Volume 95, No. 3-4 1998/1999 (ISCEV 10.4)
THIS ISSUE COMPLETES VOLUME 95

CODEN DOOPAA / ISSN 0012-4486

Documenta Ophthalmologica

Special Issue
Parallel Visual Processes in Health and Disease
Guest Editor: Werner Spileers

Kluwer Academic Publishers

Publication programme, 1998: Volumes 95-97.
Subscription prices:
(3 volumes of 12 issues): NLG 1719.00 / USD 882.00.
These prices are for institutions only.
Subscriptions should be sent to *Kluwer Academic Publishers Group, P.O. Box 322, 3300 AH Dordrecht, The Netherlands,* or at *P.O. Box 358, Accord Station Hingham, MA 02018-0358, U.S.A.,* or to any subscription agent.
Changes of mailing address should be notified together with our latest label.
For advertisement rates, prices of back volumes, and other information, please apply to Kluwer Academic Publishers, P.O. Box 17, 3300 AA Dordrecht, The Netherlands.

REPORT DOCUMENTATION PAGE

Form Approved OMB No. 0704-0188

1. AGENCY USE ONLY (Leave blank)	2. REPORT DATE	3. REPORT TYPE AND DATES COVERED
	18 November 1999	Conference Proceedings

4. TITLE AND SUBTITLE

Parallel Visual Processes in Health and Disease

5. FUNDING NUMBERS

F6170897W0180

6. AUTHOR(S)

Conference Committee

7. PERFORMING ORGANIZATION NAME(S) AND ADDRESS(ES)

Dienst Oogziekten
UZ Sint Rafael, Kapucijnenvoer 33
B-3000 Leuven
Belgium

8. PERFORMING ORGANIZATION REPORT NUMBER

N/A

9. SPONSORING/MONITORING AGENCY NAME(S) AND ADDRESS(ES)

EOARD
PSC 802 BOX 14
FPO 09499-0200

10. SPONSORING/MONITORING AGENCY REPORT NUMBER

CSP 97-1064

11. SUPPLEMENTARY NOTES

12a. DISTRIBUTION/AVAILABILITY STATEMENT

Approved for public release; distribution is unlimited.

12b. DISTRIBUTION CODE

A

13. ABSTRACT (Maximum 200 words)

The Final Proceedings for Parallel Visual Processes in Health and Disease, 20 June 1997 - 20 June 1997

Neurophysiology of Parallel Visual Processes as Applied to Color and Motion Processing, Modelling Parallel Processes in the Electroretinogram and Cortical Evoked Potentials, Motion Processing in Human Vision, Parallel Visual Processes and the Control of Eye Movements and Higher Visual Processes, Measurement of Parallel Visual Processes in Humans

14. SUBJECT TERMS

EOARD, Vision

15. NUMBER OF PAGES

378

16. PRICE CODE

N/A

17. SECURITY CLASSIFICATION OF REPORT	18. SECURITY CLASSIFICATION OF THIS PAGE	19. SECURITY CLASSIFICATION OF ABSTRACT	20. LIMITATION OF ABSTRACT
UNCLASSIFIED	UNCLASSIFIED	UNCLASSIFIED	UL

International Society for Clinical Electrophysiology of Vision

Editorial statement. *Documenta Ophthalmologica* publishes articles in the field of ophthalmology. Apart from regular journal articles longer manuscripts will also be considered for publication, for example monographs, theses or reviews.

ISCEV. *Documenta Ophthalmologica* includes 5 issues which constitute the official journal of the International Society for Clinical Electrophysiology of Vision (ISCEV). Editor of these issues is Dr. J.V. Odom, Department of Ophthalmology, RC Byrd Health Sciences Center, P.O. Box 9193, Morgantown, WV 26506, USA.

The year program of *Documenta Ophthalmologica* includes 1 issue on the History of Ophthalmology under the auspices of the Cogan Ophthalmic History Society.

Documenta Ophthalmologica is published monthly.
Subscription prices (1998, 3 volumes of 12 issues): NLG 1719.00 / USD 882.00; including postage and handling.
Periodicals postage paid at Rahway, N.J. USPS No. 568–410.
U.S. Mailing Agent: Mercury Airfreight International Ltd., 365 Blair Road, Avenel, NJ 07001.
Published by Kluwer Academic Publishers, Spuiboulevard 50, P.O. Box 17, 3300 AA Dordrecht, The Netherlands, and 101 Philip Drive, Norwell, MA 02061, U.S.A.
Postmaster: Please send all address corrections to: *Documenta Ophthalmologica,* c/o Mercury Airfreight International Ltd., 365 Blair Road, Avenel, NJ 07001, U.S.A.

Printed on acid-free paper

Special issue
Parallel Visual Processes in Health and Disease

Symposium for the Francqui International Interuniversity Chair in Biomedical Sciences 1997

Guest editor

Werner Spileers

Dienst Oogziekten, UZ Sint Rafael, Kapucijnenvoer 33, B-3000 Leuven, Belgium

The symposium received the financial support of the Francqui Foundation and the United States Air Force European Office of Aerospace Research and Development (EOARD).

DOCUMENTA OPHTHALMOLOGICA

CONTENTS Volume 95 No. 3-4 1998/1999 (ISCEV 10.4)

Documenta Ophthalmologica **95:** 181–184, 1999.

Parallel visual processes in health and disease

Symposium for the Francqui International Interuniversity Chair in Biomedical Sciences 1997

J. VERNON ODOM, PH.D.
Department of Ophthalmology, Robert C. Byrd Health Science Center of West Virginia University, Morgantown, WV, USA

It is common place in contemporary visual science to describe the brain and the human visual system as a distributed processor or to think in terms of hierarchical and parallel visual processes. These words borrowed from contemporary computers provide new, useful insights to visual processes. Although, these insights are real, they have a history, especially in visual science.

We in visual science have described the visual system in terms of hierarchically organized parallel processes at least since the 19th century, although we have not always used those words. How else would one describe Hering's theory of binocular function based on corresponding retinal points? Similarly, before World War II, Jameson and Hurvich described color vision in terms of parallel long, medium and short wavelength pathways which were hierarchically organized into three subsequent parallel red-green, blue-yellow, and black-white opponent pathways. Ideas of the separateness of rod and cone system function have similar overtones. What is new is the increasing number of parallel systems, the increasing number of hierarchical levels which increasing anatomical knowledge and improved analysis have brought to our attention, and our ability to quantitatively describe these parallel processes. Perhaps this is epitomized by the increasing work on magnocellular and parvocellular streams of visual processing or on-pathways and off-pathways of the visual system.

Our increasing refinement of ideas of parallel pathways has also begun to assist us in understanding how these systems cooperate in normal, healthy persons and how they are disrupted or altered in various disease states. At least one way of viewing many ophthalmic diseases, is to think in terms of which parallel pathways are disrupted by the disease process. Much of my career has been dedicated to developing methods of assessing functions specific to one or another disease and to identifying the pathways involved.

When the Francqui Foundation awarded me an Francqui International Interuniversity Chair in Biomedical Sciences in 1996–1997 (Flemish: Interuniversitaire Buitenlandse Francqui-Leerstoel Biologische en Medische Wetenschappen; French: Chaire Francqui Interuniversitaire au Titre Etranger

Sciences Biomédicales), they requested that I present an inaugural lecture on a topic of my specialty and organize a symposium on some topic of my choosing. It did not take me long to choose the topic for either. The inaugural lecture presented December 3, 1996 in the Promotiezaal of the Universiteitshal was entitled When Two Eyes Are Better than One: Binocular Luminance Interactions Studied with Models, Visually Evoked Potentials, and Behavior. The symposium held on June 20, 1997 was entitled, Parallel Visual Processes in Health and Disease. The purpose of the symposium was to gather a group of scholars, largely from Belgium and neighboring countries, to present papers on a wide range of topics related to parallel visual processes. I have appended a list of those presenting at the symposium and the titles of their presentations to provide an indication of the diversity and interest of the papers presented. Most but not all of the presentations are represented in this special issue of Documenta Ophthalmologica.

I wish to make several acknowledgments. First, I wish to thank the Francqui Foundation for the joy of a sabbatical year in Belgium. As a result of their confidence, I had some truly remarkable experiences, including my lecture, my symposium, Thanksgiving Dinner, shaking hands with the King and giving my first lectures in French. Prof. Eyckmans was the human face associated with the Foundation. He always was helpful and kind. Secondly, I wish to thank the United States Air Force European Office of Aerospace Research and Development (EOARD) for their support of the symposium. Their generous support permitted us to offer the symposium without charge to those attending and to sponsor several speakers who would not have been able to attend otherwise. The one requirement of EOARD was that we publish the proceedings. Third, Gerald Fishman, the editor of Documenta Ophthalmologica in 1996 agreed that we could create a special issue. Fourth, I wish to acknowledge my sponsors in Belgium: Professor Luc Missotten in Leuven and Professor Jean-Jacques DeLaey in Gent. Fifth, I wish to acknowledge the assistance of Werner Spileers who nominated me for the Francqui Chair, provided a stimulating work environment during my stay in Belgium, assisted in the planning and organizing of the Symposium, and finally was the guest editor for this volume. His laboratory personnel, especially Lidwine van Malderen, were stimulating collaborators. Lastly, I wish to thank all of those who came and presented papers at a delightful symposium. I list the presenters names and the titles of their presentations below. For considerations of space, I have omitted co-authors and abstracts.

Address for correspondence: J. Vernon Odom, Department of Ophthalmology, Robert C. Byrd Health Science Center of West Virginia University, P.O. Box 9193, Morgantown, WV 26506-9193, USA
Phone: 1- 304-293-3757; Fax: 1-304-293-7139; E-mail: jodom@wvu.edu

PARALLEL VISUAL PROCESSES IN HEALTH AND DISEASE
Symposium President: A. De Rouck
Organizers: Werner Spileers and J. Vernon Odom
Welcome: A. De Rouck, W. Spileers and J. Vernon Odom
Introduction by Prof. Eyckmans

Session I: Parallel processes and the retina
J. Robson – *Keynote speaker:* Dissecting the electroretinogram to reveal the parallel contributions of many retinal cell types.
C. Flaxel: Correlation between genotype and phenotype in X-Linked Retinitis Pigmentosa.
G. Holder: Dominant optic atrophy: Clinical, genetic, and electrophysiological findings.
P. Kestelyn: Deficits of the on-pathway in melanoma associated retinopathy.
K. van der Torren: Progression together with decrease in function of congenital hypertrophy of the pigment epithelium.
B. Zrenner: Subretinal mircrophotodiodes to replace the function of photoreceptors in degenerative retinal diseases.

Session II: Parallel processes and basic cortical processes: I
G. Orban – *Keynote speaker:* The physiology of visual motion processing areas in the monkey.
Jan Kremers: Parvocellular and magnocellular systems in dichromatic and trichromatic primates.
Peter Janssen: Stereo VEPs in man and monkey.

Session III: Parallel processes and basic cortical processes II
H. Spekreijse – *Keynote speaker:* Visual processing in man and monkey: an integrated brain imaging approach.
G. Arden: Separation of parallel visual pathways by disease processes.
W. Spileers: VEPs elicited by two dimensional noise stimuli.
J. Charlier: The pupil as an indicator of visual suppression: methods and preliminary results.

Session IV: Parallel processes and higher visual processes
J. Wagemans: Parallel visual processes in symmetry perception: Normality and pathology.
P. de Graaf: Parallel object processing in real world scenes.
M. Bach: Electrophysiological correlates of texture segregation.
J. T. Yates: Parallel pathways, noise masking and glaucoma detection.

Session V: Posters

K. Claeys: Parallel visual and memory processes.

J. Shallo-Hoffmann: A motion aftereffect in congenital nystagmus and avestibular patients.

M. L.M. Tant: Visual field defects, visual-spatial attention and driving: assessment of attention and fitness to drive in older persons with visual field defects due to CNS damage.

T.R.M. Coeckelbergh: Age-related changes throughout the functional visual field.

J. V. Odom: Visually evoked potentials evoked by moving stimuli: Effects of contrast, spatial frequency, active electrode location, reference electrode location, and stimulus type.

Documenta Ophthalmologica **95:** 185, 1999.

Introduction

It is a great pleasure, and an honour, to open this Symposium, dedicated to *Parallel Visual Processes in Health and Disease*, honouring the presence in Belgium of Professor Vernon Odom. Professor Odom is the recipient of an *International Francqui Chair in Biomedical Sciences*.

What is the Francqui Foundation? It is a Belgian Institution, devoted to the promotion of higher education and research in this country. It was founded jointly by Emile Francqui, a Belgian Officer turned financier, and Herbert Hoover, who had been president of the United States. These two had collaborated, within the frame of the Committee for the Relief of Belgium, that provided the Belgian population with essential food during World War I. Later, they took upon them to help in the reconstruction of Belgium, by various initiatives centered upon the Universities.

Today, the Francqui Foundation has three main directions in its actions:

The **Francqui Prize**, which is given each year, is meant as an encouragement for a young Belgian scientist. The selection is made by an international Jury; the Prize itself is the only prize which is handed over by the King. It carries an important sum of money, and substantial support for the laboratory or the team of the Laureate.

The **Belgian Francqui Chairs**: each year, every complete university has the possibility to invite two prominent Professors from other Belgian universities, to organize a cycle of conferences. This is usually the opportunity for a reception of all scientists involved in this discipline, where collaboration is enhanced and new initiatives can be started.

The **International Francqui Chairs** (Chaires Francqui Interuniversitaires au titre étranger – Interuniversitaire Buitenlandse Francqui-Leerstoelen): the Francqui Foundation invites every year three top-level scientists for a six-months stay in Belgium. This is meant at the inter-universitary level, one of the universities involved acting as the 'host institution'. These Chairs are distributed as follows: one in the exact sciences, one in the *human sciences* and one in the *biological and medical sciences*. Last year, the personalities proposed by the universities were so outstanding, that the Francqui Foundation decided to extend exceptionally its invitation to five such scientists, to accept an International Francqui Chair. We are very pleased that Professor Odom, of the University of West-Virginia, is with us today, and has accepted our invitation to organize this Symposium in order to crown his stay in Belgium.

PROFESSOR DR. LUC EYCKMANS
Executive Director of the
Francqui Foundation

Documenta Ophthalmologica **95:** 187–215, 1999.

Dissecting the dark-adapted electroretinogram

JOHN G. ROBSON & LAURA J. FRISHMAN
College of Optometry, University of Houston, Houston, TX 77204-6052, USA

Accepted 15 January 1998

Abstract. Although gross recordings of the ganzfeld flash-evoked electroretinogram (ERG) can potentially provide information about the activity of many, if not all, retinal cell types, it is necessary to dissect the ERG into its components to realize this potential fully. Here we describe various procedures that have been used in intact mammalian eyes to identify and characterize the contributions to the dark-adapted ERG of different cells in the retinal rod pathway. These include (1) examination of the very early part of the response to a flash (believed to reflect directly the photocurrent of rods), (2) application of high-energy probe flashes to provide information about the underlying rod photoreceptor response even when this component is obscured by the responses of other cells, (3) pharmacological suppression of responses of amacrine and ganglion cells to identify the contribution of these cells and to reveal the weaker responses of bipolar cells, (4) use of pharmacological agents that block transmission of signals from rods to more proximal neurons to separate responses of rods from those of later neurons, (5) examination of the ERG changes produced by ganglion-cell degeneration or pharmacological block of nerve-spike generation to identify the contribution of spiking neurons, (6) modeling measured amplitude-energy functions and timecourse of flash responses and (7) using steady backgrounds to obtain differential reductions in sensitivity of different cell types. While some of these procedures can be applied to humans, the results described here have all been obtained in studies of the ERG of anaesthetized cats, or macaque monkeys whose retinas are very similar to those of humans.

Key words: A-wave, B-wave, electroretinogram, retina, STR

Introduction

Because the activity of nerve cells involves changes in the electrical potential across their bounding membrane, transmission of signals through the nervous system is usually accompanied by electrical currents that flow in the surrounding tissues and give rise to voltages that can be recorded with extracellular electrodes. Although the extracellular current generated by a single neuron is small, much larger currents can be produced when many cells are simultaneously active. This is the situation when a flashed light falling on an extended area of the retina synchronously activates large numbers of cells and thereby produces currents large enough to provide a change in trans-retinal voltage that can be recorded as the electroretinogram (ERG).

The ERG that is evoked by a ganzfeld flash that uniformly illuminates the whole visual field can easily be recorded non-invasively from electrodes outside the eye and it clearly has the potential to provide information about the operation of those cells that contribute to it. Such information should be of use in ascertaining the nature of certain retinal disorders and in diagnosing retinal disease in individuals, as well as in furthering our understanding of normal retinal function. However, full realization of the diagnostic and scientific potential of the ERG requires that the contributions to the ERG of the many different types of cell in the retina be identified so that ERG recordings can be analysed into their components and observed alterations in the ERG can be attributed to the appropriate retinal elements. This is not a trivial problem because, although the responses of retinal neurons are initiated in sequence from the photoreceptors to the fibers of the optic nerve, the electrical activity of each type of cell is long-lasting compared with the delay in propagation from one stage to the next and the ERG is therefore the sum of many signals that overlap substantially in time.

In this context, we review the results of a number of experiments (in macaques and cats) designed to identify, isolate and characterize the contributions to the dark-adapted ERG of the various retinal cell types that comprise the 'rod pathway'. This pathway is peculiar to the mammalian retina; it runs from rods to ganglion cells via specific rod bipolar and amacrine cells and carries signals that result from the activation of individual rods by single quanta of light [e.g. Ref. 1, 2]. In the dark-adapted eye it provides useful

Figure 1. (A) Simplified schema of the mammalian 'rod pathway'. Signals from a number of rods, roughly 25 (15–60 depending on the species and location in the retina [3–5], converge onto each rod bipolar cell. Each rod makes a discrete synaptic connection with the bipolar cell. Output signals from many rod-bipolar cells, 5–25 [2, 6] converge onto each AII amacrine cell. Amacrine-cell outputs pass via either depolarizing or hyperpolarizing (cone) bipolar cells to ON or OFF ganglion cells respectively. There is further convergence at this stage also. Both ON and OFF ganglion cells generate action potentials that are transmitted to the optic nerve over unmyelinated fibers running over the retinal surface. Neither horizontal nor Müller cells are shown. The latter contribute to the dark-adapted ERG as a result of their response to changes in extra-cellular concentration of K^+. The involvement of horizontal cells in generating the dark-adapted ERG is unknown. (B) Typical recordings of dark-adapted ERG in cat, macaque and human. Records are shown for four flash energies to illustrate (a) the primarily negative STR obtained with the weakest stimulation, (b) the emergence of a positive-going b-wave as the energy is raised, (c) the growth and eventual saturation of the b-wave accompanied by the appearance of an earlier negative a-wave and (d) the growth and eventual saturation of the a-wave. See methods for recording procedures in cats and macaques. Procedures for recording ERGs from alert human subjects were similar to those in anesthetized macaques except that the DTL fibers were placed in the lower canthus of the eye (for details see [7]).

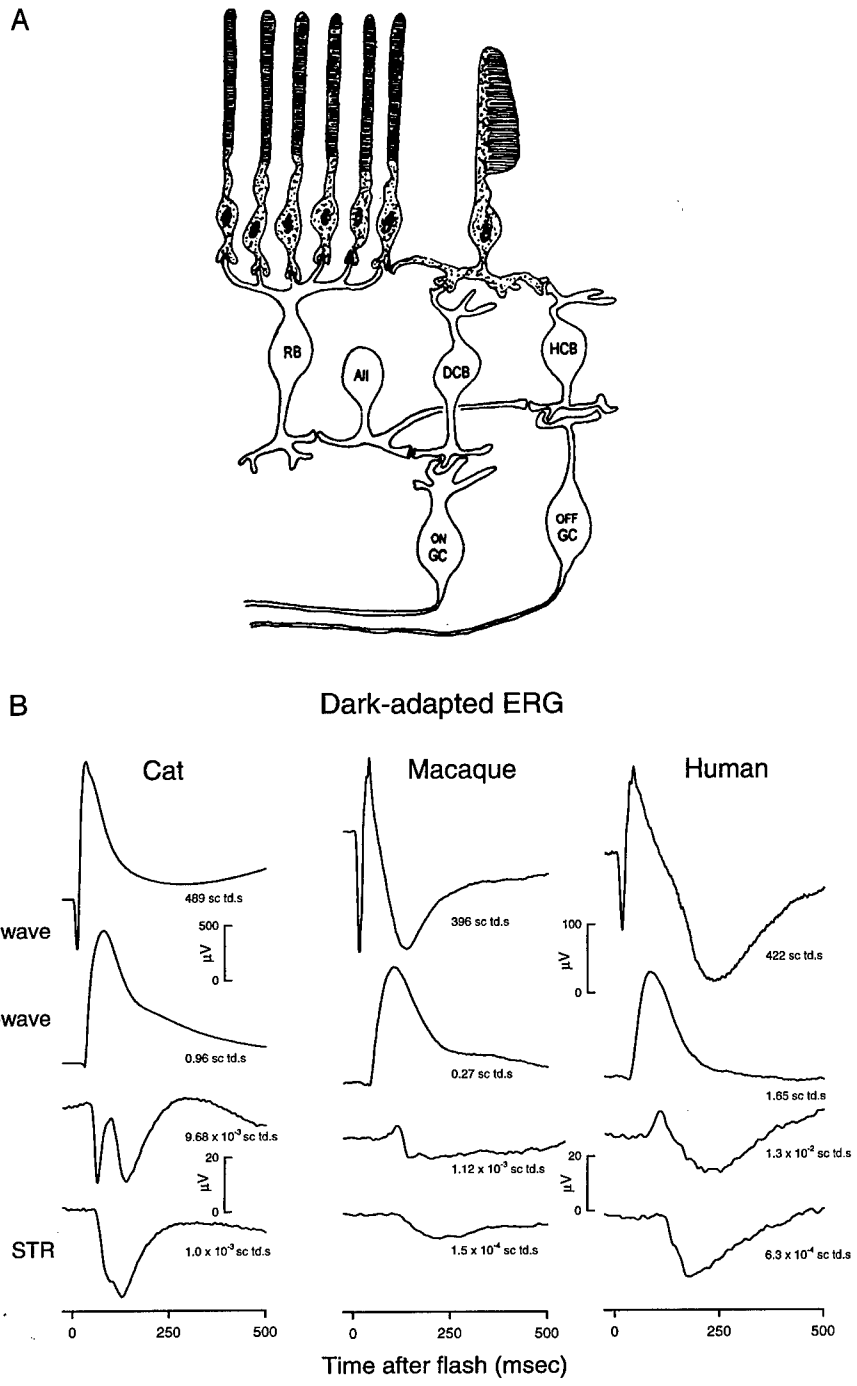
A
RB
AII
DCB
HCB
ON GC
OFF GC
B
Dark-adapted ERG
Cat
Macaque
Human
a-wave
b-wave
STR
489 sc td.s
0.96 sc td.s
9.68 x 10-3 sc td.s
1.0 x 10-3 sc td.s
396 sc td.s
0.27 sc td.s
1.12 x 10-3 sc td.s
1.5 x 10-4 sc td.s
422 sc td.s
1.65 sc td.s
1.3 x 10-2 sc td.s
6.3 x 10-4 sc td.s
500
100
20
μV
0
250
Time after flash (msec)

visual sensitivity at those very low light levels at which each rod receives no more than a few photons per second from a continuous light or more than a single photon from a flash. A cartoon of the cells involved in the rod pathway appears as Figure 1A while Figure 1B shows examples of dark-adapted ERGs that can be recorded from the intact eye of cat (left), macaque (middle) and similarly from human (right).

The form of the electroretinogram that is recorded when the rod pathway is excited by a flash of light varies greatly according to the strength of the flash and the state of adaptation of the retina. When the retina is fully dark-adapted and the flash is very weak (Figure 1B, bottom), the response is a predominantly a cornea-negative potential reflecting activation of amacrine and ganglion cells. This response peaks more than 100 ms after the flash and has been called the 'scotopic threshold response' (STR) [8, see Ref. 9 for review]. Although the amplitude of this negative wave grows with increasing stimulus energy, it always appears to saturate at a fairly low level (less than 100 μV even in cats, in which it is relatively large). When the stimulus energy is raised further an earlier positive-going b-wave appears. In the cat the b-wave, which first appears in the trough of the STR, is always preceded by an obvious negative-going wave of inner-retinal origin even when the stimulus energy is raised to levels at which the amplitude of the b-wave itself reaches saturation (second traces from the top). In the macaque and human, the preceding negative-going inner retinal contribution is not always :clearly visible.

The b-wave is primarily a reflection of the activity of the bipolar cells [10–16] although smaller positive contributions to the ERG may be made by other inner-retinal cells [e.g. 7, 17]. At still higher levels of stimulus energy the direct contribution of the rods themselves becomes evident as an even earlier negative wave (the a-wave) that can ultimately grow to an amplitude (typically hundreds of microvolts) that is several times greater than that of the saturated STR (top records). The time to the negative a-wave peak is quite short (always less than 25 ms, shorter at very high energies) and does not generally reflect the timing of the peak in the rod photocurrent response (which occurs considerably later). Rather, it may be assumed that the a-wave peak occurs when the relatively slowly rising negative signal from the rods is overtaken by a more-delayed but faster-rising positive response of other retinal neurons. Indeed the timing of all the peaks in the ERG as well as their amplitudes are complex functions of the waveforms of the underlying responses of the various retinal cell types and the way in which they change with stimulus energy [e.g. 18]. Interpretation of the ERG in terms of its basic components is difficult if attention is limited to the times and amplitudes of the obvious peaks and troughs in the records; as we shall see it is generally

more useful to consider the amplitude of the ERG at various fixed times after a stimulus flash.

Although much basic information about the cells involved in the rod pathway has come from experimental work on isolated retinas and retinal cells, this is insufficient in itself to enable ERGs from the intact eye to be exactly analyzed into their elementary components. However, the information that is now available about the behavior and pharmacology of retinal cells, together with the results of studies of the neural circuitry of the retina of primates and other mammals [19–21 for recent major reviews], can be used to guide such an analysis and to design and interpret the experimental studies in intact eyes that are required to validate it.

Among the various procedures that can be used in intact eyes to identify and characterize the contributions to the ERG of different cells in the retinal rod pathway are (1) examination of the very early part of the response to a flash (believed to reflect directly the photocurrent of rods), (2) application of high-energy probe-flashes to provide information about the underlying rod photoreceptor response even when this component is obscured by the responses of other cells, (3) use of pharmacological agents that suppress responses of amacrine and ganglion cells to identify the contribution of these cells and to reveal the weaker responses of bipolar cells, (4) use of pharmacological agents that block transmission of signals from rods to more proximal neurons to separate response of rods to high-energy stimuli from those of later neurons, (5) examination of the ERG changes produced by ganglion-cell degeneration or pharmacological block of nerve-spike generation to identify the contribution of spiking neurons, (6) location of current sources within the retina using intra-retinal microelectrodes, (7) modeling measured amplitude-energy functions and timecourse of flash responses and (8) using steady backgrounds to obtain differential reductions in sensitivity of different cell types. While some of these procedures can be applied to humans, others can only be performed in experimental animals. Even those procedures that can be used in humans may best be validated in animal experiments and we shall restrict our attention to describing results obtained in studies of the ERG of anaesthetized cats and macaque monkeys whose retinas are very similar to those of humans. These studies have been most successful in isolating and characterizing the response of rods and rod-bipolar cells and we shall primarily concentrate on these cells.

Methods

In all the experiments to be reviewed ERGs have been recorded in anaesthetized cats and macaques using protocols approved by the Institutional Animal

Care Committee; details of the procedures have been given in previous publications [15, 17, 22] and are only briefly summarized here. For all recordings the pupil is dilated with mydriatics and the cornea protected by a contact lens. In non-recovery experiments on cats the ERG is recorded between an intravitreal silver wire electrode and another silver electrode in the orbit behind the eye while in macaques that are anesthetized for only a few hours before being allowed to recover, the ERG is recorded differentially from DTL [23] fibers sandwiched between the cornea and a contact lens in each eye. In some cats glass micropipettes are used to record local potentials at different depths in the retina. All signals are amplified in a band from 0 to 300 Hz before being digitized at 1 kHz for storage, averaging and subsequent analysis. Ganzfeld stimulus flashes of very short duration are generated by computer-controlled light-emitting diodes located behind a diffusing screen in front of one eye; flashes of much higher luminous energy are provided by a xenon flash tube behind the same diffuser. Pharmacological agents are delivered to the retina by intravitreal injection in small volumes of sterile balanced salt solution.

Results

The rod photocurrent component of the dark-adapted ERG

The primary event in the generation of a visual response to a weak flash of light is the absorption of photons by the photopigment in the rods. The absorption of each photon that is effective in isomerizing a molecule of rhodopsin triggers an amplifying cascade of chemical reactions that ultimately results in a change in permeability of the membrane of the rod outer segment and a consequential reduction in the current that circulates between the inner and outer segments in the dark. This current change appears in the ERG as a cornea-negative potential.

Over much of the scotopic range both visual and ERG responses are obtained with stimuli that result in the isomerization of single molecules of rhodopsin in only some of the rods. To put this in perspective, the light required to produce, on average, a single photoisomerization in each rod is about 0.2 scotopic (scot) td.s in cats, 0.08 td.s in macaques and 0.11 td.s in humans [see Ref. 15 for the method of calculation]. The human psychophysical threshold for a ganzfeld flash is rather less than 10^{-5} scot td.s, i.e. less than about one photoisomerization in every 12,000 rods [7].

Linearity and saturation. Although the absorption of photons is a stochastic (random) process, the average number of photons absorbed from a flash cf light increases in direct proportion to the energy of the flash. Moreover it

has been shown in individual isolated rods that so long as the circulating current is reduced by no more than a fairly small proportion of its initial value in the dark, the magnitude of the reduction in photocurrent increases in direct proportion to the number of photons absorbed [24]. This is found to be true whether the response of the rod is small at all times after the flash (because the stimulus delivers only a few photons) or whether the response amplitude is small because it is measured at some short time after a stronger flash. However, once the stimulus energy is sufficiently great, the amplitude of the response at a given time no longer increases in proportion to stimulus energy but levels off at some maximum saturated value. In isolated rods this transition from linearity at low energies to saturation at high energies is well described by the exponential relation (in toad [24]; in primate [25]; in cat [26].

$$R(i, t) = \hat{R}(1 - \exp(-iT_r(t))) \tag{1}$$

where $R(i, t)$ is the average response amplitude at a fixed time t after a stimulus of energy i, $\hat{R}$ is the maximum value of the response amplitude and $T_r(t)$ is a function to be considered later.

On this basis it has been supposed that if the earliest part of the ERG response to a flash is entirely provided by the photocurrent of the rods then the amplitude of the ERG measured at a fixed short time after the stimulus would initially increase in proportion to the flash energy and then show the same exponential saturation as isolated rods. Hood and Birch [27] have demonstrated that the human ERG behaves in this way and we have now confirmed that the ERGs of both cat and macaque behave similarly. As an example Figure 2 shows the amplitude of cat ERG responses to flashes of various strengths measured at several different times after the stimulus; flash energy is given both in scot td.s and photoisomerizations per rod (calculated assuming that 1 td.s produces 5 photoisomerizations per rod). For each time at which the amplitude is plotted (between 5 and 25 ms after the flash) the continuous line that fits the lower amplitude points (and is continued by a dotted line at higher levels) corresponds to an initially linear response that saturates exponentially at a fixed level (Equation (1) with $\hat{R} = 620\ \mu V$). Thus each of these curves has the same shape but is displaced along the energy axis. It can be seen that at all times the amplitude increases at least up to 20–30 μV in proportion to stimulus energy even though at the shortest times this may require a stimulus giving thousands of photoisomerizations per rod. However, what happens when the stimulus energy is increased beyond the level giving this response depends greatly upon the time at which the amplitude is measured. At short times (10 ms and somewhat less) the response amplitude continues to grow as expected nearly up to the saturation level, although in the experiments illustrated here

this level was never quite attained with the strongest stimulus available (800 scot td.s)[1]

At later times after the flash (13 ms and greater) the amplitude stops rising along the predicted exponential path when the flash energy is much lower and the response is much smaller than the saturation level; at these times a further increase in stimulus energy results in a reduction in ERG amplitude. This behaviour is closely related to the reduction in the duration of the a-wave that is seen when stimulus energy is raised over the relevant range (see inset to Figure 2 which shows the timecourse of responses at the three stimulus-energy levels indicated by arrows a, b and c). This relationship may be made clearer by noting that the stippled line in Figure 2 plots the peak amplitude of the a-wave as a function of stimulus energy (straight lines join the measured values). From this it may be more easily appreciated that the envelope of the amplitude-energy curves plotted for different fixed times after the flash is the a-wave peak amplitude-energy function. Thus, since the different fixed-time functions have maxima that are very different from each other, it is understandable that the a-wave peak amplitude may show no sign of the proportionality with stimulus energy that is characteristic of each fixed-time function and of the underlying rod responses.

While the results of Figure 2 are consistent with the idea that the earliest part of the ERG (10 ms and less after the flash) is a reflection of the rod photocurrent alone, it is clear that at times of 13 ms and more (i.e. at times at which the amplitude no longer follows an exponential path to the saturation level), the responses of other cells must also be contributing to the ERG. Moreover, it should be noted in Figure 2 that the amplitudes measured at the longest times after the flash (20 and 25 ms) deviate markedly from the expected rod amplitude-energy functions at levels at which these are still well within the effectively linear range. This indicates that it is not simply the saturation non-linearity of the rod responses that causes an increase in stimulus energy to result in a rapid reduction in amplitude and to change the timing of the initial negative phase of the ERG. Rather we must suppose that to counteract the still linearly-increasing amplitude of the negative rod component there must be cells that add to the ERG a net positive contribution

[1] In other experiments we have seen that with slightly stronger stimuli the ERG amplitude at times between about 5 and 8 ms can indeed reach its final saturation level along an exponential path. However, when measurements are made at shorter times (e.g. 2–4 ms after the flash) the amplitude does not continue to increase according to Equation (1) all the way to saturation but shows an earlier slowing down at stimulus energy levels corresponding to those giving rise to the 'rate-saturation' of rod photocurrent described in rat rods by Penn and Hagins [28] and in the human ERG by Breton, Schueller, Lamb and Pugh [29].

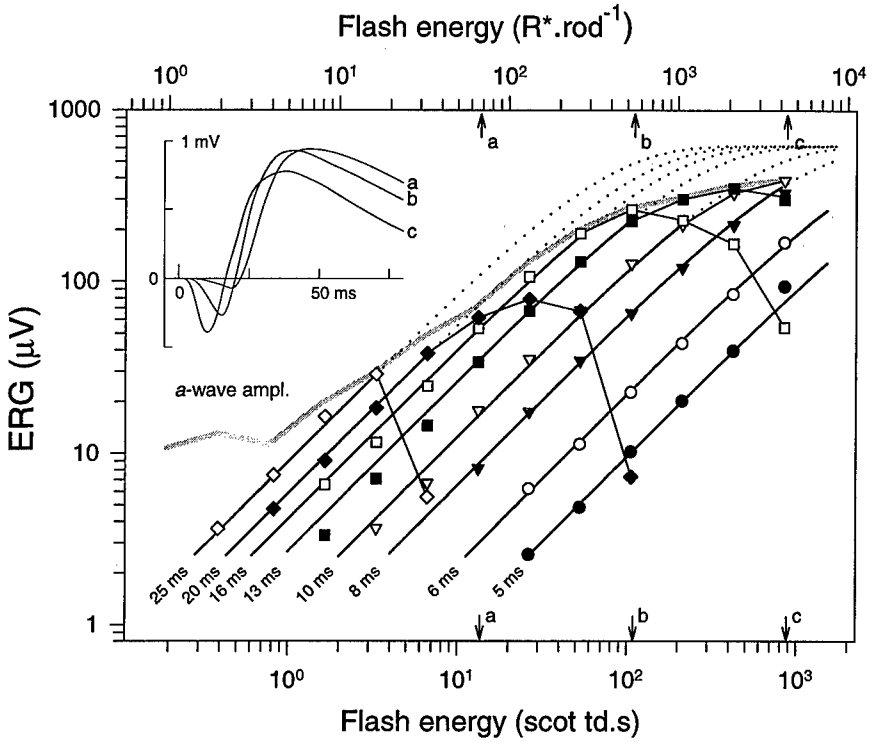

Figure 2. The amplitude of the normal cat ERG measured at various short times after flashes of various energies. Note that at all times and for all energies the amplitude initially rises in proportion to flash energy (slope of 1 on this log-log plot). At the shortest times the amplitude grows to a high level while demonstrating only a slight tendency to saturate. The smooth solid and dotted lines predict the amplitude of the underlying photoreceptor response assuming an exponential relation (see Equation (1)) and an ultimate saturation level of 620 μV, a value indicated by recordings made with stronger stimuli than those illustrated. At longer times, the amplitude reaches a much lower maximum and then declines abruptly. The stippled line shows the measured a-wave peak amplitude for different flash energies. This curve forms the envelope of the measurements made at different times. *Inset.* Timecourse of the cat ERG at three stimulus energies indicated on the energy scales by a, b and c. Note that both the time of the negative a-wave peak as well as the time of the zero-crossing change markedly with stimulus energy, indicating that some aspects of the response are very non-linear. (Cat 95).

whose amplitude is an accelerating function of stimulus energy (i.e. show a threshold type of behavior).

Timecourse of the early ERG. A detailed consideration by Lamb and Pugh [30] of the kinetics of the various intermediate steps involved in generating a rod's photoresponse predicts that when the stimulus is sufficiently strong for the circulating current to be completely suppressed before the onset of the

recovery process that terminates the response, the timecourse of the leading edge of the current waveform will be a slightly delayed Gaussian function of time.

$$R_r(i, t) = \hat{R}_r\,(1 - \exp(-k_r i(t - \tau_r - \tau_i)^2)) \tag{2}$$

i.e. in Equation (1) $T_r\,(t) = k_r\,(t - \tau_r - \tau_i)^2$

In this formulation the kinetic behaviour that is provided by the term $(t - \tau_r - \tau_i)^2$ reflects (a) three stages of integration provided by the G-protein cascade underlying phototransduction (as the exponent 2), (b) various small delays related to diffusion and chemical reactions within the rod as well as the delay involved in converting conductance changes into external currents [31], lumped together into τ_r, and c) an instrumental delay, τ_i introduced by the low-pass filtering applied to the electrical signals prior to recording them[2]. In the recordings illustrated here, τ_r and τ_i are about 2 ms and 1 ms respectively. It should be noted that while the rod response is small compared with its maximum value it can be approximated (at times longer than $\tau_r + \tau_i$) by

$$R_t(i, t) \approx \hat{R}_r\, k_r i(t - \tau_r - \tau_i)^2 \tag{3}$$

It has already been shown experimentally that the responses of isolated human rods conform to the predictions of Equation (2) [32] and that the early part of the human ERG does so too [27, 29]. We now examine the leading edge of ERGs from both cat and monkey to see to what extent this same behaviour applies.

Figure 3A shows three ERG records from a cat obtained with stimuli whose energies increase by successive factors of 8 (these are the same responses that are shown in the inset to Figure 2; they can be assumed to have produced on average about 70, 560 and 4480 photoisomerizations per rod). Although increasing the stimulus energy may appear to reduce the time delay involved in generating the leading edge (of the response, in fact the earliest part of all three responses is well described by the simple relation of Equation (3) with a fixed time delay of 3.2 ms (0.9 ms of which is introduced by the low-pass filter). These fits are plotted in Figure 3A as the thinner stippled lines. While the earliest part of the response is adequately described by this small-response approximation of the Lamb and Pugh [30] model, we can

[2] The representation of the various physiological delays and the instrumental delay as simple transport delays is an approximation that only applies for times that are long compared with the delay. Moreover, the lumping together of all the physiological delays into a single delay is only appropriate in so far as the delays follow the saturating non-linearity implicit in the Lamb and Pugh [30] model.

obtain a good fit to a larger part of the ERG records by using the more complete non-linear formulation of Equation (2). Curves generated by this model are shown by the thicker stippled lines in Figure 3A. Although the fits of the more complete model are better than those of the simple linear approximation, they still deviate from the recorded responses at times that are well before that of the negative peak, even when this is already quite short. For the response to the strongest stimulus shown in Figure 3A (with a time to peak of about 10 ms), the deviation is already apparent as early as 6 or 7 ms after the flash. While this deviation could result from some unexpected failure of the rod photocurrent to appear undistorted in the ERG, it seems more likely that it simply reflects the onset of a significant positive contribution from more proximal cells in the retina. This interpretation is considerably strengthened by examining the effect on the ERG of the intravitreal injection of a combination of APB and NMDA. These agents together block the transmission of signals from the rods to the ON bipolar cells (APB) and suppress the activity of all neurons proximal to the bipolar cells (NMDA). The effect of this cocktail on the leading edge of the ERG response to the strongest of the three stimuli illustrated in Figure 3A is shown by the filled squares. It is clear that suppressing the responses of at least a large proportion of the retinal neurons other than photoreceptors results in the postponement of the deviation of the ERG from the expected timecourse for another few ms, as would be expected if the deviation reflected the activation of those neurons. Unfortunately we have not so far round any combination of pharmacological agents that appear to be able to suppress completely the light-evoked response of all other retinal cells (i.e. including Müller and retinal epithelial cells) and make the ERG correspond exactly to the timecourse of the outer-segment current of rods *in vitro* for other than very short times after the flash or, indeed, to make an unequivocal estimate of the true saturation level of the signal that is provided by the photoreceptors alone. To examine the timecourse of the later part of the rod response, it is necessary to adopt an alternative approach that will be described later.

Intensity-scaled rod responses. While the existence of an initial, low amplitude region of the ERG that reflects linear operation of the generating mechanisms has been identified both from amplitude-energy plots (Figure 2) as well as from model fits to original ERG records (Figure 3A), a particularly simple and convenient way to examine the linearity of responses of this kind is to replot the records (e.g. those of Figure 3A) after scaling each one by the energy of the stimulus with which it was obtained. The result of doing this is shown in Figure 3B. Note that the same symbols are used in Figures 3A and 3B so that, for example, the largest energy-scaled record (open circles in

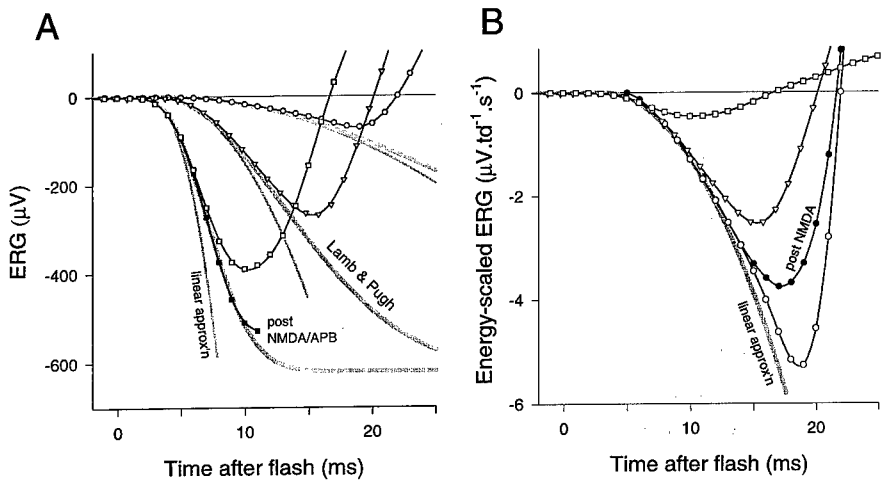

Figure 3. (A) The early part of three normal cat ERG responses (open symbols) to flashes of different energies (14, 112 and 896 scot. td.s corresponding to 70, 560, and 4480 $R^*.rod^{-1}$); these are the same records as shown in Figure 2 inset. Thick stippled lines show fits of the Lamb and Pugh [30] model (Equation (2)) to the measurements while the thinner lines show the equivalent small-response linear approximations (Equation (3)). Filled squares show the response to the strongest of the stimuli after the responses of post-receptoral neurons had been blocked as far as possible with a mixture of NMDA and APB. (B) Open symbols replot the same pre-drug data after it has been energy-scaled (i.e. each record divided by the stimulus energy with which it was generated). Filled circles show the energy-scaled response to the weakest stimulus obtained after blocking post bipolar-cell responses with NMDA. (Cat 95).

Figure 3A) corresponds to the smallest original ERG recording obtained with the weakest stimulus (open circles in Figure 3B).

It can now be seen that the initial part of each of the records falls on a common trajectory indicated by a stippled line that shows the relation

$$R'_r(t) = R_r(i, t)/i = \hat{R}_r\, k_r(t - \tau_r - \tau_i)^2 \qquad (4)$$

which is the energy-scaled version of Equation (3) (with the same constants k_r and τ_r). It will also be evident from this figure that although the fit to the largest of the scaled responses (i.e. the response to the weakest stimulus) is not far from being an adequate description over the whole extent of the leading edge, it is a *good* fit only over the first half. Given that the peak negative amplitude of the original record was only 70 μV (see Figure 3A), the deviation over the later portion of the leading edge is not likely to have been due to the exponential saturation of the rod photocurrent. Again, while it might be hypothesized that the deviation reflects the beginning of the positive-going response of the rod bipolar cells, a more probable explanation is revealed when the responses of amacrine and ganglion cells are suppressed by intravitreal injection of NMDA. Although this agent does not affect bipolar

cells, a substantial part of the response around the negative peak is removed and the linear approximation becomes a good fit over a *relatively* larger part of the leading edge. This demonstration of a significant net *negative* contribution to the ERG from cells other than bipolar cells as early as 15 to 20 ms after the flash indicates that considerable caution should be exercised in ascribing all the leading edge of the ERG to the response of the rods, even if it has a waveform closely similar to that expected from this source.

High-energy probe-flash technique. Although the earliest part of the ERG response to a relatively strong flash shows the timecourse that would be expected if it were derived from the rod photocurrent, it is clear that simple inspection of the ERG is unable to provide information either about the later stages of the response to these flashes or about more than a rather small part of the responses to stimuli that are within the functional range of rods. However, although it does not seem possible satisfactorily to isolate the responses of rods using pharmacological methods even in animals, the complete timecourse of the rod response can be revealed in the intact eye by using the high-energy probe-flash technique introduced by Pepperberg, Hood and Birch [33].

In this technique a brief white probe flash strong enough to drive the rods (and cones) into full saturation within 6 to 7 ms (about 10^4 scot td.s) is delivered at various times following a test flash. At times as soon as this after the probe flash it may be assumed that the contribution to the response of bipolar and other cells is minimal. The amplitude of the added response to the probe flash therefore indicates how close to saturation the test flash has driven the photoreceptors at the time that the probe-flash amplitude is measured; the larger the response of the photoreceptors has been to the test flash, the smaller will be their response to the probe. The reduction in amplitude of the response to the probe flash when it is delivered at various times after the test flash maps out the timecourse of the response of the photoreceptors to the test flash. In many cases the response of the cones to the test flash will be small enough to be ignored. If this is not the case, then the response of the cones alone can be examined either by using a steady background light that is sufficiently strong to saturate the rods without affecting the cones or by preceding the test flash with a conditioning flash which will drive the rods into saturation long enough for the response of the cones to be measured.

The application of this technique may best be understood from Figure 4A which shows a composite record of macaque ERG responses to a test flash of 1.6 td.s presented alone (stippled line) together with short stretches of responses obtained when an additional probe flash (black lines show 10 ms preceding and 10 ms following each probe flash) is presented as well. Each

successive 20 ms record is the response to a probe flash delivered at a different time after the test flash. Of course, only one probe flash is presented following each test flash and a long enough time (1.5 to 2 minutes) is allowed between successive test flashes for the photoreceptors to recover from the previous probe flash. In Figure 4B each 20 ms record shows the result of subtracting each response to paired test and probe flashes from the response to the test flash alone. The point on each resulting record that corresponds to a fixed time after the probe flash (7 ms in this case) is indicated by a circle and the set of circles then delineates the *derived* response of the rods to the test flash. In Figure 4C the response of the rods is replotted (open circles) so that it can be more easily compared with the original ERG (solid line, no points) and the difference between the original ERG and the derived rod response (filled circles), this latter being our best estimate of the combined responses to the test flash of all the non-receptoral cells (presumably mainly rod bipolar cells).

Concealed rod responses. It will be clear from Figure 4C that a test flash of 1.6 td.s that produces only a very small a-wave can in fact be generating a rod response of quite substantial amplitude although this is not obvious in the original ERG recording. Moreover, although the early part of the ERG is provided by the rod response and the contribution of the bipolar cells only becomes evident later on, the rod signal in fact peaks later than that of the bipolar cells and lasts longer (in this case it provides the long negative tail that continues past 600 ms). It also will be evident that because the rod response rises relatively slowly compared to the albeit delayed rise of the non-receptoral components of the ERG, the conventional measure of b-wave amplitude – from the a-wave minimum to the b-wave maximum – substantially underestimates the true amplitude of these components at these stimulus energies.

Rod amplitude-energy function. Using the probe-flash technique it is possible to examine the way in which the waveform and amplitude of the rod response depend upon stimulus energy. Figure 5A shows derived responses of macaque rods for three stimulus energies while Figure 5B shows the amplitude of the response in another macaque measured 147 ms after a test flash as a function of stimulus energy. When the stimulus energy is small the amplitude of the response increases in proportion to it and the timecourse of the response remains more or less unchanged. However, when the stimulus energy is increased the amplitude saturates and the waveform develops the flat top characteristic of saturating responses of rods studied in vitro. At this stage the entire leading edge of the waveform can be fitted with the delayed Gaussian function predicted by the Lamb and Pugh [30] model, i.e. equation (2), as plotted with the stippled line for the largest derived rod response shown in

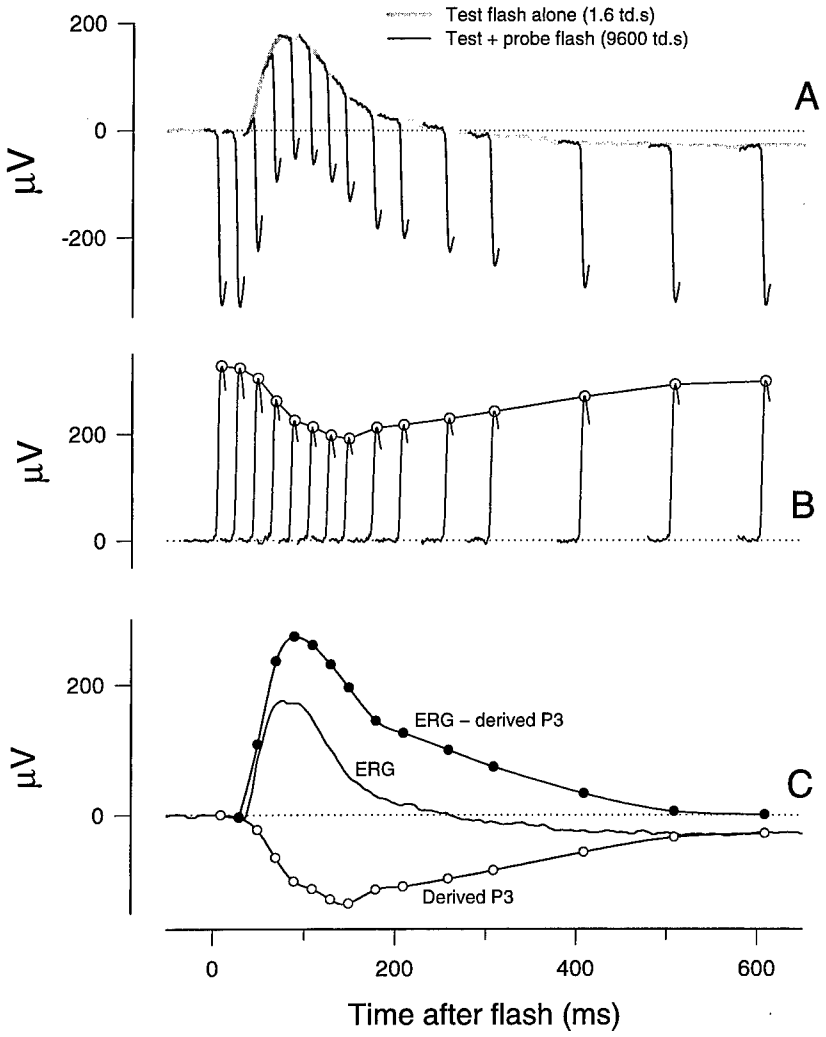

Figure 4. (A) Macaque ERG responses to a test flash of 1.6 scotopic td.s both alone (stippled line) and in combination with a probe flash of 9600 td.s at various times relative to the test flash. The response to the combination is only shown as a solid line for times between 10 ms before and 10 ms after the probe flash (at earlier times the response is the same as to the test flash alone). (B) The response to each combination of probe and test flash has been subtracted from the response to the test flash alone. The amplitude of the probe-flash response 7 ms after the probe flash is indicated with an open circle. The open circles map the reduction in probe-flash amplitude caused by the test flash; this may be considered to be the *derived response* of the photoreceptors. (C) The derived photoreceptor response from B is replotted (open circles) from a zero base together with the original ERG (line without points) and the result of subtracting the photoreceptor component from the original ERG (filled circles). Note that the negative photoreceptor response peaks later and lasts longer than the positive non-photoreceptor components of the ERG. (Monkey SM124).

Figure 5A. Amplitude-energy measurements made at a time close to the peak of the rod response (147 ms in Figure 5B) can be reasonably well described by an exponential function (Equation (1)) as found for isolated macaque [25] and human rods [32].

The rod-bipolar cell component of the dark-adapted ERG

Over a wide range of stimulus energies the most prominent feature of the dark-adapted ERG is the b-wave (Figure 1B). However, although it is generally accepted that the b-wave primarily reflects the activity of bipolar cells, it is clear that the contribution to the ERG made by other cells is always sufficiently large for it to be impossible to ascertain the exact form or behavior of the bipolar-cell response directly from the ERG. As we have already seen, strong stimuli evoke rod responses (as well as responses from inner retina) that partially obscure and distort the bipolar-cell signals. On the other hand, weak stimuli to which the rod bipolar-cell responses are of much greater functional significance, preferentially elicit responses from more proximal cells (the STR) that also effectively conceal the responses of the bipolar cells (see Figures 1B and 6A). Fortunately, in order to examine the characteristics of the rod-bipolar cell at these low stimulus levels it is sufficient to suppress the responses of the more proximal cells alone since the responses of the rods themselves are of negligible amplitude (see Figure 5B). Although a substantial reduction in the amplitude of the STR can be achieved simply by providing a suitable weak background light to adapt the more responsive proximal cells [7, 34–35], a more certain effect can be achieved in experimental animals by using pharmacological agents to suppress their activity. This can be done as illustrated in Figure 6A (thick lines) by disabling transmission from the rod bipolar cells to amacrine cells with kainate- and AMPA-receptor antagonists or by preventing the downstream cells from responding to visual stimulation by depolarizing them with NMDA [15, 36].

Prior to giving NMDA, measurements of ERG amplitude made close to the time of the b-wave peak 80 ms after the flash clearly show that the negative STR is more responsive than the positive bipolar-cell component at the lowest stimulus energies. Following removal of the contributions to the ERG of the more responsive inner-retinal cells, it can be seen that from the very lowest levels at which the b-wave can be distinguished from noise, its amplitude measured at fixed time after the stimulus (Figure 6C, open circles) increases in proportion to stimulus energy, indicating that rod-bipolar cells are operating linearly at these stimulus levels. By contrast, if the amplitude of the positive b-wave peak is estimated directly from the control ERG by measuring its height above the preceding most negative point on the waveform, there appears to be a distinct threshold level of stimulus energy below

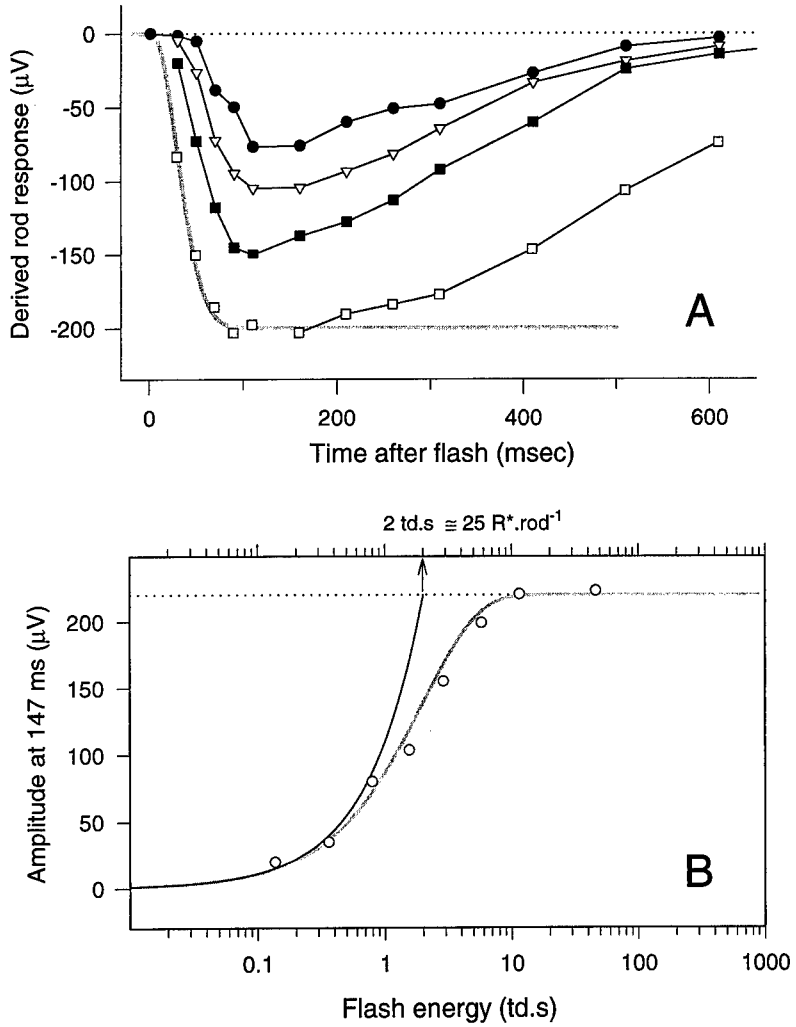

Figure 5. (A) Derived macaque photoreceptor responses to flashes of various energies (0.79, 1.6, 2.9, 8.7 scot td.s). The strongest stimulus drove the rod response (open squares) into saturation. These results have been fitted with a delayed Gaussian curve (Lamb and Pugh [30] model, Equation (2)). (B) Amplitude of macaque derived rod response measured 147 ms after the stimulus (i.e. approximately the time of the peak) as a function of flash energy. The stippled line plots an exponential relation (Equation (1)) while the solid line continues the initial linear approximation all the way to the saturation level. (Monkey SM145).

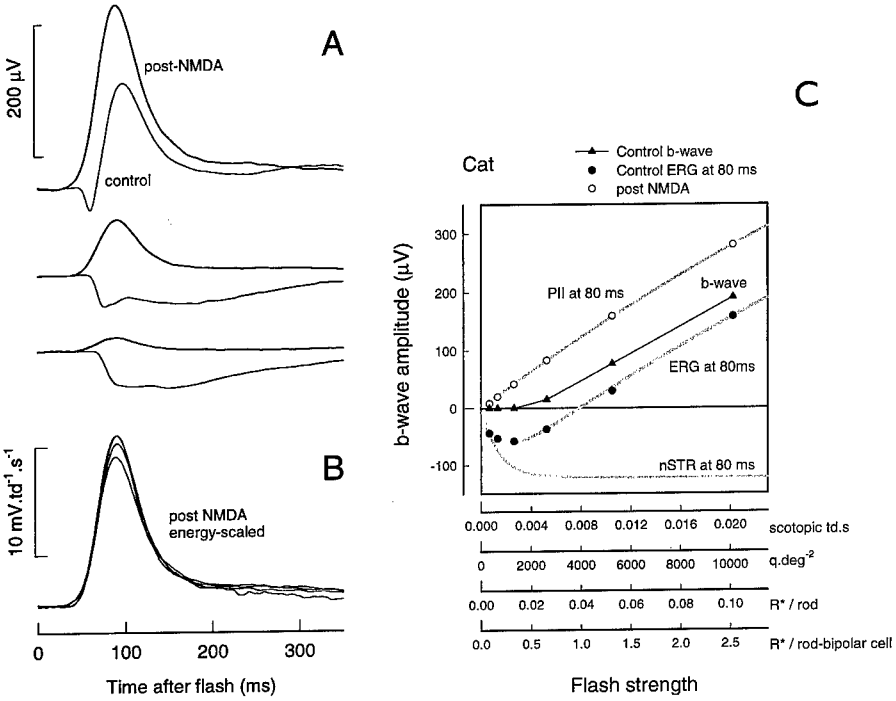

Figure 6. (A) Dark-adapted cat ERG responses to three weak stimuli (0.00125, 0.005 and 0.02 scot td.s) before and after intravitreal injection of NMDA. (B) Post-NMDA responses from A replotted after energy-scaling (each record divided by the energy of the stimulus used to generate it). (C) Amplitude of dark-adapted cat ERG responses to various low energy flashes. Filled triangles (joined by straight lines) plot the conventional b-wave amplitude, measured from the maximally negative point preceding the b-wave to the following positive peak, while filled circles plot the amplitude measured from the baseline at a fixed time of 80 ms after the flash. Open circles show the amplitude at 80 ms after suppression of inner-retinal responses with NMDA. The thicker stippled line shows the fit of a simple model (Equation (7)) to the normal 80 ms measurements while the thinner stippled lines show the amplitudes of the individual assumed positive and negative components. (Cat 13).

which the b-wave is absent (Figure 6C, filled triangles). However, we must conclude from the post-NMDA records that such appearances are deceptive. In fact it will be clear from the energy scales of Figure 6C that bipolar-cell responses can be recorded in the ERG when the stimulus energy is so low that each of the small number of bipolar cells that are activated must have received only a single quantal signal from just one of the twenty-five or so rods to which it is connected. This should not be surprising as microelectrode recordings from individual ganglion cells in the dark-adapted cat retina [37–38] have previously shown that signals generated by the absorption of single photons in rods can clearly be identified at the output of the retina, and it must

therefore be possible for each of the intermediate cell types to signal single photons also.

It will also be clear from the records in Figure 6A that although the shape of the normal ERG (thinner lines) undergoes considerable changes as the stimulus energy is increased, once the response of inner-retinal cells has been suppressed by NMDA (thicker lines), the increase in amplitude of the rod-bipolar cell response to stimuli of moderate energy is unaccompanied by any obvious change in shape. This invariance of the shape of the bipolar-cell response as well as the near proportionality of response amplitude to stimulus energy is made clearer by superimposing the responses to stimuli of different strengths after scaling each response according to the energy of the stimulus evoking it (Figure 6B). While the observed invariance under stimulus-energy scaling is consistent with the idea that the rods and rod-to-bipolar cell synapses operate linearly for small signals, it should be noted that the invariance over the whole of the timecourse is limited to stimulus levels at which only a small proportion of the rods absorb a photon and hence to levels at which only a few of the synapses are activated. It should be noted that since under these conditions an insignificant proportion of either the rods or synapses will be responding to more than a single photon, this finding would be consistent with non-linear processes being involved in the generation and transmission of discrete quantal signals to the bipolar cells, so long as the bipolar cells then sum linearly the discrete post-synaptic signals derived from different rod inputs.

Rod and rod bipolar cell components of the early ERG. A fair idea of the timecourse of the bipolar-cell response can be obtained from the post-NMDA ERG records of Figure 6B; however, even in these records the 'b-wave' is in reality distorted to some extent by the contribution to the ERG of the rod photocurrent, particularly at early times after the stimulus. Indeed, although it only becomes easily visible when the stimulus energy is high enough to cause the positive b-wave to approach saturation, the early part of the post-NMDA ERG is in fact always negative (although the positive bipolar-cell component ultimately rises faster than the negative rod component, the latter signal is initially larger). This can be seen very clearly in Figure 7A and its inset which show a number of records of cat ERGs obtained with stimuli increasing by successive factors of two from 0.81–51.8 scot td.s. Moreover it might be surmized from looking at this set of records that even though the stimuli are strong enough for the b-wave amplitude to have reached its saturation level, the whole of the early part of the ERG is still growing in proportion to the stimulus energy. In this context a particularly telling feature of the post-NMDA records (not seen in pre-drug records) is that the times of

both the negative a-wave peak and the first zero-crossing are independent of stimulus energy. In contrast, prior to delivery of the NMDA (Figure 3A), the times of both the a-wave peak and the zero-crossing are very dependent on stimulus strength. As before, the linearity of the whole initial negative phase of the ERG can be confirmed by replotting the records of Figure 7A after energy-scaling. While the main positive part of the response clearly does not scale with stimulus energy for any of the responses shown (c.f. Figure 6B at lower stimulus energies), the initial negative phase of the responses to the weakest four stimuli (shown in the inset to Figure 7B) clearly scale well, indicating that so long as their responses are small all cells contributing to the ERG at these times behave linearly.

Isolated P2. In any case, before we can determine the complete timecourse of the bipolar-cell signal that presumably underlies the b-wave, we must remove the contribution to the ERG of all cells other than the rod bipolar cells. One approach to this (applied by Hood and Birch [39] to human ERG) is to assume that the only contribution to be removed from the whole ERG is that provided by the rod photocurrent and that this can be calculated at the relevant stimulus energies by application of the Lamb and Pugh model [30] (Equation (2)), the magnitude of the parameters having been ascertained from measurements made at very short times after very strong stimuli. Alternatively, in animal experiments it is possible to assess directly the contribution of the rod photocurrent and any other non-neural signals related to the rods (i.e. responses of glial and RPE cells) after pharmacologically blocking synaptic transmission from the photoreceptors with a mixture of APB and CNQX [15, 22]. The response of these cells can then be subtracted from the post-NMDA ERG to obtain the contribution to the normal ERG of the rod bipolar cells, a signal we shall now refer to as *isolated P2*. Figure 8 shows a family of such isolated P2 curves plotted on double logarithmic scales after scaling them by the stimulus energy.

Kinetics of the leading edge of P2. Although only those energy-scaled records of isolated P2 obtained with the weakest stimuli are superimposed at times near the peak of the response, it will be clear that over more than four decades of voltage (more than three decades of stimulus energy) the initial segments of the rising phase of the records form a continuous curve. This curve is an approximately straight line with a slope of five (on this double logarithmic plot) indicating that while the responses of the bipolar cells are within their linear range the voltage rises approximately as the fifth power of the time after the flash. In fact the results are better fitted by a slightly

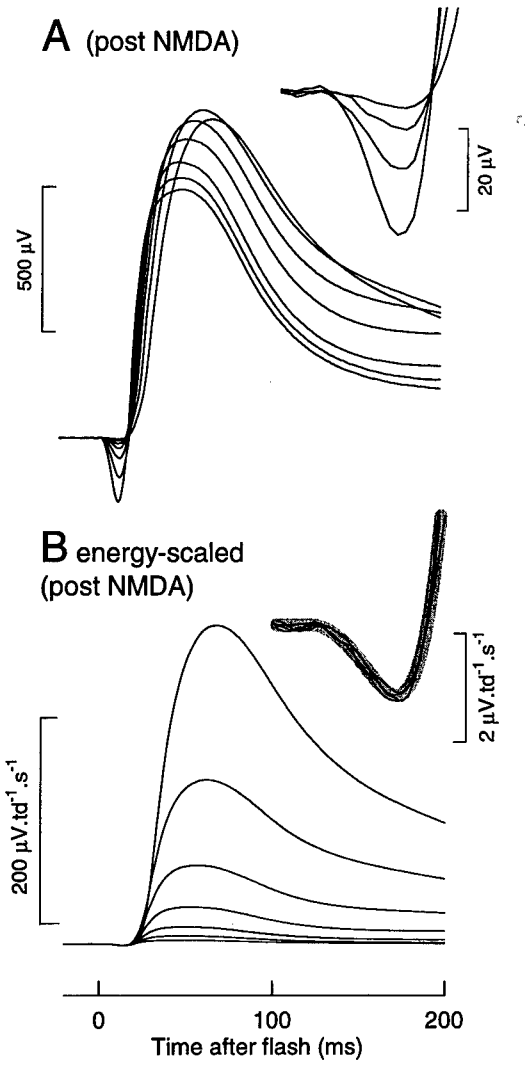

Figure 7. (A) Dark-adapted cat ERG responses to stronger stimuli (0.81–51.8 scot td.s increasing by factors of two) after inner-retinal responses have been blocked with NMDA. The inset shows the early portions of the same records on expanded scales. (B) The same records as in A after energy-scaling. The inset shows the energy-scaled responses to the weakest four stimuli on expanded scales. The stippled line in the inset shows the kinetic model of Equation (6). (Cat 60).

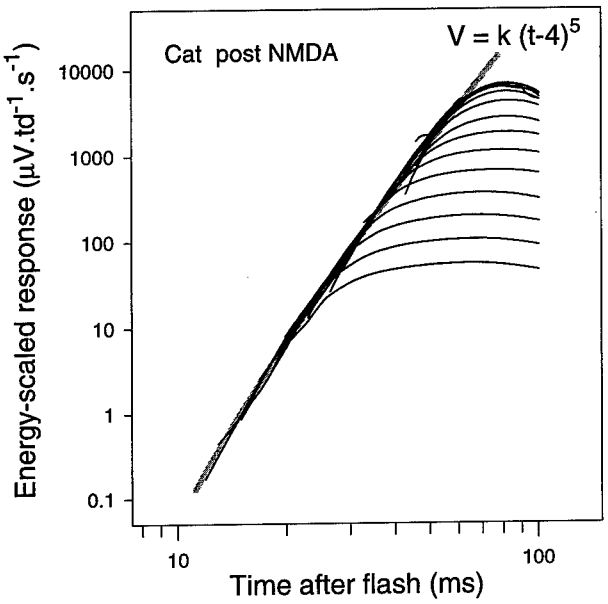

Figure 8. The energy-scaled records of Figure 7B together with records obtained with weaker stimuli are replotted on double logarithmic scales. The stippled line has the form of Equation (5). (Cat 60).

modified relation

$$R'_b(t) = \hat{R}_b\, k_b (t - \tau_b - \tau_i)^5 \qquad (5)$$

The delay, τ_b. is about 2.8 ms. This relation is very similar to the one that describes the early linear part of the rising edge of the rod response except that the delay is about 1 ms longer and the exponent is five rather than two (the subscript b indicates that the variables and constants relate to bipolar cells). This can be interpreted to mean that the response of the rod bipolar cells involves three further stages of integration and a small additional time delay of the kind attributable to several stages of diffusion over short distances. This suggestion is consistent with the findings of Shiells and Falk [40] and Nawy and Jahr [41] who attribute synaptic transmission from photoreceptors to depolarizing-bipolar cells to the operation of a three-stage glutamate-activated G-protein cascade similar to that in the photoreceptors themselves.

The initial negative phase of the post-NMDA ERG. To the extent that the initial part of the ERG is simply the sum of signals from rods and rod-bipolar cells, the time course of this part of the energy-scaled ERG should

be described by summing Equations (4) and (5).

$$R'_{erg}(t) = R'_t(t) + R'_b(t)$$
$$\approx \hat{R}_r\, k_r(t - \tau_r - \tau_i)^2 + \hat{R}_b\, k_b(t - \tau_b - \tau_i)^5 \quad (6)$$

The stippled line in the inset to Figure 7B shows how well Equation (6) can describe such records. It must be emphasised that these recordings were obtained *after blocking the responses of more proximal cells with NMDA* and that this formulation does not provide a good description of the early part of the normal dark-adapted ERG in either cat or macaque, though reduction of the responsiveness of the more proximal cells with background light can considerably improve the fit [see 22].

Recovery of P2. While the kinetics of the rising edge of the rod bipolar-cell response can apparently be explained in terms of the known mechanism of synaptic transmission, the nature of the recovery processes underlying the declining phase of the response are less well understood. However it is instructive to look at the waveform of the recovery phase of the isolated P2 response (e.g. Figures 6A and B). It is clear that as recorded in the ERG the decline of the response from its peak does not have the form of a single exponential but shows an initial rapid decline followed by a slower, extended tail. This is seen again in Figure 9 (the heavier line) which shows a smoother record of intensity-scaled isolated P2 responses that are in the linear range.

Fast and slow components of P2. Although the form of the declining phase of isolated P2 might represent the existence of a two-stage recovery process within the rod-bipolar cells, studies on isolated bipolar cells [42] have not described a similar two-phase recovery waveform or suggested that there might be more than a single recovery process. An alternative explanation for the ERG finding is that the recorded P2 is really the sum of two signals, a faster signal that directly reflects the post-synaptic current of the bipolar cells and a second, slower signal that is related to the Müller cell response to the K^+ carried by the bipolar-cell current into the extracellular space [11, 43–44]. This explanation is supported by our finding (not illustrated here) that the long tail of isolated P2 in the cat is removed by intravitreal injection of the K^+-conductance blocker, Ba^{++}, and by the observation [37] that the response of cat ganglion cells to very weak flashes shows no sign of the long tail. If this alternative explanation is correct, then it is possible to analyse the total recorded P2 response into its two components if two assumptions are made: the post-synaptic current of the bipolar cell must be assumed to be all positive and the glial-cell response must be a simple low-pass filtered version of the current response. On this basis we have computed the two components

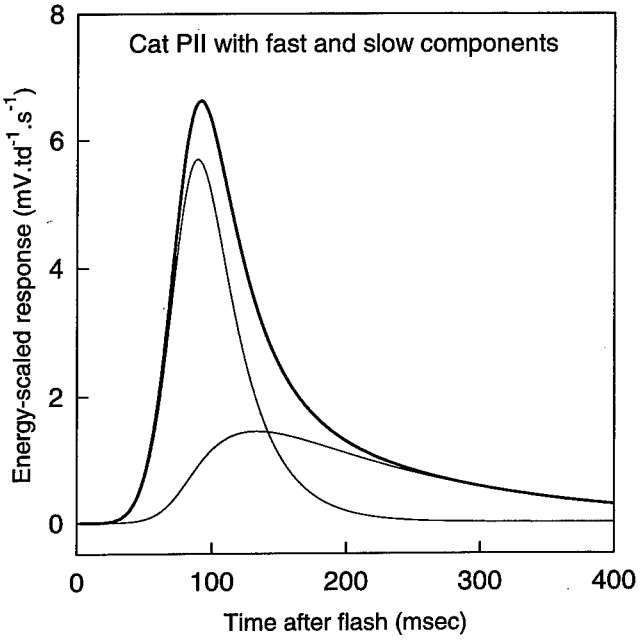

Figure 9. An energy-scaled isolated cat P2 response analysed into fast and slow components (see text) (Cat 64).

shown by thinner lines in Figure 9. The faster component that directly reflects the post-synaptic current of the rod-bipolar cell is mainly responsible for the timing of the leading edge of the the total isolated P2 response while the tail is nearly all provided by the longer-lasting, delayed Müller-cell component. It is interesting to note that although the amplitude of the slower component (in response to a brief flash) is much less than that of the faster one, the area under the two curves is about the same. This means that with the longer stimulus durations used in previous studies of Müller cell involvement, the contributions to the ERG of the two sources would be approximately equal.

STR contributions to the dark-adapted ERG

As illustrated in Figure 1B (lowest records) and Figure 6A, for flashes of sufficiently low luminous energy the normal ERG response is predominantly a negative wave (the STR) originating from inner retina. Previous work in cat and primate has indicated that the response originates substantially from amacrine cells and is mediated via K^+ currents in Müller cells [8–9, 45–48]. More recent work in macaques with ganglion cell degeneration resulting from experimentally elevated intraocular pressure, suggests that it originates,

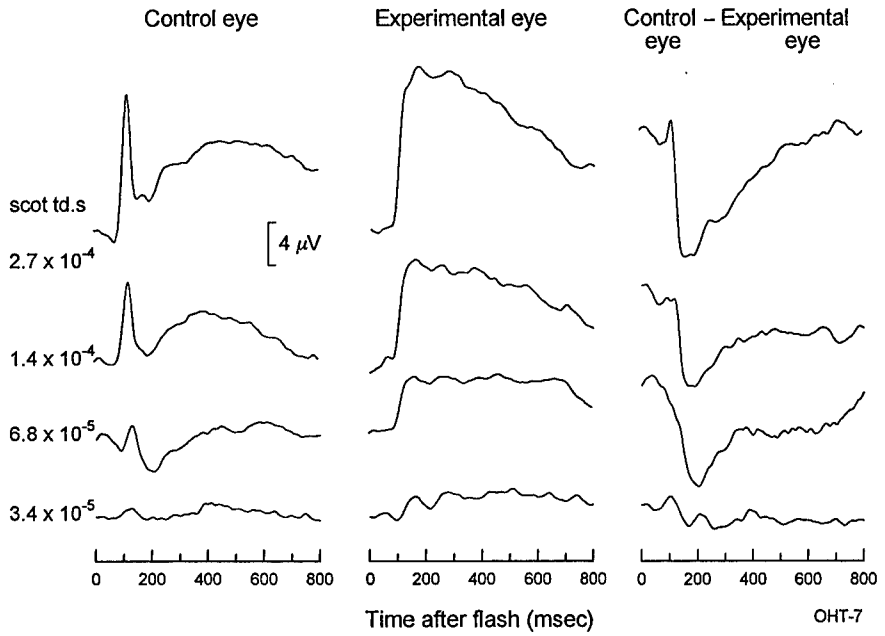

Figure 10. ERG responses to weak stimuli obtained from both normal and experimental eyes of a dark-adapted macaque. The ganglion cells in the experimental eye had essentially all degenerated as a result of experimentally induced chronic ocular hypertension (Frishman et al., 1996a). Although the normal ERG of this animal shows only a very low amplitude negative STR, the subtracted records in the right-hand column show that the effect of destroying the ganglion cells is to remove a substantial negative component peaking about 200 ms after the stimulus flash. Adapted from Ref. [17]. (Monkey OHT-7).

at least in part, from ganglion cells as well [17]. This is illustrated in Figure 10.

Unlike the situation for the a-wave and the b-wave, it has not proved possible to isolate pharmacologically the activity of any single one of the various cell types believed to contribute to the STR. Unfortunately, specific glutamate receptors do not appear to be sufficiently well segregated within the various classes of amacrine and ganglion cells in cats and monkeys to allow selective suppression or isolation of just one of them (e.g. All amacrine cells). In fact drugs acting on both NMDA and KA/AMPA receptors appear to affect the entire STR (e.g. Figure 6A). The most effective separation that has been achieved so far has been in preliminary studies using tetrodotoxin to block the Na^+-dependent spiking activity of amacrine and ganglion cells. These studies have indicated that the STR receives contributions from both the spiking and non-spiking activity of inner retinal neurons ([49–50] and

unpublished observations), and that the contribution from spiking activity is of relatively slower time course.

In addition to the problem of separating the contributions of different cell types even where these are known, another complication is provided by the observation that the inner retina also appears to generate positive components that can be detected in the ERGs of cats and monkeys at light levels where the negative STR dominates. These may originate from OFF rather than ON-center neurons, or have a more specific origin related to the particular current flow paths involved. The various positive and negative components appear to have slightly different sensitivities and levels of saturation. Thus the STR is a complex waveform that, at present, is not amenable to the detailed kinetic modeling described earlier in this review for the single classes of bipolar cells and photoreceptors.

STR and P2 (bipolar-cell) responses. Although a complete separation of the various components of the STR has not yet been achieved, it is possible to provide a quantitative explanation of some aspects of the behavior of the ERG at very low light levels in terms of the summation of the STR with the response of the rod-bipolar cells. Thus, the amplitude-energy relation measured in normal dark-adapted cat ERG at a time close to that of the b-wave peak (80 ms after the flash, shown in Figure 6C as filled circles) can be well described by assuming that the ERG amplitude at this time is the sum of a positive rod bipolar-cell component that saturates hyperbolically and a negative STR component that saturates exponentially (both, of course, being linear for very weak stimuli).

$$V_{erg}(i) = \hat{V}_b(i/(1 + i/i_{b0})) - \hat{V}_{nSTR}(1 - \exp(i/i_{nSTR0})) \qquad (7)$$

The stippled line through the filled circles in Figure 6C shows the best-fitting relation of this kind while the other two stippled lines show the P2 and STR components separately. It will be seen that the uppermost stippled line, representing the amplitude of the P2 component alone, passes through the open circles that plot experimental measurements of amplitude made after all STR components have been suppressed with NMDA and lies substantially above the conventional 'b-wave amplitude' measurements plotted as filled triangles. This strongly suggests that if an experimenter only has information about the normal ERG, the best way to estimate the amplitude of the bipolar-cell response would be to fit a function of the kind used here rather than to make an essentially arbitrary alternative measurement on the ERG record. While it has not so far been possible to identify precisely the source of the negative STR component that is dominant at 80 ms, the simple nature of its presumed amplitude-energy function at least makes it appear as though it is a single component.

Concluding comments

By judicious application of pharmacological agents, and the fitting of plausible models of neuronal activity, it is possible to learn a good deal about the origins of the ERG, and to gain some insights into basic visual function in the retina. This is particularly true in those cases where is possible to isolate single classes of cells that generate ERG components. The challenge is to extend this analysis to situations where the individual cells types are not so amenable to study.

Acknowledgements

This work was supported by NEI EY06671 to L.J. Frishman and Core Grant P30 EY07751. We thank Suresh Viswanathan, Li Xu, for help with experiments, and Clifford Stratton for the human ERG records in Figure 1B.

References

1. Smith RG, Freed MA, Sterling P. Microcircuitry of the dark-adapted cat retina: functional architecture of the rod-cone network. J Neurosci 1986; 6: 3505–17.
2. Sterling PE, Cohen E, Freed MA, Smith RG. Microcircuitry of the on-beta ganglion cell in daylight, twilight and star light. Neurosci Res 1987; 6; s269–s285.
3. Freed MA, Smith RG, Sterling P. Rod bipolar array in the cat retina: pattern of input from rods and GABA-accumulating amacrine cells. J Comp Neurol 1987; 266: 445–55.
4. Grünert U, Martin PR. Rod bipolar cells in the macaque monkey retina: immunoreactivity and connectivity. J Neurosci 1991; 11: 2742–58.
5. Kolb, H, Linberg KA, Fisher SK. Neurons of the human retina: A Golgi study. J Comp Neurol 1992; 318: 147–87.
6. Wässle H, Grünert U, Chun MH, Boycott BB. The rod pathway of the macaque monkey retina: identification of AII-amacrine cells with antibodies against calretinin. J Comp Neurol 1995; 361: 537–51.
7. Frishman LJ, Reddy MG, Robson JG. Effects of background light on the human dark-adapted electroretinogram and psychological threshold. J Opt Soc. Soc Am A1996; 13: 601–12.
8. Sieving PA, Frishman LJ, Steinberg RH. Scotopic threshold response of proximal retina in cat. J. Neurophysiol 1986; 56: 1049–61.
9. Steinberg RH, Frishman LJ, Sieving PA. (1991) Negative components of the electroretinogram from proximal retina and photoreceptor. In: NN Osborne and GJ Chader, eds. Progress in Retinal Research. Oxford, UK: Pergamon Press 1990; 10: 121–60.
10. Newman EA. Current source-density analysis of the b-wave of frog retina. J Neurophysiol 1980; 43: 1355–66.
11. Newman EA, Odette LL. Model of electroretinogram b-wave generation: a test of the K^+ hypothesis. J Neurophysiol 1984; 51: 164–82.

12. Stockton RA, Slaughter MM. *b*-Wave of the electroretinogram: a reflection of ON bipolar cell activity. J Gen Physiol 1989; 93: 101–22.
13. Gurevich L, Slaughter MM. Comparison of the waveforms of the ON bipolar neuron and the b-wave of the electroretinogram. Vision Res 1993; 33: 2431–35.
14. Xu XJ, Karwoski CJ. Current source density analysis of retinal field potentials. 2. Pharmacological analysis of the *b*-wave and *m*-wave. J Neurophysiol 1994; 72: 96–105.
15. Robson JG, Frishman LJ. Response linearity and dynamics of the cat retina: the bipolar cell component of the dark-adapted ERG. Vis. Neurosci 1995; 12: 837–50.
16. Tian N, Slaughter MM. Correlation of dynamic responses in the ON bipolar neuron and the *b*-wave of the electroretinogram. Vision Res 1995; 35: 1359–64.
17. Frishman LJ, Shen FF, Du L, Robson JG, Harwerth RS, Smith III EL, Carter-Dawson U, Crawford MLJ. The scotopic electroretinogram of macaque after retinal ganglion cell loss from experimental glaucoma. Invest Ophthalmol Vis Sci 1996; 37: 125–41.
18. Breton ME, Montzka DP. Empiric limits of rod photocurrent component underlying a-wave response in the electroretinogram. Doc Ophthalmol 1992; 79: 337–61.
19. Massey SC. Cell types using glutamate as a neurotransmitter in the vertebrate retina. In: NN Osborne and GJ Chader, eds. Progress in Retinal Research. Oxford, UK: Pergamon Press 1990; 9: 399–425.
20. Sterling P. Retina. In: G Shepherd ed. Synaptic Organization of the Brain. Oxford, UK: Oxford Univ. Press, chapt. 6, 1990.
21. Wässle H, Boycott BB. Functional architecture of the mammalian retina. Physiol Rev 1991; 71: 447–80.
22. Robson JG, Frishman LJ. Photoreceptor and bipolar-cell contributions to the cat electroretinogram: a kinetic model for the early part of the flash response. J Opt Soc Am A 1996; 13: 613–22.
23. Dawson WW, Trick GL, Litzkow CA. Improved electrode for electroretinography. Invest. Ophthalmol Vis Sci 1979; 18: 988–91.
24. Lamb TD, McNaughton PA, Yau KW. Spatial spread of activation and background desensitization in toad rod outer segments. J Physiol (Lond) 1981; 319: 463–96.
25. Baylor DA, Nunn BJ, Schnapf JL. The photocurrent, noise and spectral sensitivity of rods of the monkey *macaca fascicularis*. J Physiol (Lond) 1984; 357: 575–607.
26. Tamura T, Nakatani K, Yau K-W. Light adaptation in cat retinal rods. Science 1989; 245: 755–58.
27. Hood DC, Birch DG. Light adaptation of human rod receptors: the leading edge of the human a-wave and models of rod receptor activity. Vision Res 1993; 33: 1605–18.
28. Penn RD, Hagins WA. Kinetics of the photocurrent of retinal rods. Biophys J 1972; 12: 1073–94.
29. Breton ME, Schueller AW, Lamb TD, Pugh EN, Jr. Analysis of ERG a-wave amplification and kinetics in terms of the G-protein cascade of phototransduction. Invest Ophthalmol & Vis Sci 1994; 35: 295–309.
30. Lamb TD, Pugh EN. A quantitative account of the activation steps involved in phototransduction in amphibian photoreceptors. J. Physiol 1992; 449: 717–57.
31. Smith NP, Lamb TD. The *a*-wave of the human electroretinogram recorded with a minimally invasive technique. Vision Res 1997; 37: 2943–52.
32. Kraft TW, Schneeweis DM, Schnapf JL. Visual transduction in human rod photoreceptors. J Physiol (Lond) 1993; 464: 747–65.
33. Pepperberg DR, Birch DG, Hood DC. Photoresponses of human rods *in vivo*. Visual Neurosci 1997; 14: 73–82.

34. Frishman LJ, Sieving PA. Evidence for 2 sites of adaptation affecting the dark-adapted ERG of cats and primates. Vision Res 1995; 35: 435–42.
35. Hood DC, Birch DG. (1996) The b-wave of the scotopic (rod) ERG as a measure of the activity of human on-bipolar cells. J Opt Soc Am A 1996; 13: 623–33.
36. Vaegan, Millar TJ. Effect of kainic acid and NMDA on the pattern electroretinogram, the scotopic threshold response, the oscillatory potentials and the electroretinogram in the urethane anaesthetized cat. Vision Res 1994; 34: 1111–25.
37. Barlow HB, Levick WR, Yoon M. Responses to single quanta of light in retinal ganglion cells of the cat. Vision Res Suppl 1971; 3: 87–101.
38. Mastronarde DN. Correlated firing of cat retinal ganglion cells. II. Responses of X- and Y-cells to single quantal events. J Neurophysiol 1983; 49: 325–49.
39. Hood DC, Birch DG. A computational model of the amplitude and implicit time of the *b*-wave of the human ERG. Vis Neurosci 1992; 8: 107–26.
40. Shiells RA, Falk G. Glutamate receptors of rod bipolar cells are linked to a cyclic GMP cascade via a G-protein. Proc Roy Soc Lond, Series B: Bio Sci 1990; 242: 91–4.
41. Nawy 5, Jahr CE. Suppression by glutamate of cGMP-activated conductance in retinal bipolar cells. Nature 1990; 346: 269–71.
42. Ashmore JF, Falk G. The single-photon signal in rod bipolar cells of the dogfish retina. J Physiol (Lond) 1980; 300: 151–66.
43. Miller RF, Dowling JE. Intracellular responses of the Müller (glial) cells of mudpuppy retina: their relation to b-wave of the electroretinogram. J Neurophysiol 1970; 33: 323–41.
44. Wen R, Oakley B. K^+-evoked Müller cell depolarization generates b-wave of electroretinogram in toad retina. Proc Nat Acad Sci (USA) 1990; 87: 2117–21.
45. Wakabayashi K, Gieser J, Sieving PA. Aspartate separation of the scotopic threshold response (STR) from the photoreceptor *a*-wave of the cat and monkey ERG. Invest Ophthalmol Vis Sci 1988; 29: 1615–22.
46. Frishman LJ, Steinberg RH. Intraretinal analysis of the threshold dark-adapted ERG of cat retina. J Neurophysiol 1989; 61: 1221–32.
47. Frishman LJ, Steinberg RH. Light-evoked increases in $[K^+]_o$ in proximal portion of the dark-adapted cat retina. J Neurophyisol 1989; 61: 1233–43.
48. Sieving PA. Retinal ganglion cell loss does not abolish the STR of the cat and human ERG. Clin Vision Sci 1991; 6: 149–58.
49. Frishman LJ, Robson JG, Du L. Contributions of the positive and negative scotopic threshold responses to the scotopic cat ERG. Invest Ophthalmol Vis Sci Suppl 1993; 34: 1273.
50. Robson JG, Frishman LJ, Du L. Component potentials of the dark-adapted cat ERG. Soc Neurosci Abs 1993; 1413.

Address for correspondence: L.J. Frishman, College of Optometry, University of Houston, 4901 Calhoun Road, Houston, TX 77204-6052, USA
Phone: 1-713-742-1972; Fax: 1-713-743-2053; E-mail: lfrishman@uh.edu

Documenta Ophthalmologica **95:** 217–228, 1999.

Electrophysiological findings in Dominant Optic Atrophy (DOA) linking to the OPA1 locus on chromosome 3q 28-qter

G.E. HOLDER[1], M. VOTRUBA[1,2], A.C. CARTER[1],
S.S. BHATTACHARYA[2], F.W. FITZKE[2] & A.T. MOORE[1]
Moorfields Eye Hospitals[1] and Institute of Ophthalmology[2], London, UK

Abstract. Pattern and flash visual evoked cortical potentials (PVEP, FVEP), and pattern electroretinograms, (PERG) were recorded in 13 affected individuals from 8 families with DOA. These were selected as representative from 87 affected members of 21 pedigrees with DOA who were examined, and who underwent genetic linkage analysis. Linkage to the OPA1 locus on chromosome 3q 28-qter was demonstrated in all families. VA ranged from 6/9 to HM; visual fields showed a variable centro-caecal defect; SLO (when performed) showed diffuse nerve fibre loss; MRI (when performed) showed small intra-orbital optic nerves. In 9/13 patients the PVEP was absent in one or both eyes. Most recordable PVEPs were of abnormal latency, but the delays were not marked (peak times 116–135 msec); amplitudes were low or subnormal. PERG fell within the normal range in 9 eyes of 7 patients. 14 eyes showed an abnormal N95:P50 ratio in keeping with ganglion cell dysfunction. Some severely affected eyes showed P50 component involvement, but in no eye was the PERG extinguished. Significant interocular asymmetries in at least one electrophysiological measure were present in 6/13 patients. Colour contrast thresholds were significantly elevated for all three colour confusion axes, with tritan being most affected.

Key words: optic atrophy, pattern electroretinogram, colour vision, visual evoked potential

Introduction

Kjer type dominant optic atrophy (DOA), [1] is an autosomal dominantly inherited disorder resulting in reduced visual acuity and pallor of the optic disc [2]. The clinical features of progressive visual loss, pallor of the optic disc, centro-caecal visual field defect and defective colour vision, first described by Batten [3], have subsequently been confirmed by other authors [4–8]. Histopathological studies suggest that the fundamental pathology is degeneration of the retinal ganglion cells leading to optic atrophy [9, 10].

As part of a re-evaluation of the phenotypic and genotypic features of DOA, we report the electrophysiological and colour contrast sensitivity findings in thirteen patients with DOA in various stages from mild to severe. These were selected as representative from a cohort of 87 affected patients

from 21 pedigrees who received full clinical examination and genetic linkage analysis. All families showed linkage to the *OPA1* gene locus on chromosome 3q28-qter, in accordance with previous studies which also demonstrated linkage to chromosome 3q [11–17]. Some patients from the cohort also had other investigations such as scanning laser ophthalmoscopy, magnetic resonance imaging or motion detection. The main clinical findings are addressed in detail elsewhere [18], but will be summarised herein when relevant.

Methods

The thirteen patients described in detail came from eight affected families, and form part of the greater cohort of 87 patients. All had a full clinical history taken, with data also being obtained in relation to schooling, blind registration, employment status etc. Ophthalmic examination was performed to include best corrected visual acuity and ocular motility. All eyes were examined by slit-lamp biomicroscopy, with particular attention to the nerve head and the nerve fibre layer. The optic nerve head was classified as normal; subtle diffuse pallor; temporal pallor; or total atrophy. Any nerve fibre layer abnormalities visible with the direct ophthalmoscope and the 90 diopter (Volk aspheric) lens were noted. All clinical examinations were performed by the same observer (MV).

When undertaken, perimetry was performed using the 30-2 program on the Humphrey perimeter; high resolution fine matrix mapping (FMM), [19] was also performed using the Humphrey automated perimeter; imaging of the nerve head and nerve fibre layer by scanning laser ophthalmoscopy was performed using a Zeiss SLO [20].

Colour contrast sensitivity was measured for the protan, deutan and tritan axes using the Moorfields colour vision system [21], which has been previously been described and validated (e.g. [22, 23]), and which provides a sensitive measure of colour vision by examining the colour contrast thresholds for each of the three colour confusion axes.

Electrophysiological measurement comprised pattern and flash VEP, and pattern electroretinography (PERG), using techniques in consideration of published ISCEV Standards and Recommendations [24, 25]. For the VEP, check size was 40 min; field size was 10 × 7 degrees; contrast was 85%; mean luminance was 200cd/m^2 and reversal rate was 2/sec. Silver/silver chloride electrodes were placed at O1, OZ and O2 with Fz reference. Recording bandwidth was 1–100Hz (–3dB). Pattern ERG was performed using a black and white reversal stimulus with check size of 60 min in a 18 × 14° field. Reversal rate was 6/sec; contrast was 95%; mean luminance was 200cd/m^2. Focal ERG was performed using a large check (8°) displayed by the same monitor used

for the PERG, and with all parameters other than check size held constant. Gold foil corneal electrodes were used to record the PERG, with reference electrodes at the ipsilateral outer canthi. Recording bandwidth was 1–100Hz–3dB. Particular attention was paid to the technical factors, particularly blink, movement and muscle artefact, to which the PERG is particularly susceptible [26–28].

Analysis of the electrophysiological data involved measurement of the amplitude and latency of the P100 component of the PVEP, and the P2 component of the FVEP [29]. The amplitudes of the PERG P50 and N95 components [30, 31] were measured, together with the latency of the P50 component. N95 is often broadened which precludes accurate estimation of latency.

The study was approved by The Ethical and Scientific Committee of Moorfields Eye Hospital and written informed consent was obtained from all participating patients.

Results

The findings in the thirteen patients are shown in Table 1.

The pattern VEP was absent in at least one eye of 9/13 patients.; when present there were usually latency delays, but these were not profound (P100 latency usually less than 135msec; normal <110msec). There was no significant inter-hemispheric asymmetry in any of the PVEP parameters measured, and only the mid-line data are presented. Flash VEP P100 component amplitude and latency failed to show significant abnormality, other than in two severely affected brothers (patients 10, 11) in whom there was a major positive component amplitude of 2.5μV or less. The PERG was abnormal in the majority of patients, with 14 eyes showing an abnormal N95:P50 ratio. In some severely affected patients there was involvement of P50, but in most of those there was also a reduced N95:PSO ratio. Focal ERG was usually unaffected. Note the not infrequent inter-ocular asymmetry.

The colour contrast thresholds were invariably elevated for all three colour confusion axes. The tritan axis was usually most affected, but note the very high incidence of mixed defects. A high incidence of mixed defects was also observed in the results obtained in a larger number of patients from the main cohort [18] using the Mollon-Reffin test of colour vision, a simplified version of the 100-Hue [32].

Electrophysiological data from six patients are shown in Figures 1-6, chosen to represent the spectrum of disease from mildly to severely affected. See legends for full details.

Table 1. Clinical, electrophysiological and colour contrast sensitivity findings

Patient	Family	Age	Onset	Discs'	NFL[2]	Eye	VA	PVEP lat (msec; N<110)	PVEP amp (μV; N>2.0)	FVEP lat (msec; N<135)	FVEP amp (μV; N>2.5)	PERG P50 (μV; N>1.8)	PERG N95 (μV; N>2.2)	N95:P50 N>1.1)	FERG (μV; N>1.5)	CCS: protan % N<10	CCS: deutan % N<10	CCS: tritan % N<15	Comments	Fields
1	A	68	6	A	N	OD	HM	abs	0.0	118	14.0	1.2	1.4	1.17	1.8	-	-	-		
						OS	HM	abs	0.0	118	12.0	1.4	1.5	1.07	1.6	-	-	-		
2	A	37	2	T	N	OD	2/60	abs	0.0	105	8.5	2.2	2.2	1.00	1.6	-	-	-		CCD
						OS	2/60	abs	0.0	108	6.5	1.8	2.2	1.22	1.6	-	-	-		
3	B	42	5	T	N	OD	6/18	125	2.5	106	10.0	3.2	3.4	1.06	2.7	16	30	100		
						OS	6/18	114	3.0	106	9.0	2.6	3.3	1.27	2.4	16.5	31	92		
4	C	40	25	T	A	OD	6/18	114	2.0	114	5.0	2	2.6	1.30	1.9	55	62	83		CCD
						OS	6/18	118	1.5	111	4.0	1.9	2.4	1.26	1.6	63	59	90		
5	C	41	?	N	N	OD	6/9	102	5.0	123	7.0	2.9	3.6	1.24	2.8	11.5	9.5	29		CCD
						OS	6/9	107	2.5	123	5.0	2.6	2.2	0.85	2.9	14.5	16.5	34		
6	C	43	3	T	N	OD	6/24	abs	0.0	115	2.5	1.4	1.9	1.36	1.9	100	50	40	MRI abn[3]	
						OS	6/12	120	1.0	126	1.5	2.2	2.2	1.00	2.1	71	89	57		CCD
7	D	36	7	T	N	OD	6/60	130	1.0	124	7.0	1.9	2.2	1.16	2.0	100	70	100		
						OS	6/60	abs	0.0	126	5.0	2	2.5	1.25	2.2	100	95	100		
8	E	28	4	S	N	OD	6/36	155?	1.0?	109	9.5	2.1	2.2	1.05	1.7	69	85	100	MRI abn[3]	CCD
						OS	6/18	120	2.0	106	6.5	2.7	2.4	0.89	2.2	53	78	100		
9	F	36	3	T	N	OD	6/36	abs	0.0	110	9.5	1.2	1.4	1.17	2.0	97	100	100		
						OS	6/36	abs	0.0	110	9.5	1.2	1	0.83	2.0	100	100	100		
10	G	65	3	A	A	OD	CF	abs	0.0	125	2.0	0.7	0.5	0.71	1.0	-	-	-	SLO DL	GL
						OS	CF	abs	0.0	123	2.0	0.7	0.6	0.86	1.0	-	-	-	SLO DL	
11	G	62	3	A	A	OD	3/60	abs	0.0	132	2.5	1.5	1.6	1.07	1.6	-	-	-	SLO DL	GL
						OS	3/60	abs	0.0	130	2.5	1.2	1.1	0.92	1.6	-	-	-	SLO DL	
12	H	15	1	T	A	OD	6/60	125	1.5	106	6.5	2.7	3.4	1.26	3.0	75	60	90		CCD
						OS	6/60	abs	0.0	101	6.0	2.4	2.6	1.08	2.2	65	60	95		
13	H	43	3	T	A	OD	3/60	abs	0.0	113	10.5	2.9	2.9	1.00	2.2	100	100	100		
						OS	3/60	135	1.0	112	11.5	2.3	2.6	1.13	2.2	100	100	100		

[1] N= Normal; S = subtle pallor; T = temporal pallor; A = total atrophy. CCS = colour contrast sensitivity

[2] NFL = nerve fibre layer. N = normal; A = abnormal N=normal

[3] MRI - thinned optic nerves Fields: CCD = centro-caecal defect

DL = marked diffuse nerve fibre loss GL = Generalised loss

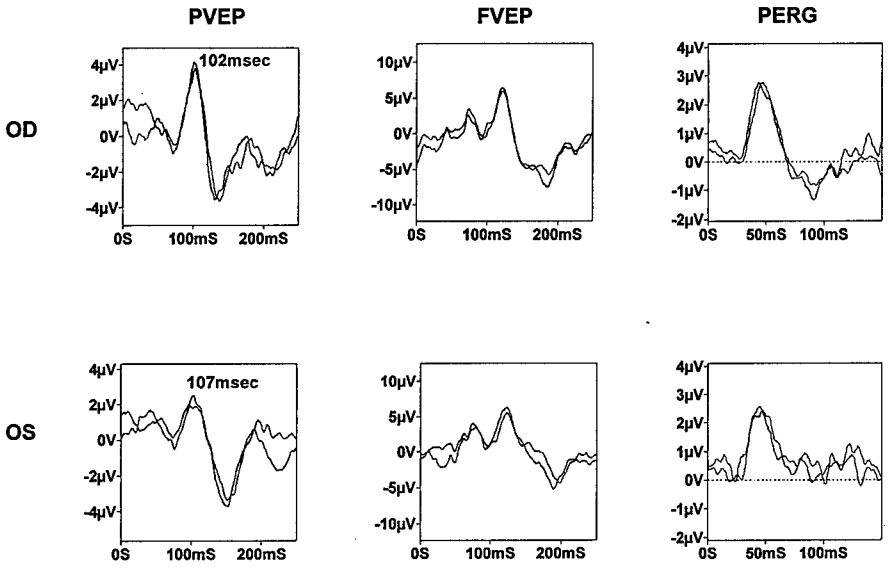

Figure 1. (Patient 5). The right eye findings fall within the normal range. The left eye VEPs, although within the absolute limits of normal, show mild relative amplitude loss and latency delay:, the left eye PERG shows N95 component reduction with sparing of P50.

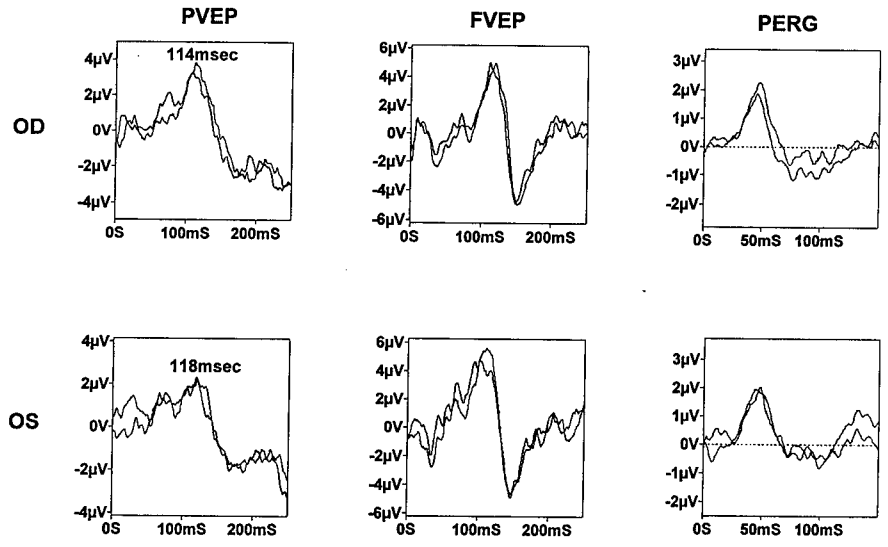

Figure 2. (Patient 4). The pattern VEP P100 component from both eyes is delayed (>110msec). Flash VEPs are unremarkable. Right eye PERG falls within the normal range; that from the left shows no definite abnormality, but there is possible early N95 component reduction.

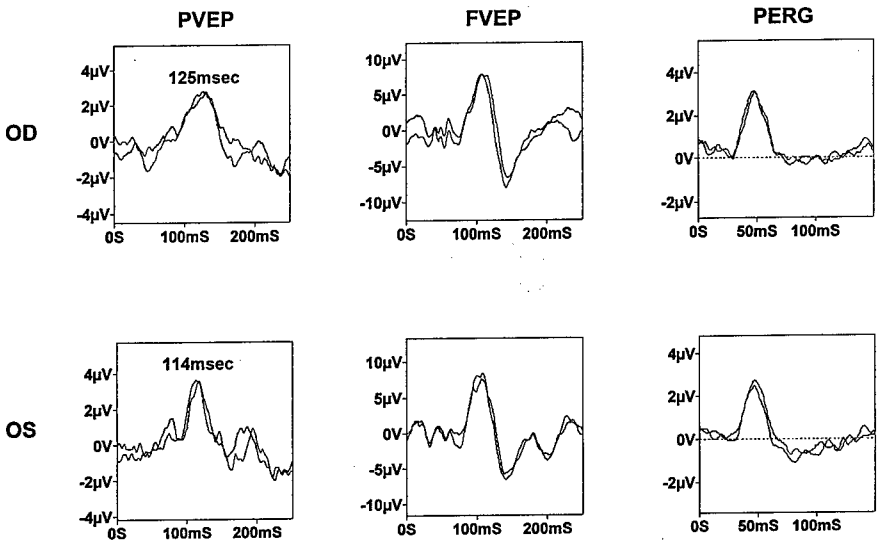

Figure 3. (Patient 3). The pattern VEP P100 component from both eyes is delayed (>110msec). Flash VEPs are unremarkable. Right eye PERG shows N95 component reduction (N95:P50 ratio <1.1); left eye PERG falls within the normal range.

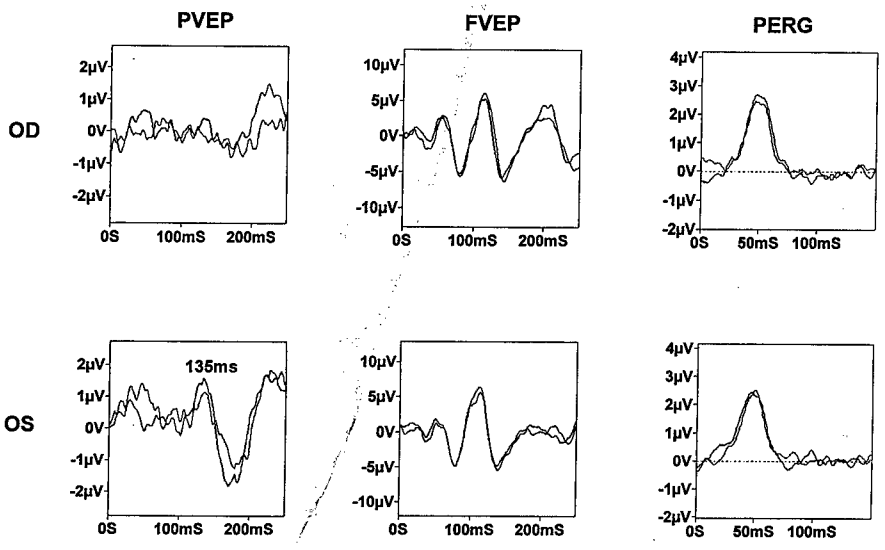

Figure 4. (Patient 13). The pattern VEP from the right eye is unrecordable; that from the left is delayed. Flash VEPs are unremarkable. PERG from both eyes shows N95 component reduction (N95:PSO ratio <1.1).

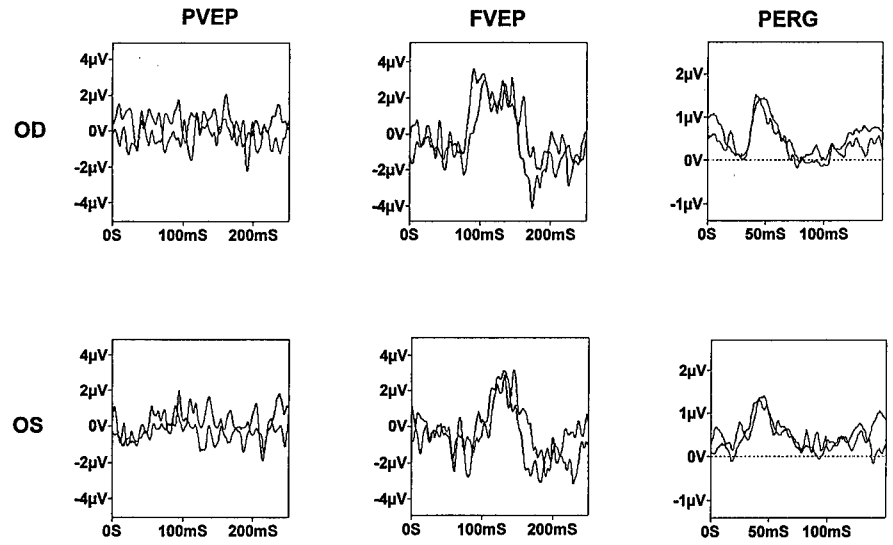

Figure 5. (Patient 11). The pattern VEP from both eyes is unrecordable. Flash VEP is approximately 2.5μV bilaterally. PERG from both eyes shows reduction in N95 (N95:P50 < 1.1), with additional P50 involvement (P50 <2.0μV).

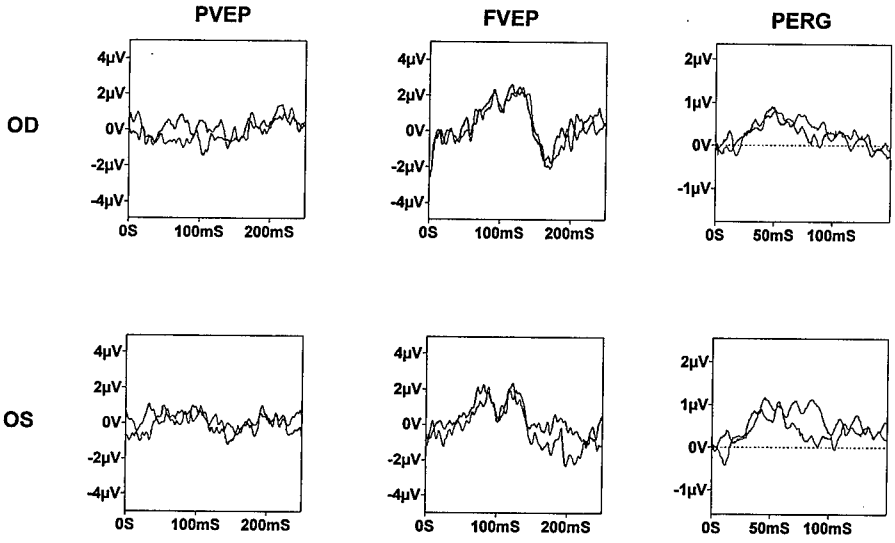

Figure 6. (Patient 10). The pattern VEP from both eyes is unrecordable. Flash VEP is <2.5μV bilaterally. PERG from both eyes shows residual P50 amplitude with loss of the N95 component.

Discussion

Despite the genetic homogeneity in these patients, there is wide phenotypic variation, both within and between families. However, there are some common electrophysiological features. The pattern VEP, as would be anticipated from the often poor visual acuity values, was often absent. When present, the P100 component was delayed in most affected eyes. Flash VEPs were usually normal, other than in two severely affected brothers. The lower sensitivity of the FVEP than the PVEP to optic nerve dysfunction is well known. The PERG, however, was not extinguished in any eye, even when visual acuity was severely affected and the PVEP absent. Most more severely affected eyes showed involvement of the P50 component, but P50 was never extinguished. Fourteen eyes showed an abnormal N95:P50 ratio. These findings extend, and are consistent with, most previous reports [33–36]. Other optic nerve diseases, including optic atrophy, have also been reported to show N95 component reduction, but this is not confirmed by all authors, e.g. Bach and colleagues [37]. However, the latter group studied 'optic atrophy' as a number of diverse pathologies including glaucoma, and their results may not be directly comparable to those of the present study.

It is known from the histopathology that DOA is a disease of the retinal ganglion cells [9, 10]. The high incidence of PERG N95 component reduction is therefore in keeping with the postulated ganglion cell origin of that component [31, 34, 35, 38–40], but the finding of a consistently measurable P50 component, even in eyes which can be assumed by disc appearance, severely reduced VA and SLO findings to be virtually devoid of a normally functioning central retinal ganglion cell population, further suggests a more distal origin than the ganglion cells for some of the P50 component. This relative preservation of P50, albeit abnormal, is in keeping with earlier observations of some P50 retention in various patients with severe optic nerve dysfunction, including optic nerve section [35, 41, 42], based upon which a more distal origin for some of the P50 component of the PERG has been proposed [43]. It is in contrast with observations in cat [44] where abolition of the PERG accompanies retinal ganglion cell degeneration following optic nerve section, and cautions to the possible dangers inherent in inter-species comparisons. Some cat work has shown a greater effect on N95 than P50 in the early stages following optic nerve section [45]. Also of relevance here are the focal ERG (FERG) findings; usually normal, but reduced in two eyes with very severe disease. Some trans-synaptic dysfunction is not excluded on electrophysiological grounds.

It is also further possible, from the pattern of results, to postulate the sequence of electrophysiological abnormalities which occur in DOA. Initially

there is a mild delay in the PVEP which may or may not be accompanied by PERG N95 component reduction; there is little or no effect on PERG P50 in the early stages. As disease progresses there is usually N95 reduction in the PERG, and the PVEP reduces in amplitude and becomes progressively more delayed. Further disease progression results in the PVEP becoming undetectable, and involvement of the P50 component of the PERG, which may shorten in latency. By now visual acuity is extremely poor. The flash VEP may become involved by this stage, but shows no significant abnormality in milder disease. Although it is likely that there would be observable FVEP deterioration in association with disease progression, this study does not provide the longitudinal data necessary to confirm that suggestion. Most FVEP findings were within the normal range at the time of examination, but this does not preclude deterioration in relation to the pre-morbid state. It is not established whether this proposed sequence of events is always equally applicable to other optic nerve diseases, but it is not an unfamiliar picture in progressive optic nerve disease (Holder, unpublished observations).

Colour vision deficiencies, as evidenced by the elevated colour contrast sensitivity values in the patients studied, were not confined to the tritan axis although this was the more severely affected. Even in mildly affected patients, or early in the disease process, all colour axes could be involved. Indeed, in the overall cohort there were a number of children with marked protan or protan/deutan deficits and who had relatively good visual acuities [18]. This does not support the suggestion that the ganglion cell population affected in DOA is that mediating the blue-yellow colour channel e.g. [46]. Jaeger [7] previously reported that protan and deutan defects could occur in advanced disease. It is of interest that in one patient the VEP and PERG in one eye were normal. The PVEP from the fellow eye showed relative amplitude reduction and latency delay while falling within the absolute limits of normal, with additional N95 loss in the PERG, but there was significant elevation of the tritan threshold from the eye with normal electrophysiology. A subtle colour vision abnormality may be an initial sign of DOA; as this tends to be in the tritan axis it would not be detectable by the use of Ishihara charts.

In clinical practice, the PERG findings are worthy of note. Even though the PVEP could be extinguished or markedly delayed, the PERG was never extinguished in such cases as would invariably occur in macular dysfunction with an equal amount of acuity loss. This should alert to the possibility of macular dysfunction secondary to generalised cone dysfunction in the occasional retinal dystrophy which presents with pale discs but minimal or no macular abnormality on ophthalmoscopy, is initially assumed to be an heredofamilial or idiopathic optic atrophy, and in whom the PERG is unrecordable. The finding of a delayed or extinguished PVEP should not be assumed to

reflect optic nerve dysfunction unless accompanied either by a normal PERG or by a PERG with N95 component reduction. Absence of P50 is usually associated with dysfunction distal to the retinal ganglion cells [43, 47].

Acknowledgements

This study was supported by a grant from The Guide Dogs for The Blind Association, Berkshire, England, and The Wellcome Trust, London, England. M.V. is a Wellcome Trust Vision Research Fellow. The MRI data are courtesy of Dr. Ivan Moseley. We thank the families who co-operated with this study, and Dr. Marcelle Jay, who helped trace family members.

References

1. Kjer P. Infantile optic atrophy with dominant mode of inheritance: a clinical and genetic study of 19 Danish families. Acta Ophthalmol 1959; 37 (Suppl 54): 1–146.
2. Eliott MD. Visual prognosis in autosomal dominant optic atrophy (Kjer type). Am J Ophthalmol 1993; 115: 360–7.
3. Batten B. A family suffering from hereditary optic atrophy. Trans Ophthalmol Soc UK 1896; 16: 125.
4. Caldwell JBH, Howard RO, Riggs LA. Dominant juvenile optic atrophy: A study of two families and review of the hereditary disease in childhood. Arch Ophthalmol 1971; 85: 133–47.
5. Smith DP. Diagnostic criteria in dominantly inherited juvenile optic atrophy: A report of three new families. Am J Opt & Physiol Optics 1972; 49: 183–200.
6. Hoyt CS. Autosomal dominant optic atrophy: a spectrum of disability. Ophthalmology 1980; 87: 245–51.
7. Jaeger W. Diagnosis of dominant infantile optic atrophy in early childhood. Ophthalmic Paediatrics and Genetics 1988; 9: 7–11.
8. Kline LB, Glaser JS. Dominant optic atrophy. The clinical profile. Arch Ophthalmol 1979; 97: 1680–6.
9. Johnston PB, Gaster RN, Smith VC, Tripathi RC. A clinicopathological study of autosomal dominant optic atrophy. Am J Ophthalmol 1979; 88: 868–75.
10. Kjer P. Histopathology of eye, optic nerve and brain in a case of dominant optic atrophy. Acta Ophthalmol 1982; 61: 300–12.
11. Eiberg H, Kjer B, Kjer P, Rosenberg T. Dominant optic atrophy (OPA1) mapped to chromosome 3q region. I. Linkage analysis. Hum Molec Genet 1994; 3: 977–80.
12. Bonneau D, Souied E, Gerber S, Rozet J-M, D'Haens E, Journel H, et al. No evidence of genetic heterogeneity in dominant optic atrophy. J Med Genet 1995; 32: 951–3.
13. Brown J, Fingert JH, Taylor CM, Lake M, Sheffield VC, Stone EM. Clinical and genetic analysis of a family affected with dominant optic atrophy (OPA1). Arch Ophthalmol 1997; 115: 95–9.
14. Johnston RL, Burdon MA, Spalton DJ, Bryant SP, Behnam JT, Seller MJ. Dominant optic atrophy, Kjer type: Linkage analysis and clinical features in a large British pedigree. Arch Ophthalmol 1997; 115: 100–3.

15. Jonasdottir A, Eiberg H, Kjer B, Kjer P, Rosenberg T. Refinement of the dominant optic atrophy locus (OPA1) to a 1.4-cM interval on chromosome 3q28-3q29, within a 3-Mb YAC contig. Hum Genet 1997; 99: 115–20.
16. Stoilova D, Child A, Desai SP, Sarfarazi M. Refinement of the locus for autosomal dominant juvenile optic atrophy to a 2cM region on 3q28. Ophthalmic Genetics 1997; 18: 1–6.
17. Votruba M, Moore AT, Bhattacharya SS. Genetic refinement of dominant optic atrophy (OPA1) locus to within a 2cM interval of chromosome 3q. J Med Genet 1997a; 34: 117–21.
18. Votruba M, Fitzke FW, Holder GE, Carter AC, Bhattacharya SS, Moore AT. Clinical features in affected individuals from 21 pedigrees with dominant optic atrophy. Arch Ophthalmol 1997b; in press.
19. Fitzke FW, Poinoosawmy D, Ernst W, Hitchings RA. Peripheral displacement thresholds in normals, ocular hypertensives and glaucoma. In: Greve EL, Heijl A, ed. Seventh International Visual Field Symposium. 1987: 447–52.
20. Cioffi GA, Robin AL, Eastman RD, Perell HF, Sarfarazi FA, Kelman SE. Confocal laser scanning ophthalmoscope. Reproducibility of optic nerve head topographic measurements with the confocal laser scanning ophthalmoscope. Ophthalmology 1993; 100: 57–62.
21. Arden GB, Gunduz K, Perry, S. Colour vision testing with a computer graphics system. Clin Vis Sci 1988; 2: 303–20.
22. Berninger TA, Canning C, Strong N, Gunduz K, Arden GB. Using Argon laser blue light reduces Ophthalmologists' colour contrast sensitivity. Arch Ophthalmol 1989; 107: 1453–8.
23. Gunduz K, Arden GB. Changes in colour contrast sensitivity associated with operating Argon lasers. Br J Ophthalmol 1989; 73: 241–6.
24. Harding GFA, Odom JV, Spileers W, Spekreijse H. Standard for Visual Evoked Potentials 1995. Vision Res 1996; 36: 3567–72.
25. Marmor MF, Holder GE, Porciatti V, Trick G, Zrenner E. Guidelines for pattern electroretinography. Recommendations by the International Society For Clinical Electrophysiology of Vision. Doc Ophthalmol 1996; 91: 291–8.
26. Holder GE. Recording the pattern electroretinogram with the Arden gold foil electrode. J Electrophysiol Technol 1988; 14: 183–90.
27. Odom JV, Holder GE, Feghali JG, Cavender S. Pattern electroretinogram intrasession reliability: A two center comparison. Clin Vis Sci 1992; 7: 263–82.
28. Arden GB, Hogg CR, Holder GE. Gold foil electrodes: a two centre study of electrode reliability. Doc Ophthalmol 1994; 86: 275–84.
29. Harding GFA. The visual evoked response. in Roper-Hall MJ et al., eds. Advances in Ophthalmology. Karger, Basel, 1974, 2–28.
30. Holder GE. Pattern ERG abnormalities in anterior visual pathway disease. Electroenceph clin Neurophysiol 1985; 61: S135.
31. Holder GE. Significance of abnormal pattern electroretinography in anterior visual pathway dysfunction. Br J Ophthalmol 1987a; 71: 166–71.
32. Mollon ID, Astell S, Reffin JP. A minimalist test of colour vision. In: Drum B, Moreland ID, Serra A, ed. Colour vision deficiencies vol X. Kluwer, Dordrecht 1991: 59–67.
33. Harding GFA, Crews SJ, Pitts SM. Psychophysical and visual evoked potential findings in hereditary optic atrophy. Trans Ophthalmol Soc UK 1979; 99: 96–102.

34. Holder GE. Abnormalities of the pattern ERG in optic nerve lesions: changes specific for proximal retinal dysfunction. in Barber, C. and Blum, T. eds. Evoked Potentials III, Butterworths, London, 1987b: 221–4.
35. Holder GE. The incidence of abnormal pattern electroretinography in optic nerve demyelination. Electroenceph clin Neurophysiol 1991a; 78: 18–26.
36. Berninger TA, Jaeger W, Krastel H. Electrophysiology and colour perimetry in dominant infantile optic atrophy. Br J Ophthalmol 1991; 75: 49–52.
37. Bach M, Gerling J, Geiger K. Optic atrophy reduces the pattern electroretinogram for both fine and coarse stimulus patterns. Clin Vis Sci 1992; 7: 327–34.
38. Berninger TA, Schuurmans RP. Spatial tuning of the pattern ERG across temporal frequency. Doc Ophthalmol 1985; 61: 17–25.
39. Holder GE. Pattern electroretinography in the evaluation of glaucoma and in optic nerve function. in Heckenlively, JR and Arden GB. eds. Principles and Practice of Clinical Electrophysiology of Vision, Mosby Year Book, St. Louis, 1991b: 549–56.
40. Ryan S, Arden GB. Electrophysiological discrimination between retinal and optic nerve disorders. Doc Ophthalmol 1988; 68: 247–55.
41. Sherman J. Simultaneous pattern reversal electroretinograms and visual evoked potentials in diseases of the macula and optic nerve. Ann NY Acad Sci 1982; 388: 214–226.
42. Harrison JM, O'Connor PS, Young RS, Kincaid M, Bentley R. The pattern ERG in man following surgical resection of the optic nerve. Invest Ophthalmol Vis Sci 1987; 28: 492–499.
43. Holder GE. The pattern electroretinogram in anterior visual pathway dysfunction and its relationship to the pattern visual evoked potential: A personal clinical review of 743 eyes. Eye 1997; 11: 924–34.
44. Maffei L, Fiorentii A. Electroretinographic responses to alternating gratings before and after section of the optic nerve. Science 1981; 211: 953–5.
45. Tobimatsu S, Celesia G, Cone SB, Gujrati M. Electroretinograms to checkerboard pattern reversal in cats: physiological characteristics and effect of retrograde degeneration of ganglion cells. Electroenceph clin Neurophysiol 1989; 73: 341–52.
46. Rodieck RW. Which cells code for colour? In Valberg A and Lee BB. eds. From Pigment to Perception. Plenum. NY: 83–93.
47. Holder GE. Pattern electroretinography in patients with delayed pattern visual evoked potentials due to distal anterior visual pathway dysfunction. J Neurol Neurosurg Psychiat 1989; 52: 1364–8.

Address for correspondence: G.E. Holder, Moorfields Eye Hospital, City Road, London EC1V 2PD, UK
Phone: +44-171-566 2120; Fax: +44-171-566 2556; E-mail: gholder@cix.co.uk

Documenta Ophthalmologica **95:** 229–245, 1999.

Spatial and temporal response properties of the major retino-geniculate pathways of Old and New World monkeys

JAN KREMERS
Dept. of Experimental Ophthalmology, University of Tübingen Eye Hospital, Röntgenweg 11, 72076 Tübingen, Germany

Abstract. Old World monkeys, apes and humans all enjoy trichromatic colour vision, and the absorption spectra of the photopigments are very similar in all species and all individuals. Colour vision in New World monkeys however, is very heterogeneous. In many species, the majority of individuals is dichromatic. Recently, anatomical and electrophysiological studies revealed that the retinal organisation in Old World monkeys and New World monkeys is very similar, although the cells belonging to the parvocellular pathway do not show any colour opponency and their spectral sensitivity is similar to that of the magnocellular cells. Apparently, the magnocellular and parvocellular pathways in the retina and the LGN have not developed as an adaptation to luminance and chromatic processing. It is more likely that the two pathways originally evolved to cover different ranges in the spatio-temporal domain. In the present paper, several spatial and temporal properties of parvo- and magnocellular cells (which are identical for dichromatic and trichromatic animals) are compared.

Key words: magnocellular, New World monkeys, Old World monkeys, parvocellular

Abbreviations: LGN – lateral geniculate nucleus; M – magnocellular; P – parvocellular

Introduction

The only mammals that enjoy trichromatic colour vision are primates. But not all primates are trichromatic. Figure 1 shows a family tree of the primates, with a summary about the number of cone types and the spectral characteristics (given by the maximally absorbed wavelengths) of the photopigments. Of course, not all primate species have been investigated yet, but it seems to be clear that trichromacy is not found in the strepsirhines. The galago is probably even a monochromat, lacking functional S-cones [1, 12]. This is probably influenced by their nocturnal life style. The diurnal strepsirhines are probably dichromatic [3]. Tarsiers are probably more closely related to the anthropoids [4, 5]. Nothing is known yet about colour vision in this group with mainly nocturnal species. The anthropoids can be subdivided into the catarrhines or Old World monkeys (including apes and humans) and the platyrrhines or the

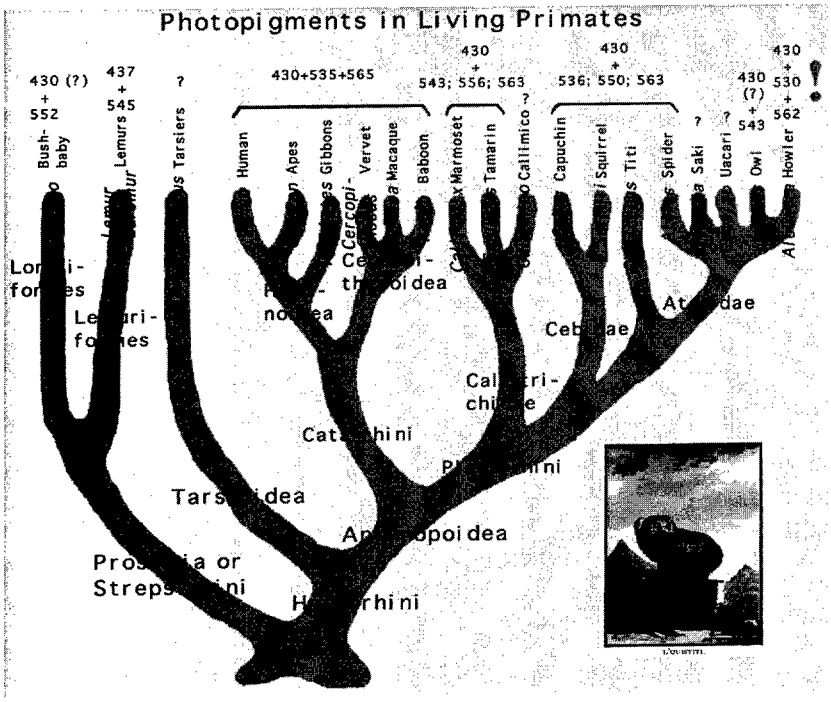

Figure 1. The primate tree according to Fleagle [4] and Martin [5] together with a compilation of about what is known about the photoreceptor types. The pigment data are obtained from several different studies [3, 6, 7, 11, 12, 61–72]. We used the definition of Napier and Napier [46] for the prosimians as a synonym for the strepsirhini. Other authors include the tarsiers in the prosimians, but they probably form a monophylogenetic group (the haplorhini) with the anthropoids. The inset shows a print of a marmoset by de Buffon.

New World monkeys. The cone types in these groups have been studied in more detail. All catarrhines have three cone types with only little variation in the absorption spectra of the cone-pigments within species and between species. They are all trichromatic, because they additionally possess post-receptoral mechanisms which compare the outputs of the three cone types. The New World monkeys are much more heterogeneous. The species of the genus *Alouatta* (the howler monkeys) all seem to be completely trichromatic [6]. The nocturnal owl monkeys (*Aotus*) are probably monochromatic, lacking functional S-cones [1, 7]. Colour vision in all other platyrrhine species studied so far is polymorphic [8–12]. This polymorphism is sex-linked and has a genetic origin: all the males and about one-third of the females are dichromats. All other females are trichromatic.

Anatomical studies revealed that there are only minor morphological differences between the retinae of diurnal catarrhines and platyrrhines [13–21]. Further, a comparison between the electrophysiological properties of retinal

ganglion cells and cells in the LGN of platyrrhine capuchin monkeys and marmosets with those of the catarrhine macaques shows that there only few functional differences in the neuronal organisation of the retina [17, 22–26]. Thus, the retinal wiring seems to be basically identical in catarrhines and platyrrhines, despite the differences in cone arrangements. This is surprising, because colour opponent processing in the P-pathway is so distinct, that it has led to the proposition that it has evolved as an adaptation to trichromatic colour vision [27]. But because the retinal organisation also seems to be present in dichromats, this hypothesis becomes questionable. Possibly, the subdivision in P- and M-pathways has another cause. In the present paper, I try to discuss the possible factors which might play a role, and explore the differences between the response characteristics of dichromatic and trichromatic anthropoids. I will substantiate the discussion with experimental data in which electrophysiological responses of P- and M-cells in the LGN of marmosets (*Callithrix jacchus* a platyrrhine monkey with routine dichromacy and trichromacy) are compared.

Parts of the presented data were used in previous publications on the temporal [24] and the spatial properties [23] of M- and P-cells.

Methods

Animal preparation We recorded from cells in the LGN of marmosets (*Callithrix jacchus*). The surgical procedure has been described in detail elsewhere [23–25]. Briefly, the animals were initially sedated by administration of ketamine hydrochloride (Ketanest®; 15–30 mg/kg) and Xylazin hydrochloride (Rompun®; 0.15 ml/kg 2% solution). After tracheotomy the animals were artificially respired with a 70% NO_2/30% O_2 mixture. Anaesthesia was achieved by adding Enflurane (Ethrane®; 0.4–0.8% during surgery and 0.2–0.4% during recording) to the respired air. The depth of anaesthesia was controlled by monitoring EKG and EEG continuously. After the experiments, the animals were sacrificed with an overdose of sodium pentobarbital (Nembutal®). The experiments were conducted in accordance with the European Communities Council Directive of 24 November 1986 (86/609/EEC).

Tungsten in glass electrodes were lowered into the LGN and we recorded extracellularly from single cells. The cell type we recorded from could be determined from the sequence of ocular input, and from post-mortem histological reconstructions of the recording depth relative to small lesions, which were made occasionally.

Visual stimuli

Visual stimuli were presented using a BARCO Calibrator monitor (CCID 7751 MKII; 100 Hz frame rate) in combination with a VSG 2/2 graphics card (Cambridge Research Systems). The luminance output of the monitor was calibrated regularly using the internal measuring device of the monitor. Gamma corrections were performed by the VSG-Software. The luminance output of the each phosphor was checked using a UDT luminance detector and an IL1700 radiometer. The spectral output of the monitor was measured with a Spectrascan spectroradiometer.

In the described experiments, several stimuli were used in order to investigate different aspects of signal processing in the peripheral visual system.

Temporal response properties

The responses to sine-wave luminance modulation were measured. The stimuli were spatially uniform and covered the receptive field completely. We measured at several temporal frequencies, and at several Michelson contrasts (defined as $100\% \times \frac{(L_{max}-L_{min})}{(L_{max}+L_{min})}$, in which L_{max} and L_{min} are the maximal and the minimal luminance output in the stimulus respectively) for each frequency [24].

Receptive field dimensions

To measure the spatial properties of the cells' receptive fields, a bipartite field stimulus and drifting gratings were used [23]. The two halves of the bipartite field stimulus modulated in counterphase but otherwise identically (4 Hz luminance modulation; 75% contrast). The common edge of these halves was positioned on different locations within the receptive fields. Receptive field sizes were also obtained from the responses to drifting gratings with different spatial frequencies [28]. The moving gratings had, similar to the bipartite field stimulus, a 75% luminance contrast and a temporal frequency of 4 Hz.

Responses to rotating hemi-circles

Finally, some preliminary results are presented of measurements in which we stimulated with rotating hemi-circles, that were displayed on the monitor. The hemi-circles were produced by the red and green phosphors of the monitor each having a luminance of 5 cd/m^2. The hemi-circles therefore were yellow with a luminance of 10 cd/m^2. The background of the monitor on which the hemi-circle was displayed had a luminance of less than 0.1 cd/m^2. This hemi-circle rotated 360° rotated around ist midpoint in one second. The midpoint of the hemi-circle was positioned at different locations within the cells' receptive fields. The advantage of this stimulus is that the phase of maximal response is directly linked with an orientation of the straight edge of

the hemi-circle. The response phase therefore depends on the position of the hemi-circles relative to the receptive field mid-point and on the temporal characteristics of the cells. Thus, it can be determined to which spatio-temporal aspects of the stimulus the cells respond. Cells with eccentric receptive fields might receive rod input at the used luminances of the stimulus [25]. This probably influences the temporal characteristics and therefore the response phase of the cells.

Results

The majority of the data are obtained from dichromatic marmosets. The data stemming from trichromats are treated equally as those from dichromats and they are not explicitly distinguished, because the results were not obviously different between dichromatic and trichromatic anthropoids [26]. Furthermore, it is the aim of this paper to find differences between parvo- and magnocellular cells in both dichromats and trichromats, rather than differences between dichromats and trichromats.

Temporal modulation

Figure 2 displays the response amplitudes and phases (defined as the amplitudes and phases of the fundamental component obtained from the Fourier analysis on the response histograms) of an off-centre M-cell and an off-centre P-cell from dichromatic marmosets as a function of temporal frequency for a 75% contrast sine-wave modulation of a spatially uniform field. The response amplitudes of the P-cell are smaller than those of the M-cell by about a factor of two, which is similar to the differences found in a larger population of cells [24]. Larger response differences were described for M- and P-cells in the macaque retina [29]. Further, the response phases of the M-cell are advanced relative to the P-cell response phases, especially at low temporal frequencies, indicating that the M-cell responds in a more transient manner than the P-cell. This also was found in a larger cell population.

Spatial dimensions

The receptive field dimensions were measured with a bipartite field stimulus and with drifting gratings. Stimulus contrast was 75% in both measurements. Figure 3 shows the response amplitudes for an on-centre P-cell to both sets of stimuli. We modelled the responses based on the assumptions that the receptive field centres and surrounds have Gaussian responsivity profiles, and that their responses were antagonistic [23, 30, 31]. Based on this model, we

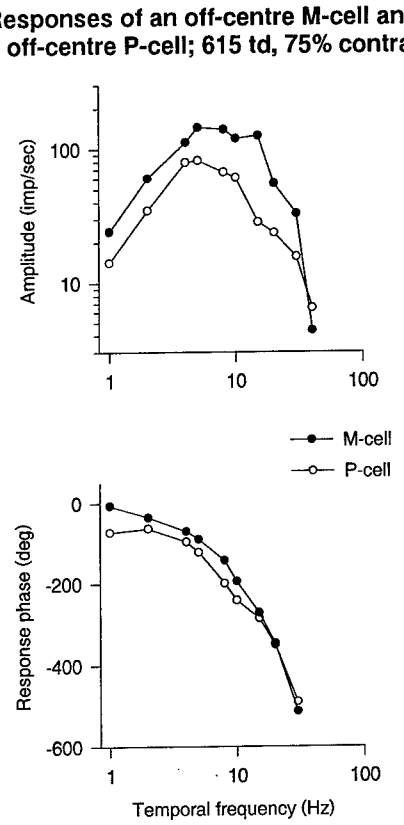

Figure 2. Response amplitudes (upper panel) and response phases (lower panel) of an off-centre M-cell and an off-centre P-cell to 75% contrast luminance sine-wave modulation as a function of temporal frequency. These data are representative for all cells found in the marmoset LGN [24]. The P-cell has a lower response amplitude than the M-cell, but the response difference is smaller than those found in for macaque retinal ganglion cells. Further, the response phases of the two cells differ.

were able to obtain good descriptions of both sets of data. The drawn curves in Figure 3 are best fits of the model through the data. From these fits we obtained the size of the receptive field centre and surround expressed as the standard deviation of the Gaussian profiles. For the cell displayed in Figure 3 we obtained a centre size of 7.2 mm of arc and a surround size of 14.4 min of arc with the bipartite field stimuli, whereas the grating data yielded a centre size of 7.6 min of arc and a surround size of 17.0 mm of arc. Other parameters which were obtained are described in the legends.

We measured the centre sizes of 50 P-cells and 28 M-cells with the bipartite field stimulus. The centre sizes of these cells are plotted in Figure 4. A large subpopulation of these cells was measured in two directions using

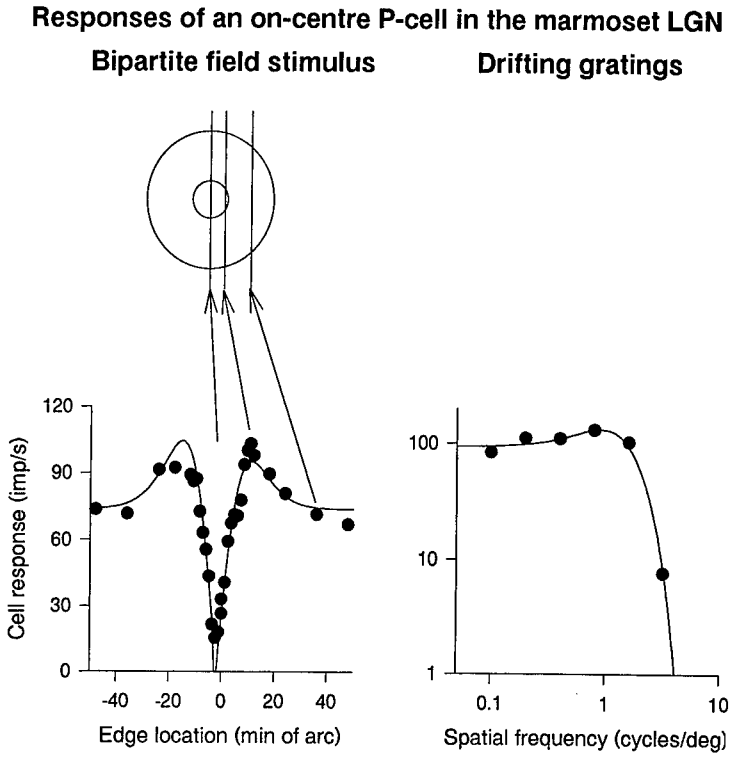

Figure 3. Amplitudes of the responses of a on-centre P-cell to a bipartite field stimulus (left graph) and to moving gratings (right graph). The response amplitudes are given as a function of the location of the edge of the bipartite field stimulus and as a function of the spatial frequency of the moving grating. The sketch above the graph for bipartite field stimulus displays three approximate locations of the edge relative to the receptive field of the cell. Both data sets were fitted with a model based on the assumption that centres and surrounds have Gaussian sensitivity profiles. For the bipartite field stimulus there were six free parameters and for the moving gratings there were four free parameters. The fit parameters for the bipartite field data were: centre position: −2.4 min of arc; surround position: −3.6 min of arc; centre size: 7.2 min of arc; surround size: 14.4 min of arc; centre amplitude: 179 imp/sec; surround amplitude: 105 imp/sec. The fit parameters for the drifting gratings: centre size 7.6 min of arc; surround size: 17.0 min of arc; centre peak sensitivity 2135 imp/(sec.%contrast.deg^2); surround peak sensitivity: 245 imp/(sec.%contrast.deg^2). Thus, the two fits gave similar centre and surround sizes. Peak sensitivities in the fits to the moving grating data are not directly comparable with the amplitudes obtained from the bipartite field data because they are normalised to the centre and surround sizes and to the stimulus contrast.

horizontal and vertical edges. The average centre size are displayed for those cells. Only a few cells showed a clear elongation of the receptive field centres. There is a considerable variability in the centre sizes between individual cells, but the linear regressions through the P- and M-cell data (dotted and drawn

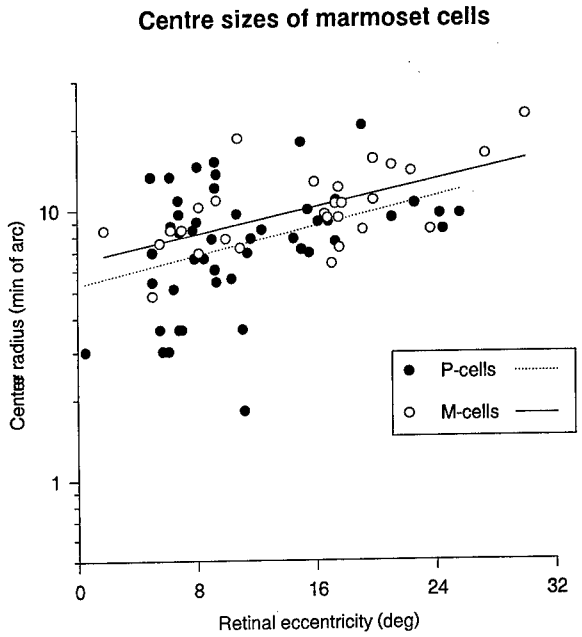

Figure 4. Centre sizes of marmoset LGN cells measured with the bipartite field stimulus as a function of the retinal eccentricity. Moving gratings yielded very similar results. The centre sizes were often measured in the horizontal and the vertical direction. In that case, the mean of the two values are plotted. The majority of the data are published before [23]. Five new data points are included. The linear regressions through the data in this semi-logarithmic plot are shown (drawn line for the M-cells; dotted line for the P-cells).

lines, respectively) show that there is a shallow increase of centre size with increasing retinal eccentricity. Further, M-cells are only slightly larger than P-cells. Similar results have been obtained in the macaque [30–36], although other in studies [37, 38] it was found that M-cell had considerably larger receptive field centres than P-cells. The cause of the discrepancy in results is still unresolved. A closer comparison of the marmoset and the macaque data reveals that the slope of the linear regressions are similar in both species [31], but cells in the marmoset LGN have about 1.5–3 times larger centre sizes than macaque LGN cells and retinal ganglion cells. The difference in centre size can be attributed to optical factors, because the marmoset eye is a factor of about 1.6 smaller than the macaque eye [39]. It therefore seems that the neuronal spatial processing is similar in marmosets and macaques.

Responses to rotating hemi-circles

To study more closely the spatio-temporal processing in the marmoset peripheral visual system, we performed experiments, in which rotating hemi-

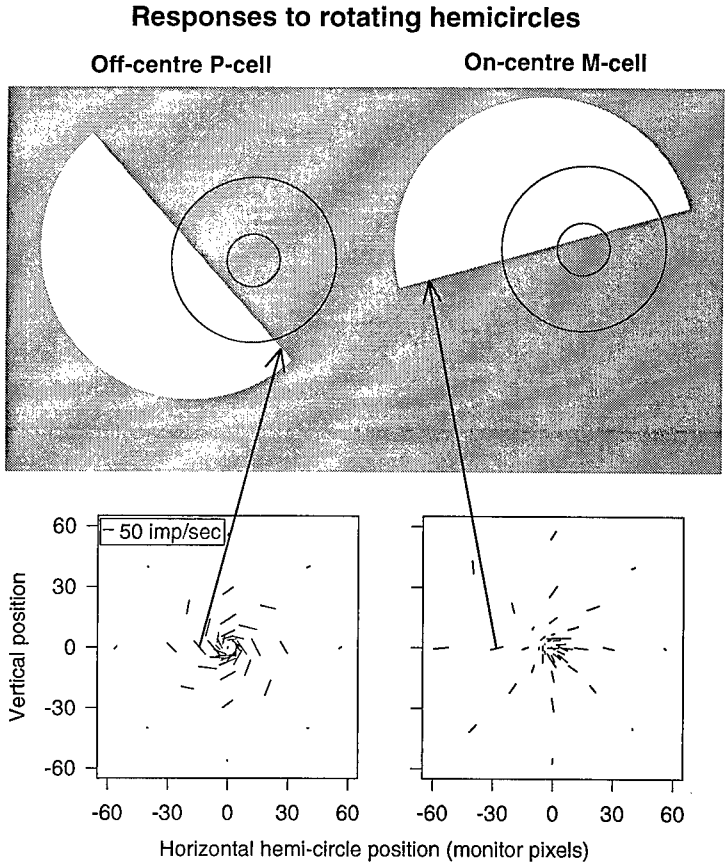

Figure 5. Responses of an off-centre P-cell and an on-centre M-cell to rotating 10 cd/m^2 yellow hemi-circles upon a dark background. The lower plots display the responses as line segments. The midpoints of the line segments coincide with the position of the midpoints of the hemi-circles. The length of the line segments quantifies the response amplitude, and the orientation of the line segments gives the response phase. The orientation of the line segments is very similar to the orientation of the straight edge of the hemi-circle when the cell responds maximally. For a position of the hemi-circle left of the receptive field centre in the two cells (which is encoded by the position of the line segments) this is visualised by the sketch above the plot: the orientation of the line segments and the straight edges of the hemi-circles are similar. This is the orientation of the hemi-circle when the cell responds maximally. In contrast to the drawing, the hemi-circles are actually much larger than the receptive fields. All the line segments of the P-cell responses do not point towards the receptive field centre. Thus the cell responds maximally when the receptive field centre is minimally illuminated. The response line segments of the M-cell all point more in the direction of the receptive field centre, indicating that the cell mainly responds when the illuminance in the receptive field centre increases.

circles were employed as a stimulus. In the present paper, some preliminary results are presented. The plots in the lower part of Figure 5 display the responses of an on-centre M-cell and an off-centre P-cell as line segments. Each line segment gives the response characteristic of the cell at a certain position of the hemi-circles. The positions of centres of the line segments identify the locations of the hemi-circles. The lengths of the line segments quantify the response amplitudes and the angles of the line segments with the abscissa equal the response phases. By this definition, the orientation of the line segments is approximately equal to the orientation of the hemi-circles when the cell responds maximally. Two examples for the orientation of the hemi-circles at maximal response are sketched above the plots. In these examples, the hemi-circles were located left of the receptive field midpoint. The M-cell responded maximally when the straight edge of the hemi-circle passed through the receptive field centre, and thus when the illuminance within the receptive field centre changes. The P-cell, however, responded when the hemi-circle did not cover the receptive field centre, suggesting that the cell mainly responded to levels of illuminances rather than to changes in illuminances. The plots show that this is the case for every position of the hemi-circle. These results were very characteristic for nearly all P- and M-cells we encountered.

Discussion

As already argued in the introduction, retinal ganglion cells and LGN cells of plathyrrhines and catarrhines have very similar electrophysiological response properties [17, 22–25]. Additionally, the morphological retinal organisation [13–21] is very similar in both groups. Thus, it seems that there are only minor differences in the retinal organisation and wiring, despite the fact that colour vision is different in the two groups. It is very unlikely that this similarity is the result of a parallel or a convergent evolution. It is much more probable that the retinal organisation was already present in the common ancestor of the platyrrhines and catarrhines. If colour vision had only a small influence on the retinal organisation, then it also becomes questionable whether the P-pathway is an adaptation to trichromatic colour vision as has been proposed by Shapley and Perry [27]. Thus this proposal either needs some extension or alternatives must be considered. I will discuss three different proposals in relation to the above described results and data given in the literature.

(1) The P-pathway was present before trichromatic colour vision developed but its organisation has been significantjy altered since then. Strepsirhines and tarsiers have, similar to anthropoids, layered LGNs [40, 41]. The morphology of the retinal ganglion cells in the strepsirhine galago resembles

those found in the anthropoids (Yamada, pers. comm.). The few electrophysiological data available [42–44] indicate some similarities with P- and M-cells in anthropoids, but a more detailed comparison will be needed to get a better notion about organisational differences between the retinae of anthropoids and non-anthropoid primates. But, this indicates that the presence of a parvocellular pathway is probably a primitive feature of primates. The first primate was probably a dichromat (or possibly even a monochromat) because trichromacy seems to be lacking in strepsirhines, and because of the nocturnal life style of the first primates [45]. Trichromacy has so far only been found in diurnal primates. However, the first anthropoids were probably diurnal [46, 47] and it cannot be excluded that some sort of trichromatic colour vision (either full trichromacy as in the catarrhines or a platyrrhine-like polymorphism) had developed at that stage. The P-pathway might have changed concurrently with the development of trichromacy, to increase colour opponent processing. These properties were then passed onto the catarrhines and the platyrrhines. Indeed, there are some arguments that the functional advantage of the connection of one cone to one midget bipolar cell and further to one midget ganglion cell in the foveal P-pathway is probably an increase of colour opponent responses in the parvocellular retinal ganglion and LGN cells rather than an increase of the spatial resolution [48].

This version has the advantage that no parallel evolution needs to be assumed. Colour opponent processing and the one cone–one bipolar cell–one ganglion cell connection was already in the common ancestor. But even if the first anthropoid was polymorphic, it cannot be conceived that a large part of the visual system underwent drastic changes, only to bring some advantage to a minority of the individuals. Indeed, if the evolutionary advantages of trichromacy is so large, that it brings these radical changes, it leaves the question why not all anthropoids have developed full trichromacy. Since full trichromacy has evolved twice independently in the anthropoids (in the catarrhines and in the platyrrhine howler monkeys, *Alouatta*) it does not seem to be a very improbable that it could have developed more often. Furthermore, if the first anthropoid was a full trichromat and if trichromacy had many advantages, it seems improbable that most platyrrhines have lost full trichromacy again and that it reappeared in the howler monkeys. These considerations seem to support the idea that the ancestral anthropoid was a dichromat, implying that the basic organisation of the P- and M-pathways has developed for reasons not related with colour vision. Some possible reasons are discussed in the next two sections.

(2) The P-pathway is an adaptation to high acuity spatial vision. Differences in spectral sensitivity cannot have been the cause for the division between M-

and P-pathways, when they were already present before trichromatic colour vision appeared. Other possible origins for the division must be considered. One purpose of the original division might have been a specialisation of the P-pathway for higher spatial acuity and of the M-pathway for higher temporal acuity. Indeed midget ganglion cells, which are the anatomical equivalents of the P-cells, have smaller dendritic trees than the parasol cells [14, 20, 21, 49–51]. For cat ganglion cells, a correlation between dendritic tree size and receptive field centre size has been established [52]. However, the receptive field centre sizes of P- and M-cells in the marmoset (Figure 4) and macaques do not differ much [30–36] (but see Croner and Kaplan [38] and de Monasterio and Gouras [37] for conflicting results), suggesting that the correlation between receptive field centre size and dendritic tree size does not hold for primates. A direct comparison between LGN receptive field centers and dendritic tree sizes in marmosets reveals two types of mismatches between the physiological and the anatomical data [23]. Receptive field centres and dendritic trees of M-cells match well close to the fovea, but at large retinal eccentricities the receptive field centres are smaller. This is possibly caused by the large contrast gain of M-cells which results in a decrease of the receptive field sizes. On the other hand, P-cell receptive field centres match the dendritic tree sizes at retinal eccentricities above about 15°, but the receptive field sizes are larger for more centrally located cells. This might have been caused by optical blur [31, 53]. In summary, although the dendritic tree sizes of midget and parasol cells are different, the receptive field centre sizes and thus the spatial resolutions of P- and M-cells are much more similar, thus excluding this factor as a driving force for the division between the two pathways.

However, spatial acuity of the pathways is probably not only determined by the receptive field centre sizes of the individual cells, but also by the number of cells which sample the visual scene. The P-pathway may have some advantage in spatial vision because of the larger amount of cells and the smaller average nearest neighbour distances. But, also the M-pathway can deliver very accurate spatial signals which are probably used in hyperacuity vision [36, 54]. Furthermore, the requirement of a cell system with a high density cannot be the reason for the division between M- and P-pathways, because if all the ganglion cells would belong to only one pathway the density of these cells would be even larger. There probably were other differences between the P- and M-pathways which might have influenced their separate development. A solution to this problem might be found in the temporal responses of P- and M-cells.

Possibly, requirements of higher spatial resolution in anthropoids, owing to an diurnal and arboreal lifestyle, led to a decrease of receptive field size and

to an increase in density of both P- and M-cells. A decrease of receptive fields in P-cells might have ultimately led to the situation in which their centres received their input from only a few cones. A further decrease would not be advantageous for spatial vision, since optical blur rather than receptive field centre size would be limiting the spatial resolution. But, at this stage, in trichromats colour opponency might have been automatically present in many cells, even when the inputs were randomly drawn from the cones within its reach. Possibly, the driving force for a further decrease of the centre size to the size of one cone might be an increase in the colour opponent signal in P-cells.

(3) There are temporal differences between P- and M-cells. Our data show that the spatial dimensions of P- and M-cells in dichromatic and trichromatic marmosets seems to be very similar. Our data also show that M-cells in these dichromatic animals are more sensitive to illuminance changes than P-cells, but the difference in the LGN does not seem to be as large as in the retina. However, one consistent difference can be found in the temporal domain. The response phases to low temporal frequency sine-wave modulation are quite different between P- and M-cells. M-cells respond in a transient manner, and mainly respond to changes in illuminance. P-cells respond less transiently and their response is mainly determined by illuminance levels. The responses to the rotating hemi-circles confirm this conclusion: the M-cells responded mainly when the straight edge of the hemi-circle passed through the receptive field centre, whereas P-cell responded maximally when the edge was outside the receptive field centre. Possibly, this is one of the main reasons for subdividing the retino-geniculate system of primates. When the M-system is more sensitive to changes in illuminance it will code for contours and movements. A P-pathway will be more sensitive for illuminance levels (and for chromaticities in trichromatic animals) and might 'fill in' the contours, thus establishing a coherence in the visual scene. For object recognition both systems therefore might be necessary. The different requirements in the temporal domain might have kept them separated in primate evolution, and eventually caused that colour processing was only subserved by the P-pathway.

This proposal comes close to the earlier ideas, that the visual system can be subdivided into transient and sustained systems [55]. Others have tried to explain the division by combining temporal and spatial factors [56–60]. They argue that the P- and M-pathway are complementary in the temporal and spatial domain, due to which the spatio-temporal range in which the visual system can respond is expanded.

At this moment, it is not possible to decide which (parts) of above mentioned proposals are correct. Furthermore, it should be pointed out that these

hypotheses are not mutually exclusive. More data, also from non-anthropoid primates are needed to resolve more firmly the role of the subdivision in P- and M-pathways.

Acknowledgements

I would like to thank my collaborators Eva Burkhardt, Sabine Meierkord, Dr. Tomoaki Usui and Dr. Stefan Weiss for help with the experiments, Prof. Eberhard Zrenner for his continuous support, and Profs. Luiz Silveira and Barry Lee for useful discussions. Barry Lee provided the idea for Figure 1. I would also like to thank two anonymous referees for their constructive comments. This work was supported by DFG grant Zr 1/9-3 , DFG SFB 430/C3 and a DFG Heisenberg fellowship.

References

1. Wikler KC, Rakic P. Distribution of photoreceptor subtypes in the retina of diurnal and nocturnal primates. J Neurosci. 1990; 10: 3390–401.
2. Deegan II JF, Jacobs GH. Spectral sensitivity and photopigments of a nocturnal prosimian, the bushbaby (*Otolemur crassicaudatus*). Amer J Primatol. 1996; 40: 55–66. (Abstract).
3. Jacobs GH, Deegan II JF. Photopigments underlying color vision in ringtail lemurs (*Lemur catta*) and brown lemurs (*Eulemur fulvus*). Amer J Primatol 1993; 30: 243–456.
4. Fleagle JG. Primate Adaptation and Evolution. San Diego, London: Academic Press Inc., 1988.
5. Martin RD. Primate origins: plugging the gaps. Nature 1993; 363: 223–34.
6. Jacobs GH, Neitz M, Deegan JF, Neitz J. Trichromatic colour vision in New World monkeys. Nature 1996; 382: 156–158.
7. Jacobs GH, Deegan II JF, Neitz J, Crognale MA, Neitz M. Photopigments and color vision in the nocturnal monkey, *Aotus*. Vis Res 1993; 33: 1773–83.
8. Mollon JD, Bowmaker JK, Jacobs GH. Variations of colour vision in a new world primate can be explained by polymorphism of retinal photopigments. Proc Soc B 1984; 222: 373–99.
9. Jacobs GH. Within-species variations in visual capacity among squirrel monkeys (*Saimiri Sciureus*): color vision. Vis Res 1984; 24: 1267–77.
10. Jacobs GH, Neitz J. Color vision in squirrel monkeys: sex-related differences suggest the mode of inheritance. Vis Res 1985; 25: 141–43.
11. Jacobs GH, Neitz J. Polymorphism of the middle wavelength cone in two species of South American monkey: *Cebus apella* and *Callicebus moloch*. Vis Res 1987; 27: 1263–68.
12. Jacobs GH, Neitz J, Crognale M. Color vision polymorphism and its photopigment basis in a callitrichid monkey (*Saguinus fuscicollis*). Vis Res 1987; 27: 2089–100.
13. Ghosh KK, Goodchild AK, Sefton AE, Martin PR. The morphology of retinal ganglion cells in the new world marmoset monkey *Callithrix jacchus*. J Compar Neurol 1996; 366: 76–92.

14. Goodchild AK, Ghosh KK, Martin PR. Comparison of photoreceptor spatial density and ganglion cell morphology in the retina of human, macaque monkey, cat, and the marmoset *Callithrix jacchus*. J Compar Neurol 1996; 366: 55–75.
15. Wilder HD, Grünert U, Lee BB, Martin PR. Topography of ganglion cells and photoreceptors in the retina of a new world monkey: The marmoset (*Callithrix jacchus*). Vis Neurosci 1996; 13: 335–52.
16. Chan TL, Goodchild AK, Martin PR. The morphology and distribution of horizontal cells in the retina of a New World monkey, the marmoset *Callithrix jacchus*: A comparison with macaque monkey. Vis Neurosci 1997; 14: 125–40.
17. Lee BB, Silveira LCL, Yamada E, Kremers J. Parallel pathways in the retina of old and new world primates. Rev Brasil Biol 1996; 56: 323–38.
18. Lima SMA, Silveira LCL, Perry VH. Distribution of M retinal ganglion cells in diurnal and nocturnal new world monkeys. J Compar Neurol 1996; 368: 538–52.
19. Silveira LCL, Yamada E, Perry VH, Picanco-Diniz CW. M and P retinal ganglion cells of diurnal and nocturnal new-world monkeys. NeuroReport 1994; 5: 2077–81.
20. Yamada ES, Silveira LCL, Perry VH. Morphology, dendritic field size, somal size, density and coverage of M and P retinal ganglion cells of dichromatic *Cebus* monkeys. Vis Neurosci 1996; 13: 1011–29.
21. Yamada ES, Silveira LCL, Gomes FL, Lee BB. The retinal ganglion cell classes of New World primates. Rev Brasil Biol 1996; 56: 381–96.
22. Yeh T, Lee BB, Kremers J, Cowing JA, Hunt DM, Martin PR, Troy JB. Visual responses in the lateral geniculate nucleus of dichromatic and trichromatic marmosets (*Callithrix jacchus*). J Neurosci 1995; 15: 7892–904.
23. Kremers J, Weiss S. Receptive field dimensions of lateral geniculate cells in the common marmoset (*Callithrix jacchus*). Vis Res 1997; 37: 2171–81.
24. Kremers J, Weiss S, Zrenner E. Temporal properties of marmoset lateral geniculate cells. Vis Res 1997; 37: 2649–60.
25. Weiss S, Kremers J, Maurer J. Interaction between rod and cone signals in responses of lateral geniculate neurons in dichromatic marmosets (*Callithrix jacchus*). Vis Neurosci 1998; 15: 931–43.
26. Kremers J, Lee BB. Comparative retinal physiology in Anthropoids. Vis Res 1998; 38: 3339–44.
27. Shapley RM, Perry VH. Cat and monkey retinal ganglion cells and their visual functional roles. Trends Neurosci. 1986; 9: 229–35.
28. Enroth-Cugell C, Robson JG. The contrast sensitivity of retinal ganglion cells of the cat. J Physiol (London) 1966; 187: 517–52.
29. Lee BB, Pokorny J, Smith VC, Martin PR, Valberg A. Luminance and chromatic modulation sensitivity of macaque ganglion cells and human observers. J Opt Soc Amer A 1990; 7: 2223–36.
30. Kremers J, Lee BB, Yeh T. Receptive field dimensions of macaque retinal ganglion cells; In: Drum B, ed. Colour vision defiencies XII. Dordrecht, Boston, London: Kluwer Academic Publishers, 1995: 399–405.
31. Lee BB, Kremers J, Yeh T. Receptive field structure of primate retinal cells studied with a novel technique. Vis Neurosci 1998; 15: 161–75.
32. Derrington AM, Lennie P. Spatial and temporal contrast sensitivities of neurones in lateral geniculate nucleus of macaque. J Physiol 1984; 357: 219–40.
33. Blakemore CB, Vital-Durand F. Organization and post-natal development of the monkey's lateral geniculate nucleus. J Physiol 1986; 380: 453–91.

34. Crook JM, Lange-Malecki B, Lee BB, Valberg A. Visual resolution of macaque retinal ganglion cells. J Physiol 1988; 396: 205–24.
35. Kaplan E, Shapley RM. X and Y cells in the lateral geniculate nucleus of macaque monkeys. J Physiol 1982; 330: 125–43.
36. Lee BB, Wehrhahn C, Westheimer G, Kremers J. Macaque ganglion cell responses to stimuli that elicit hyperacuity in man: Detection of small displacements. J Neurosci 1993; 13: 1001–9.
37. de Monasterio FM, Gouras P. Functional properties of ganglion cells of the rhesus monkey retina. J Physiol 1975; 251: 167–95.
38. Croner LJ, Kaplan E. Receptive fields of P and M ganglion cells across the primate retina. Vis Res 1995; 35: 7–24.
39. Trollo D, Howland HC, Judge SJ. Visual optics and retinal cone topography in the common marmoset (*Callithrix jacchus*). Vis Res 1993; 33: 1301–10.
40. Kaas JH, Huerta MF, Weber JT, Harting JK. Patterns of retinal terminations and laminar organization of the lateral geniculate nucleus of primates. J Compar Neurol 1978; 182: 517–54.
41. Rosa MGP, Pettigrew JD, Cooper HM. Unusual pattern of retinogeniculate projections in the controversial primate *Tarsius*. Brain Behav Evol 1996; 48: 121–9.
42. Norton TT, Casagrande VA, Irvin GE, Sesma MA, Petry HM. Contrast-sensitivity functions of W-,X-, and Y-like relay cells in the lateral geniculate nucleus of bush baby, *Galago crassicaudatus*. J Neurophysiol. 1988; 59: 1639–55.
43. Norton TT, Casagrande VA. Laminar organization of receptive-field properties in Lateral Geniculate Nucleus of bush baby (*Galago crassicaudatus*). J Neurophysiol 1982; 47: 715–41.
44. Irvin GE, Casagrande VA, Norton TT. Center/surround relationships of magnocellular, parvocellular, and koniocellular relay cells in primate lateral geniculate nucleus. Vis Neurosci 1993; 10: 363–73.
45. Martin RD. Primate Origins and Evolution. A Phylogenetic Reconstruction. London: Chapman and Hall Ltd, 1990.
46. Napier JR, Napier PH. The Natural History of the Primates. London: British Museum (Natural History), 1985.
47. Kay RF, Ross C, Williams BA. Anthropoid origins. Science 1997; 275: 797–804.
48. Lee BB. Receptor inputs to primate ganglion cells. In: Gegenfurtner KR, Sharpe LT, eds. Color Vision: From Molecular Genetics to Perception. New York: Cambridge University Press, 1997: in press.
49. Perry VH, Oehler R, Cowey A. Retinal ganglion cells that project to the dorsal lateral geniculate nucleus in the macaque monkey. Neuroscience 1984; 12: 1101–23.
50. Rodieck RW, Binmoeller KF, Dineen J. Parasol and midget ganglion cells of the human retina. J Compar Neurol 1985; 233: 115–32.
51. Dacey DM, Petersen MR. Dendritic field size and morphology of midget and parasol ganglion cells of the human retina. Proc Nat Acad Sci USA 1992; 89: 9666–70.
52. Peichl L, Wässle H. Size, scatter and coverage of ganglion cell receptive field centres in the cat retina. J Physiol 1979; 291: 117–41. Lee BB. Receptive field structure in the primate retina. Vis Res 1996; 36: 631–44.
53. Lee BB, Wehrhahn C, Westheimer G, Kremers J. The spatial precision of macaque ganglion cell responses in relation to Vernier acuity of human observers. Vis Res 1995; 35: 2743–58.
54. Kulikowski JJ, Tolhurst DJ. Psyhophysical evidence for sustained and transient detectors in human vision. J Physiol 1973; 232: 149–62.

55. Merigan WH. P and M pathway specialization in the macaque; In: Valberg A, Lee BB, eds. From Pigments to Perception.Advances in Understanding Visual Processes. New York, London: Plenum Press, 1991: 1–9.
56. Merigan WH. Chromatic and achromatic vision of macaques: Role of the P pathway. J Neurosci 1989; 9: 776–83.
57. Schiller PH, Logothetis NK, Charles ER. Role of the color-opponent and broad-band channels in vision. Vis Neurosci 1990; 5: 321–46.
58. Schiller PH, Logothetis NK. The color-opponent and broad-band channels of the primate visual system. Trends Neurosci 1990; 13: 392–8.
59. Silveira LCL. Joint entropy loci of M and P cells: A hypothesis for parallel processing in the primate visual system. Rev Brasil Biol 1996; 56: 345–67.
60. Bowmaker JK, Astell S, Hunt DM, Mollon JD. Photosensitive and photostable pigments in the retinae of old world monkeys. J Exper Biol 1991; 156: 1–19.
61. Harosi FI. Cynomolgus and rhesus monkey visual pigments. Application of Fourier transform smoothing and statistical techniques of the determination of spectral parameters. J Gen Physiol 1987; 89: 717–43.
62. Baylor DA, Nunn BJ, Schnapf JL. Spectral sensitivity of cones of the monkey *macaca fascicularis*. J Physiol 1987; 390: 145–60.
63. MacNichol EF, Levine JS, Mansfield RJW, Lipetz LE, Collins BA. Microspectrophotometry of visual pigments in primate photoreceptors. In: Mollon JD, Sharpe LT, eds. Colour Vision. London: Academic Press, 1983: 13–38.
64. Dartnall HJA, Bowmaker JK, Mollon JD. Human visual pigments: microspectrophotometric results from the eyes of seven persons. Proc R Soc London, B 1983; 220: 115–30.
65. Jacobs GH, Neitz J. Inheritance of color vision in a New World monkey (*Saimiri Sciureus*). Proc Nat Acad Sci USA 1987; 84: 2545–9.
66. Jacobs GH, Deegan II JF, Neitz M, Neitz J. Presence of routine trichromatic color vision in new world monkeys. Inves Ophthalmol Vis Sci (Suppl) 1996; 37: 346 (Abstract).
67. Jacobs GH, Deegan II JF. Polymorphism of cone photopigments in new world monkeys: is the spider monkey unique? Invest Ophthalmol Vis Sci (Suppl) 1993; 34: 749 (Abstract).
68. Tovée MJ, Bowmaker JK, Mollon JD. The relationship between cone pigments and behavioural sensitivity in a new world monkey (*Callithrix jacchus jacchus*). Vis Res 1992; 32: 867–78.
69. Bowmaker JK. Visual pigments and colour vision in primates; In: Valberg A, Lee BB, eds. From Pigments to Perception. Advances in Understanding Visual Processes. New York, London: Plenum Press, 1991: 1–9.
70. Dartnall HJA, Arden GB, Ikeda GB, Luck CP, Rosenberg ME, Pedler CMH, Tansley K. Anatomical, electrophysiological and pigmentary aspects of vision in the bush baby: an interpretative study. Vis Res 1965; 5: 399–24.
71. Petry HM, Harosi FI. Visual pigments of the tree shrew (*tupaia belangeri*) and greater galago (*galago crassicaudatus*): A microspectrophotometric investigation. Vis Res 1990; 30: 839–51.

Address for correspondence: J.F. Kremers, Dept. of Experimental Ophthalmology, Röntgenweg 11, 72076 Tübingen, Germany
Phone: +7071 2985031; Fax: +7071 295777; E-mail: jan.kremers@uni-tuebingen.de

Documenta Ophthalmologica **95:** 247–255, 1999.

Assessment of stereopsis in rhesus monkeys using visual evoked potentials

PETER JANSSEN, RUFIN VOGELS & GUY A. ORBAN
Laboratorium voor Neuro- en Psychofysiologie, K.U. Leuven, B-3000 Belgium

Abstract. Rhesus monkeys can have deficiencies in stereo vision, making it necessary to screen monkey subjects intended for single cell studies of stereo-based depth processing. We measured VEPs in two monkeys using a dynamic random-dot display in which a stereo-defined checkerboard reversed in depth. Monkeys fixated upon a small dot during stimulus presentation. One monkey showed clear evoked potentials in response to changes in disparity that were similar to those obtained in human subjects, using an identical stimulus paradigm. Controls with presentations of the monocular stimulus sequences (in which no depth reversal can be perceived) yielded no or much weaker VEPs. In the other animal, however, there was no difference in evoked potential between the two conditions. These electrophysiological findings closely match the performance of these same two subjects in a disparity discrimination task in which they were previously trained. We conclude that VEPs using this type of stimulus display can be used to screen monkeys for single cell or behavioral studies of stereopsis.

Key words: macaque, stereopsis, VEP

Introduction

It has been shown that monkeys can see depth in random-dot stereograms (RDSs), and that their thresholds are very similar to those of humans [1–6]. Little is known, however, about abnormal stereopsis in rhesus monkeys. Experimentally induced binocular misalignment during the critical period can cause stereoblindness [7, 8], but the spontaneous incidence of stereodeficiencies in monkeys is unknown. The assessment of stereopsis is particularly important in single cell recording studies of disparity processing in extrastriate cortex, since stereodeficiencies could remain undetected if no behavioral control is present. However, monkeys that have been made stereoblind (and have very few binocular neurons in V1) can still be trained to discriminate depth in RDSs [9]. It is therefore possible that these animals perform at or just above their threshold level, which permits them to solve the task while still having poor stereopsis. Thus, the behavioral performance in a supra-threshold discrimination task is not a reliable indicator of the quality of stereoscopic depth perception. A possible solution is to measure stereo-thresholds behaviorally. However, this is very time-consuming, since it requires long training. Be-

cause we wanted a rapid and objective tool with which to screen monkeys for stereoblindness, and because VEPs have been recorded in both nonverbal and stereoblind human subjects [10, 11], we applied this technique for assessing stereopsis in rhesus monkeys.

Materials and methods

Subjects

Two male rhesus monkeys (*Maccaca mulatta*), weighing 8 and 10 kg respectively, were trained to sit in a primate chair and to fixate a small target on a computer screen. Both monkeys had a stainless steel head post cemented on the skull and a recording well implanted over the left frontal lobe (for surgical procedures see [12]). Both had a mild myopia (−2.5D) in the right eye, which was corrected for the VEP recordings. The left eye showed no refractive error. Two human observers with normal or corrected to normal vision and excellent stereopsis also served as subjects.

Apparatus

The stimuli were presented dichoptically by means of two liquid crystal shutter glasses which were placed in front of the monkey's eyes. The shutters opened alternately at a rate of 60 Hz, synchronized with the frame rate of the computer monitor (Barco MWD 321, frame rate 120 Hz). Figure 1 gives a schematic illustration of the stimulus presentation. During the recordings, the monkey was placed in a dimly lit room at a distance of 86 cm from the screen. Head movements were restrained by a head post and eye movements were monitored using the scleral search coil technique [13]. The animal was required to fixate a small spot in the center of the screen for 500 msec, after which the stimulus was presented. Reward (a drop of apple juice) was given at randomized intervals as long as the animal continued to fixate. The human subjects viewed the stimulus through identical shutters (adjusted for the difference in interpupillary distance). They were placed in a chin rest at the same viewing distance, and were instructed to fixate the small spot on the screen. Timing of events and recording of the VEP were identical to the procedure described above.

Stimuli

The stimulus was a 12 degree diameter dynamic RDS (dot size 7', density 50%, luminance 125 cd/m^2). When viewed stereoscopically, it was perceived as a 2×2 checkerboard that reversed in depth. The random-dot pattern

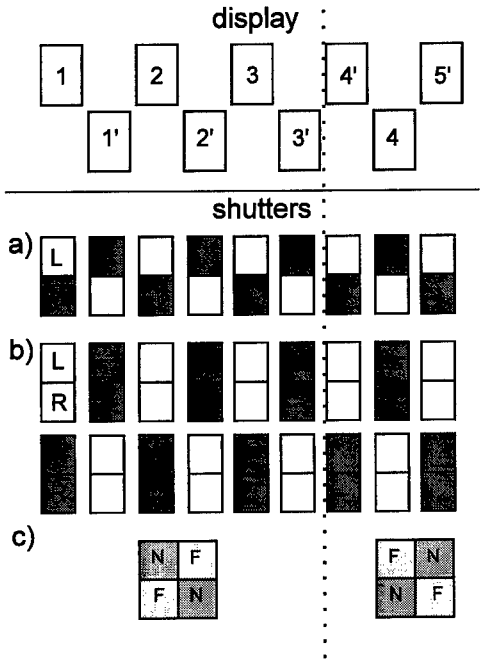

Figure 1. Schematic illustration of the dichoptic stimulus presentation. Top: 1, 2, 3, etc. represent different noise patterns presented successively to the left eye. 1′, 2′, 3′, etc. are the noise patterns presented to the right eye, which are identical except for a horizontal shift in position of the dots in order to create disparity. The dotted vertical line indicates the change in disparity at which the VEP-recording was triggered. At this point, the noise patterns are switched between the left and the right eye. Bottom: in the stereo-condition (a), both shutters open and close alternately at 120 Hz. In the monocular control condition (b), both shutters open and close together, so both eyes view either the left eye image or the right eye image. In (c), a schematic illustration of the stimulus in the stereo condition is depicted (F= far, N= near).

changed at a rate of 60 Hz. To obtain a reversal in depth, the random-dot patterns for the two eyes were switched (Figure 1, top row): the pattern which should have been presented to the right eye was shown to the left eye and vice versa. In the control condition, the same stimulus sequence on the display was run, but the shutters for the left and right eye opened and closed together at 60 Hz. Thus, the images were always identical for both eyes. Since no disparity is present, one perceives only a flat plane with a texture of moving random dots. Blocks in which both eyes viewed the left eye image were averaged with blocks in which both eyes viewed the right eye image (Figure 1, bottom row).

We also recorded VEPs in both animals using random-dot correlograms (RDCs). In this type of stimulus, both eyes view the same noise pattern which is changed at 40 Hz (correlation). The impression is identical to the

monocular presentation of the dynamic RDS. After a certain period of time, different patterns are presented to left and right eye (uncorrelation), which yields a vague, unstable percept of depth. The monocular control condition is created in the same way as for the RDSs (Figure 1, bottom row). Since the two patterns are always correlated in this case, one also perceives a flat plane of moving random dots.

VEP recording

The active electrode was positioned on a screw that was fixed in the skull of each animal, approximately above central V1 of the left hemisphere. The reference electrode was attached to the recording chamber above the left frontal lobe. The signal was sampled at 1000 Hz, amplified 200,000 times and filtered with a low frequency cut-off of 1 Hz and a high frequency cut-off of 30 Hz. Experimental and control conditions were carried out in blocks of 200 sweeps and interleaved to control for changes in VEP amplitude. VEP recording started 1400 msec after stimulus onset, 500 msec later the checkerboard reversed in depth and another 500 msec later it returned to its original disparity. This sequence was repeated as long as the subjects maintained fixation. The evoked potentials were averaged over 3 or 5 blocks of 200 sweeps (yielding a total of 600 or 1000 sweeps, respectively), and smoothed by adjacent averaging, whereby every data point is replaced by the average of that point and 8 points on either side.

In the human subjects, 10 mm diameter silver oxide cup electrodes were placed at OZ (90% of the distance between nasion and inion), on the forehead (reference electrode) and at the left mastoid (ground). Timing of events and recording of the VEP was identical to the procedure described above.

Results

Figure 2 shows the evoked potentials of both monkeys and human subjects at different disparities. For the disparity of 29 arc min, the second monkey's VEP consists of a positive peak with a latency of 175 msec, followed by a negative trough after 249 msec. The control condition yielded a very different response. Moreover, the shape and latency of the stereo-VEP were very similar to those of our human observers (latencies of 169 and 177 msec, respectively). The first monkey's VEP, however, has a much smaller latency (95 msec) and is almost identical to the potential in the control condition. The presence or absence of binocular disparity did not yield a difference in VEP in this animal, which suggests that this subject has poor stereopsis. These results fit well with the performance of both monkeys in a disparity discrimination

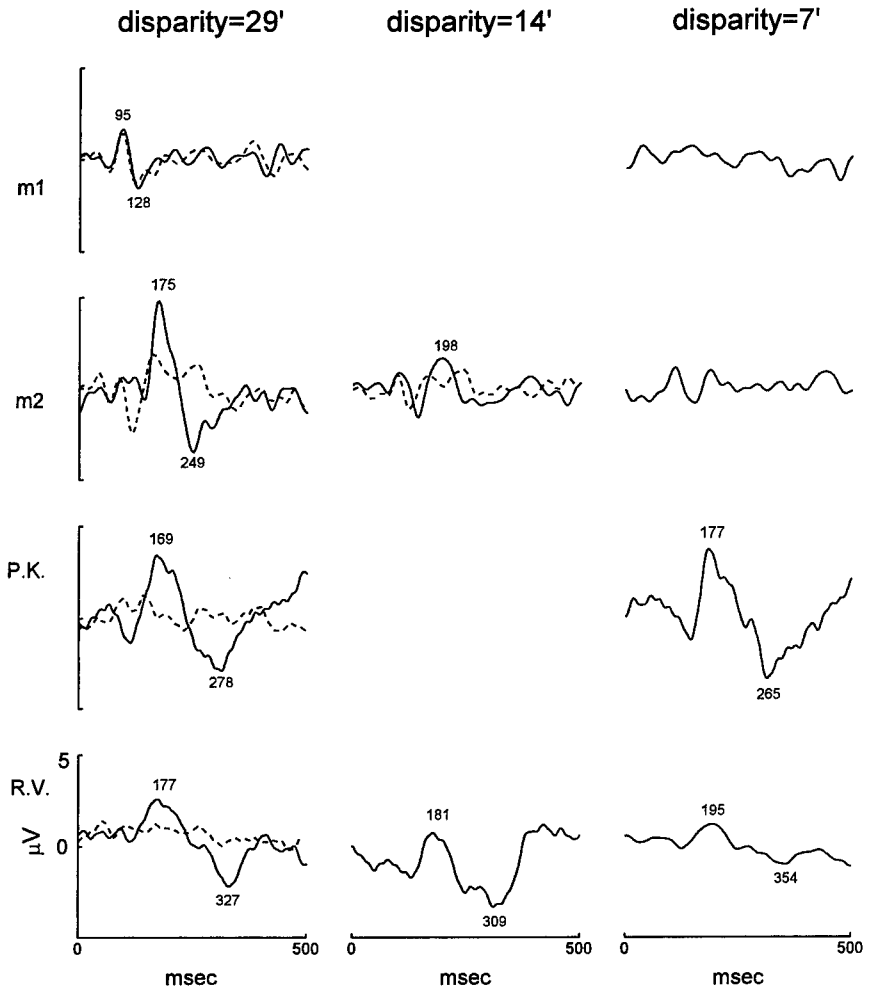

Figure 2. VEPs recorded in monkeys (m1 and m2, averages over 1000 sweeps) and in humans (P.K. and R.V., averages over 600 sweeps) with RDSs at three different disparities (columns). Full lines represent the evoked potentials in the stereo-condition and dashed lines the evoked potentials of the monocular control condition. The numbers in every plot indicate the latencies of the peaks in msecs. The change in disparity was at 0 msec.

task in which they were previously trained. Whereas the mean performance of monkey 2 was 84% correct responses (chance level was 50%), monkey 1 only reached 72% correct after extensive training.

When the disparity in the stimulus was reduced to 7 arc min, a clear VEP was no longer present in monkey 2, although both human observers still showed a response at this disparity. A small VEP could be seen only at

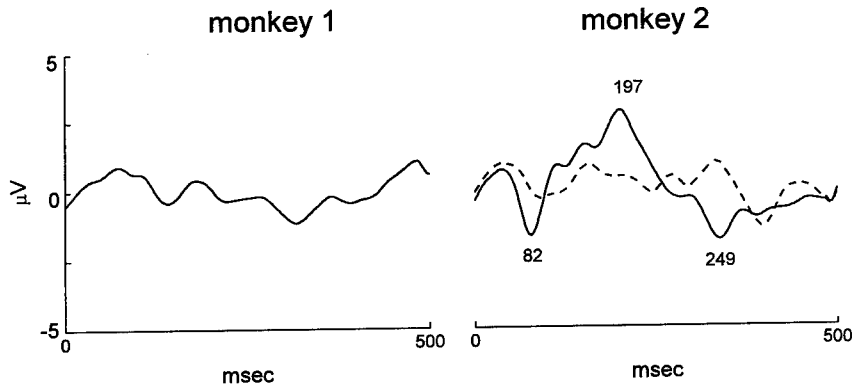

Figure 3. VEPs in monkeys recorded with RDCs. Full lines represent the evoked potentials in the stereo-condition and dashed lines the evoked potentials in the monocular control condition (averages over 600 sweeps). The change from correlation to uncorrelation was at 0 msec.

the intermediate disparity of 14 arc min., suggesting that – at least in terms of evoked potentials – this animal has an elevated stereo threshold. As was the case for the larger disparity, monkey 1 did not show an evoked potential at the smallest disparity. In all subjects tested, there was a tendency towards longer VEP latencies with smaller disparities.

There is a theoretical possibility that binocular neurons could be present even though no disparity-tuned cells exist [14]. To test this, we recorded the evoked potentials elicited by RDCs in both monkeys. A clear VEP with this type of stimulus indicates the presence of binocular cells. In Figure 3, it can be seen that no VEP was recorded in monkey 1 when the stimulus changed from correlated to uncorrelated. On the other hand, monkey 2 showed – as expected from the results with the RDSs – a distinct response relative to the monocular control condition.

Discussion

Numerous authors have recorded stereo-VEPs in verbal and nonverbal human subjects [15–24]. In macaque monkeys, Miezin et al. [25] recorded evoked potentials in response to dynamic RDCs, and proposed this technique as a test for cyclopean perception. However, as explained above, the presence of a VEP to correlated-uncorrelated shifts simply suggests the presence of neurons which receive input from the two eyes. Our recordings with the RDC match closely with the stereogram-VEPs, and to our knowledge no dissociation in VEP has been reported between these two types of stimuli. Nevertheless, because evoked potentials to RDCs do not actually depend on

the presence or absence of disparity-tuned cells (which are believed to be crucial for stereoscopic depth perception), this test is of little use to researchers who wish to screen monkeys for stereoblindness.

Our results demonstrate that evoked potentials to dynamic RDSs can be reliably recorded in rhesus monkeys. Moreover, the electrophysiological assessment of stereopsis has several advantages over the behavioral training of the animals in a disparity discrimination task. Since the evoked potential is the result of the firing of large groups of neurons, the finding of a clear VEP not only permits to conclude that there is stereoscopic depth perception, but also that the disparity in the stimulus is well above threshold. Secondly, a stereodeficiency is revealed by the absence of an evoked potential following a change in disparity: monkey 1 had great difficulties in doing the task, and showed no response to the disparity shift or to the correlated-uncorrelated shift, whereas monkey 2 could discriminate depth and had a clear stereo-VEP. Note, however, that the performance of our stereodeficient monkey (72% correct) was significantly above chance level (50%). It is very well possible that after prolonged training, this monkey would have reached a higher level of performance, despite the apparent lack of input from corresponding points on the two retinas. Finally, VEP-recording is a very time-saving technique: training can take several months, and rhesus monkeys very easily learn to discriminate on the basis of any monocular cue in the stimulus that has been overlooked [2].

The second finding of this study is that stereo-VEPs in monkeys are remarkably similar to those of human subjects. In all three subjects with stereo vision (monkey 2, P.K. and R.V.), the latencies of the first peak of the evoked potential lay within a range of 10 msec (between 169 and 177 msec), while the negative trough was more variable between subjects. The results of the control condition differed between monkeys and humans, since in this condition, a small and early potential was recorded in both monkeys while the human observers showed no response at all. One possible source of these 'monocular' VEPs could be the cross-talk between the images for the left and the right eye. At slow speeds of motion, human observers could see some low-contrast dots belonging to the other image in this condition. Although this was not the case at the high speed (60 Hz) used in the VEP-recordings, it is possible that our monkeys responded to these small stimulus artifacts. However, the latency of this response was clearly different from the latency of the stereo-VEPs.

Several studies have used VEPs to estimate the psychophysical stereothreshold [11, 20]. Since we were unable to test more than one disparity in a single session (due to technical limitations) and since there was a large variability in VEP-amplitude from day to day in our monkeys, it was difficult

to interpret these differences. Therefore, we did not apply linear regression to the VEP-amplitudes in order to estimate the stereo-threshold of monkey 2. Additionally, the disparities used in the behavioral training were relatively large (33 arc min). Thus, based on the absence of an evoked potential with small disparities, we can only speculate that this animal has an elevated stereothreshold.

We conclude that the electrophysiological assessment of stereopsis in macaque monkeys is useful. It is a rapid, time-saving technique and has the important advantage of being objective, in that it reflects the presence of true stereopsis.

Acknowledgements

We thank W. Spileers for the eye coil surgery and for his help on the VEP recordings, J.V. Odom for his suggestions on the stimulus, S. Raiguel for his critical reading of the manuscript, M. Depaep who did the programming and P. Kayenbergh and G. Meulemans for technical assistance. This study was supported by the FWO Vlaanderen (research grant G.0172.96) and by GOA 95/6. P. Janssen is a research assistant and R. Vogels is a research associate of the FWO Vlaanderen.

References

1. Bough EW. Stereoscopic vision in the macaque monkey: a behavioural demonstration. Nature 1970; 225: 42–44.
2. Cowey A, Parkinson AM, Warnick L. Global stereopsis in rhesus monkeys. Quater J Exp Psych 1975; 27: 93–109.
3. Julesz B, Petrig B, Buttner U. Fast determination of stereopis in rhesus monkeys using dynamic random-dot stereograms. J Opt Soc Am 1976; 66: 1090.
4. Harwerth RS, Boltz RL. Stereopsis in monkeys using random dot stereograms: the effect of viewing duration. Vis Res 1979; 19: 985–991.
5. Harwerth RS, Smith EL, Siderov J. Behavioral studies of local stereopsis and disparity vergence in monkeys. Vis Res 1995; 1755–1770.
6. Crawford MLJ, von Noorden GK, Harwerth RS, Smith EL. Judgments by monkeys of apparent depth in dynamic random-dot stereograms. Behav Brain Res 1996; 79: 219–225.
7. Crawford MLJ, Pesch TW, von Noorden GK. Excitatory binocular neurons are lost following prismatic binocular dissociation in infant monkeys. Behav Brain Res 1996; 227–232.
8. Harwerth RS, Smith EL, Crawford MLJ, von Noorden GK. Stereopsis and disparity vergence in monkeys with subnormal binocular vision. Vis Res 1997; 37: 483–493.
9. Crawford MLJ, Harwerth RS, Smith EL, von Noorden GK. Loss of stereopsis in monkeys following prismatic binocular dissociation during infancy. Behav Brain Res 1996; 79: 207–218.

10. Petrig B, Julesz B, Kropfl W, Baumgartner G, Anliker M. Development of stereopsis and cortical binocularity in human infants: electrophysiological evidence. Science 1981; 213: 1402–1405.
11. Chao G-M, Odom JV, Karr D. Dynamic stereoacuity; a comparison of electrophysiological and psychophysical responses in normal and stereoblind observers. Doc Ophthalmol 1988; 70: 45–58.
12. Kovacs G, Vogels R, Orban GA. Selectivity of macaque inferior temporal neurons for partially occluded shapes. J Neurosc 1995; 15: 1984-1997.
13. Judge SJ, Richmond BJ, Chu FC. Implantation of magnetic search coils for measurement of eye position: an improved method. Vis Res 1980; 20: 535–538.
14. Livingstone MS, Nori S, Freeman DC, Hubel DH. Stereopsis and binocularity in the squirrel monkey. Vis Res 1995; 35: 345–354.
15. Regan D, Spekreijse H. Electrophysiological correlate of binocular depth perception in man. Nature 1970; 225: 92–94.
16. Julesz B, Kropfl W, Petrig B. Large evoked potentials to dynamic random-dot correlograms and stereograms permit quick determination of stereopsis. Proc Natl Acad Sci USA 1980; 77: 2348–2351.
17. Herpers MJ, Caberg HB, Mol JMF. Human cerebral potentials evoked by moving dynamic random dot stereograms. Electroenceph Clin Neurophysiol 1981; 52: 50–56.
18. Fukai S. Topographic visually evoked potentials induced by stereoptic stimulus. Br J Ophthalmol 1984; 69: 612–617.
19. Norcia AM, Sutter EE, Tyler CW. Electrophysiological evidence for existence of coarse and fine disparity mechanisms in human. Vis Res 1985; 25: 1603–1611.
20. Wesemann W, Klingenberger H, Rassow B. EIectrophysiological assessment of the human depth-perception threshold. Graefe's Arch Clin Exp Ophthalmol 1987; 225: 429–436.
21. Teping C, Silny J. Evidence of pericentral stereopsis in random dot VECP. Doc Ophthalmol 1987; 66: 261–266.
22. Manning ML, Finlay DC, Dewis SAM, Dunlop DB. Detection duration thresholds and evoked potential measures of stereosensitivity. Doc Ophthalmol 1992; 79: 161–175.
23. Rawlings SC, Yates JT. Dynamic depth reversal stereograms. Ophthalmology 1979; 86: 1462–1470.
24. Skandries W. Depth perception and evoked brain activity: the influence of horizontal disparity and visual field location. Vis Neurosc 1997; 14: 527–532.
25. Miezin FM, Myerson J, Julesz B, Allman JM. Evoked potentials to dynamic random-dot correlograms in monkey and man: a test for cyclopean perception. Vis Res 1981; 21: 177–179.

Address for correspondence: R. Vogels, Laboratorium voor Neuro- en Psychofysiologie, Herestraat 49, 3000 Leuven, Belgium
Phone: (0)16 34 58 57; Fax: 34 59 93

Documenta Ophthalmologica **95:** 257–269, 1999.

Maturation of Binocular Luminance Interaction in normal young and adult rhesus monkeys

J. VERNON ODOM[1,2], RICK J. BROWN[1,3] & RONALD G. BOOTHE[1,3]
[1]*Yerkes Regional Primate Research Center, Emory University, Atlanta, GA 30322, USA;* [2]*Departments of Ophthalmology and Psychology, West Virginia University Health Sciences Center, Morgantown, WV 26506, USA;* [3]*Departments of Psychology and Ophthalmology, Emory University, Atlanta, GA 30322, USA*

Abstract. Purpose: Our aim was to answer three questions 1) Do adult rhesus monkeys have binocular luminance interactions (BLIs) similar to those found in adult humans? 2) Is BLI in very young rhesus monkeys functionally mature? 3) If not, how does it change with age?

Methods: We recorded visually evoked potentials (VEPs) in response to sinusoidally modulated uniform fields. The fields were presented dichoptically by varying the relative temporal phase between the two eyes. Monkeys varied in age from 5.6 weeks to 5.25 years.

Results: VEPs were Fourier analyzed and the relative second harmonic amplitudes were taken as the response measure. The second harmonic amplitudes in adult monkeys had an asymmetrical 'V-shaped' function as interocular phase difference (IPD) varied from 0° to 180°, as had been observed previously in adult humans [1]. The youngest monkeys exhibited a symmetrical pattern which became more asymmetrical at older ages and was adult like by about 19 weeks. Asymmetry magnitude and log age correlated 0.97 ($p < 0.05$) in the monkeys younger than 19 weeks.

Conclusions: The adult rhesus data are consistent with a model derived from humans which involves two types binocular luminance processing. One combines monocular responses nonlinearly (MNL) and a second combines monocular responses linearly followed by a binocular nonlinearity (MLBNL). These two processes have been associated with the parvocellular (P-) and magnocellular (M-) streams. Within this framework, the data from the youngest monkeys indicate that BLI in the P-stream is relatively less mature at birth than that in the M-stream and develops reaching functional maturity on these measures by around 19 weeks.

Key words: binocular vision, magnocellular and parvocellular pathway, rhesus monkey, visual development, vision models

The magnocellular (M) and parvocellular (P) pathways form two partially separable streams of visual processing up to the cortex [1, 2]. These two pathways appear to subserve different aspects of normal binocular vision [3], the P-stream serving fine, static stereopsis and the M-stream coarse, dynamic stereopsis. Moreover, the two pathways are differentially affected by abnormal binocular visual experience; mild blur of the retinal image in one eye during early development appears to affect mostly the P-stream [4], while other developmental abnormalities, such as congenital esotropia, appear to affect primarily the M-stream [3]. However, little is known about the relative development of the two pathways and their respective binocular functions.

Anatomically, parvocellular neurons in the lateral geniculate nucleus and parvocellular derived afferents in visual cortex appear to mature earlier than their magnocellular counterparts [4]. However, based on functional grounds, one might expect the M-stream to mature earlier due to the fact that functions such as sensitivity to flicker and motion asymmetry appear to reach functional maturity at an early age, whereas fine spatial resolution develops over a more protracted postnatal period [4].

If one varies the phase of sinusoidally modulated light presented to one eye relative to that presented to the other eye in humans, the resulting VEPs and behavioral thresholds show evidence of two types of processing, one of which combines monocular nonlinear responses (MNL) and a second which first combines monocular linear responses followed by a purely binocular nonlinearity (MLBNL) [5–8]. Based on evidence such as the fact that the second pathway is not needed to describe binocular luminance interactions at higher temporal frequencies, these two pathways have been identified with the M- and P-streams, respectively [5].

In the current study, we wished to provide a description of the normal development of binocular luminance interaction in monkeys. To determine if normal adult monkeys would show the same pattern of binocular luminance interactions as adult humans, we first tested an adult monkey and an adult human under conditions similar to those used by Odom and Chao [5]. This initial study established that the normal adult monkey exhibited binocular luminance interactions qualitatively similar to those seen in normal adult humans. Then, we tested young monkeys over an age range of 5 to 19 weeks to determine the normal development of these interactions. These developmental results were analyzed to obtain, by inference, a measure of the relative development of the M- and P-streams.

Methods

Subjects

Three sets of subjects were tested for different purposes. One normally-reared, adult, female rhesus macaque aged 5 years was tested to determine if the pattern of binocular luminance interaction observed in human adults would also be observed in adult rhesus monkeys. Four normally-reared, young rhesus macaques aged 5.6, 7.6, 12, and 19 weeks were tested to determine if there was an age related trend in the development of binocular luminance interaction. The youngest and oldest were females and the two middle monkeys were male. All procedures performed on these monkeys were done in strict compliance with the ARVO resolution on the Use of Animals in Research.

One woman, aged 22 years, served as a human control tested under stimulus conditions identical to those used with the young monkeys. She was informed of the nature and purposes of the experiments and gave her informed consent. She had normal visual acuity and no history of binocular vision problems.

Stimulus

Uniform field stimuli were presented to the subjects dichoptically with goggles. The luminances of red light emitting diodes (peak wavelength of 660 nm) were modulated sinusoidally in each goggle. The fields presented to each eye had the same mean luminance (51 cd/m^2), temporal frequency (2 Hz) and modulation depth (70%). Young monkeys tended to close their eyes during testing so that the luminance through their lids during their tests approximated 2.5 cd/m^2. The adult monkey was tested under two luminance conditions; with unattenuated goggles and with a neutral density and diffusing filter in place that achieved an attenuation of 1.3 log units (2.5 cd/m^2). The adult human was instructed to keep her eyes closed during testing so that the luminance would approximate that of the young monkeys.

During the experiment, the phase of the stimulus presented to the right eye was kept constant while the phase of the stimulus presented to the left eye was varied. The relative phase difference between the two eyes, the interocular phase difference (IPD), ranged from 0° to 180° in 45° steps. The order of the five IPDs was pseudo-randomly assigned during a given experimental replication. A minimum of three replications were performed for each subject.

VEP recording

Prior to electrode placement and testing young monkeys were injected with a mild sedative, butorphanol tartrate (Torbutrol), at a dose of 0.05 mg/kg and wrapped in a cloth blanket. The young animals tended to close their eyes during testing, probably due to their sedated state and the repetitive stimulus conditions. However, this did not appear to be a sleep state as removing the goggles usually resulted in immediate opening of the eyes and alert looking around. The adult rhesus was anesthetized with a low dose of ketamine to facilitate placing her in a primate testing chair. She was permitted to recover from the anesthetic, sedated with the butorphanol tartrate as with the young monkeys, and then tested. Even under sedation she remained alert and generally appeared to keep her eyes open.

VEPs were recorded in monkeys using subdermal electrodes of about 10 mm in length. In young monkeys, the active electrode was placed 10 mm

above the inion and 5–15 mm to the left of the midline, referred to the vertex along the midline and grounded to a midfrontal location. In the adult monkey, the position of the active electrode was 20 mm above the inion and 10-20 mm to the left of the midline. VEPs were recorded from the adult human using a midline electrode configuration with an active electrode at O_Z, referred to the vertex and grounded to the forehead. Signals were amplified using a Grass amplifier (model P511) with a half amplitude band pass of 0.3 to 100 Hz. The amplified electroencephalograms were averaged using an Apple II^+ computer and stored for later analysis. Averaging was triggered by a pulse synchronized with the stimulus with constant phase presented to the right eye. The duration of each sweep was 1480 ms.

VEP amplitudes at the second harmonic of the stimulus frequency were used as the response measure. These were derived from the averaged VEP responses using the Fast Fourier Transform (FFT). The amplitudes and phases of ti : second harmonics for a particular subject at a particular IPD were vector averaged within a session. Across sessions or subjects amplitudes and phases were averaged using scalar values.

We standardized second harmonic amplitudes and phases for each subject to allow comparisons across conditions where absolute levels might differ and to permit comparison of experimental results with modeled results. The relative amplitudes were obtained by dividing the absolute amplitudes by the amplitude at IPD=0°, and the relative phases were obtained by subtracting the phase at IPD=0° from the absolute phases for each condition.

Results

1) Model's predicted results

The lights used as the stimuli in the experiment were sinusoidally modulated. Thus we can use the following formulas to express the inputs to the left eye

*Figure 1.*a) Schematic of the model described by Odom and Chao [5]. Linear operations are designated by boxes and nonlinear operations by triangles. The output that contributes to the VEP comes from two types of internal processing: one which combines monocular nonlinear responses (MNL) is illustrated with dashed lines and a second which combines monocular linear responses followed by a purely binocular nonlinearity (MLBNL) is shown by the thin solid lines. b) The model's predicted second harmonic amplitudes as the relative contributions of the two pathways varies. The asterisk (*) indicates the prediction if only the MNL pathway is operating such that the MLBNL makes no contribution. Filled symbols show predictions in cases where the MLBNL process sums, open symbols when the MLBNL subtracts. Squares indicate the prediction if only the MLBNL process is operating. Circles indicate the predictions if both pathways are present and make an equal contribution.

(a)

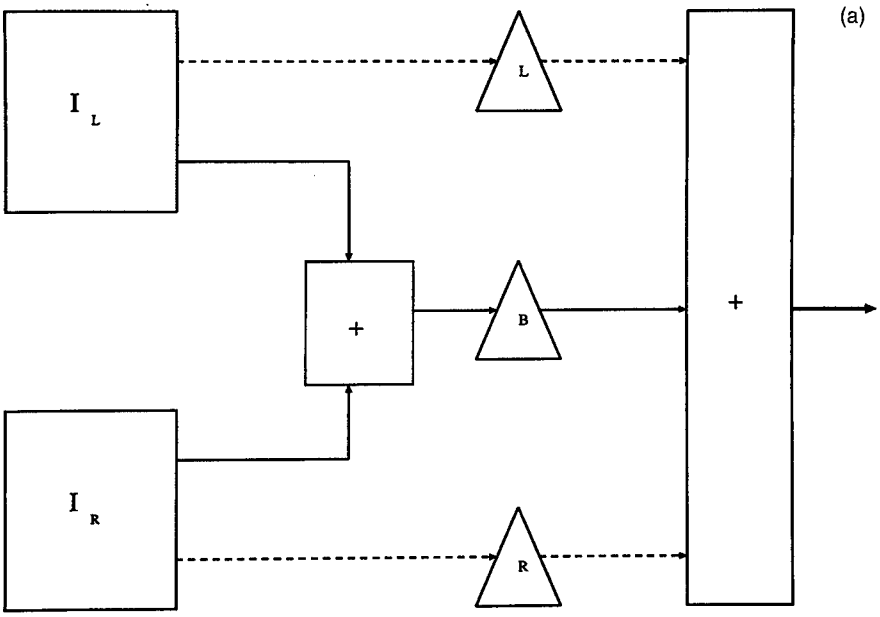
I L
I R
L
B
R
+
+

(b)

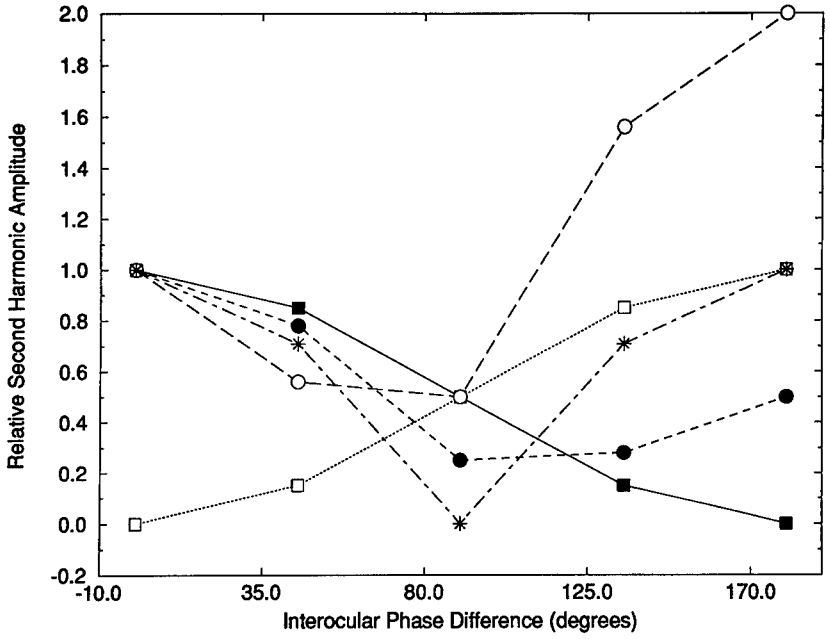
Relative Second Harmonic Amplitude
2.0
1.8
1.6
1.4
1.2
1.0
0.8
0.6
0.4
0.2
0.0
-0.2
-10.0
35.0
80.0
125.0
170.0
Interocular Phase Difference (degrees)

and right eye:

$$I_L = L + S^* cos(2\pi f t + \phi)$$

$$I_R = L + S^* cos(2\pi f t)$$

where I_L and I_R are the inputs as a function of time (t) to left and right eyes, respectively; L is the mean luminance, f is the temporal frequency, S the modulation depth, and ϕ the initial phase. Note that L, S, and f are constant so that ϕ is the only parameter allowed to vary.

If I_L and I_R provide the input to the model of Odom and Chao [5] that is illustrated schematically in Figure 1a, then the outputs from the model can be predicted through appropriate calculations [6, 7]. Some examples of predicted relative second harmonics amplitudes as a function of phase are shown in Figure 1b. As long as the MNL makes some contribution to the output, the predicted responses have a 'V' shaped function as interocular phase difference (IPD) varies from 0° - 180° with a trough at IPD=90°. The relative strengths of the contributions MLBNL and MNL adjust the asymmetric property of the 'V' shape as illustrated in Figure 1b. When the contribution from the MLBNL is zero, the 'V' shape is symmetrical because the relative amplitudes at IPD=180° and at IPD=0° are the same. With increasing contribution from the MLBNL the amplitude, one observes an increasingly asymmetric 'V' shape. Relative amplitude at IPD=180° decreases relative to that at IPD=0° if the linear responses are summed prior to the binocular nonlinearity, but relative amplitude at IPD=180° decreases relative to that at IPD=0° if the linear responses are subtracted prior to the binocular nonlinearity.

Comparison of adult rhesus with adult humans and with the model of binocular luminance interaction

Some typical examples of averaged VEP waveforms are shown in the panel on the left in Figure 2. The data were collected from the adult monkey for the 0°, 90° and 180° IPD conditions during one replication in which the luminance level was 2.5 cd/m^2. The shape and waveform of the VEPs varies with IPD. The second harmonic amplitudes and phases of the waveforms on the left of Figure 2 were calculated using FFTs and displayed on the right in Figure 2 along with the second harmonic amplitudes and phases of three other replications acquired under the same conditions. The results in Figure 2 indicate that second harmonic amplitude is largest at 0° reaches a minimum at 90° and has a second maximum at 180°.

In Figure 3, the relative second harmonic amplitudes are presented for our adult monkey subject at the two luminance levels. For comparison, human

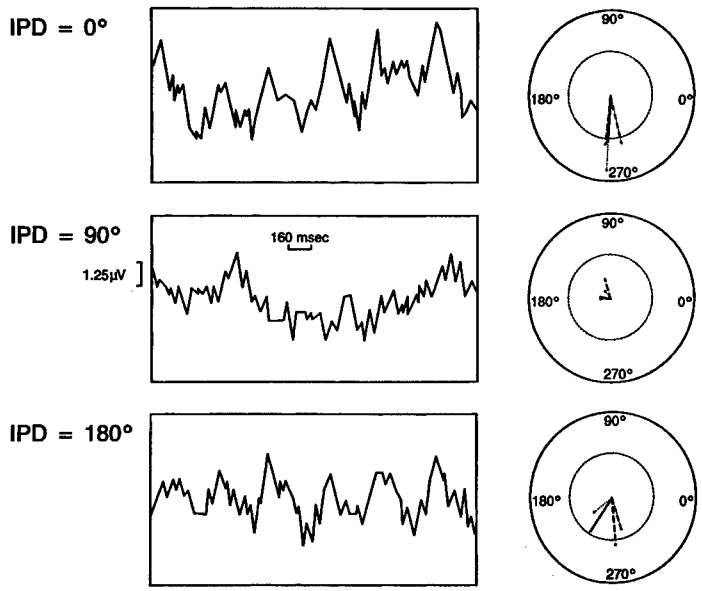

Figure 2. Data for the 0°, 90° and 180° interocular phase difference (IPD) conditions are presented for the adult monkey. On the left of the figure waveforms from one replication of the 0°, 90° and 180° interocular phase difference (IPD) conditions are presented. Mean luminance was 2.5 cd/m^2. Large vertical divisions are separated by 1.25 microvolts (μV). Large horizontal divisions are separated by 160 msec. On the right second harmonic amplitudes and phases for the four replications, calculated using a Fast Fourier Transform (FFT), are plotted as vectors on polar coordinates. The inner circle represents an amplitude of 0.4 μV and the larger circle represents an amplitude of 0.8 μV. The replications, one through four, are represented by different lines, solid, dotted, dashed and dot-dash, respectively. In those cases where four lines cannot be resolved in the figure, it indicates that two replications had very similar amplitudes and phases.

data from three adult human subjects tested previously by Odom and Chao [5] are presented as well. The results obtained at low luminance levels are presented in Figure 3a, including the results for the additional human subject tested during this study. As discussed previously [5, 6], the results are consistent with an additive model at low light levels and this conclusion can be verified by comparing the results in Figure 3a with the additive model predictions in Figure 1b. Similarly, as discussed previously [5], the results are consistent with a subtractive model at higher light levels which can be verified by comparing the results in Figure 3b with the subtractive model prediction in Figure 1b. The results from the monkey observer and the human observers have similar shapes at both luminances from which we conclude that IPD and mean luminance have the same qualitative effects on binocular interaction in the two species.

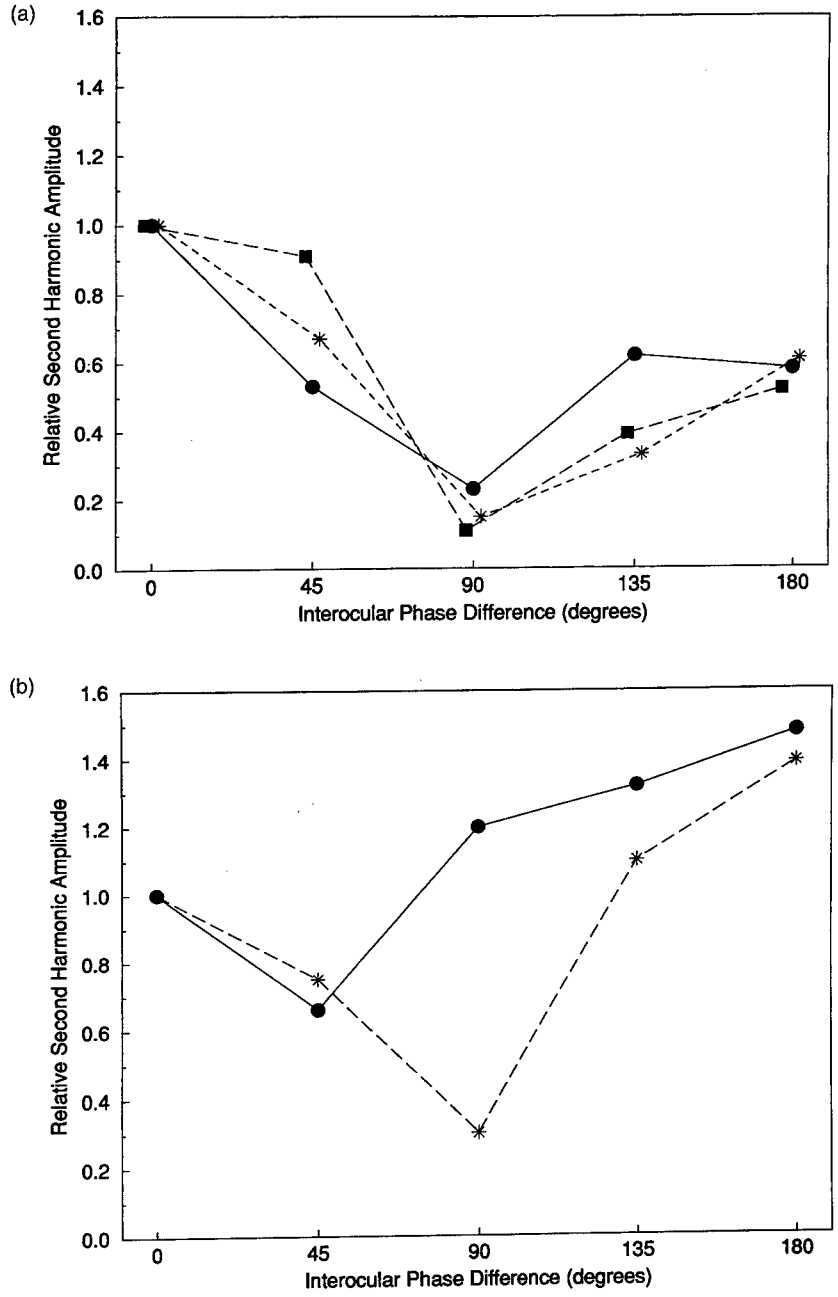

Figure 3. The relative second harmonic amplitude of the adult rhesus is presented as a function of interocular phase difference under two luminance conditions. Low luminance data are presented in Figure 3a. The circle symbols show results for the adult monkey and the square symbols results for the adult human. Asterisk symbols are mean values for three adult human subjects tested by Odom and Chao [5]. High luminance data are presented in Figure 3b for the adult monkey and for the three adult humans tested by Odom and Chao [5]. Symbols in 3b are the same as in 3a.

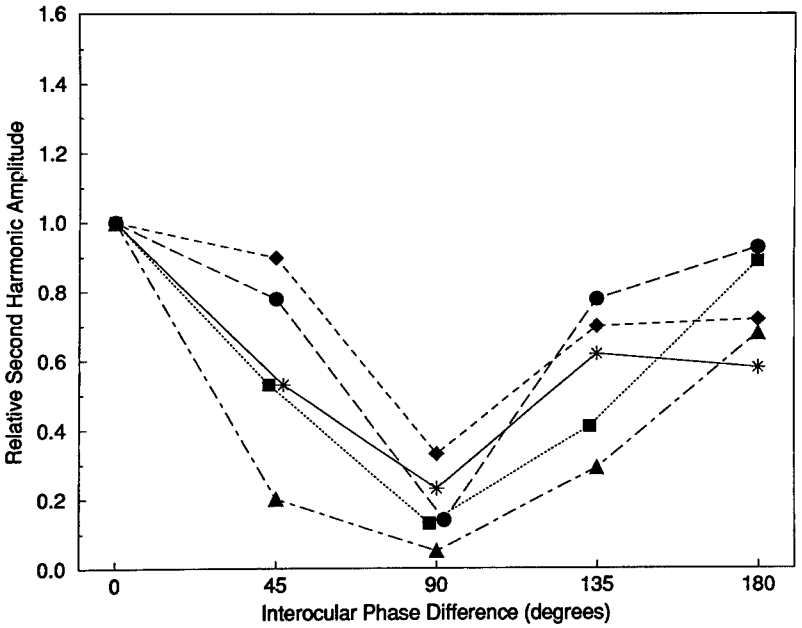

Figure 4. The relative second harmonic amplitudes are shown for each of the four young-rhesus subjects. The young rhesus macaques aged 5.6, 7.6, 12, and 19 weeks are represented by circles, squares, diamonds, and triangles, respectively. Mean values for the adult monkey are replotted from Figure 3a for comparison using asterisks as symbols.

The magnitudes of second harmonics in the VEP responses at various IPDs reflect cortical binocular interaction. The similarity of monkey and human binocular interaction demonstrated by the data in Figure 3, suggest an underlying similarity in the neural processes of the two species by which information from the two eyes are combined. Comparing the monkey and the human results to the prediction of the model presented in Figure 1 confirms that results from both are consistent with a combination of MLBNL and MNL processing.

Maturation of binocular luminance interaction: comparisons of young rhesus monkeys with adult rhesus and humans

All of the results for our young subjects were obtained at low luminance levels. Figure 4a shows a plot of the relative amplitudes of the second harmonics versus IPDs for these young subjects. The second harmonic amplitudes show asymmetrical 'V' shaped curves with troughs at IPD=90°. The relative values of the amplitudes at IPD=180° are consistently smaller than that at

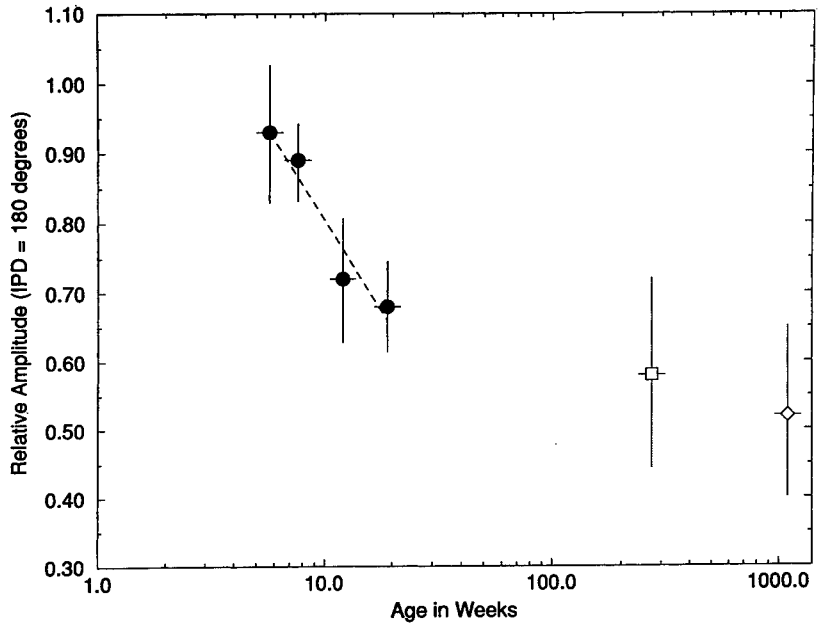

Figure 5. The relative amplitude at IPD = 180° is plotted as a function of log age in weeks. The data of the four younger monkeys have been fit with a regression line with the equation: Relative Amplitude = –0.52 * (log weeks of age) + 1.325. The data for the adult monkey (about 273 weeks) and adult human (about 1144 weeks) are presented for comparison. Error bars represent the standard error of the relative amplitude calculated across different replications.

IPD=0°. The magnitude of this relative asymmetry varies with age. In the youngest monkey it is slight, 0.93, and increases so that it is 0.58 in the adult rhesus. These results are consistent with the hypothesis that the contribution from MLBNL processing is relatively weak compared to that from MNL processing at early ages, and increases in relative strength with age (compare Figure 4 with the model predictions for conditions of summation shown in Figure 1b).

We used linear regression to determine whether there was a significant age trend in the magnitude of the asymmetry. The linear function relating relative amplitude of the response at 180° to log age over the four young ages is shown by the dashed line in Figure 5. This relationship is significant (r = –0.968, $p < 0.05$). We plot the values for the adult monkey (5 years old) and the adult human (22 years old) on the same graph for comparison.

Discussion

The present report has three major findings. First, the binocular luminance interaction of a normally-reared adult rhesus as measured with VEPs is similar to that observed with visually normal human adults tested under similar conditions. Second, binocular luminance interaction is qualitatively and quantitatively different in young rhesus monkeys as compared to the adult. Lastly, the changes seen with age in the four young monkeys are consistent with a model that assumes a difference in the relative maturation of two processes (MLBNL and MNL) involved in binocular luminance interaction. We infer that these two processes reflect the relative maturation of the M and P streams [5]. These three findings are discussed in greater detail below.

Binocular luminance interactions elicited by dichoptically presented sinusoidal luminance modulation which varies in the relative phase presented to the two eyes have different characteristics depending on the mean light level. When the light is bright, the VEP second harmonic amplitude is greatest at an IPD of 180°. At lower light levels, it is largest at an IPD of 0°, is minimal at an IPD of 90° and increases to a second maximum at 180°, which is smaller than at 0°. The adult monkey data are qualitatively the same as in adult humans studied previously [5,6] and in the present situation. Odom and Chao [5] proposed a model of binocular luminance interaction to describe their human data. If binocular luminance interaction reflected the activity of a single process which summed nonlinear monocular inputs (MNL), the VEP second harmonic would be perfectly symmetrical about an IPD of 90° such that the relative amplitudes at IPDs of 0° and 180° would be exactly the same and the relative amplitude at 90° would be approximately 0. The deviations from perfect symmetry of the relative amplitudes at 0° and 180° reflect the influence of a second process in binocular luminance interaction which sums monocular linear inputs (MLBNL). The direction of the deviation depends on whether this process sums or subtracts the monocular linear inputs. If it subtracts them, the relative amplitude will be greater at 180° than at 0°, while if it sums them it will be smaller. The model proposed by Odom and Chao to account for human results across luminance levels includes both an MNL and a MLBNL process. The MLBNL sums linear monocular inputs at lower stimulus intensities but subtracts them at higher stimulus intensities. The two pathways in the model were identified with the M and P pathways, respectively, based on their temporal characteristics. The similarity of the monkey and human data indicate that the same model can be used to describe the monkey data as has been used to describe the human data. In other words, two processes are needed to describe the adult monkey relative second harmonic amplitudes as a function of IPD and the putative origins of these two processes are the M and P streams.

We were only able to test infant monkeys at the lower luminance condition due to the fact that they closed their eyes during testing. Under these low luminance conditions the young monkeys exhibited a pattern of binocular luminance interaction different from adults. The relative amplitudes of the second harmonic were almost perfectly symmetrical about 90° in the youngest animal, the relative amplitude at 180° being 93% of that at 0°. This would imply that there was little or no binocular interaction in the MLBNL process, i.e, the P stream. As age increases a pattern of binocular luminance interaction emerges that is more similar to that of adults. This is reflected in the correlation of age and relative amplitude at 180° see Figure 5). Our interpretation of this finding is that the binocular MNL process (i.e., the M stream) is relatively more mature in early infancy and that the MLBNL process (i.e., the P pathway) matures more slowly so that as the monkeys increase in age its relative contribution increases. The slower relative maturation of the binocular interactions subserved by the P stream relative to the M stream, is consistent with an accumulating body of evidence such as the fact that flicker sensitivity and symmetry of the OKN response become adult like earlier than resolution of fine spatial detail, that mild monocular deprivation affects primarily the P pathway [5, 8] and that VEP binocular beat frequencies are diminished in monkeys with monocular deprivation [9]. The differential maturation of binocular luminance interactions subserved by the two streams of processing provides another measure of binocular vision which can be utilized in future studies to try to understand both normal visual development and its impairment in animal models of blinding visual disorders.

Acknowledgments

The authors thank the veterinary and animal care staff at the Yerkes Regional Primate Research Center for their expert assistance. The Yerkes Center is fully accredited by the American Association for Accreditation of Laboratory Animal Care.

References

1. van Essen DC, Anderson CH, Felleman DJ. Information processing in the primate visual system: An integrated systems perspective. Science 1992; 255: 419–423.
2. Merigan WH, Maunsell JHR. How parallel are the primate visual pathways? Annu Rev Neurosci 1993; 16: 369–402.
3. Tychsen L. Binocular vision. In: Hart WM Jr, ed. Adler's Physiology of the Eye: Clinical Applications, 9th ed. St. Louis, MO: C.V. Mosby, 1992: 773–853.

4. Boothe RG, Dobson V, Teller DY. Postnatal development of vision in human and nonhuman primates. Annu Rev Neurosci 1985; 8: 495–545.
5. Odom JV, Chao GM. Models of binocular luminance interaction evaluated using visually evoked potential and psychophysical measures: A tribute to M. Russell Harter. Internat J Neurosci 1995; 80: 255–280.
6. Chao GM, Odom JV. A model of binocular luminance interaction: Effects of interocular phase difference on visual evoked potentials. Biomedical Engineering, Applications Basis Communications. 1993; 5: 482–495.
7. Zemon V, Pinkhasov E, Gordon, J. Electrophysiological tests of neural models: Evidence for nonlinear binocular interactions in humans. Proc Natl Acad Sci USA. 1993; 90: 2975–2978.
8. Chao GM, Odom JV, Schwartz TL. Binocular luminance interaction of stereo abnormals: visually evoked potentials. Proceedings of the 14th Annual Meeting of the Engineering in Medicine and Biology Society. Piscataway, NJ: IEEE, 1992: 576–1577.
9. Baitch LW, Ridder WH, III, Harwerth RS, Smith EL, III. Binocular beat VEPs: losses of cortical binocularity in monkeys reared with abnormal visual experience. Invest Ophthalmol Vis Sci 1991; 32: 3096–3103.

Address for correspondence: J. Vernon Odom, Department of Ophthalmology, Robert C. Byrd Health Science Center of West Virginia University, P.O. Box 9193, Morgantown, WV 26506-9193, USA
Phone: 1-304-293-3757; Fax 1-304-293-7139; E-mail: jodom@wvu.edu

Documenta Ophthalmologica **95:** 271–281, 1999.

The separation of parallel visual systems by disease processes

JANET WOLF & GEOFFREY ARDEN
City University, Centre for Applied Vision Science, London, UK

Abstract. Aim: to investigate psychophysics and electrophysiology in disease states with altered retinal function.

Methods: determination of colour and luminance contrast sensitivity functions using computer controlled VDUs: recording of flash and pattern ERGs to short and long flashes of coloured lights under differing conditions of light adaptation: recording of pattern ERG.

Results: In melanoma-associated retinopathy (MAR) low spatial frequency temporal flicker loss occurs for achromatic Gaussians, but colour Gaussians are seen normally. Low spatial frequency luminance contrast sensitivity and motion losses are severe while red-green gratings are seen normally. In Cuban Tropical Amblyopia, achromatic luminance contrast sensitivity may be normal, in the presence of considerable losses of colour vision, to spatial frequencies as high as 32 c/degree. There are supernormal cone ERGs.

Conclusions: these 2 conditions represent highly selective loss of 'M' and 'P' pathways respectively. Almost the entire 'bell shaped curve' normally represents M activity. In CTA, there may be a selective loss of the receptive field surrounds of P ganglion cells.

One of the main discoveries of the last decades concerns the structure of the primate retina. We and the great apes are unique in possessing midget ganglion cells: about 90% are of this type [1]. The midget system continues through the layers of the retina. Each ganglion cell, at least near the macula, is served by a single midget bipolar, and each midget bipolar connects to a single cone – a private pathway [2–4]. Such a system is naturally colour coded: the single cone can only be green or red. The small receptive fields of these ganglion cells and their dense sampling of the visual image suggests that they subserve visual acuity [5, 6]. But there are other, larger ganglion cells – the so-called parasols. What function do they serve? They have larger receptive fields, and inputs from all classes of cone, so they cannot signal colour [7–11] but can signal luminance contrast. Evidently, evolution sets great store by the difference between these systems [12], for the chromatic midget ganglion cells synapse – completely segregated from the remainder – in the parvocellular layers of the LGN, while the achromatic pathway synapses in the magnocellular layers. This explains the usual naming of these pathways, P and M. The segregation continues up to the visual cortex, and beyond, so the data-processing of the ocular input must be specialised along these lines [11–13]. The function of the P-cells is self evident, but what about

the remainder? Livingstone and Hubel [14] described various possible visual illusions which might depend upon the achromatic system: the ability to see 3-D effects in a flat image, for example. A vast amount of work was done by the neuroscientists, to try and pin down the elusive functions.

One way in which vision is investigated clinically is to measure contrast sensitivity, using gratings of various spatial frequencies, and the 'bell shaped curve' is characteristic of the contrast sensitivity (CS) function. The question arises which of the retinal subsystems, parvo- or magno-, mediates this curve? For the highest spatial frequencies, at the acuity limit, the visual neuroscientist would unhesitatingly say the midget cells must be responsible. In a series of experiments on operantly trained monkeys, lesions have been made in the magnocellular layers of the lateral geniculate, and the contrast sensitivity function remained unchanged, even at low spatial frequencies: so it has become accepted that this curve is determined by midget cell input [15, 16]. But let us see what clinical evidence has to say.

Metastasising cutaneous malignant melanoma is almost always rapidly lethal. However, in some sufferers, always elderly men, even though secondary tumours can be found, they do not enlarge and may actually dwindle and vanish, so that the patient can remain in good health for many years. The reason is that the melanoma is a very antigenic tumour, and in some cases the patient's immune system produces such a titre of antibodies that the tumour cells are destroyed. However, the antibodies may not be specific to melanoma, but also attack the retina, producing a melanoma-associated retinopathy, MAR [17].

This develops over the space of a few days. The patients experience a screen of golden scintillating photopsiae and become night blind [17–19]. The MAR patients' serum, as Milam has shown [20], binds to bipolar cells. The condition does not appear to progress, but the visual disturbance is profound, even though acuity and colour vision may remain quite good. What the three such patients we have examined are suffering from seems to be a loss of the M-pathway [21, 22]. The M-optic axons are large, and this makes them more liable to damage in a number of conditions, for example glaucoma [23, 24]. However, in MAR the condition appears to dissect out the M pathway very selectively.

The principle of selective stimulation of the P and M pathway is very simple: only the P pathway can transmit colour information, and the M pathway apparently does not transmit information about detailed patterns and is optimally sensitive at high temporal frequencies. Thus, if we use large Gaussian blobs (containing only very low spatial frequencies) as targets, making them appear against the background by achromatic luminance contrast reversal, they should be picked up by the M system: and if the Gaussians are

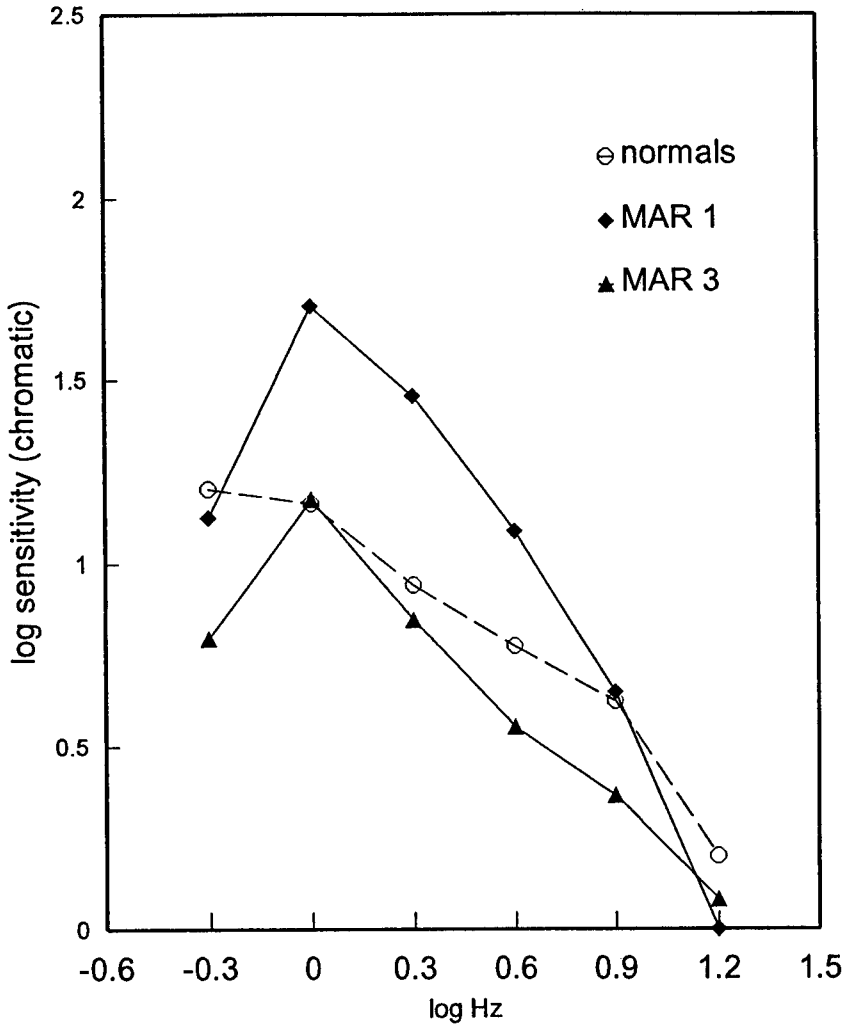

Figure 1. The variation of colour contrast sensitivity with temporal frequency for Gaussian stimuli with a half width of 3 deg. The equiluminance colour stimuli reversed at the temporal frequencies indicated. The colours changed along a protan axis. Data of patient 2 are not shown since he was known to be a colour defective. There is no loss of colour contrast sensitivity in the remaining 2 patients.

visible only by a colour contrast (for example, reddish on a greenish background of equal luminance), then the P pathway, the colour coded midget cells, must detect the targets.

We made the luminance or colour contrast of the Gaussians flicker at various rates. For colour reversal, the MAR patients' thresholds are the same as the (age-matched normal (Figure 1), but if the patches are achromatic they

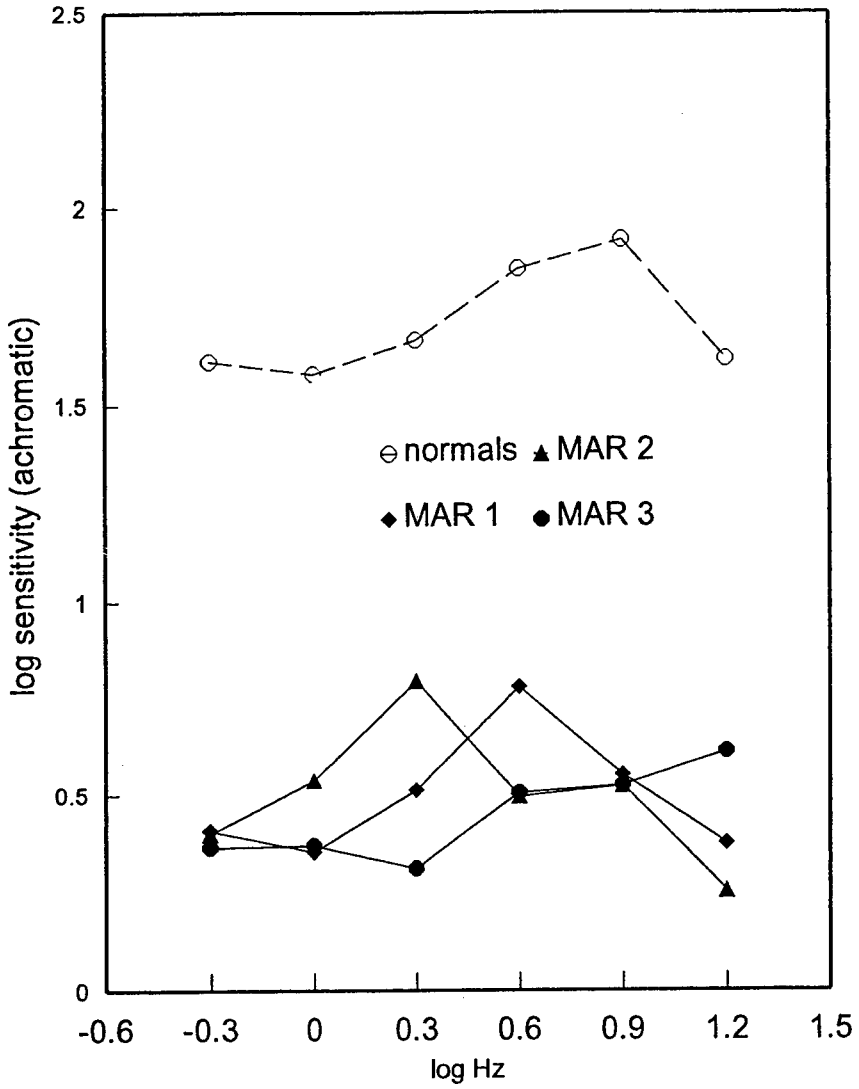

Figure 2. Gaussian stimuli with the same spatial and temporal characteristics as Figure 1, but with achromatic luminance contrast. Note the loss of sensitivity in the MAR patients.

have a profound sensory loss (Figure 2) of approximately the same amount for all temporal frequencies. At temporal frequencies of 10 Hz it would be universally accepted that the thresholds reflect M-cells activity. The only economical explanation of an equivalent loss at all temporal frequencies is that threshold is again being set by the M-cells for these conditions of viewing. So, what happens if we use gratings to get the spatial contrast frequency

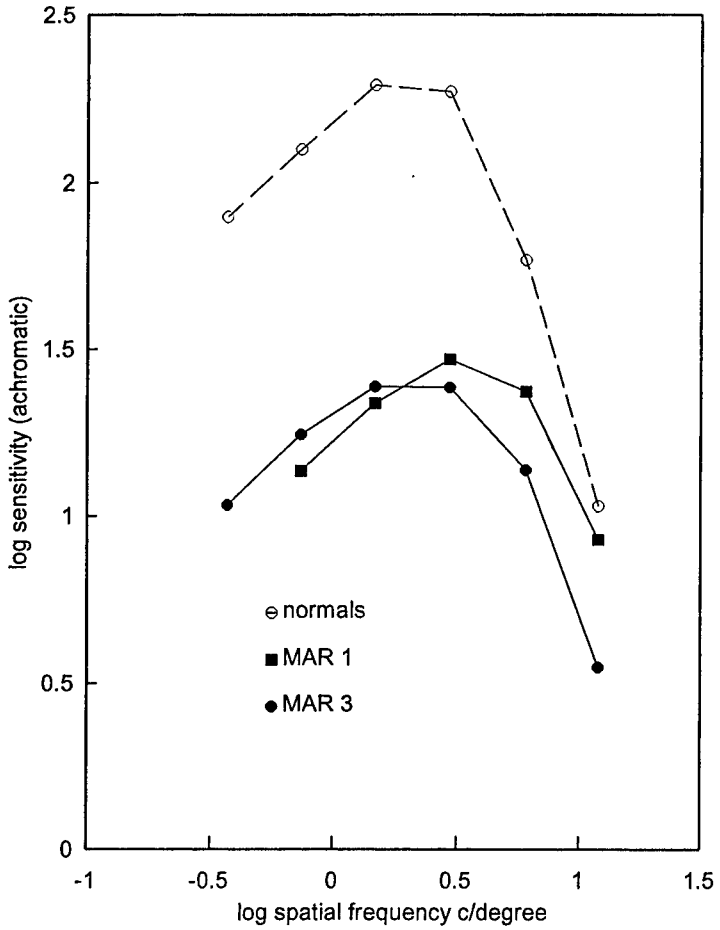

Figure 3. Grating contrast sensitivity in normals and MAR patients. The stimuli were vertical gratings appearing on the monitor for 200 ms each second. Thresholds were determined using a modified binary search technique(MOBS). Major loss of sensitivity in patients at low spatial frequencies.

function? If the grating is green/red there is no loss. But if the gratings are achromatic, there is a huge loss at lower spatial frequencies (Figure 3). At higher spatial frequencies, the normal and patients' curves converge. This would be expected if there was P-cell sparing in our patients [15, 16].

The losses associated with the lower spatial frequencies can be explained if large magnocellular ganglion cells normally signal low contrast at low spatial frequencies – even at low temporal frequencies – and these are damaged in our patients. The peak CS in the patients is about 5%, which is within the capabilities of the P pathway [25].

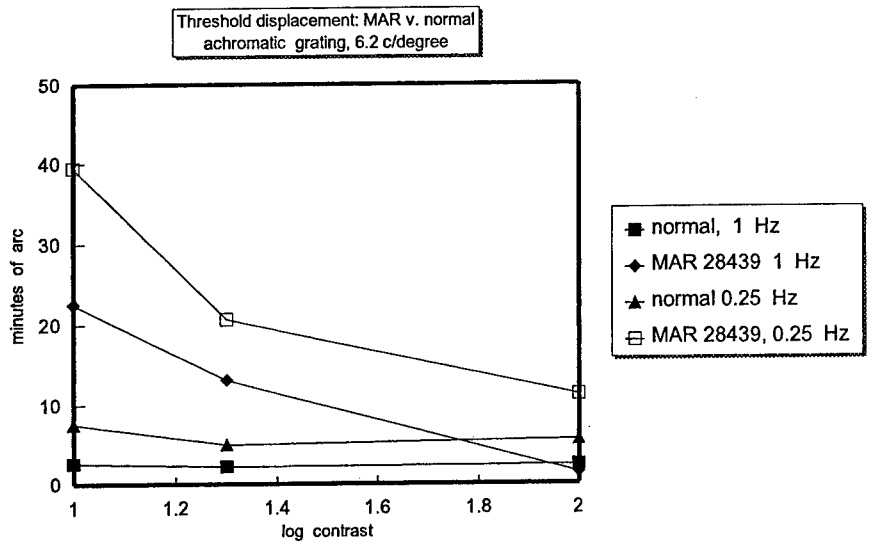

Figure 4. Motion detection threshold for achromatic gratings in a normal and MAR patient as a function of contrast. The patient's motion detection is only significantly raised at low contrasts.

However, in some lesion experiments of the P-pathway, there appears to be a loss of sensitivity for low spatial and temporal frequencies, and it is argued that the M system sensitivity to low contrast at low spatial and temporal frequency is less than that of the P system. At first sight seems at variance with the conclusion above. But there is a simple explanation. The lesions made in the LGN were very small, and in the projection of peripheral retina, so the monkey could still fixate properly: the area of the test grating was therefore so small, that the maximal M-cell sensitivity could not be achieved [15]. Tests to determine the 'bell shaped curve' in man are always performed with the subject freely viewing a rather large target. Under these circumstances, with the eye movements enabling there to be a relatively transient presentation, our thresholds for low spatial frequencies correspond to those of the M system.

But, what more do parasol ganglion cells signal than low contrasts at low spatial frequencies? Animal experiments tell us that M cells are very sensitive to motion [14, 16, 25, 26]. In our patients, motion sensitivity is certainly reduced, but only under specific circumstances. Figure 4 shows a normal's motion detection ability (using gratings), compared to a patient. At high contrast, the patient does nearly as well, but when the contrast is reduced to levels where the M cells start to take over, his thresholds rise enormously. What insights have we got into the change in the quality of vision that such a patient experiences? They complain in fact of very little. One of our patients

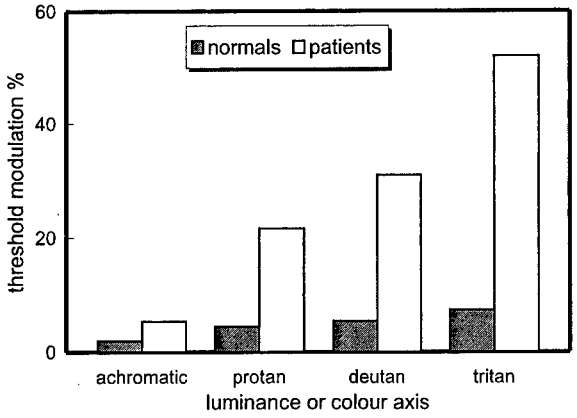

Figure 5. Achromatic luminance contrast and equiluminant colour contrast thresholds in patients with the Cuban dietary retinopathy and matched normals. The stimuli in all cases were subsets of Sloane optotypes subtending 3 degrees at the eye . Stimuli appeared for 200 ms each second. Thresholds determined by MOBS. The patients had visual acuity >6/9. Note the disproportionate loss of colour contrast sensitivity.

described how he could no longer understand pictures, or derive pleasure from looking at them. But the main problem, which he said ruined his life, was that he could no longer play golf. Every time he made a stroke, the ball vanished, and he could only see it when it came to rest!

What would happen if we could obtain the reverse of this patient, and study vision mediated by the M system only? We have been very fortunate in encountering a syndrome in which there appears to be a nearly pure loss of the midget, or P-system [22]. The condition is usually called a Tropical Neuropathy [27, 28], but it was first recorded in Cuba and named a century ago [29, 30]. In 1992 (as in earlier times) there was widespread shortage of food in Cuba. An epidemic developed. The symptoms were weakness and pain particularly in the lower limbs, loss of memory, deafness and poor sight. Because the Cuban public health service was still functioning, they realised that three groups were not affected, namely the elderly, pregnant women and children. These were the groups who received supplemental food rations, so it seemed pretty clear that the epidemic was due to malnutrition [31]. Multivitamins were prescribed to all, and the epidemic ended abruptly.

We only investigated recovered cases about a year afterwards. Without going into the entire symptomatology, there was clear evidence both of an optic atrophy and also a retinal degeneration. The missing nerve fibre bundles were easily visualised in the dark fundi of many ex-sufferers, and also, the electroretinograms were affected. This test monitors the activity of the cells in the outer retina. Even after recovery, many persons suffered from reduced

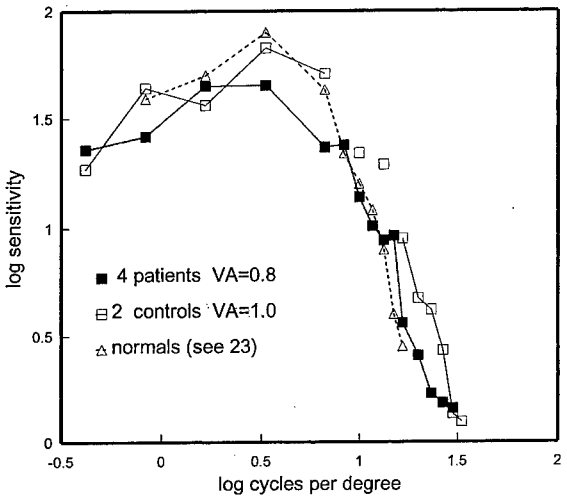

Figure 6. Luminance contrast sensitivity function in patients and Cuban normals. The dashed lines are from normals in a previous study [32]. In the patients the high spatial frequency grating contrast sensitivity does not differ significantly from the normals up to 30 c/deg.

visual acuity, though in some, it was normal. What we discovered was that there was a most interesting dissociation between achromatic luminance contrast sensitivity, and colour contrast sensitivity (Figures 5 and 6). Even in persons with normal visual acuity and a normal 'bell shaped curve', there remained a profound loss of colour vision. We were so impressed by these findings that we returned and reinvestigated the most mildly affected of our patient group. Figure 6 shows that the peak and the descending arm of the curve, right up to the visual acuity limit are normal. This is a most surprising finding. The midget, chromatic, system is clearly affected, yet there is no evidence of it in the contrast sensitivity function! Once it was believed that the entire curve represented the limit of function of the midget cells: but now it looks as though the entire curve may be generated by the M system.

This may not however be the entire story. The latest work on the M system has reached the conclusion that M cells are capable of a far higher spatial resolution than was once thought, so possibly P cells are required for only the most finicky tasks. Another explanation is even more interesting. Visual acuity is limited by the size of the receptive field centres and the distances between the foveal cones, but there is another constraint on colour vision. This depends upon the interactions between the central receptive fields of retinal ganglion cells, and their antagonistic, colour-coded surrounds. If in the tropical neuropathy, the antagonistic surround mechanism were to be blocked, it would be entirely possible to preserve acuity even though there was a col-

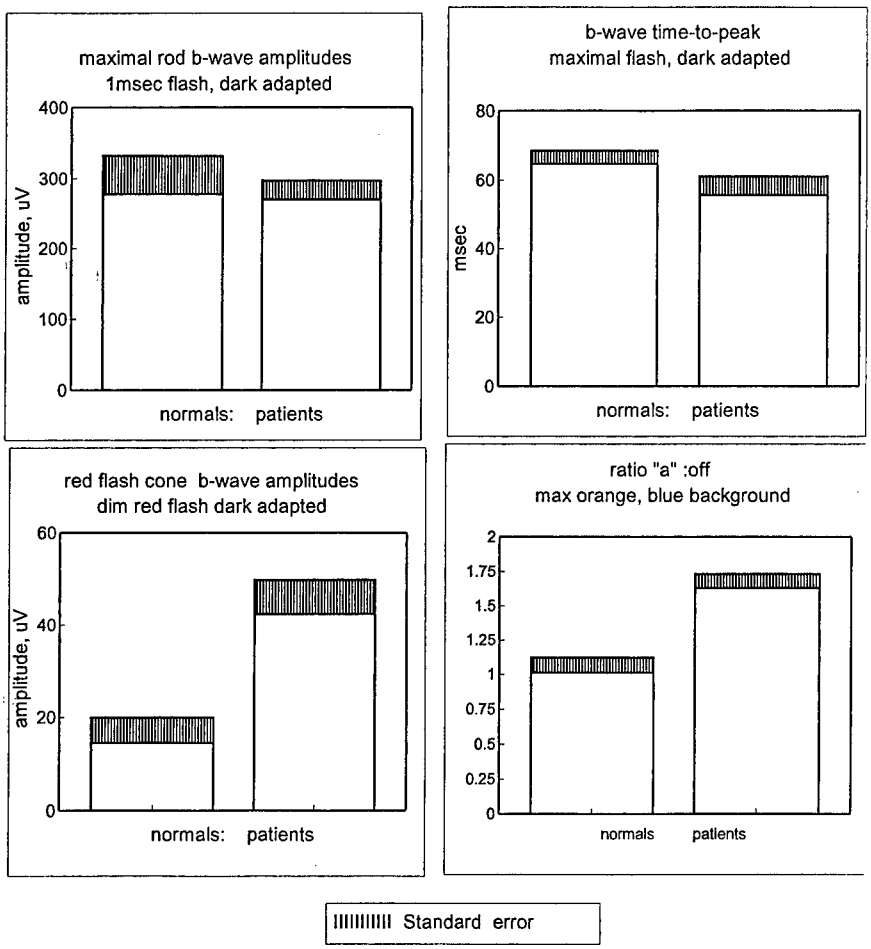

Figure 7. Histograms illustrating the ERG properties of patients with the Cuban dietary retinopathy compared with Cuban normals. Although the rod ERG is normal, the photopic 'on' and 'off' responses show characteristic changes: a supernormal 'on' response' and a reduced 'off' response.

our vision deficiency. In fact there is evidence that outer retinal function is disturbed in the way one would expect. The ordinary dark adapted ERGs of our patients are normal (for the technique see [33]), but the cone b-waves are supernormal (Figure 7). This would be expected if the centre-surround antagonism was to be interrupted. In addition, there is a highly specific loss of the 'off' responses to long flashes: this does not occur in UK patients with optic atrophy and retinal damage due to tobacco.

Analysis of the properties of the visual system is continuing but the most refined methods seem gross when compared to the dissections caused by

these diseases. There must be proteins on the surface of M cells that are immunologically distinct from those of P cells: and horizontal and amacrine cells which construct the receptive field surrounds of midget cells must have a metabolism so distinct from the bipolars that they are selectively damaged by a particular pattern of deprivation of micronutrients.

References

1. Calkins DJ, Schein SJ, Tsukamoto Y, Sterling P. Ganglion Cell Circuits in Primate Fovea. pp 267–274. In: Drum B, ed. Colour Vision Deficiences XII. Documen Ophthalmologica Proc Ser 1995; 57. Kluwer Academic Publishers, Dordrecht.
2. Croner LJ, Kaplan E. Receptive fields of P and M ganglion cells across the primate retina. Vision Res 1994; 35: 7–24.
3. Schiller PH, Logothetis NK, Elliot RC. Functions of the colour-opponent and broadband channels of the visual system. Nature 1990; 343: 68–70.
4. Kolb H (1991). The neural organisation of the Human Retina. Chapter 5 of Principles and practice of Clinical Electrophysiology of Vision. Editors: Heckenlively JR & Arden GB. Mosby -Year Book, Inc. St. Louis. pp 25–52.
5. Kolb H. The architecture of functional neural circuits in the vertebrate retina. Investigative Ophthalmology & Visual Science 1994; 35: 2385–2404.
6. Merigan WH, Eskin TA. Spatio-temporal vision of macaques with severe loss of pβ ganglion cells. Vision Res 1986; 26: 1751–1761.
7. Kremers J, Lee BB, Kaiser PK. Sensitivity of macaque retinal ganglion cells and human observers to combined luminance and chromatic temporal modulation. Journal of the Optical Society of America 1992; 9: 1477–1485.
8. Kremers J, Lee BB, Yeh T. Receptive field dimensions of monkey retinal ganglion cells. In: Drum B ed. Colour Vision Deficiences XII. pp 399–408. Doc Ophthalmologica Proc Ser 1995; 57. Kluwer Academic Publishers, Dordrecht.
9. Lee BB, Martin PR, Valberg A. Sensitivity of Macaque retinal ganglion cells to chromatic and luminance flicker. J Physiol Lond 1989; 414: 223–243.
10. Lee BB, Pokorny J, Smith VC, Martin PR, Valberg A. Luminance and chromatic modulation sensitivity of macaque ganglion cells and human observers. Journal of the Optical Society of America 1990; 7(12): 2223–2236.
11. Schiller PH, Malpeli JG. Functional specificity of lateral geniculate nucleus laminae of the rhesus monkey. Journal of Neurophysiology 1978; 41: 788–797.
12. Schiller PH, Logothetis NK, Elliot NK. Functions of the colour-opponent and broadband channels of the visual system. Nature 1990; 297: 580–583.
13. Merigan WH, Maunsell JHR. How parallel are the primate visual pathways? Annu. Rev. Neurosci 1993; 16: 369–402.
14. Livingstone MS, Hubel DH. Psychophysical evidence for separate channels for the perception of form, colour, movement, and depth. Journal of Neuroscience 1987; 7: 3416–3468.
15. Merigan WH. Chromatic and achromatic vision of macaques: role of the P pathway. Journal of Neuroscience, 1989; 9: 776–783.
16. Merigan WH, Maunsell JHR. Macaque vision after magnocellular lateral geniculate lesions. Visual Neuroscience 1990; 5: 347–352.

17. Alexander KA, Fishman GA, Peachey NS, Marchee AL, Tso MOM. 'On' response defects in paraneoplastic night blindness with cutaneous malignant melanoma. Investigative Ophthalmology and Visual Science 1992; 33: 477–483.
18. Berson EL, Lessell S. Para-neoplastic night blindness with malignant melanoma. American Journal of Ophthalmology 1988; 106: 307–311.
19. Kim RY, Retsas S, Fitzke FW, Arden GB, Bird AC. Cutaneous melanoma-associated retinopathy. Ophthalmology 1994; 101: 1837–1843.
20. Milam AH, Saari JC, Jacobson SG, Lobinski WP, Feun LG, Alexander KR. Autoantibodies against retinal bipolar cells in cutaneous melanoma-associated retinopathy. Investigative Ophthalmology & Visual Science 1993; 34: 91–100.
21. Wolf J, Arden GB. Selective loss of magnocellular function in a patient suffering from melanoma-associated retinopathy (MAR). J. Physiol (1994): 475: 42p.
22. Wolf JE, Arden GB, Plant GT. Selective damage to either the 'M' or 'P' pathway in human retinal disease: implications for visual processing. European Journal of Ophthalmology 1996; 6: 208–214.
23. Quigley HA, Dunkelburger GR, Green WR. Chronic human glaucoma causing selectively greater loss of large optic nerve fibres. Ophthalmology 1988; 95: 357–363.
24. Drance SM, Lakowski R, Schultzer M, Douglas GR. Acquired color vision changes in glaucoma. Arch Ophthalmol 1981; 99: 829–831.
25. Kaplan E, Shapley RM. The primate retina contains two types of ganglion cells, with high and low contrast sensitivity. Proceedings of the National Academy of Science, USA, 1986; 83: 2755–2757.
26. Shapley R, Perry VH. Cat and monkey retinal ganglion cells and their visual functional roles. T.I.N.S. 1986; 9: 229–235.
27. Thomas PK, Plant GT, Baxter PJ, Santiago Luis R. An epidemic of optic neuropathy and painful sensory neuropathy in Cuba: clinical aspects. J Neurol in press.
28. Roman GC. An epidemic in Cuba of optic neuropathy, sensineural deafness, peripheral sensory neuropathy and dorsolateral myeloneuropathy. J Neurol Sci 1994; 127: 11–28.
29. Strachan H. On a form of multiple peripheral neuritis prevalent in the West Indies. Practitioner 1897; 59: 417–484.
30. Madan D. Notas Sobre una forma sensitiva de neuritis perifica. Ambliopia por neuritis óptica retrobulbar. Crónica Médico-Quirúrgica de la Habana. 1897; 24: 81–86.
31. Grupo Operativo Nacional Cuidad de la Habana. Neuropatia Epidemica en Cuba. 30 de Julio de 1993.
32. Swanson WH, Wilson HR, Giese CG. Contrast matching data predicted from contrastincrement thresholds. Vision Research 1984; 24: 63–75.
33. Spileers W, Falcao-Reis F, Arden GB. Evidence from human ERG a- and off-responses that colour processing occurs in the cones. Invest Ophthalmol Vis Sci 1993; 34: 2079–2091.

Address for correspondence: G. Arden, City University, 311 Goswell Rd., London ECIV 7DD, UK
Phone: 44-171-477-8000 (ext. 4313); Fax: 44-171-4778355; E-mail: g.arden@city.ac.uk

Documenta Ophthalmologica **95:** 283–299, 1999.

Parallel pathways, noise masking and glaucoma detection: behavioral and electrophysiological measures

J. TERRY YATES[1], MONIQUE J. LEYS[2], MARC GREEN[2], WEI HUANG[2], JUDIE CHARLTON[2], JANIS REED[2], BAO-ZHONG DI[2] & J. VERNON ODOM[2]

[1]*AL/AOCOC, Brooks Air Force Base, TX;* [2]*Department of Ophthalmology, Robert C. Byrd Health Science Center of West Virginia University, P.O. Box 9192, Morgantown WV 26506, USA*

Abstract. Purpose: We tested the hypothesis that because of their reduced neural efficiency, glaucoma patients should have increasingly impaired thresholds as external noise is added to a stimulus. Method: We compared the performance of 20 normals (mean age = 39 years) with that of 15 patients with early glaucoma or at very high risk for glaucoma (mean age 45 years). All patients had normal visual acuity. Contrast thresholds were measured on two sets of tasks: (1) behavioral and (2) sweep visually evoked potentials (VEPs). Two stimuli were used (a) 7.5 Hz reversing gratings of 0.69 cpd, and (b) 5.5 cpd gratings. Noise was binary and contrast varied from 0 to 80%. Psychophysical thresholds were determined using a staircase which employed a spatial four alternative forced choice procedure (4AFC) and converged on 50% correct. Sweep VEP thresholds were determined by extrapolation to zero volts as a function of log contrast. Results: Differences between normal subjects and patients with early glaucoma were not significant without noise. Both the absolute size of the difference and its significance increased as noise level increased. For the behavioral thresholds these trends were clearer with the 5.5 cpd grating, while for the sweep VEPs they were more clear for the 0.69 cpd grating. Conclusion: The performance deficit of glaucoma patients which may be minimal under normal testing conditions is magnified when external noise is added to the stimulus. VEPs and psychophysical thresholds show interesting differences in their sensitivity to this effect. Implications for the early detection of glaucoma are discussed.

Key words: early detection, glaucoma, ideal observer, magneocellular pathway, noise, parallel pathways, parvocellular pathway, signal detection theory

Introduction

Primary open angle glaucoma is the second leading cause of blindness; in the industrialized world [1]. It is characterized by (1) increased intraocular pressure, (2) visual field losses, and/or (3) increased cupping of the optic disc. Visual field losses and increased disc cupping are presumed to result from ganglion cell death secondary to elevated intraocular pressure [2]. The

degenerated optic nerve fibers are distributed throughout the ON, indicating that ganglion cell damage is not limited to one area or type [3–5]. However, there does seem to be a greater loss of larger diameter ganglion cells [3–5]. Early treatment may be essential for preventing reversible loss of visual function; therefore, development of sensitive tests for early detection of primary open angle glaucoma would be a major step in blindness prevention [1].

Efforts at early primary open angle glaucoma (POAG) detection using visual fields and intraocular pressure have proven disappointing. A 5-db visual field deficit is required to demonstrate the presence of POAG. By the time visual field deficits of this magnitude may be detected about 20% of the optic nerve fibers in the affected region have degenerated [6]. Patients with increased intraocular pressure develop glaucoma at $\leq 1\%$ per year [7]. Consequently, intraocular pressure while a major risk factor is not very predictive of who will develop glaucoma. Consideration of the underlying pathology might provide clues for creating sensitive glaucoma screening tests.

One way of conceptualizing the visual system is to think of it as consisting of a series of parallel pathways. One such set of pathways is the magnocellular (large cell) and parvocellular (small cell) pathways of the lateral geniculate nucleus. These two systems are segregated at the level of the retina and remain segregated at least until the visual cortex. More importantly they show distinctly different response properties. The magnocellular pathway is achromatic and responds physically to stimuli with lower spatial frequencies especially if they change rapidly. The parvocellular system has many color-opponent cells and responds tonically to stimuli which change slowly and/or have higher spatial frequencies [8–14].

Evidence suggests that glaucoma is marked by a loss of specific classes of retinal cells, large diameter retinal ganglion cells [3–6]. Some authors have interpreted this to suggest that glaucoma produces a loss in functions subserved by the magnocellular pathways (e.g., [15]). Early diagnosis would then best be accomplished by testing functions which are presumably mediated primarily by the magnocellular pathway such as flicker and motion detection [15–17]. However, there is also evidence of poor color vision in glaucoma patients [18]. Specifically, there is a marked deficit in the ability to detect blue objects on a yellow background [19]. Since color vision is a function mediated by the parvocellular system [9, 17], the effects of glaucoma cannot be assumed to be pathway specific (see [16, 17]).

An alternate hypothesis is that glaucoma affects a broad range of retinal cells, especially in its early stages [3–6]. Why then is it diagnosed by testing in the periphery and why are functions which depend on blue cones and large diameter ganglion cells often affected? It may be because these cell types are relatively few in number in the normal retina: (1) ganglion cell density is

lower in the periphery, (2) large diameter ganglion cells have lower density and (3) blue cone density is far lower than other cone classes. A general loss may affect these cells more, relatively speaking, because they are distributed more sparsely. This hypothesis has been referred to as the reduced redundancy hypothesis [16]. The functions of sparsely distributed cells may be more easily affected because of their smaller number under relatively standard testing conditions [16, 17].

Because of the potential benefits from early detection, there are many efforts to develop primary open angle glaucoma screening tests. These include measures of structure, e.g., optic nerve anatomy, retinal nerve fiber layer thickness, optic nerve blood flow, and measures of function, e.g., electrophysiological (pattern electroretinograms) [20] and behavioral tests (flicker sensitivity) [21]. Each of these strategies is recommended by a particular perspective or theory, either (1) of the underlying mechanism by which primary open angle glaucoma is generated or (2) of the effects of glaucoma on visual structures or functions. For example, the fact that ganglion cells die as a result of glaucoma underlies efforts at quantifying nerve fiber layer thickness. Similarly, suggestions that larger ganglion cells are more affected by glaucoma have led to the design of tests designed to test presumptive functions of these cells [15–17].

The inherent population variability of normal function presents severe problems for the development of successful tests of early glaucomatous damage. For example, the number of optic nerve fibers in normals has a standard deviation of about 20% of the mean [22, 23]. If the average number of optic nerve fibers and their standard deviation is initially the same in patients who do and do not develop glaucoma, then the number of fibers in an individual optic nerve must be reduced at least 40% before the nerve can be identified as abnormal with 95% confidence. Given the variability of the underlying anatomy, it seems unlikely that structural parameters will be considerably less variable than functional tests.

New approaches are needed to successfully screen for the early stages of glaucoma. Because the causes of early glaucomatous damage and the consequences of early damage remain uncertain, a new strategy should be general enough not to depend on any of the current assumptions about mechanisms of damage. One strategy is to develop tests that increase the mean difference between normals and primary open angle glaucoma suspects with early primary open angle glaucoma and/or reduce the groups' response variability. One may decrease the variability of normal subjects by using tasks to which they are very sensitive, for example, full field flicker [21]. Alternatively, one may increase the difference in group means. One means of increasing the differences between normals and patients with minimal defects should be

to increase the external noise. Therefore, visual tasks that artificially stress the visual system, increasing the demands placed on it, by adding external noise may be even more effective in identifying early neural damage from glaucoma (see the appendix for a derivation of the ideal observer model on which the strategy is based). The success of this strategy depends on the presumption that the visual system of the glaucoma patients is less efficient than that of normals [24–29]. However, the loss of cells in glaucoma requires that the system be less efficient.

There are several lines of evidence which support the utility of adding noise to stimuli. Simply presenting noise (snow) on a television screen has been shown to be a useful adjunct to perimetry. Patients experience scotomata which they otherwise fail to see subjectively [33]. Asking patients to detect a pattern as the correlation of its elements vary (i.e., noise is varied) [34, 35] can be useful in glaucoma detection. Most importantly, adding external noise has been used successfully to reveal functional visual loss in the elderly [30, 31] and in glaucoma patients [32].

Whether the same approach which appears to be successful with behavioral measures would also be successful with electrophysiological measures may be questioned. First, most electrophysiological measures make use of signal averaging which is a noise cancellation procedure. Nonetheless, several studies that used VEPs as a measure have suggested that VEPs elicited by stimuli which preferentially stimulate the magnocellular system may be useful in glaucoma detection [36, 37]. However, at least one study has argued that psychophysical measures and other measures may differ in their effectiveness for certain purposes [38] because they tap different levels of the visual system and reflect different internal noise sources [39]. In other words because they reflect different levels of visual processing, thresholds determined using VEPs and behavior might not behave the same way when noise is added to the stimuli. Another reason for being uncertain about the effects of noise is the question of what a threshold represents in the case of VEPs and behavior. In the case of behavior, we know that a threshold of a specific level corresponds to a d' of a certain level. There is no clear analogy in the case of VEP thresholds for stating that a VEP threshold represents a particular likelihood of identifying the stimulus correctly or that this corresponds to a particular d′ level.

In the present study we wished to compare contrast thresholds determined using stimuli thought to preferentially stimulate, either the parvocellular system (5.5 cpd) or the magnocellular system (7.5 Hz reversal of 0.69 cpd gratings). We wished to determine if adding noise improved the separation of the two normal and glaucoma groups as would be predicted by the theory.

Lastly, we wished to determine if adding noise to stimuli would affect contrast thresholds determined using VEPs or psychophysical methods differently.

Methods

Subjects

We tested 20 normal patients with a mean age of 39 years and 15 patients with early glaucoma with a mean age of 45 years. The six-year difference in mean ages was not statistically significant ($p > 0.1$). All patients had visual acuity of 20/20 or better at the viewing distance of 1 m. No patients had other visual diseases or systemic diseases that might have visual complications.

Stimuli and experimental procedures: Psychophysical estimates of contrast thresholds

Contrast thresholds were measured on two tasks: (1) 7.5 Hz reversing gratings of 0.69 cpd and (2) stationary 5.52 cpd gratings. Each task was tested at 5 noise levels ranging from 0 to 80% contrast. The screen size was 11.59 arc degrees at the viewing distance of one m. The mean screen illuminance was 68 lux. Noise was binary and was changed every 1/45th of a second (22.2 ms). Stimuli appeared for 666.67 ms (60 of 90 frames per second).

Thresholds were determined using a spatial four alternative forced choice method in conjunction with a staircase with a 1 up, 1 down rule, i.e., 50% correct ($d' = 0.84$). Prior to the beginning of each task, the subject was given an opportunity to practice the task. The choice of which task to present first was randomized. The sequence of testing within tasks was fixed. It began with the no added noise condition and progressed through the lower noise levels to the highest added noise condition.

Stimuli and experimental procedures: Sweep VEP estimates of contrast thresholds

The dependent measure in the sweep VEP experiments is an estimate of contrast threshold derived from the contrast sweep. It was calculated by extrapolating sweep VEP amplitude as a function of log contrast to zero voltage. In all of the sweeps, stimulus contrast decreased from high to low. The spatial frequency of the two stimuli was 5.5 cpd and 0.69 cpd. Noise was binary and changed every 1/30th of a second (33.3 ins). The stimulus frequency was 7.5 Hz. The stimuli appeared for 80 stimulus cycles or about 10.5 s. During each sweep, eight contrasts levels were presented for 10 stimulus

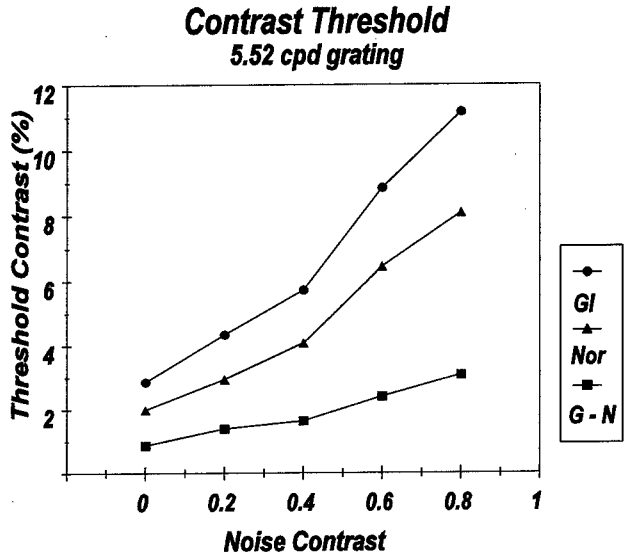

Figure 1. Psychophysical contrast thresholds of static 5.52 cpd grating as a function of noise contrast. Circles represent patients with early glaucoma, triangles represent normal subjects and squares represent the differences between the two groups. In the absence of added external noise there is not statistical significance between the groups ($p = 0.114$); a: 20% noise contrast the difference is statistically significant ($p = 0.046$) and becomes increasingly significant as noise contrast increases (at 40%, $p = 0.029$; at 60%, $p = 0.014$; at 80%, $p = (.00079)$.

cycles each, about 1.3 s per contrast step, for a total of 80 stimulus cycles and 10.5 seconds. The sweeps were repeated at three noise levels: 0%, 20% and 60% (rounded to nearest full percent).

Results

Psychophysical estimates of contrast thresholds

Differences in contrast thresholds were not statistically significantly different between the normal and patient groups at zero noise levels: Contrast thresholds of 5.52 cpd grating as a function of noise contrast ($p = 0.11$; see Figure 1), contrast thresholds of 0.69 cpd gratings reversing at 7.5 Hz ($p = 0.26$; see Figure 2).

The statistical significance of differences between normal and patients with early glaucoma in contrast thresholds of 5.52 cpd gratings increases as a function of noise contrast (see Figure 1); the difference is statistically significant at 20% noise contrast ($p = 0.046$) and becomes increasingly significant

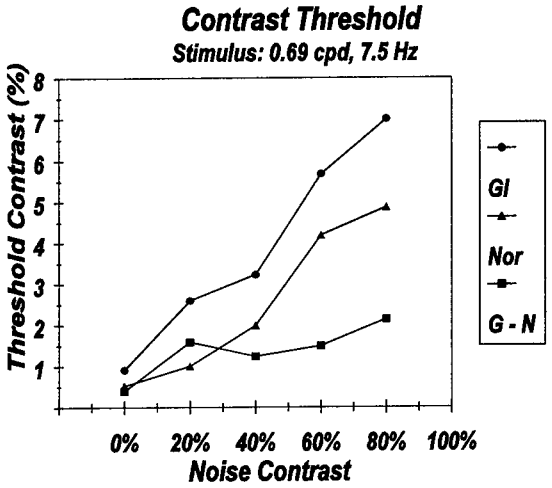

Figure 2. Psychophysical contrast thresholds of 0.69 cpd gratings reversing at 7.5 Hz as a function of noise contrast. Circles represent patients with early glaucoma, triangles represent normal subjects and squares represent the differences between the two groups. In the absence of added external noise there is not statistical significance between the groups ($p = 0.26$); at 20% noise contrast the difference is statistically significant ($p = 0.01$) and remains at approximately the same level as noise is increased (40%, $p = 0.026$; 60%, $p = 0.04$; and 80%, $p = 0.02$).

as noise contrast increases (at 40%, $p = 0.029$; at 60%, $p = 0.014$; at 80%, $p = 0.00079$).

The difference between glaucoma patients and normals for contrast thresholds of 0.69 cpd gratings reversing at 7.5 Hz remains relatively constant as noise is added; the level of statistical significance of the differences between the two groups is at 20%, $p = 0.01$; at 40%, $p = 0.026$; at 60%, $p = 0.04$; and at 80%, $p = 0.02$) (see Figure 2).

Sweep VEP estimates of contrast thresholds

The contrast thresholds determined using sweep VEPs were not statistically significantly different using 7.5 Hz reversal of 5.5 cpd gratings (see Figure 3). The 0.69 cpd gratings reversing at 7.5 Hz showed a statistically significant difference between the normal and glaucoma (see Figure 3). At the no noise level, the mean threshold percent contrast for the normal group was 0.382% $\pm$ 0.184 and for the glaucoma group was 1.014% $\pm$ 1.24 ($p = 0.029$). At the 20% noise contrast level, the mean threshold percent contrast for the normal group was 1.073% $\pm$ 2.911 and for the glaucoma group was 2.057% $\pm$ 4.597 ($p = 0.152$). At the 60% noise level, the mean threshold percent contrast for

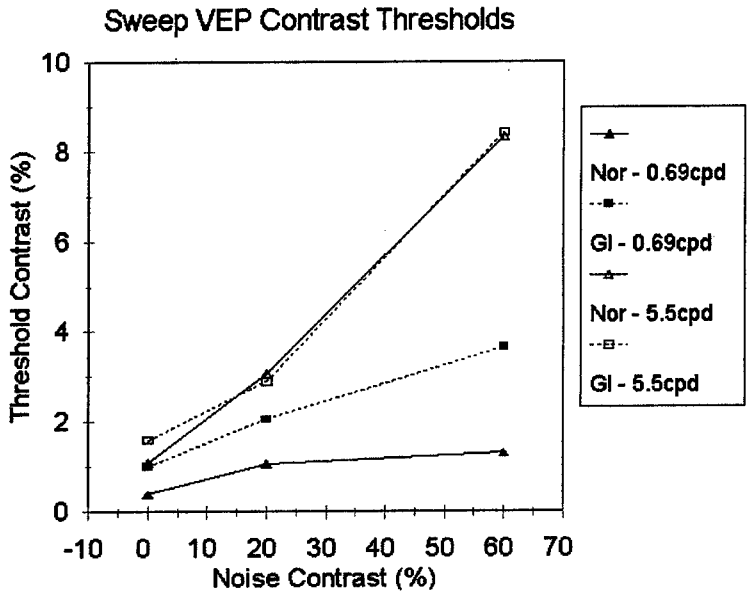

Figure 3. Sweep visually evoked potential contrast thresholds. The contrast thresholds determined using extrapolation of sweep VEP amplitude to zero voltage were not statistically significantly different at any noise level using 7.5 Hz reversal of 5.5 cpd gratings. The 0.69 cpd gratings reversing at 7.5 Hz showed a statistically significant difference between the normal and glaucoma (zero noise, $p = 0.029$; at 20% noise contrast level $p = 0.152$, and at 60% noise level $p = 0.03$).

the normal group was 1.305% ± 2.104 and for the glaucoma group was 3 660% ± 17.579 ($p = 0.03$).

Discussion

We described two major approaches to early detection of glaucoma. The first approach assumes that a specific class of retinal ganglion cells (and the related visual function) is more affected early in glaucoma. The second approach assumes that cells in general are affected even in early glaucoma. However, because some cells are more sparsely represented, some classes of cells (and related visual functions) will be more affected than others. In some ways both approaches are similar; both suggest that one should test for very specific visual functions. The difference between the approaches is in what one observes if one tests a variety of visual functions. The first approach suggests that some cells and their related functions will be unaffected by early glaucoma. The second strategy suggests that all cell classes and all functions will

be affected by early glaucoma, but that those functions subserved by more sparsely represented cells will be most affected. We noted that the inherent variability of underlying anatomy and physiology makes detecting defects in early glaucoma inherently difficult. Based on signal detection theory and ideal observers theory, we proposed a third approach. Namely we suggest that any visual function which is affected by early glaucoma will show a greater defect if external noise is added.

Under ordinary viewing conditions the difference between normal subjects and patients with early glaucoma may be minimal. As noise is added, we expected that performance would decline for both normals and patients. However, we expected that the change for patients would be greater, so that differences between the groups which were not significant when no external noise was present would be increased and become more statistically significant. We tested this general hypothesis using several different tasks. In general, our expectations were supported by our results.

Psychophysical estimates of contrast thresholds

Our data permit us to make several observations. (1) Without added noise, no statistically significant differences in contrast thresholds of gratings were present with the spatial frequencies tested. (2) When external noise was added, thresholds increased for normal subjects and patients with early glaucoma. Additionally, differences between the normal and glaucoma groups increased as noise increased both in absolute magnitude and statistical significance. This was particularly true of the 5.52 cpd, stationary grating. (3) The effects of adding noise saturated at relatively low noise contrasts when using a low spatial frequency, sinusoidally reversing grating. We discuss each of these results in more detail below.

Contrast sensitivity without external noise. Contrast sensitivity without added noise failed to discriminate between normals and patients with early glaucoma under any of the conditions that we examined. The performance deficits of patients with early glaucoma (or glaucoma suspects who have early glaucoma) are minimal when there is no added external noise. The conditions for testing contrast sensitivity without added noise were similar to standard conditions which might be used in a clinic. In other words, the conditions without added external noise would not be sensitive enough to detect differences between groups of normals and patients with early glaucoma.

External noise magnifies differences in contrast sensitivity. In general, the nonsignificant deficits which are present without added external noise are magnified when external noise is added to the stimulus. This is most clearly

seen in Figure 1 presenting data for the stationary 5.52 cpd gratings in which the differences and significance between groups increase as noise is added.

The effects of noise saturate at low contrasts for low spatial frequency stimuli. The data for the contrast thresholds of 0.69 cpd gratings reversing at 7.5 Hz presents an apparent exception to the conclusion that increasing noise contrast increases the difference between normal and glaucoma groups. While noise does increase the magnitude and significance of differences between the groups, the effect appears to saturate between a noise contrast of 20% and 40%. This particular stimulus was designed to stimulate the magnocellular system because of its low spatial frequency and relatively high temporal frequency. The response of magnocellular cells of the lateral geniculate nucleus saturate at about 30% contrast [8, 9]. This response saturation could impose a limit on the range of noise contrasts over which increasing noise contrast increasingly masks the stimulus. Drum and Bisset [35] reached a similar conclusion, observing that increasing noise contrast had little effect on coherency thresholds in a pattern discrimination task. It is possible that varying other parameters which alter noise energy (duration and spatial extent) may increase the effectiveness of masking for low spatial frequency, high temporal frequency stimuli.

Sweep VEP estimates of contrast thresholds

In the sweep VEP results, the effects of noise on thresholds were fundamentally different from those observed in the psychophysical studies and those predicted by theory. There was a significant difference between normals and patients with early glaucoma even in the absence of added noise. This significant difference was not magnified as external noise was added. The difference was not significant at 20%, but was significant at the same p level at 60% added noise as the no noise condition. Given our rate of stimulation, 7.5 Hz, we were probably preferentially stimulating the magnocellular pathway using these low spatial frequency stimuli. Therefore, the deficits revealed using the VEPs probably reflect magnocellular deficits in early glaucoma. This is consistent with previous reports that such stimuli are effective without added noise in separating normal and glaucomatous patients [35, 36]

The same pattern of results did not exist for the contrast thresholds of the 5.5 cpd gratings. At the no noise level there was no difference between the normal and early glaucoma groups. No difference emerged as external noise was added. There are two simplistic possibilities which could be used to account for these results. One may note that if no difference exists, multiplying it still yields a zero difference. This possibility is most interesting if we assume that we correctly tested the parvocellular system with the 5.5

cpd stimulus. The implication would be that there is little or no influence of glaucoma on the parvocellular system. We hesitate to draw this inference, however. First, at a temporal frequency of 7.5 Hz, we may be less effective in stimulating the parvocellular pathway. Therefore, failure to find differences between the groups using other stimuli may reflect inadequate stimulation of the parvocellular pathway. Second, we demonstrated a deficit using stationary 5.5 cpd gratings, psychophysically. A stationary 5.5 cpd grating probably more adequately stimulates the parvocellular system than the sweep VEP stimulus. Thirdly, others have demonstrated color vision deficits in glaucoma [18, 19] which are best interpreted in terms of a parvocellular effect [8–14].

In general, the effects of adding noise were minimal on the VEP contrast thresholds, at least in the ranges of noises available in the experiments. We can suggest at least three reasons for the difference between VEPs and psychophysics. First, most electrophysiological measures make use of signal averaging which is a noise cancellation procedure. Therefore, the effects of adding noise may be minimal. Second, psychophysical measures and electrophysiological measures may differ because they tap different levels of the visual system and reflect different internal noise sources [38, 39]. Third, thresholds calculated by extrapolation of VEP voltages do not represent the same differences between signal to noise as thresholds calculated from behavior. In the case of behavior, we know that a threshold of a specific level corresponds to a d' of a certain level. There is no clear analogy in the case of VEP thresholds for stating that a VEP threshold represents a particular likelihood of identifying the stimulus correctly or that this corresponds to a particular d' level. Moreover, it is not clear that thresholds calculated using extrapolation of VEP amplitudes would represent the same separation between signal and noise at the different noise levels tested.

Implications for strategies for early glaucoma detection

In the present study, we wished to determine if adding noise improved the separation of the two normal and glaucoma groups as would be predicted by theory. Also, we wished to determine if added noise might affect VEP and psychophysical contrast thresholds differently.

The present results are encouraging in that they show that our original framework for doing these studies is useful. Adding external noise does increase the separation between normals and patients with early glaucoma when psychophysical thresholds are measured. Our results confirm the observations that VEPs elicited by stimuli likely to stimulate the magnacellular pathway do discriminate between normal and glaucomatous patients. However, we failed to find evidence that adding external noise improved this separation. We have not demonstrated that the tests that we have employed could inde-

pendently be used to detect glaucoma. The results suggest that an optimized test battery of stimuli with added noise could improve screening accuracy and early detection of patients with glaucoma when measured psychophysically. Electrophysiological tests which might be a part of such a battery appear to function as well or better without added noise.

Appendix: Ideal Observer Theory/Signal Detection Theory applied to continuous representations of stimuli

In Signal Detection Theory, performance is limited by the signal-to-noise ratio [23–28].

$$d' = \sqrt{E_t/N} \tag{1}$$

where d' is the sensitivity index, E_t is the signal energy at a given performance level and N is the spectral density of image noise.

Given this view and a statistical representation of an image, it is possible to construct a model, the Ideal Observer, which has no internal noise and uses all available signal information. Such an observer performs optimally in the sense that it is limited only by the information in the image.

Real observers, however, seldom achieve ideal performance. Previous authors have suggested three general factors to account for suboptimal human performance. The first is reduced information gathering efficiency. The Ideal Observer is a Bayesian classifier which determines p(hypothesis/data) for each potential signal. It computes a likelihood ratio for any two signals from the ratio of their probabilities. A decision rule uses the likelihood ratio or its monotonic transform to specify when the observer should say 'yes' or 'no'. The response transition point, the criterion, depends on what aspect of performance the observer wishes to optimize [24]. For most applications, this is assumed to be maximum percent correct.

The main problem, as in all Bayesian classification tasks, is to derive an estimate of p(data/hypothesis). The Ideal Observer obtains p(data/hypothesis) by cross-correlation of an optimal detector, a template exactly matching the expected signal, with the image. Performance would be decreased if the cross-correlation were compromised by using a suboptimal detector, by taking fewer samples, taking samples from too large or small an area, or by taking samples from the wrong location. The importance of proper sampling is apparent from Barlow's [23] definition of efficiency, F, as

$$F\frac{sample\ size\ required\ by\ the\ idea\ observer}{sample\ size\ required\ by\ the\ human\ observer} \tag{2}$$

F can be estimated directly from sensitivity as:

$$F = \frac{d'_e}{d'_i} \tag{3}$$

where d'_e is the experimentally obtained sensitivity and d'_i, is the sensitivity of an observer who uses all available information. Substituting (3) in (1) and rearranging produces the following relationship among detectability, threshold energy, noise and efficiency:

$$d'_e = \sqrt{f}\sqrt{E_t/N} \tag{4}$$

For an experimental performance level of $d' = 1$, the equation can be rewritten in terms of the energy threshold:

$$E_t = (1/F)(N) \tag{5}$$

The second factor producing suboptimal behavior is internal noise. The Ideal Observer is presumed to possess no internal noise. However, most detection devices also have internal noise which decreases detection performance. Internal noise may be represented by adding a term to Equation (5):

$$E_t = (1/F)(N_e + N_{eq}) \tag{6}$$

N_e refers to an external noise component and N_{eq} is a constant 'equivalent noise' [28] within the observer. (It is called 'equivalent' since it is internal noise which could be mimicked by an external noise of the equivalent level.)

One way to visualize the meaning of Equation (6) is to plot data from a hypothetical experiment which measures contrast energy needed to achieve a performance of d $d' = 1$ as a function of external noise spectral density. Figure 4 shows hypothetical results for such an experiment for an Ideal Observer (dotted line) who has an intercept of zero (is noiseless) and a slope of one (uses all information). Line A shows an observer with internal noise but optimum sampling efficiency. The internal noise adds a constant term producing a horizontal shift that can be quantified by the negative of the curve's intersection with the abscissa. Line B shows an observer with no internal noise but a lowered efficiency, which is quantified as the reciprocal of the slope. The division of visual factors into separate additive and multiplicative components, depicted in Figure 4 and Equation (6), has important implications for early detection and diagnosis of primary open angle glaucoma.

- The line's slope indicates the observer's sampling efficiency. If then were a loss of sampling elements, e.g., ganglion cells, or the same number of sampling elements were less sensitive then the slope would increase. Pathological conditions causing cell loss would be manifest as increased slope.

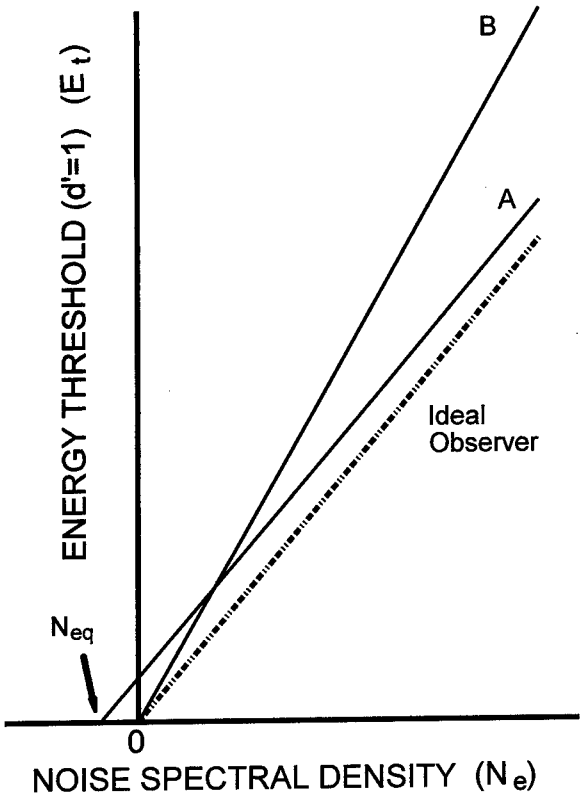

Figure 4. The results of hypothetical results of an experiment in which noise is added to stimuli and the energy threshold is measured. The results of three observers as shown. An ideal observer (dotted line) has an intercept of zero (is noiseless) and a slope of one (uses all information). Line A shows an observer with internal noise but optimum sampling efficiency (slope of one). Line B shows an observer with no internal noise but reduced efficiency (slope greater than one). The internal noise adds a constant term producing a horizontal shift that can be quantified by the negative of the curve's intersection with the abscissa. Loss of efficiency increases slope.

- The addition of external noise amplifies the visual loss. Small deficits, which may not be detectable in the absence of noise (i.e., using conventional displays at early stages of a disease), can become obvious in noise. In Figure 4, for example, the Ideal Observer and observer B are similar at low noise but different at high noise.

External noise should make it possible to detect primary open angle glaucoma earlier, when visual impairment is small and undetectable by normal methods.

- The dissociation of factors into additive and multiplicative components makes differential diagnosis more precise. At any one noise level, two observers could show identical sensitivity loss, yet one might suffer from

increased internal noise and the other from lower efficiency. The observers can be distinguished by testing at different external noise levels. For example, the effect of degraded optics, such as refractive error or reduced retinal illumination, is to add a constant internal noise which shifts the psychometric function without increasing slope (Observer A). Consequently, functional deficits due to optical factors would be distinguishable from deficits due to neural cell dysfunction or loss. Since most primary open angle glaucoma suspects are older, they may have optical losses and clinic personnel do not always correct refractions for test distances or for reduced retinal illumination.

References

1. Krieglstein G. Glaucoma: Editorial overview. Cur Opin Ophthal 1991; 4: 1–2.
2. National Advisory Eye Council. Vision Research: A National Plan, Vol. 2, Part 3. Report of the Glaucoma Panel. Washington, D.C: U.S. Department of Health and Human Services, 1983.
3. Quigley HA, Addicks EM, Green WR. Optic nerve damage in human glaucoma. III. Quantitative correlation of nerve fibre loss and visual field defect in glaucoma, ischemic neuropathy, papilledema, and toxic neuropathy. Arch Ophthal 1982; 100: 135–146.
4. Quigley HA, Sanchez RM, Dunkelberger GR, L'Hernault NL, Baziiski, TA. Chronic glaucoma selectively damages large optic nerve fibers. Invest Ophthal Vis Sci 1987; 28: 913-920.
5. Quigley HA, Dunkelberger GR, Green WR. Chronic human glaucoma causing selectively greater loss of large optic nerve fibers. Ophthalmology 1988; 95: 357–363.
6. Quigley HA, Dunkelberger GR, Green WR. Retinal ganglion cell atrophy correlated with automated perimetry in human eyes with glaucoma. Amer J Ophthal 1989; 107: 453–64.
7. Migdal C. Primary open-angle glaucoma. In: Tasman W, Jaeger EA, eds. Duane's Clinical Ophthalmology, Vol. 3, Chapter 52. Philadelphia: J.B. Lippincott Co., 1992.
8. Derrington AM, Lennie P. Spatial and temporal contrast sensitivities of neurones in lateral geniculate nucleus of macaque. J Physiol 1984; 357: 219–240.
9. Kaplan E, Lee BB, Shapley RM. New views of primate retinal function. Prog Ret Res 1990; 9: 273–336.
10. Livingstone M, Hubel D. Segregation of form, color, movement, and depth: Anatomy, physiology, and perception. Science 1988; 240: 740–749.
11. Merrigan WH, Eskin TA. Spatio-temporal vision of macaques with severe loss of P_β retinal ganglion cells. Vis Res 1986; 26: 1751–1761.
12. Merrigan WH, Maunsell JH. Macaque vision after magnocellular lateral geniculate lesions. Vis Neurosci 1990; 5: 347–352.
13. Shapley R. Visual sensitivity and parallel retinocortical channels Ann Rev Psychol 1990; 41: 635–658.
14. Shiller PH, Logothetis NK, Charles ER. Role of color-opponent and broad-band channels in vision. Vis Neurosci 1990; 5: 321–346.

15. Bassi CJ. Parallel processing in the human visual system. In: Wall M, Sadun A, eds. New Methods of Sensory Visual Testing in Clinical Ophthalmology. Berlin: Springer-Verlag, 1989: 1–13.
16. Johnson C. Selective versus nonselective losses in glaucoma. J Glaucoma 1994; 3: S32–S44.
17. Breton ME, Drum BA. Functional testing in glaucoma: visual psychophysics and electrophysiology. In: Ritch R, Shields MB, Krupin T, eds. The Glaucomas: Basic Sciences, 2nd ed. St. Louis: Mosby, 1996: 677–699.
18. François J, Veriest G. Lens dyschromatopsies aquises dans le glaucome primaire. Ann Ocul (Paris) 1959; 192: 191–194.
19. Sample PA, Weinreb RN. Color perimetry for assessment of primary open angle glaucoma. Invest Ophthalmol Vis Sci 1990; 31: 1869–1879.
20. Odom JV, Feghali JG, Jin JC, Weinstein GW. Retinal visual function deficits in glaucoma: Electroretinogram (ERG) pattern and luminance nonlinearities. Arch Ophthalmol 1990; 108: 222–227.
21. Feghali JG, Bocquet X, Charlier J, Odom JV. Static flicker perimetry in glaucoma and ocular hypertension. Curr Eye Res 1991; 10 205–212.
22. Repka MX, Quigley HA. The effect of age on normal human optic nerve fiber number and diameter. Ophthalmology 1989, 96, 26–32.
23. Jonas JB, Mueller-Bergh JA, Schloetzer-Schrehardt UM, Naumann GO. Histomorphometry of the human optic nerve. Invest Ophthalmol Vis Sci 1990; 31: 736–44.
24. Barlow H. The efficiency of detecting changes of density in random dot patterns. Vis Res 1978; 18: 637–650.
25. Green DM, Swets JA. Signal detection theory and psychophysics. New York: John Wiley and Sons, Inc., 1966.
26. Kersten D. Spatial summation in visual noise. Vis Res 1984; 24: 1977–1990.
27. Legge E, Kersten D, Burgess A. Contrast discrimination in noise. J Opt Soc Amer A 1987; 4: 391–404.
28. Meeteren van A, Barlow H. The statistical efficiency for detecting sinusoidal modulation of average dot density in random figures. Vis Res 1981, 21, 765–777.
29. Pelli DG. The quantum efficiency of vision. In: Blakemore C, ed. Vision: Coding and Efficiency Cambridge: Cambridge University Press, 1990: 3–24.
30. Walsh D. Aging and human visual information processing. Geriatr Ophthalmol 1986; 2: 29–35.
31. Pardhan 5, Gilchrist J, Beh G, Elliott D. The decrease in sampling efficiency with age. Invest Ophthalmol Vis Sci 1993; 34 (Suppl): 1418.
32. Pardhan 5, Gilchrist J, Yap M. Contrast detection in noise in open angle glaucoma. Invest Ophthalmol Vis Sci 1994; 35 (Suppl): 1752.
33. Aulhorn E, Koest G. Noise field campimetry: a new perimetric method (snow campimetry). In: Heijl A, ed. Perimetry Update 1988/1989 Amsterdam: Kugler, 1990: 331–336.
34. Drum B, Breton M, Massof R, Quigley H, Krupin T, Leight, J, Magnat-Rai I, O'Leary D. Pattern discrimination perimetry: a new concept in visual field testing. Doc Ophthalmol Proc Series 1987; 49: 433–440.
35. Drum B, Bissett R. Optimizing dot size and contrast in pattern discrimination perimetry. In: Mills RP, Heijl A. Perimetry Update 1990/9 1. Amsterdam: Kluger, 1991: 373–379.
36. Towle VL, Moskowitz A, Sokol S, Schwartz B. The visual evoked potential in glaucoma and ocular hypertension: effects of check size, field size, and stimulation rate. Invest Ophthalmol Vis Sci 1983; 24: 175–183.

37. Schmeisser ET, Smith TJ. High-frequency flicker visual-evoke I potential losses in glaucoma. Ophthalmology 1989; 96: 620–623.
38. Brown A. Intrinsic contrast noise and infant visual contrast discrimination. Vis Res 1994; 34: 1947–1964.
39. Sperling G. Three stages and two systems of visual processing. Spatial Vis 1989; 2/3: 183–207.

Address for correspondence: J. Vernon Odom, Department of Ophthalmology, Robert C. Byrd Health Science Center of West Virginia University, P.O. Box 9193, Morgantown, WV 26506, USA
Phone: 1- 304-293-3757; Fax: 1-304-293-7139; E-mail: jodom@wvu.edu

Documenta Ophthalmologica **95:** 301–314, 1999.

Reduced duration of a visual motion aftereffect in congenital nystagmus

JOSEPHINE SHALLO-HOFFMANN[1], CLIVE J. WOLSLEY[1], JAMES F. ACHESON[2] & ADOLFO M. BRONSTEIN[1]
[1]*MRC Human Movement and Balance Unit, National Hospital, London and* [2]*Department of Neuro-Ophthalmology, London, UK*

Abstract. Congenital nystagmus (CN) is a primarily horizontal, involuntary, conjugate eye movement which can be observed soon after birth or during the first half-year of life. Individuals with CN rarely complain of oscillopsia. Using a motion aftereffect (MAE), we investigated if individuals with CN have abnormalities in motion perception and if any such abnormality could be due to nystagmus or to compensatory mechanisms to avoid oscillopsia.

In task A, patients (n= 10) and control subjects (n= 10) indicated the direction, duration and relative velocity of MAEs. The subjects binocularly viewed a high contrast, grey scale grating (0.23 cyc/deg; visual angle: 18.3 deg) moving upward or downward at 1, 3, and 6 deg/sec for 60 sec. Vertical optokinetic nystagmus (OKN) was monitored. In task B, patients (n=8) and control subjects (n=8) viewed similar spatial frequency gratings (visual angle: 40.7 degs; 0.5, 0.2, 0.08 cyc/deg) which moved at 4, 10, and 16 deg/sec for 60 sec. In task C, five control subjects, with induced vestibular nystagmus, viewed a grating (0.2 cyc/deg; visual acuity: 28.5 deg), moving upward for 40 sec. In all three tasks, after adaptation with the moving grating, subjects viewed the then static grating and reported the duration and direction of the MAE. One CN patient and eight control subjects reported MABs at all three test velocities in task A. When patients exhibited OKN, the gain was close to one, as in the control group. In task B, seven of the eight patients and all of the control subjects had MABs at the faster adaptation velocities. CN patients had less MAEs at an adaptation velocity of 4 deg/sec and when MAEs were observed, the duration of the illusory motion was reduced by approximately 48%. Control subjects, with induced vestibular nystagmus, reported MAEs at 4 deg/sec (task C).

These findings indicate that nystagmus cannot be the only factor accounting for the suppression of motion perception and suggest that compensatory mechanisms used to avoid oscillopsia contribute to the differences found between the groups.

Key words: congenital nystagmus (CN), motion after effect (MAE), motion perception, oscillopsia

Introduction

The purpose of this study was to investigate if individuals with congenital nystagmus (CN) have impaired processing of visual motion by using a mo-

tion aftereffect (MAE) and whether any such impairment can be attributed to nystagmus or due to compensatory mechanisms to avoid oscillopsia.

A visual motion aftereffect (MAE) can be generally described as the apparent motion of a stationary object which is caused by adaptation to a moving pattern over some period of time. The stationary object appears to move in the opposite direction for an interval of approximately 1/3 or less of the adaptation period [1]. Numerous studies have been concerned with the cortical location of mechanisms coding direction and elicitation of MAEs [2]. Recently, functional magnetic resonance imaging was used to measure local haemodynaniic changes in normal human visual cortical area MT and showed the production of visual MAEs [3]. Motion aftereffects are useful to study motion processing since they are a pure motion event, eliminating the parameter of object displacement, a factor which can confound motion perception in individuals with nystagmus.

The cause of congenital nystagmus (CN) is unknown. CN is a benign, primarily horizontal, conjugate nystagmus that may be noted at birth or in early infancy. It can be inherited and is sometimes associated with other congenital disorder, such as, albinism, aniridia, congenital cataracts and inherited optic atrophy. CN patients rarely complain of oscillopsia and the manner by which they avoid it, is unclear. Studies have indicated that persons with CN develop mechanisms which could account for their visual stability, suggesting that extraretinal signals cancel out the involuntary eye movement, [4, 5], post-saccadic backward masking of motion signals [6] and a central elevation of motion perception thresholds [7].

In the case of motion perception, Dieterich and Brandt [7] concluded that both nystagmus and a central adaptive process were responsible for elevation of motion perception thresholds. Kommerell, Horn and Bach [8] suggested that patients may have a reduced sensitivity to shifts of the retinal image. Both these studies used stimuli which moved in the same direction as the patients nystagmus which may have confounded finding.

Using a luminous dot target for detecting horizontal and vertical oscillatory motion to evaluate if CN subjects might be less sensitive to retinal image motion than a control group, Bedell [9] evaluated motion thresholds to oscillatory target motion in the meridian of the CN patient's nystagmus and found them elevated as well as showing that thresholds were raised in control subjects when the target underwent continuous sinusoidal motion to stimulate the retinal motion that occurs with nystagmus eye movement. The author suggested that the motion deficits could not account for the visual stability of CN subjects and proposed that perceptual adaptation may be one mechanism contributing to their visual constancy.

Table 1. Clinical status: Congenital Nystagmus patients

Subjects case no.	Age in yr/sex	Visual acuity cc	Head turn	Ocular alignment	Clinical diagnosis
1	27/M	0.7; 0.7	right, 10 deg	orthotropia	idiopathic CN
2	30/M	0.7; 0.7	right, 15 deg	esotropia	nystagmus blocking syndrome
3	28/M	0.3; 0.3	right, 10 deg	esotropia	idiopathic periodic alternating nystagmus
4	45/M	0.3; 0.3	right, 10 deg	orthotropia	OX recessive: ocular albinism
5	39/M	0.17; 0.17	chin down- 15 deg, left tilt, 5–10 deg	esotropia	inherited optic atrophy associated with CN
6	48/M	0.25; 0.33	nil	orthotropia	OX recessive: ocular albinism
7	26/M	0.5; 0.5	chin down- 5 deg, right tilt, 5 deg	orthotropia	idiopathic CN
8	25/M	1.2; 1.0	right or left 10 deg	orthotropia	idiopathic periodic alternating nystagmus
9	38/M	0.67; 0.67	left, 10 deg	orthotropia	idiopathic periodic alternating nystagmus
10	53/M	0.7; 0.7	nil	orthotropia	idiopathic CN

Key: OX recessive – X- chromosomal recessive, M – male, F – female, yr – year, no. – number.

Recently, we investigated motion detection thresholds in patients with CN and found that visual motion which was orthogonal to the plane of nystagmus motion, was not sufficient to reduce thresholds to normal [10].

Therefore, in this study we have used adaptation stimuli which involved motion orthogonal to nystagmus motion and measured a response which did not depend on the physical movement of a stimulus.

Materials and methods

Subjects

Congenital nystagmus patients, who did not complain of oscillopsia and did not have a vertical component to their nystagmus, were recruited from the Neuro-Ophthalmology service of the National Hospital. Control subjects were age-matched staff and student volunteers drawn from the hospital population. Ten orthotropic control subjects (23–52 years; 2 females, 8 males) participated in task A, eight orthotropic control subjects (25–48 years; 8 males) participated in task B and five orthotropic control subjects (24–38 years, 1 female, 4 males) participated in task C. The control subject groups had normal corrected visual acuity. All participants underwent ophthalmological examin-

ation before testing. The clinical status of the patients (1–10) are presented in Table 1.

It was the first time any of the subjects had viewed a motion aftereffect and they were naïve, not only to the predicted outcome of exposure to an adaptation stimulus but also to the purposes of the study. Investigations were performed according to the guidelines of the 'Declaration of Helsinki' as well as the medical ethics committee of the National Hospital. Subjects were fully informed about the nature of the procedures and gave their written consent before the beginning of the experiment. Eight of the ten patients (Case numbers 1, 3–9) returned to participate in task B. Two of the control subjects, who participated in task B, returned to perform task C.

Eye movement recordings

Eye movements were recorded using an infra-red limbal reflection technique (DC – 250 Hz bandwidth, resolution 0.1 deg). Eight minute recordings of horizontal (range: ± 20 deg) and a one minute recording of vertical eye movements (range: ± 10 deg) were performed on the patients to document the characteristics of their waveforms as part of the initial screening.

Task A – MAEs at adaptation velocities of 1, 3 and 6 deg/s

All subjects were naïve, light adapted to the ambient illumination of the grating, and viewed a stimulus binocularly with their head and chin restrained by rests. The stimulus consisted of a high contrast, back-projected, grey scale, sinusoidal grating (0.23 cyc/deg, 43 cm in diameter), subtending 18.3 deg, moving upward or downward at 1, 3 and 6 deg/sec, presented for 60 sec. It was vignetted with a circular mask to eliminate both flicker and motion cues derived from the edge of the stripe. Subjects indicated the direction, duration and relative velocity of a MAE using a subject-operated device which recorded these variables on a strip chart during testing. Vertical optokinetic (OKN) responses (right eye) and horizontal CN eye movements (left eye) were monitored during testing by infra-red limbal reflection oculography as well as stimulus velocity (veridical and illusory) and stored on a PC (Figure 1).

The joystick and procedure

The purpose of the joystick was to record latency of the onset of an MAE, relative perceived velocity of an MAE as compared to the velocity of the adaptation stimulus and the duration of a MAE during the test session. Subjects were instructed in the use of and given practice in manipulating a self-zeroing

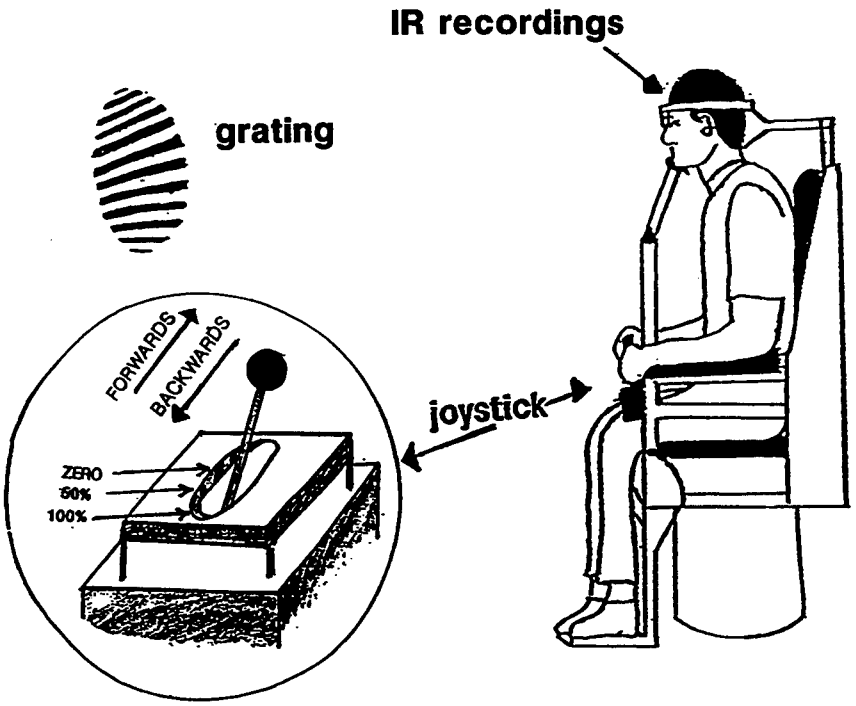

Figure 1. The subjects viewed a spatial frequency grating, moving upward or downward in the three tasks. Vertical OKN eye movements (IR, infrared recordings) and joystick deflections were simultaneously recorded during the test session in task A.

device, which had two guidepost positions in the upward motion direction and two in the downward motion direction: that is, a central - neutral position (denoted zero velocity), a full deflection position either forward (for upward motion) or backward (for downward motion), representing the velocity of the adapting stimuli as 100%, and a notch between 0 and 100%, representing 50% velocity. The device was attached to either the right or left arm of the chair used during testing, depending on the hand-dominance of the subject (Figure 1, joystick).

Subjects were not informed as to what they were expected to perceive after exposure to the adapting stimuli (either 1, 3 or 6 deg/sec). They were told that they should look at the stripes of the grating which would move either upward or downward for 60 sec. They were not to look at the edges of the grating and without looking at the joystick, they moved it to full deflection (100% velocity) in the direction of the adaptation velocity motion and kept it there until the motion stopped, which occurred after 60 sec. The subject then returned the joystick to the neutral (no-motion) position. The examiner

then asked the subject what he or she 'saw'. If a subject reported a MAE, he or she was instructed to move the joystick in the direction of the motion to a point of subjective relative velocity (any position between 0 and 100%) as compared with the adaptation stimulus velocity. During a test session, as subjects tracked the movement of the stripes, eye position was monitored by a video.

Calibration and analysis of relative velocity, latency and duration of a MAE and eye movements during task performance

Calibration of the joystick deflections was performed for each subject before and after a test session. Relative velocity of an MAE was measured in percent of absolute velocity which was calculated by dividing the full joystick deflection unit executed during adaptation velocity by the deflection unit of the illusory motion executed during an MAE.

The gain (slow phase velocity of the vertical OKN over velocity of the adaptation stimulus) was calculated, when possible, in the patient group and for all the control subjects to investigate if there was a correlation between gain and the occurrence of a MAE.

A measure of the latency of a response was calculated when subjects indicated a pause in the zero velocity position between the termination of the adapting stimulus motion and the onset of illusory motion in seconds.

Testing for a MAE under minimal nystagmus conditions in CN subjects

Five patients (Case no. 1, 3, 4, 7 and 9) who did not have MAEs at an adaptation velocity of 6 deg/sec, repeated the task while using their specific head turn which can minimise nystagmus.

Task B – MAEs at adaptation velocities of 4, 10 and 16 deg/s

Eight patients (case no. 1–2, 3–9) and age-matched control subjects reported on MAEs after viewing high contrast, grey scale, computer generated gratings (31 × 23 cm, visual angle: 40.73 deg) of 0.08, 0.2 and 0.5 cyc/deg, which moved at velocities of 4, 10 and 16 deg/sec for 60 sec. The order of presentation of the three spatial frequencies, three velocities and two directions of stimulus motion was randomised in a $3\times3\times2$ Latin square matrix of 18 trials. Subjects reported the direction and duration of illusory motion. A 60 sec rest interval was interleaved between each trial and a testing session lasted approximately 1 hour.

Task C – Induced vestibular nystagmus in control subjects and the occurrence of an MAE

Vestibular nystagmus was induced using a 25 deg centigrade 'cold' water caloric irrigation of the left ear in five control subjects. The head was tilted 60 deg backwards to stimulate the horizontal canal for 40 sec. After the nystagmus was stimulated, the subjects viewed an adaptation stimulus (visual angle: 28.5 deg; 0.2 cyc/deg) which moved at 4 deg/sec for 40 sec. When the motion stopped, subjects reported how the grating 'appeared'. Nystagmus persisted throughout the entire adaptation (40 sec) and test, lasting approximately 30 sec. Subjects reported the direction and duration of illusory motion.

Results

Task A

Number: All control subjects reported MAEs in task A. Only one patient (case no. 5) had MAEs at all three adaptation velocities compared with eight control subjects. Two patients had MAEs at an adaptation velocity of 6 deg/sec; one control subject reported MAEs only at 3 deg/sec, and one control subject reported MAEs only at 6 and 3 deg/sec (Figure 2, A).

Latency and duration of an MAE: A mean latency of 5.32 $\pm$ 5.02 sec between the stimulus offset and the perception of illusory motion occurred 35% of the time in the control group. The longest latencies occurred at an adaptation velocity of 3 deg/sec ($F2,20) = 3.496$; p=0.05. The three CN patients showed a latency in response 6 out of the 7 times that they reported MAEs (mean of 2.75 $\pm$ 1.92 sec).

No differences in the mean duration of an MAE were found due to adaptation velocities $F(2,42) = 1.392$; $p = 0.260$ in the control group (Table 2). The mean MAE duration for the one patient who reported them at all three test velocities was 19 $\pm$ 9.3 sec. A duration of 7.5 sec was reported by two patients at 6 deg/sec only.

Perceived velocity of an MAE relative to the adaptation velocity: The perceived velocity of a MAE was always found to be less than the veridical adapting velocity (Table 2). The three patients who reported MAEs, one at all three test velocities, and two at 6 deg/sec, judged the illusory velocity to have moved at a mean of 42.23 $\pm$ 20.82 percent of the adaptation velocity. The ten control subjects judged an MAE to have moved at a mean of 47.28 $\pm$ 27.43 deg/sec. Increased duration of a MAE did not correlate with perceived relative velocity (r=0.206; p=0.190).

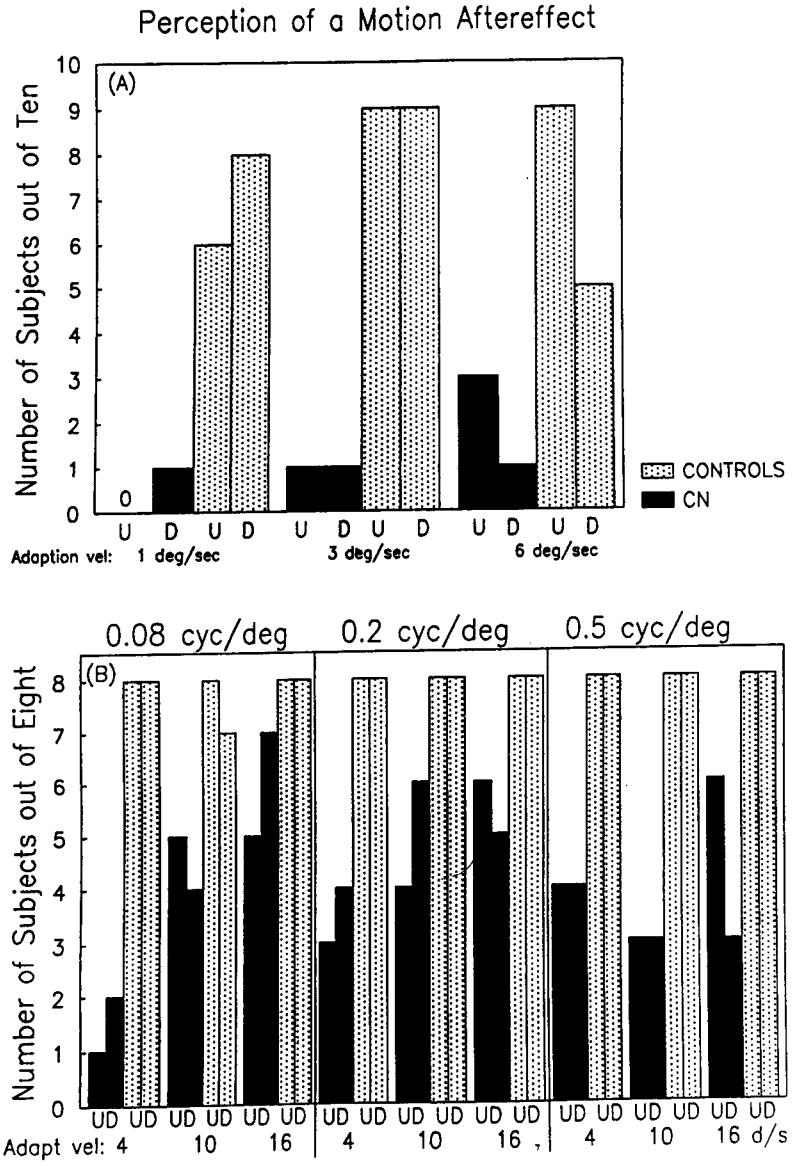

Figure 2. Number: The histograms (A) and (B) demonstrate the differences in the number of subjects who perceived a MAE from each group under task A and B test conditions. U - upward and D - downward stimulus motion. Adapt vel and Adaption vel = adaptation velocities in deg/sec.

Table 2. MAE characteristics for the control group in task A

Adaptation velocity	1 deg/sec	3 deg/sec	6 deg/sec
Latency	3.88 ± 2.34 sec	8.39 ± 6.32 sec	2.67 ± 2.79 sec
	$n = 3$	$n = 4$	$n = 4$
Duration	12.71 ± 15.97 sec	9.08 ± 8.10 sec	16.42 ± 12.08 sec
	$n = 8$	$n = 9$	$n = 9$
Relative velocity	52.39 ± 26.30%	40.79 ± 20.06%	49.95 ± 30.93%

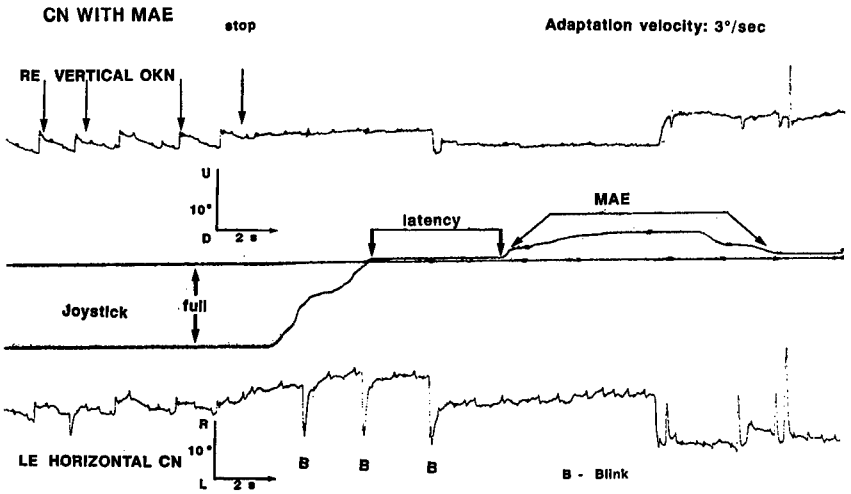

Figure 3. An example of eye movements and joystick deflections of a CN patient during downward stimulus motion at an adaptation velocity of 3 deg/sec. The top recording shows the right eye (RE) measurement of vertical optokinetic nystagmus (OKN: first three arrows). The fourth arrow shows the point where the adaptation stimulus was stopped. The middle recording displays a full joystick deflection. When the adaptation stimulus stopped (stop), the joystick was brought back to the zero deflection position by the subject. In this case, a latency occurred before the subject moved the joystick in the opposite direction (upward) to indicate the perception of an MAE. The height of the deflection disclosed the perceived velocity of illusory motion relative to the previous (full deflection) veridical stimulus velocity. The bottom trace documents the left eye (LE) horizontal CN eye movements.

Table 3. The influence of direction on the mean duration (in sec) of a MAE

Subjects	Up	Down	ANOVA
CN	9.24 ± 4.97	11.54 ± 5.4	F(1,70) = 3.826
	n = 34	n = 38	p=0.054
Control	21.74 ± 7.5	17.6 ± 6.7	F(1,141) = 12.23
	n = 72	n = 71	p = 0.001

OKN and MAEs: Vertical OKN was consistently at a gain of 1 for the control group regardless of whether a MAE was generated or not. Four of the ten patients showed some vertical OKN tracking. When OKN was present, it also had a gain close to 1 and did not correlate with MAEs (Figure 3).

Nulled nystagmus and the MAE: The five patients who repeated task A while using their specific head turn to damp nystagmus, did not report MAEs under this test condition.

Task B – The duration of an MAE as a function of adaptation velocity, spatial frequency and direction

Number: In task B, seven of the eight patients and all of the control subjects reported MAEs in, at least, one direction when adaptation velocity was either 10 or 16 degs/sec. An adaptation velocity of 4 deg/sec was least effective in eliciting MAEs in the patient group compared to their performance at faster velocities [F (2, 15)= 5.0; p<0.02)]. Figure 2B shows the number of patients, (one patient at 0.08 cyc/deg in the up direction, four patients at 0.2 and 0.5 cyc/deg), compared with all eight control subjects who reported MAEs when velocity was 4 deg/sec.

The duration of an MAE was reduced for the patient group by 49.1%, 48.7% and 46% when adaptation velocities were 4, 10, and 16 deg/sec respectively compared to the control group [F= (1, 213) 91.124; p<0.0001] (Figure 4).

Upward motion increased the duration of an MAE in the control group and decreased it in the patient group (Table 3).

No differences in MAE duration were found due to spatial frequency (F(2, 179)=0. 568; p=0.568].

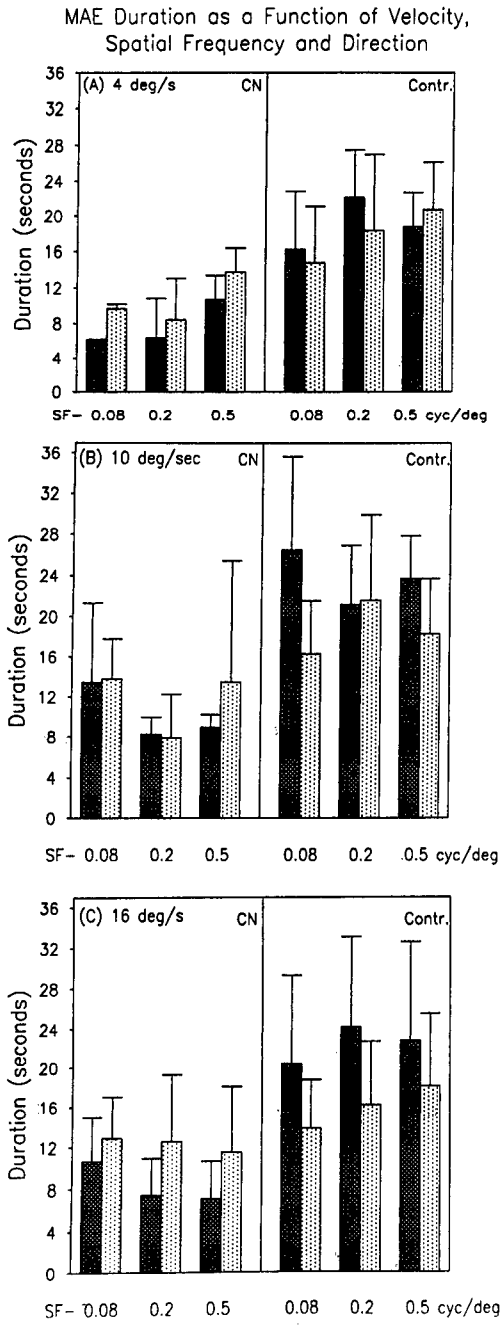

Figure 4. Comparison of the duration of the MAE for CN (CN) and control (Contr.) subjects at three adaptation velocities (A – 4 deg/sec, top; B – 10 deg/sec, middle, and C – 16 deg/sec, bottom) in task B. Note the reduced MAE duration for the patient group in all conditions as compared to the control group. No differences due to spatial frequency were found. Dark check pattern; light dot pattern – data when adaptation velocity moved upward and downward, respectively.

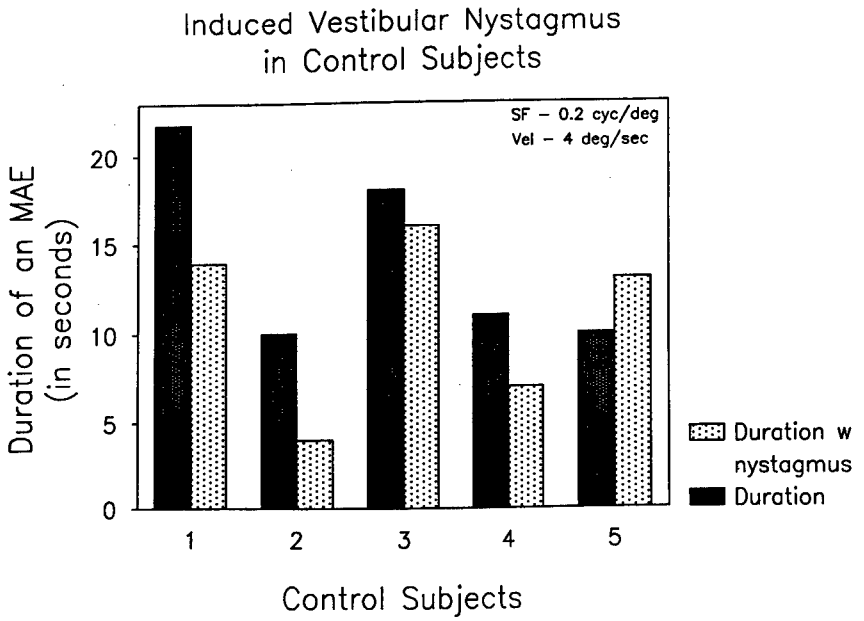

Figure 5. The duration of a MAE in five control subjects before and with (w) vestibular nystagmus.

Task C – The influence of induced vestibular nystagmus in control subjects on the elicitation of MAEs

No differences in mean duration of a MAE before (14.16 ± 5.42 sec) and after (10.77 ± 5.05 sec) caloric irrigation for the five subjects were found $F(1,8) = 1.043$; $p = 0.337$ although four of the five subjects had a reduction in the duration of an MAE after induced vestibular nystagmus (Figure 5).

Discussion

The adaptation stimuli in task A were almost completely ineffective in eliciting MAEs in the patient group, even if they used head turns to achieve minimal nystagmus. Some factors affecting performance may have been the size of the grating (visual angle: 18.3 deg), spatial frequency (0.2 cyc/deg), slow adaptation velocities, poor visual acuity in some members of the patient group or nystagmus. Results from task A suggest that visual acuity was not a factor effecting performance since the grating was of high contrast and all CN subjects reported that the grating was moving, even at the slowest adaptation velocities. Further, the only CN subject, (Table 1 – case no. 5), who reported MAEs at all velocities, had poor visual acuity (Snellen acuity: 0.17). Data

gained within the control group showed that latencies occurred one-third of the time and duration did not correlate with the illusory velocity of an MAE or veridical velocity of the adaptation stimuli. Although between group comparisons were not possible concerning MAEs, when OKN was recognisable in CN subjects, the gain of the response was similar to the control group.

Task 2 tested some of the factors mentioned above by enlarging the stimulus (visual angle: 40.7 deg); adding a finer and courser spatial frequency (0.08 and 0.5 cyc/deg) and two faster adaptation velocities (10 and 16 deg/sec). Two main effects were shown. Firstly, the stimuli were sufficient to elicit some MAEs in all patients with the exception of one (case no. 6), who never reported a MAE in either task. However, the patient group had the least number of MAEs at a slow adaptation velocity (4 deg/sec). It has been demonstrated that control subjects tolerate retinal image motion approaching 3–4 deg/sec [11] at which point visual constancy starts to decay [12]. These findings show that mechanisms operate in normal subjects to suppress the perception of image motion and smear. Our findings, that CN subjects seldom reported MAEs at velocities of 4 deg/sec and less is supported by a previous study in which we asked a similar patient group to discriminate vertically moving velocity and found that they were less accurate than control subjects when test velocities were below 4 deg/sec [10]. These studies suggest that CN patients use similar mechanisms as normally sighted individuals to suppress the perception of smear, especially when velocity is slow. One such mechanism suggested by Bedell & Bollenbacher [5] is the cancellation of retinal image motion signals that represent nystagmus eye motion, a mechanism which may be useful to avoid oscillopsia at a cost of sensitivity to motion.

Secondly, although stimulus motion was orthogonal to the CN subject's horizontal nystagmus motion, the ongoing retinal slip may have inhibited the perception of MAEs or contributed to the reduction in duration of the response found in this study. Four of the five control subjects with induced vestibular nystagmus had some reduction in the duration of MAEs. However, all five subjects reported MAEs at an adaptation velocity (4 deg/sec) which was least effective in evoking MAEs in the patient group, indicating that the nystagmus alone can not account for all the deficits found.

In summary, we have shown that the duration of MAEs was reduced and adaptation velocities of 4 deg/sec or less inhibited the elicitation of MAEs in the patient group. Nystagmus was not sufficient to account for these deficits since control subjects, with induced vestibular nystagmus, had MAEs at an adaptation velocity which was least effective in the patient group. These findings suggest that mechanisms are involved to suppress image smear, especially when velocities are slow, which may be useful to avoid oscillopsia.

Acknowledgements

The authors gratefully acknowledge Anthony Morland who suggested the MAE paradigm and David Buckwell who wrote the software for tasks B and C.

References

1. Wade NJ. A selective history of the study of visual motion aftereffects. Perception 1994; 23: 1111–1134.
2. Thompson P. Motion psychophysics. In: Miles FA & Wallmann J (eds). Visual motion and its role in the stabilisation of gaze. Elsevier Science Publishers BV, 1993: pp. 29–52.
3. Tootell RB, Reppas JIB, Dale AM, Look RB, Sereno MI, Malach R, Brandy TJ, Rosen BR. Visual motion aftereffect in human cortical area MT revealed by functional magnetic resonance imaging. Nature 1995; 373: 139–141.
4. Goldstein HP, Gottlob I, Fendick MG. Visual remapping in infantile nystagmus. Vis Res 1992; 32: 1115–1124.
5. Bedell HE, Bollenbacher MA. Perception of motion smear in normal observers and in persons with congenital nystagmus. Invest Ophthamol & Vis Sci 1996; 37: 188–195.
6. Leigh RJ, Dell'Osso LF, Yanigios SS, Thurston S]E. Oscillopsia, retinal image stabilisation and congenital nystagmus. Invest Ophthamol & Vis Sci 1988; 29: 279–282.
7. Dieterich M, Brandt T. Impaired motion perception in congenital nystagmus and acquired ocular motor palsy. Clin Vis Sci 1987; 1: 337–345.
8. Kommerell G, Horn R, Bach M. Motion perception in congenital nystagmus. In: Keller EL & Zee DS (eds). Adaptive processes in visual and oculomotor systems. Oxford: Paragon Press, 1986: 485–491.
9. Bedell HE. Sensitivity to oscillatory target motion in congenital nystagmus. Invest Opthalmol & Vis Sci 1992; 33: 1811–1821.
10. Shallo-Hoffmann J, Bronstein AM, Acheson J, Morland AB, Gresty MA. Vertical and horizontal motion perception in congenital nystagmus. Neuro-Ophthalmol 1998; 19: 171–183.
11. Steinman RM, Collewijn H. Binocular retinal image motion during active head rotation. Vis Res 1980; 20: 415–429.
12. Barnes GR, Smith R. The effects on visual discrimination of image movement across the stationary retina. Aviat, Space, & Environ Med 1981; 52: 466–472.

Address for correspondence: J. Shallo-Hoffman, College of Optometry, Nova Southeastern University, 3200 South University Drive, Fort Lauderdale, FL 33328-2018, USA
Phone: ++(1) 954 262 1464; Fax: ++(1) 954 262 3875; E-mail: shoffman@hpd.nova.edu

Documenta Ophthalmologica **95:** 315–333, 1999.

Visually evoked potentials evoked by moving unidimensional noise stimuli: Effects of contrast, spatial frequency, active electrode location, reference electrode location, and stimulus type

J. VERNON ODOM[1,2], ELS DE SMEDT[1], LIDWINE VAN MALDEREN[1] & WERNER SPILEERS[1]

[1]*Dienst Oogziekten, UZ - St. Rafael, Kapucijnenvoer 33, 3000 Leuven, Belgium and*
[2]*Department of Ophthalmology, Robert C. Byrd Health Sciences Center of West Virginia University, Morgantown, WV 26506-9192, USA*

Abstract. We determined the relative importance of electrode derivation, stimulus type, spatial frequency and contrast in determining the relative size of the late negative and early positive responses of motion elicited VEPs. Seven subjects aged 22–48 years with normal vision were tested binocularly. Motion onset and motion reversal were employed as modes of stimulus presentation. For both, pseudo-random one-dimensional noise patterns whose peak power was at 5.2, 2.6, 1.3, 0.325 and 0.1625 cycles per degree (cpd) were stimuli. Contrasts were 70% and 5%. Active electrodes were placed at Oz, 5 cm to the left of Oz, 5 cm to the right of Oz and a frontal midline position (Fpz) and referenced to linked mastoids. Transient motion reversal elicited a prominent positive response present in all subjects and at low contrasts. Motion onset VEPs have a complex waveform which may be either predominantly positive or negative. The most important variables in determining whether a prominent positivity or negativity is present in the motion onset VEP are the contrast and the spatial frequencies. Data such as these are first efforts in developing recommendations for the motion VEP.

Introduction

Visually evoked potentials (VEPs) elicited by moving stimuli were among the first potentials recorded that were elicited by patterned stimuli [1–6]. However, as the cathode ray tube displays replaced the galvanometer controlled mirror as the typical stimulus for eliciting VEPs, interest in the response declined [7]. More recently a number of investigators have reintroduced the moving stimuli as a means of eliciting VEPs [8–28]. Two major reasons appear to account for this renewed interest. First, recent data provide support for the idea that there is a cortical system relatively sensitive to motion [29–34]. Thus VEPs elicited by moving stimuli provide one means of isolating these cortical regions [12, 21–23, 34]. Secondly, several authors have suggested that the motion centers in the cortex receive their input exclusively (30) or

largely (32, 33) from the magnocellular (M) layers of the lateral geniculate nucleus. VEPs elicited by moving stimuli should reflect the output of the M pathway. Because a number of ocular and neurological diseases are thought to affect first the M pathway [20, 34], VEPs elicited by moving stimuli might come to serve a unique and useful role in diagnosis (15–19, 35).

If VEPs elicited by moving stimuli are to become clinically useful, the optimal stimulus and recording conditions must be determined. Additionally, data must be gathered which determine the variability and reliability of these responses. Different groups of investigators, however, have employed varying techniques to elicit motion VEPs. The two most common are motion onset and motion reversal. Additionally, they have used different contrasts, spatial frequencies, active electrode positions and reference electrode positions [8–28]. All of these parameters have been shown to affect the topography and morphology of the response [10, 21, 22].

The present study was conducted as part of an ongoing effort to develop electrophysiological methods to evaluate magnocellular (M) and parvocellular (P) function. In our previous work on motion onset and motion reversal [26] we employed a high contrast pattern (70%) and recorded responses using a single channel, midline montage (active: Oz, reference: Fpz, and ground: Cz). For both motion onset and motion reversal, the response we recorded was a prominent positivity. However, the new ISCEV standard for VEPs [39] calls for a minimum of three channels (active: Oz, O_3, O_4; reference: Fpz; ground: Cz). The groups most active in the clinical use of motion VEPs have recommended using an ear (or linked ears) reference [9–10, 15–16], motion onset stimuli, low spatial frequency patterns and low contrast stimuli [9, 21, 22]. Using these stimulus conditions they record a prominent late negative response. We wished to determine the relative importance of the variables indicated (electrode location, stimulus type, spatial frequency and contrast) in determining the relative size of the late negative and early positive responses. We view efforts such as these as first efforts in developing recommendations for the motion VEP.

Methods

Subjects

Seven subjects aged 22–48 years with vision corrected to 6/6 or better were tested. Subjects were excluded if they had a history of ophthalmic disease or systemic diseases which might be expected to interfere with visual function.

Apparatus

The apparatus used for the generation of the stimulus was identical to the one described in Spileers et al. (1996): a PC (IBM compatible 486, 33 Mhz) was used to generate the stimulus for the Millipede Prisma VR1000 grating generator on a display with a vertical resolution of 1024 lines at a 100 Hz frame rate (Manitron Ltd VLR 1593). To record the VEPs, a second PC IBM power station (VL4, 1486DX-266) with a multi-channel fiber isolated EEG amplifier (Stichting Vision Research Amsterdam) was used to sample the incoming signal. The sampling rate was 500 Hz.

Stimuli

The stimulus was a unidimensional noise pattern, as described previously [25, 26]. We have several reasons for selecting these patterns. First, the relative richness of the spatial frequency spectrum of the stimuli is more similar to that of most real world objects than patterns which consist of a single spatial frequency. Second, the richness of the spatial frequency content appears to elicit larger more robust VEPs under many conditions. The patterns do have the apparent disadvantage that they may activate more than one spatial frequency mechanism. Nonetheless, the patterns can be quantified rigorously as indicated below. Therefore, one can determine with some confidence the predominant mechanisms which are being stimulated.

The energy at the different spatial frequencies for a particular noise pattern was calculated using a Fourier algorithm. Each noise pattern had a characteristic range of spatial frequencies about a spatial frequency which had the maximum energy. The peak spatial frequencies were 5.2, 2.6, 1.3, 0.325, and 0.1625 cpd. The pattern was generated so that a full screen on the display always contained equal amounts of blank and dark bars and moreover that all possible widths of the bars in the noise pattern were equally represented in one screen. To provide examples of the way in which the patterns were constructed we describe several of the noise patterns in detail. The noise pattern with a peak spatial frequency of 5.2 cpd contained 4 different bars subtending, respectively, 3.3, 4.9, 6.6 and 8.2 min of arc; the pattern which had a peak spatial frequency of 2.6 cpd contained bars of 6.6, 9.8, 13.1 and 16.4 min of arc and the pattern which had a peak spatial frequency of 1.3 cpd was constructed of bars with 13.1, 19.7, 26.2 and 32.8 min of arc.

The mean luminance of the display was 105 cd/m^2. For the transient recordings, the viewing distance was 114 cm with the rectangular stimulus field subtending 14*10 visual degrees. The contrast and the spatial content of the stimulus as well as the speed, direction and duration of motion were

all computer-controlled. Stimulus velocity was 8 degrees per second for all conditions. Stimuli were presented at contrasts of 70% and 5%.

Motion onset and motion reversal were employed as modes of stimulus presentation.

Motion-onset/offset presentation: This condition consisted of a 200 ms period with the pattern moving at a given speed followed by the interstimulus interval of 1100 ms with the pattern present but stationary [see 25]. These intervals and their ratio were suggested by previous research as necessary to reduce the adaptation of the predominant negativity [8, 20]. The speed, motion duration, and interstimulus interval were all computer controlled. The direction of motion was chosen randomly to the left or to the right to prevent anticipation by the subject: the same direction of motion was repeated no more than three times consecutively.

Motion reversal presentation: The noise pattern was continuously present and moving at a constant velocity. The direction of motion reversed 180 degrees after a given time period. To avoid anticipation to the reversal, the duration of motion in one direction was randomized: for the standard condition where the motion duration was constant 400 msec in one direction, the duration was randomized between 300 to 390 msec (in 10 insec steps) for the opposite direction. This rate of transient reversal has previously been shown to provide a large response at lower contrasts [26].

Recording procedures

All VEP recordings were made in a room with a low ambient background luminance. The subjects had to fixate a small fixation spot in the middle of the stimulus field and were explicitly instructed not to make eye movements. Recording was binocular for all stimulus conditions. Ag-AgCl cup electrodes were used. Sweep averaging was continued until an acceptable signal to noise ratio was obtained. Generally approximately 200 sweeps were averaged.

Recording technique

All testing was binocular. Each stimulus condition was presented once. Two recording sessions of approximately one hour's duration were required to complete testing with all of the conditions. The first consisted of the motion onset conditions and the second session consisted of the motion reversal conditions. For each spatial frequency the low contrast condition was presented first and then the high contrast condition in order to minimize adaptation effects.

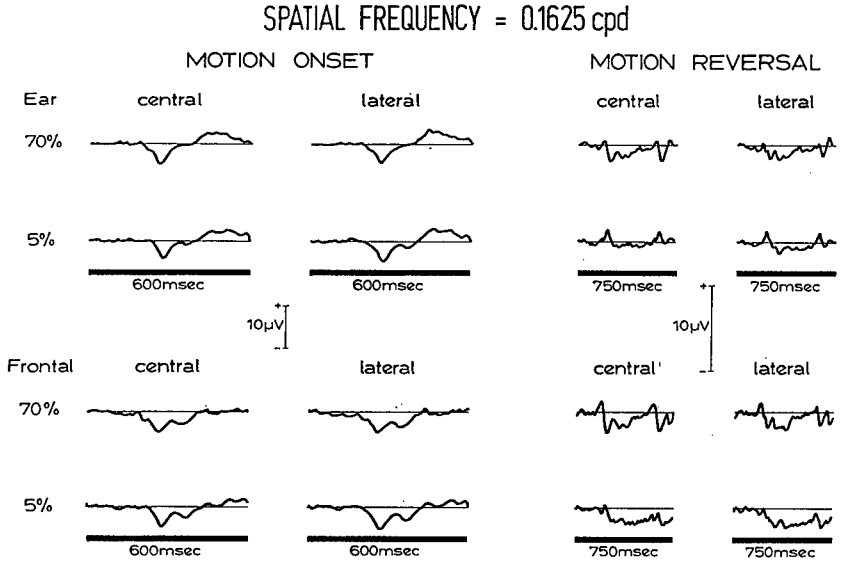

Figure 1. Visually evoked potentials elicited by moving lower spatial frequencies (0.1625 cpd): Grand means. The waveforms presented represent the average of the VEPs of all of the subjects for each condition. While these waveforms are useful for comparisons they are dominated by those subjects who had the largest amplitude responses.

Active electrodes were placed at Oz and 5 cm to the left and 5 cm to the right of Oz and a frontal midline position (Fpz). These active positions correspond approximately to Oz, O_3, O_4 and Fpz, the positions recommended in the ISCEV standard [7]. These active electrodes were referenced to linked mastoids. Linked mastoid references were constructed by placing two 5 kohm resistors in parallel, one in series to a reference at each mastoid. The purpose of this arrangement was to equalize contributions from the two references (William W. Dawson, personal communication). Electrodes were grounded to a midline, vertex position (Cz).

Representation of the VEP recordings

Transient VEP recordings are represented either as individual traces or as group averages [40] obtained by summation of the individual averages. To this end, the mean value in the 100 ms pre-trigger period was calculated and used to align the responses among different subjects before averaging over subjects. Group averages are only used to illustrate the morphology and latency of the different VEP components, while taking advantage of the low noise level (see Figures 1 and 2). These 'off-line averages' are dominated by individual signals with larger amplitudes. As in all VEP studies, the in-

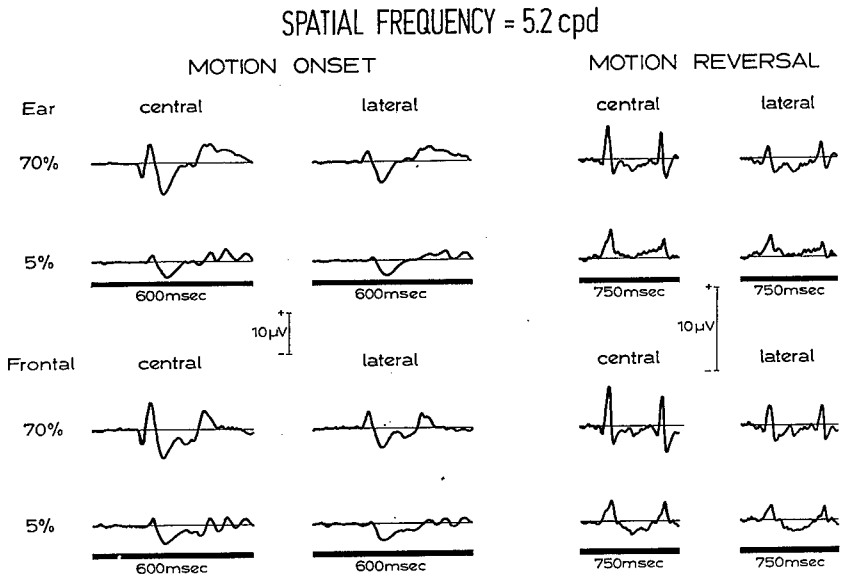

Figure 2. Visually evoked potentials elicited by moving higher spatial frequencies (5.2 cpd): Grand means. The waveforms presented represent the average of the VEPs of all of the subjects for each condition. While these waveforms are useful for comparisons they are dominated by those subjects who had the largest amplitude responses.

terindividual difference in absolute amplitude is quite large (a range of 1 to 5).

All calculations and statistics were performed using individual responses after normalizing over all conditions within each subject. The amplitudes and latencies of the prominent positive and negative peaks between 50 and 250 ms were measured for each subject and condition. Individual peaks were measured as peak to peak measures (preceding negative to positive or preceding positive to negative). In the case of motion onset VEPs, absolute amplitudes were also measured relative to a baseline determined by a 100 ms pretrigger interval. All calculations and statistics were performed using individual responses after normalizing over all conditions within each subject: the median value, the first quartile (q1; 25%) and the third quartile (q3; 75%) are given. Statistics were performed using the non-parametric Wilcoxon's rank sum test for paired observations. The probability levels of significant results are presented in parentheses.

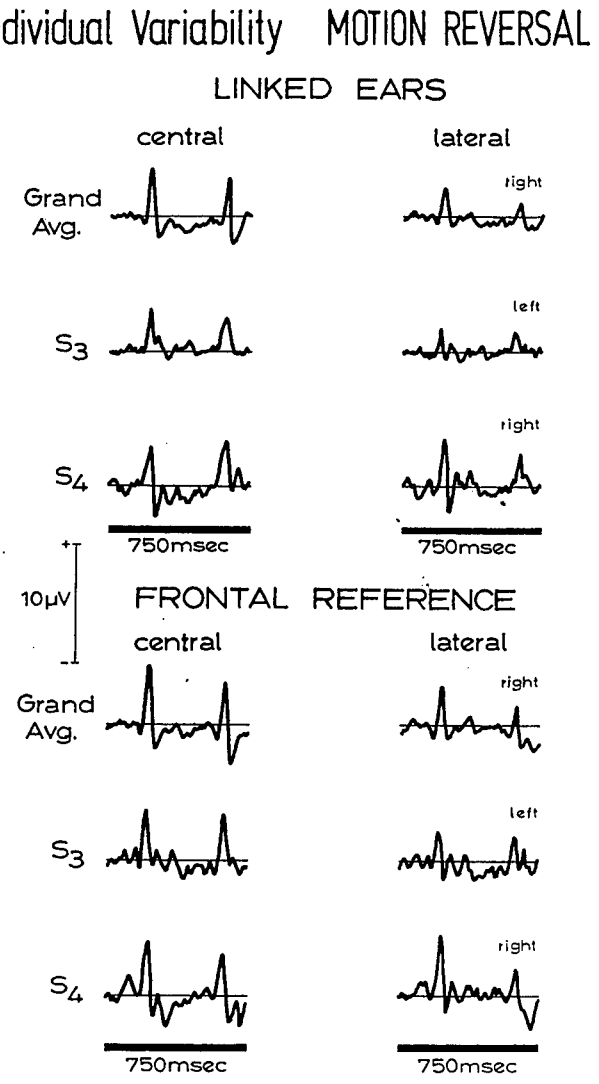

Figure 3. Individual variability of visually evoked potentials: Motion reversal. The grand mean and two individual responses are presented to provide an indication of the individual variability. The spatial frequency is 5.2 cpd and the contrast 70%.

Results

The motion reversal stimulus elicited a predominantly positive response which was present even at 5% contrast. Motion onset stimuli elicited a waveform which varied in morphology depending on the specific conditions. The grand means (averages of the evoked potentials of all subjects) are presented for

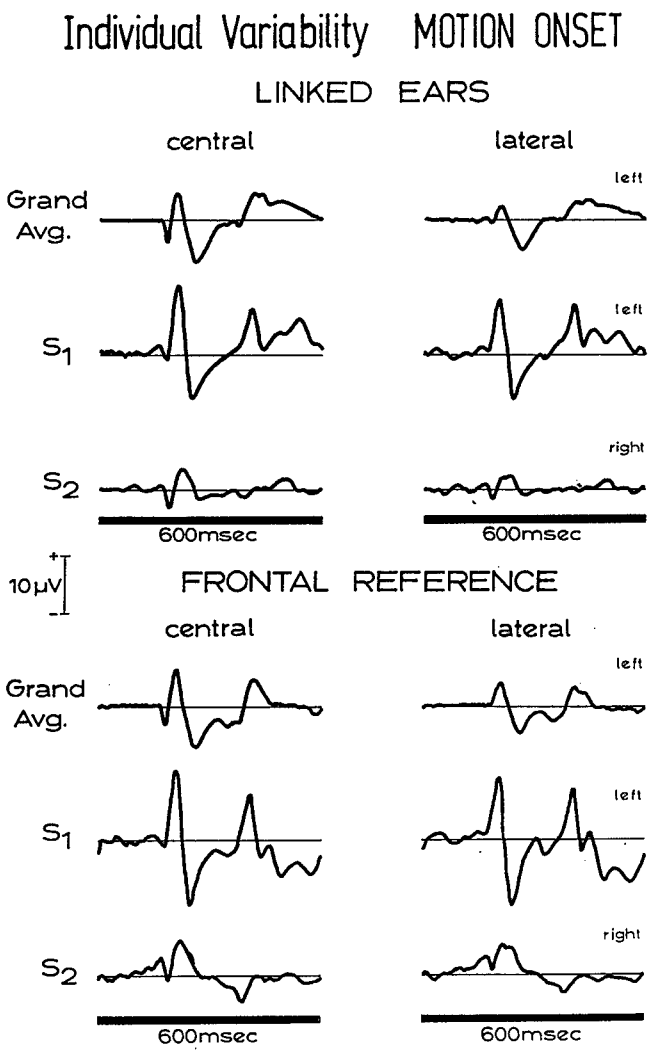

Figure 4. Individual variability of visually evoked potentials: Motion onset. The grand mean and two individual responses are presented to provide an indication of the individual variability. The spatial frequency is 5.2 cpd and the contrast 70%.

illustrative purposes in Figures 1 and 2. Figure 1 presents the VEPs elicited by the unidimensional noise pattern with the lowest maximum spatial frequency (0.1625 cycles per degree [cpd]). Figure 2 presents the grand mean VEPs elicited by the pattern with the highest maximum spatial frequency (5.2 cpd). Individual variability of the VEPs elicited by the pattern with 5.2 cpd at 70% contrast is presented in Figure 3 (motion reversal) and Figure 4 (motion onset). The individual variability observed is similar at lower contrasts and

spatial frequencies. Namely, the positive peak of the motion reversal VEP was found in all subjects, while the negative component was absent in one subject consistently and occassionally absent in two others. However, the shape of the motion onset VEP varied with subject. One subject failed to have a negative component of the motion onset VEP. Additional testing under other stimulus conditions failed to find a negativity under any conditions for this subject.

Effects of stimulus type

Reversal gave a predominantly positive response under almost all conditions. This positive response was prominent even at 5% contrast. This statement is true for all spatial frequencies, reference electrode positions, and active electrode positions. Therefore, only the peak to peak amplitude of the positive peak was measured from an earlier negative trough to the positive peak. Motion onset stimuli elicited a more complicated waveform which varied in morphology dramatically depending on the specific conditions. Two response components were measured: an earlier positive component and a later negative component. These two components were measured both as peak to peak and as absolute measures. The peak to peak positive measure was calculated from an earlier negative component to the major positive component (or the most positive component in the range of 100–130 ms). The later negative component was calculated as the absolute difference in amplitude of the earlier positive component and the major negative component following it within the range of 150–200 ms. Absolute amplitudes of these components were calculated relative to a baseline calculated from the 100 ms prestimulus interval.

In following sections we will present results for motion reversal first. Then we will present the results for motion onset with the positive and negative component results presented separately. We will present the peak to peak measures and their analyses. We will present only those absolute measures which would substantially change the interpretation of the results.

Motion reversal

The results motion reversal are presented in Figure 5. At 70% contrast and 5% contrast, the spatial frequency response function tends to peak at 2.6 cpd. Therefore, VEPs elicited by noise patterns with spatial frequencies of 1.3–5.2 cpd tend to be larger than the VEPs elicited by noise patterns with peak spatial frequencies of 0.325 and 0.1625 cpd ($p < 0.05$). The exception to this pattern is found, when the electrode derivation is the larger lateral electrode referred to linked ears and the stimulus is at 5% contrast; then, there is no difference in VEP amplitude as a function of spatial frequency. The response

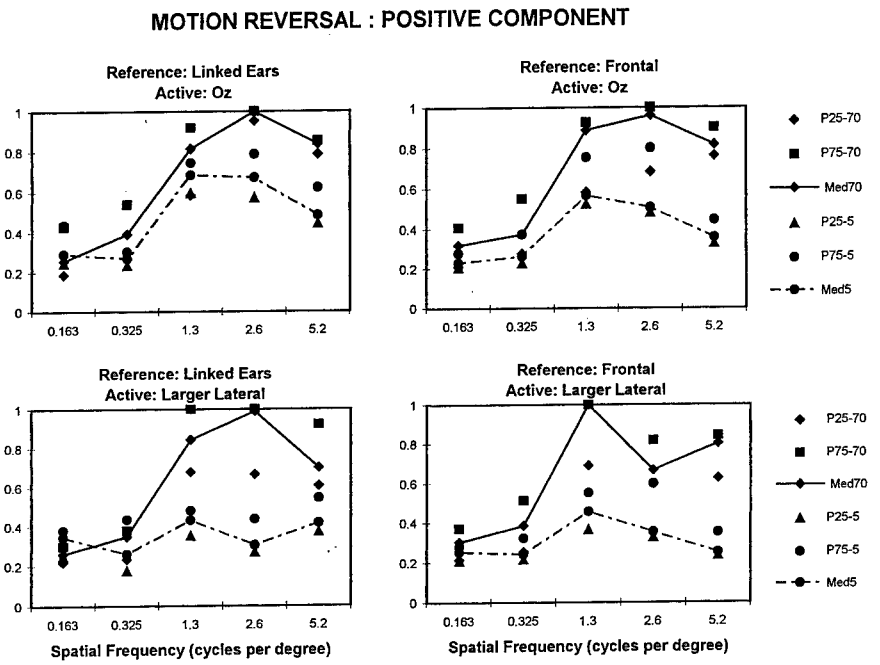

Figure 5. Motion reversal visually evoked potentials: Positive component. The median values and the 25% and 75% are calculated and presented for each condition. The x-axis of each of the four panels represents the spatial frequency containing the maximum energy in the unidimensional noise pattern. The y-axis represents the relative amplitude of the median amplitude for the conditions presented. For ease of interpretation of results we indicate the maximum amplitudes of each panel. Panel 1: Oz referenced to linked ears. Maximum amplitude = 4.59 μV. Panel 2: Larger lateral referenced to linked ears. Maximum amplitude = 3.52 μV. Panel 3: Oz referenced to frontal. Maximum amplitude = 5.07 μV. Panel 4: Larger lateral referenced to frontal. Maximum amplitude = 4.57 μV.

is larger at 70% contrast than for 5% contrast for noise patterns with 5.2 cpd peak spatial frequencies ($p<0.5$) under all of the conditions and for 2.6 cpd when the linked ears were a reference ($p<0.05$).

At 70% contrast, VEP amplitude is not influenced by active or reference electrode conditions except for the 2.6 cpd noise pattern; for it, the VEP recorded over the Oz is larger than that recorded over the larger lateral electrode position ($p<0.05$). At 5% contrast, the VEP amplitudes recorded over Oz are larger for spatial frequencies 5.2 and 2.6 cpd. The effects of reference position do not make consistent statically significant differences.

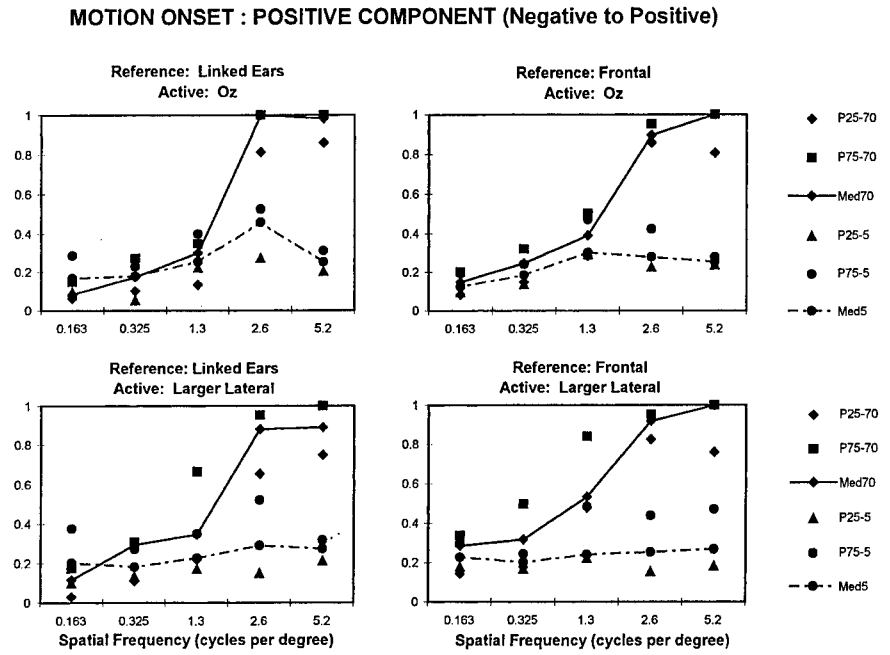

Figure 6. Motion onset visually evoked potentials: Positive component. The median values and the 25% and 75% are calculated and presented for each condition. The x-axis of each of the four panels represents the spatial frequency containing the maximum energy in the unidimensional noise pattern. The y-axis represents the relative amplitude of the median amplitude for the conditions presented. For ease of interpretation of results we indicate the maximum amplitudes of each panel. Panel 1: Oz referenced to linked ears. Maximum amplitude = 5.35 μV. Panel 2: Larger lateral referenced to linked ears. Maximum amplitude = 3.97 μV. Panel 3: Oz referenced to frontal. Maximum amplitude = 8.0 μV. Panel 4: Larger lateral referenced to frontal. Maximum amplitude = 6.62 μV.

Motion onset

Peak to peak positive component. The results for the motion onset peak to peak positive component are presented in Figure 6. At 70% contrast, the positive component tends to decrease with decreasing spatial frequency (spatial tuning), so that 5.2, and 2.6 cpd patterns elicit larger amplitude responses than those at 0.325 and 0.1625 cpd ($p<0.05$). At 5% contrast, there is no difference in VEP amplitude elicited by different patterns if the active electrode is at the larger lateral position. However, over Oz patterns with 1.3–2.6 cpd elicit larger amplitude VEPs ($p < 0.05$). In general, noise patterns whose peak spatial frequencies were 1.3–5.2 cpd elicited larger amplitude VEPs were elicited if the contrast was 70% than if it was 5% ($p<0.05$). If the spatial frequency is 1.3–5.2 cpd, the response is larger over Oz than over the larger lateral position

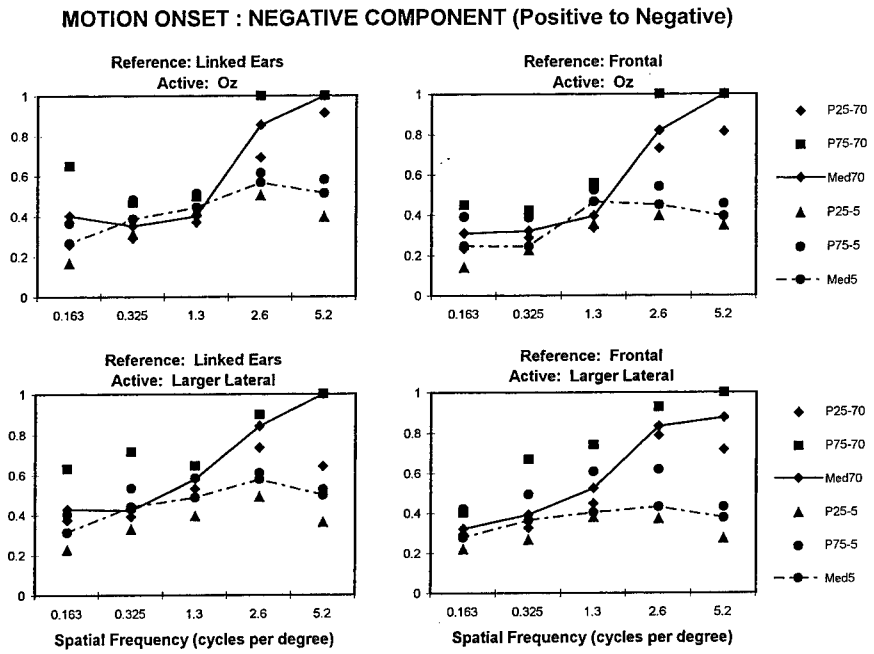

Figure 7. Motion onset visually evoked potentials: Negative component. The median values and the 25% and 75% are calculated and presented for each condition. The x-axis of each of the four panels represents the spatial frequency containing the maximum energy in the unidimensional noise pattern. The y-axis represents the relative absolute amplitude of the amplitudes for the conditions presented. For ease of interpretation of results we indicate the maximum amplitudes of each panel. Panel 1: Oz referenced to linked ears. Maximum amplitude = 11.02 μV. Panel 2: Larger lateral referenced to linked ears. Maximum amplitude = 8.26 μV. Panel 3: Oz referenced to frontal. Maximum amplitude = 13.58 μV. Panel 4: Larger lateral referenced to frontal. Maximum amplitude = 8.9 μV.

($p<0.05$). VEPs elicited by 1.3 cpd are larger when the linked ear reference is used ($p<0.03$).

Peak to peak negative component. The results for the motion onset peak to peak negative component are presented in Figure 7. At 70% and 5% contrast, VEPs elicited by noise patterns containing peak spatial frequencies of 2.6 and 5.2 cpd are larger than those elicited by noise patterns containing lower peak spatial frequencies ($p<0.05$). The exception is when the VEPs are recorded using a larger lateral–frontal reference derivation. In that case, the 1.3 cpd pattern elicits larger responses than the 0.325 cpd pattern ($p<0.05$). The responses elicited by stimuli of 70% contrast are larger than those elicited by 5% contrast for 2.6 and 5.2 cpd stimuli ($p<0.05$). If the reference is the linked ears the 0.325 cpd pattern also elicits a larger response at 70% contrast

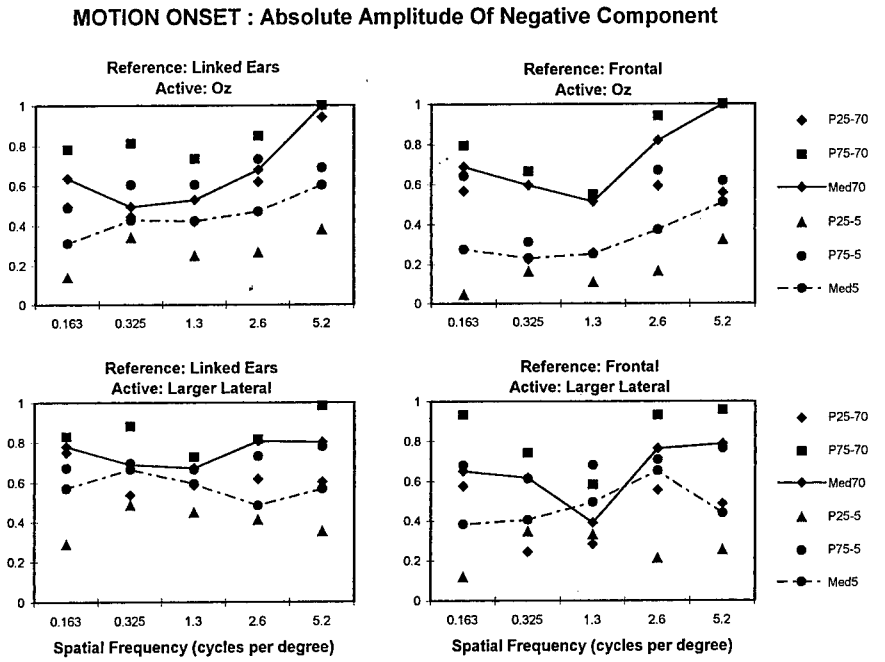

Figure 8. Motion onset visually evoked potentials: Absolute amplitude of negative component. The median values and the 25% and 75% are calculated and presented for each condition. The x-axis of each of the four panels represents the spatial frequency containing the maximum energy in the unidimensional noise pattern. The y-axis represents the relative amplitude of the median amplitude for the conditions presented. For ease of interpretation of results we indicate the maximum amplitudes of each panel. Panel 1: Oz referenced to linked ears. Maximum amplitude = 7.49 μV. Panel 2: Larger lateral referenced to linked ears. Maximum amplitude = 7.49 μV. Panel 3: Oz referenced to frontal. Maximum amplitude = 7.41 μV. Panel 4: Larger lateral referenced to frontal. Maximum amplitude = 5.58 μV.

than at 5% contrast ($p<0.05$). VEPs elicited by 5.2 cpd stimuli are larger when recorded over Oz ($p<0.05$), as are 2.6 cpd stimuli ($p<0.05$), unless the reference is frontal. VEPs recorded with linked ear references are larger than those recorded with a frontal reference at 70% contrast ($p<0.05$).

Absolute negative component. Measuring the negative component relative to the prestimulus period (i.e., absolute amplitude) rather than relative to the earlier positivity) had only a minor effect on the overall results as seen in Figure 8. When an absolute measure of late negative amplitude is used , there is no systematic effect of spatial frequency content of the unidimensional noise patterns on VEP amplitude, except in the Oz–Frontal derivation where 5.2 and 2.6 cpd patterns elicit larger responses at 70% contrast. The reference

electrode position has no systematic effect on the magnitude or spatial tuning of the negative component when measured relative to the baseline.

Discussion

In the present study we compared the relative effects of a number of parameters on the VEPs on moving unidimensional noise stimuli. Several major points emerge. First, transient motion reversal yields a prominent positive response which is present in all subjects and at contrasts of 5%. Second, motion onset VEPs have a complex waveform which may be either predominantly positive or negative. The most important variables in determining whether a prominent positivity or negativity is present in the motion onset VEP are the contrast and the maximum spatial frequencies of the unidimensional noise patterns used. Although active electrode position has some role in determining the shape of the response, on average reference electrode position does not appear to be crucial in determining the shape of the motion onset VEP. We will discuss each of these points below. Additionally we will discuss the relevance of these findings for efforts to identify magnocellular-dependent VEPs and to assumptions regarding motion VEPs.

Motion reversal stimulation

Transient motion reversal yields a prominent positive response which is present in all subjects and at low contrasts. This observation is consistent with previous research [3–6], including our own [26] which indicates that motion reversal is a useful measure of motion processing. Motion reversal VEPs are assumed to depend on directionally selective cells which respond to the onset of motion in the two cardinal directions of the motion. They have been frequently interpreted as the most direct evidence from VEPs of motion processing [3–6, 15–19].

One of the difficulties encountered in current studies of motion reversal VEPs is that the predominant response is usually positive. This is counter to a common assumption that the motion-specific component of the VEP is a late negativity [15–19]. Several authors have suggested that there is a local luminance contaminant in motion reversal [10–11]. They have attempted to overcome this contaminant by refreshing their dot pattern at each reversal and half way through the reversal (i.e., refreshing at a fourth harmonic of the reversal frequency). We considered using this control procedure. However, when we implemented it we noted that refreshing the pattern is in fact a two frame motion stimulus. In our view, this two frame motion stimulus masks the motion reversal stimulus. Therefore, the control may introduce a contaminant

to the stimulus as great or greater than the 'artifact' it is supposed to eliminate. The difficulties of this control procedure are perhaps especially apparent in transient conditions such as our own where one cannot separate second harmonic from fourth harmonic activity and one measures an amplitude.

The absence of a large negativity and the generally smaller amplitude of motion reversal VEPs may be due to the effects of adaptation [8]. This does not necessarily deny the motion specificity of the positive component which remains in this response [see 3–6].

It is important to note that although the motion reversal stimulus elicits a smaller VEP than the motion onset stimulus, VEPs elicited by motion reversal appear to be more consistent in appearance across normal subjects and they are still recordable at 5% contrast. This latter point is consistent with their being largely determined by the magnocellular system [30–34]. These two factors, their reproducibility and their relationship to the magnocellular system may make them interesting for clinical purposes.

Motion onset stimulation

Effects of contrast and spatial frequency of unidimensional noise patterns. The two most important variables in determining whether a prominent positivity or negativity is present in the motion onset VEP are the contrast and the maximum spatial frequencies of the unidimensional noise patterns used as a stimulus as can be seen in Figures 6–8. Contrast and spatial frequency interact. In general, the largest motion onset VEPs are elicited by high spatial frequency, high contrast patterns. Even when one uses absolute amplitude measures of the negative component of the motion onset response (see Figure 8) one can see residual influences of contrast and even spatial frequency, although clearly these effects are less. One might argue that varying spatial frequency and/or contrast represent means of manipulating the relative influence of magnocellular and parvocellular contributions to motion elicited VEPs. Within this view the added amplitude of increasing contrast and spatial frequency would represent the additional input of the parvocellular system to that of the magnocellular system which can be observed only at low contrasts and/or low spatial frequencies. Our use of unidimensional noise stimuli limit this interpretation because of the relatively broadband characteristics of our stimuli.

Effects of channel derivation: Active and reference electrode locations. Although active electrode position has some role in determining the shape of the response, on average reference electrode position does not appear to be crucial in determining the shape of the motion onset VEP. We should note that our conclusion on this point is somewhat at odds with the observations

of others who emphasize the importance of the ear lobe reference [8, 9, 18, 19]. In part the difference depends on their use of absolute measures of amplitude. However, this cannot fully account for the discrepancy as with absolute measurement of the late negativity in our data the largest responses are not observed with an ear lobe reference (see Figure 8).

However, in some patients channel derivation may play a role in determining the appearance of the motion onset VEP. There is considerable intrasubject variability in the shape of the motion onset VEP. In some of our preliminary trials we found one subject who never yielded a motion onset negativity and a second who yielded primarily a negativity under all of our conditions. Most of our subjects however, showed a pattern typified by the grand means which we presented in Figures 1 and 2. That is that although there was little influence of the reference electrode on the amplitude of the motion onset VEP, larger late negative components were recorded over the larger lateral active position than over the Oz. Use of motion onset stimuli in the clinic must be designed in a fashion to take this individual variability of subjects into account. Therefore, if sufficient channels are available one may also wish to use an ear lobe active and derive the response from the ear lobe.

Motion VEPs and the magnocellular system. There are two different reasons for being interested in VEPs elicited by moving stimuli. The first is as a means of probing and understanding the properties of the visual system's mechanisms for processing motion. A second reason is to use the moving stimuli as a means of probing the magnocellular system. Although there is frequently a suggestion that these two purposes are equivalent [15–29], there are substantial reasons for believing that the two purposes overlap but are not totally equivalent. In the VEP, the most frequently cited 'motion' response is a late negativity on the order of 180–300 ms. On the face of it this appears late for what is generally presumed to be the faster of the two major systems. Both in psychophysics [41–44] and VEPs [28], there is evidence for more than one motion mechanism. Similarly, motion can be perceived for high contrast stimuli even when the magnocellular system is lesioned [32, 33]. Lastly, current evidence suggests that there are a number of different cortical areas involved in the processing of motion depending on the task [45]. While it may be true that the various motion systems may feed into a common, relatively late stage of motion processing, it is far from clear that this common stage is what is being recorded in the VEP. Therefore, overly strong emphasis on a single VEP measure as the motion VEP may obscure interesting and even clinically useful information in the motion VEP.

Conclusion

Transient motion reversal elicited a positive response which was present in all subjects and at low contrasts. In many subjects but not all, a later negative response was also present, especially at low contrasts. Motion onset VEPs have a complex waveform which may be either predominantly positive or negative. The most important variables in determining whether a prominent earlier positivity or later negativity is present in the motion onset VEP are the contrast and the spatial frequencies. The negativity predominates at all electrode locations if the contrast is low and/or the spatial frequency is low. Active and reference electrode position have only minor importance in determining the dominant response. One of our seven subjects failed to show a late negative response under any of the stimulus conditions which we used. It appears then that one may use the ISCEV standard conditions in recording motion VEPs.

References

1. Barlow JS. Evoked responses in relation to visual perception and oculomotor reaction times in man. Annals of the New York Academy of Sciences, 1964; 112: 432–67.
2. MacKay DM, Rietveld WJ. Electroencephalogram potentials evoked by accelerated visual motion. 1968; 217: 677–8.
3. Clarke PGH. Visual evoked potentials to sudden reversal of the motion of a pattern. Brain Res 1972; 36: 453–8.
4. Clarke PGH. Visual evoked potentials to changes in the motion of a patterned field. Exp Brain Res 1973; 18: 145–55.
5. Clarke PGH. Comparison of visual evoked potentials to stationary and to moving patterns. Exp Brain Res 1973; 18: 156–64.
6. Clarke PGH. Are visual evoked potentials to motion-reversal produced by direction-sensitive brain mechanisms? Vision Res 1974; 14: 1281–4.
7. Harding, GFA. History of visual evoked cortical testing. In: Principles and practice of visual electrophysiology. Ed. by Heckenlively J. and Arden G.B., Mosby Year Book, 1991, pp 17–22.
8. Bach M, Ullrich D. Motion adaptation governs the shape of motion-evoked cortical potentials. Vision Res 1994; 34: 1541–7.
9. Bach M, Ullrich D. Contrast dependency of motion-onset and pattern-reversal VEPs: Interaction of stimulus type, recording site and response component. Vision Res 1997; 37: 1845–9.
10. Snowden RJ, Ullrich D, Bach M. Isolation and characteristics of a steady-state visually-evoked potential in humans related to the motion of a stimulus. Vision Res 1995 May; 35(10): 1365–73.
11. Wattam-Bell J. Development of motion-specific cortical responses in infancy. Vision Res 1991; 31(2): 287–97.
12. Dagnelie G. Pattern and motion processing in primate visual cortex. a study in visually evoked potentials. Amsterdam, thesis, 1986.

13. De Vries M, Van Dijk B, Spekreijse H. Motion-onset-offset VEPs in children. Electroenceph. din. Neurophysiol 1989; 74: 81–7.
14. Göpfert E, Müller R, Simon E-M. The human motion onset VEP as a function of stimulation area for foveal and peripheral vision. Doc. Ophthalmol 1990; 75: 165–73.
15. Kubova Z, Kuba M, Hubacek J, Vit F. Properties of visual evoked potentials to onset of movement on a television screen. Doc Ophthalmol, 1990; 75: 67–72.
16. Kuba M, Kubova Z. Visual evoked potentials specific for motion onset. Doc Ophthalmol 1992; 80: 83–9.
17. Kubova M, Toyonaga N, Kubova Z, Motion-reversal visual evoked responses. Physiol Res 1992; 41(5): 369–73.
18. Kubova Z, Kuba M. Clinical application of motion-onset visual evoked potentials. Doc Ophthalmol 1992; 81: 209–418.
19. Kubova Z, Kuba M, Spekreijse H, Blakemore C. Contrast dependent changes of motion-onset and pattern-reversal VEPs. Vision Res 1995; 35: 197–205.
20. Müller R, Göpfert E. The influence of grating contrast on the human cortical potential visually evoked by motion. Acta Neurobiol Exp 1988; 48: 239–49.
21. Müller R, Göpfert E, Shlykowa L, Anke D. The human motion VEP as a function of size and eccentricity of the stimulation field. Doc Ophthalmol 1990; 76: 81–9.
22. Probst Th, Plendll H, Paulus W, Wist ER, Scherg M. Identification of the visual motion area (area VS) in the human brain by dipole source analysis. Exp Brain Res 1993; 93: 345–51.
23. Schlykowa L, van Dijk BW Ehrenstein W. Motion-onset visual evoked potentials as a function of retinal eccentricity in man. Cogn Brain Res 1993; 1: 169–74.
24. Spileers W, Maes H, Orban GA. Visual evoked potentials to moving pattern stimuli. Doc Ophthalmol 1994; 85: 326.
25. Spileers W, Maes H, Orban GA Motion-related visual evoked potentials in normal human subjects. Electroenceph Clin Neurophysiol 1996; in press.
26. Spileers W, Joniau I, Mangelschots E, Van Malderen L, Orban G. On the contrast dependence of motion reversal visual evoked potentials in normal human subjects. Vision Research, submitted.
27. Norcia AM, Hamer RD, Jampolsky A, Orel-Bixler D. Plasticity of human motion processing mechanisms following surgery for infantile esotropia. Vision Res 1995; 35: 327–96.
28. Victor JD, Conte MM. Evoked potential and psychophysical analysis of Fourier and non-Fourier motion mechanisms. Vis Neurosci 1992; 9: 105–23.
29. Ungerleider LG, Mishkin M. (1982) Two cortical visual systems. In: Ingle DJ, Goodale MA Mansfield I. (eds), Analysis of visual behaviour. Boston, Mass: MIT Press, 1982; 549–86.
30. Livingstone MS, Hubel DH. Segregation of form, color, movement and depth: Anatomy, physiology, and perception. Science 1988; 240: 740–40.
31. Maunsell JHR, Nealey TA De Priest DD. Magnocellular and parvocellular contributions to responses in the middle temporal visual area (MT) of the Macaque Monkey. J. Neurosci 1990; 10: 3323–34.
32. Merigan WH, Byrne CE, Maunsell JHR. Does primate motion perception depend on the magnocellular pathway? J. Neurosci 1991; 11: 3422–9.
33. Merigan WH, Maunsell JHR. How parallel are the primate visual pathways? Ann Rev Neurosci 1993; 16: 369–402.
34. Tootell RBH, Hamilton SL, Switkes E. Functional anatomy of macaque striate cortex. IV. Contrast and magno-parvo streams. J. Neurosci 1988; 8: 1594–1609.

35. Bassi CJ. Parallel processing in the human visual system. In: Wall M Sadur AA (eds). New Methods of Sensory Visual Testing. Springer-Verlag: New York, 1989.
36. Livingstone MS, Rosen GD, Drislane FW, Galaburda AM. Physiological and anatomical evidence for a magnocellualr defect in developmental dyslexia. Proc Natl Acad Sci USA 1991; 88: 7943–7.
37. Tychsen L. Binocular vision. In: Hart WM Jr (ed). Adler's Physiology of the Eye: Clinical Applications, 9th ed. St. Louis, MO: C.V. Mosby, 1992: 773–853.
38. Regan D. The Charles F. Prentice Award Lecture 1990: specific tests and specific blindnesses: keys, locks, and parallel processing. Optom Vis Sci 199; 68: 489–512.
39. Harding GFA, Odom JV, Spileers W, Spekreijse H. Standard for Visual Evoked Potentials 1995. Vision Research 1996; 36: 3567–72.
40. Kriss, A. Recording technique. In: Evoked potentials in clinical testing. Ed. by Halliday AM, Churchill Livingstone, 1993, p. 38.
41. Green M. Visual masking by flickering surrounds. Vision Research 1983; 23: 735–44.
42. Green M, Odom J. Comparison of monoptic and dichoptic masking by light. Perception and Psychophysics 1984; 34; 291–6.
43. Green M. Masking by light and the sustained-transient dichotomy. Perception and Psychophysics 1984; 34: 617–35.
44. Green M, Odom J. Correspondence matching in apparent motion: Evidence for three-dimensional spatial representation. Science 1986; 233: 1427–29.
45. Dupont P, Orban GA, De Bruyn B, Verbruggen A, Mortelmans L. Many areas in the human brain respond to visual motion. J. Neurophysiol 1994; 72: 1420–4.

Address for correspondence: J. Vernon Odom, R.C. Byrd Health Sciences Center of West Virginia University, Department of Ophthalmology, P.O. Box 91193, Morgantown, WV 26506, USA

Documenta Ophthalmologica **95:** 335–347, 1999.

Electrophysiological correlates of human texture segregation, an overview

MICHAEL BACH[1] & THOMAS MEIGEN[2]
[1]*Elektrophysiologisches Labor, Universitäts-Augenklinik Freiburg, Germany;*
[2]*Univ.-Augenklinik, Würzburg, Germany*

Abstract. 'Texture segregation' results from parallel processing in the visual cortex. It occurs when the stimulus contains spatial gradients within a visual dimension. We here present an introductory overview of the field, concentrating on electrophysiological correlates in the human EEG ('tsVEPs') of the neuronal processes underlying texture segregation. We describe the isolation of the tsVEP from the background EEG, give examples of the correlation between saliency and tsVEP amplitude and compare texture segregation between visual dimensions.

Key words: electrophysiology, human, texture segregation, VEP

Abbreviations: tsVEP – VEP associated with texture segregation

Introduction

'Texture segregation' refers to an active research field that deals with the capability of our visual system to segment (segregate) areas of our visual field. Texture segregation is closely related to 'grouping' and 'pop out' (Figure 1) and is a fundamental mechanism to segregate a Gestalt from the background. The common feature of these perceptual phenomena is parallel processing of the visual field, without conscious or automatic sequential scanning (foveation). By definition, texture segregation occurs if detection of a certain feature is not compromised by an increasing number of detracting stimuli [1]. Our eventual goal is to understand how our visual system detects figures and objects from the 'flat' retinal image out of a distracting background. Texture segregation is an important intermediate step in figure-ground-segmentation (Figure 2).

Beck first noticed parallel processing of certain line elements [2]. Julesz first analyzed local statistical properties and later based his 'texton theory' on the presence of certain local features (line endings etc) [3]. We now believe that texture segregation is not determined by the presence or absence of local features, but rather by *spatial (or temporal) gradients* in the expression of a *visual dimension* [1, 4–6]. We consider as visual dimensions those properties of the visual world, for which our visual system has developed specific

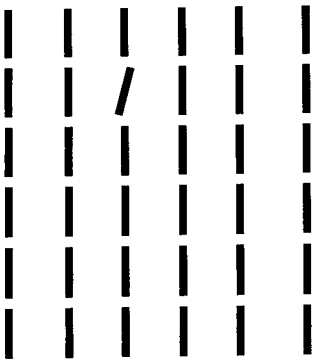

Figure 1. In this arrangement of vertical lines the oblique line is obvious at first glance, without sequential scanning of the image, a typical case of 'pop out'.

neuronal filters (receptive fields). The following list of visual dimensions is probably incomplete, it includes: luminance, orientation, spatial frequency, motion, stereo disparity and color (Figure 3).

Electrophysiological correlates of texture segregation

Texture segregation occurs spontaneously, without scanning of the visual field, as it is based on parallel processing. Such massive processing should leave its traces in the EEG, and consequently in the VEP. VEP findings provide a link between psychophysical results in humans and neuronal measurements in animal experiments and provide a fascinating possibility to analyze neural mechanisms of visual processing in the human visual system. In search of a VEP correlate of texture segregation, we wanted to introduce many orientation gradients in the stimulus and chose a 'global orientation checkerboard' as stimulus (Figure 4). The subject fixates the center of the screen, initially blank. Suddenly the pattern appears, evoking a VEP (Figure 5).

This VEP does not yet represent a specific correlate of texture segregation. Any visual change will trigger visual processing and consequently evoke a VEP. We will call the VEP evoked by the onset of the line elements themselves the 'low-level-VEP'. To extract a component associated with texture segregation (the 'tsVEP') we used the following rationale: The 'global orientation checkerboard' contains both vertical and horizontal line elements, so we also presented a pattern 'vertical only' and another 'horizontal only'. Since the 'global orientation checkerboard' contains half vertical and half horizontal line elements, we subtracted from the evoked VEP-mixture half of the response to the vertical and half of the response to the horizontal pattern.

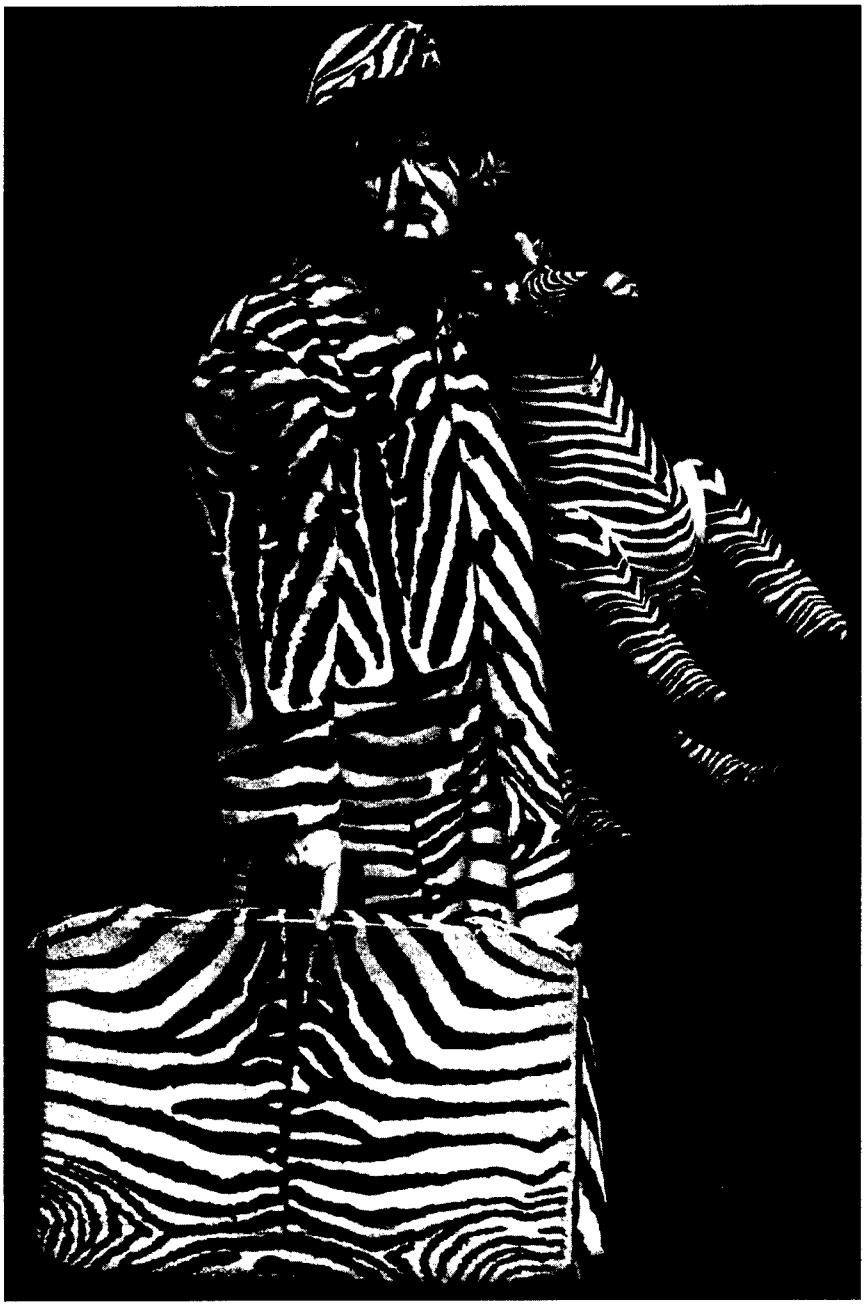

Figure 2. 'Cirque Invisible' Victoria Chaplin & Jean-Baptiste Thierrée (photo: F. Simon, Hamburg 1994, with permission). Three Gestalten (clown, zebra and suitcase) segregate from each other and from the background by boundaries that are defined by gradients in luminance, orientation and spatial frequency (cf. Figure 3). For instance, between clown and zebra there is an orientation gradient (lines oblique on the coat, horizontal on the zebra), as well as a gradient in spatial frequency (stripes wide apart on the coat, close in the zebra).

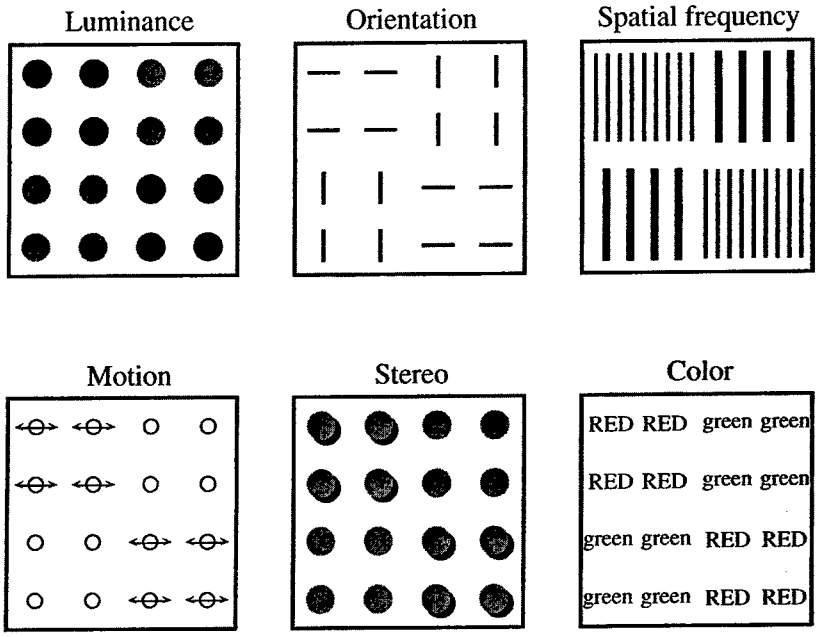

Figure 3. Texture segregation in different visual dimensions. The six squares segregate into 4 segments each, based on different visual dimensions. The vivid segregation by motion, stereo and color cannot be adequately presented here.

In other words: We assumed linearity and calculated the linear combination:

$$tsVEP = VEP_{checkerboard} - \frac{VEP_{vert.lines} + VEP_{horiz.lines}}{2} \quad (1)$$

Assuming linearity at this stage, the low-level VEP should thus be eliminated and a negative component just before 200 ms after stimulus onset appeared [7, 8]. The latency was in an 'interesting' range: clearly after the low-level-VEP, but before the time for cognitive potentials that occur typically at 300 ms. These results were confirmed and extended to segregation by motion, topographic- and cortical depth-analysis and recordings in monkeys by the Amsterdam group [9–11]. The assumption of linearity at this stage cannot easily be tested directly. Rather, to assess the viability of the tsVEP as a measure of segregation processing, we will now quantitatively compare the tsVEP and psychophysical measures.

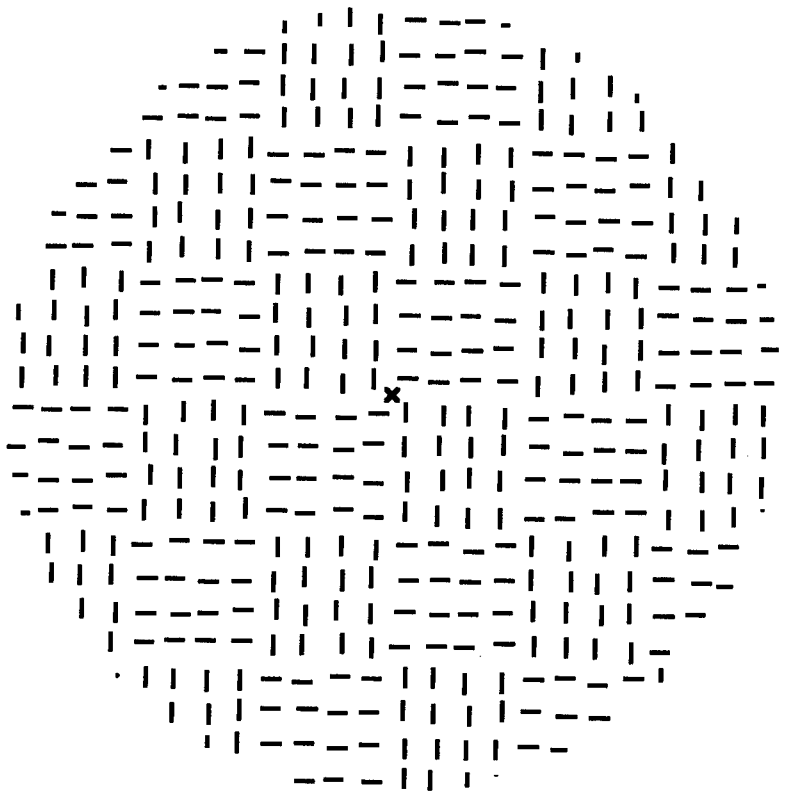

Figure 4. An 'orientation checkerboard' as seen by the subjects. The checks are defined by orientation gradients. The small displacements ('jitter') of the individual line elements against their regular lattice position are introduced to reduce luminance artifacts.

Correlation between psychophysical and electrophysiological findings in texture segregation – Four textons

Having isolated the tsVEP, we proceeded to study its relation to psychophysical saliency. Saliency of texture segregation depends on many stimulus parameters. We compared saliency, quantified in a ranking paradigm, and the tsVEP amplitude across four patterns that were inspired by Julesz' texton patterns.

All patterns were constructed from identical line elements, in Figure 6 the four patterns are depicted in a simplified way. When the line elements build up groups of 'U's that are rotated by 90° between groups (Figure 6 left, second pattern from bottom left), there appears a clear, if weak, percept of a global checkerboard (orientation based texture segregation, caused by the contrasting of 2 lines horizontal and 1 line vertical to 1 line horizontal and

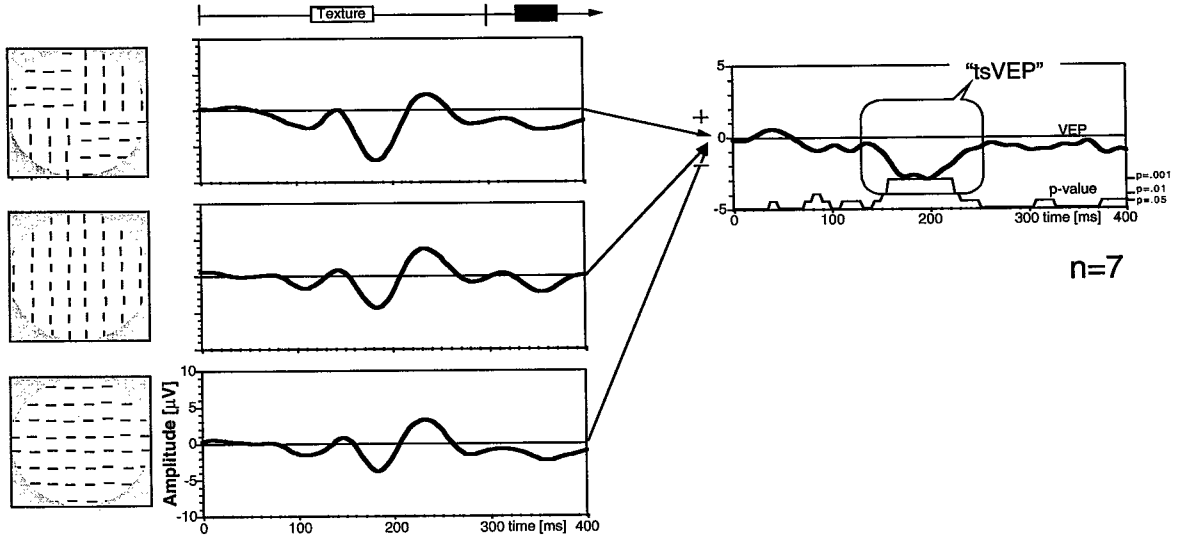

Figure 5. Isolation of a VEP component associated with texture segregation. At the very left are icons of the stimulus patterns (cf. Figure 4), the center shows the VEPs in response to onset of these patterns (grand mean of 7 subjects). On the right is a linear combination [Equation (1)] of these three responses, designed to cancel the local, or 'low-level VEPs'. This results in the 'tsVEP', a negativity around 200 ms. (Modified after [8]).

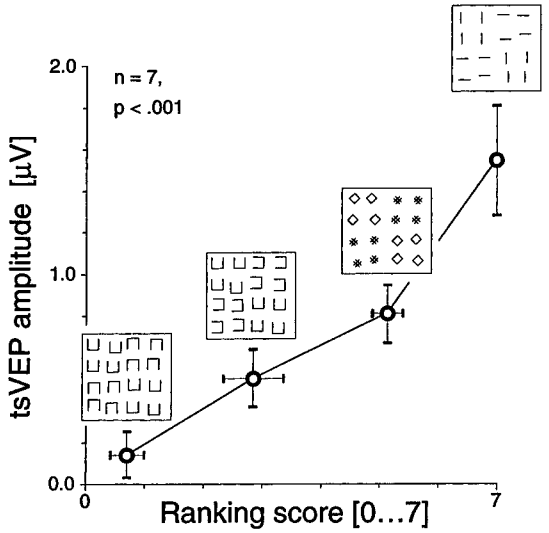

Figure 6. 'Four textons' experiment. Comparison of psychophysical saliency and tsVEP amplitude, grand mean of 7 subjects. The subjects estimated the 'strength of the global checkerboard' of four patterns. The actual patterns were arranged like Figure 4. Saliency as expressed by the ranking score and tsVEP amplitude are closely correlated. (Modified after [12]).

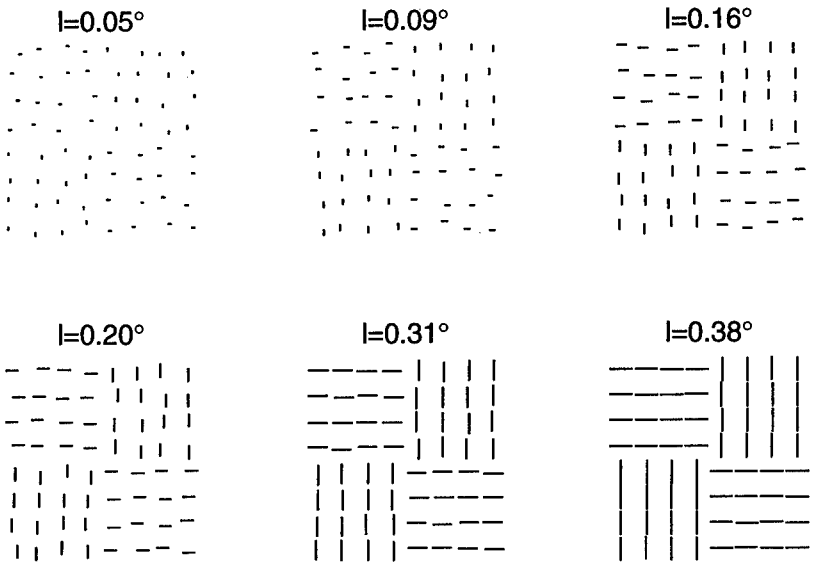

Figure 7. Line-length experiment, simplified stimulus patterns. The relative size of the line elements and the checks are as seen by the subjects, the full stimuli resembled those from Figure 4. Six different line lengths were presented, with length l from 0.05° to 0.38° with a constant raster width of 0.4° to manipulate the magnitude of orientation gradients.

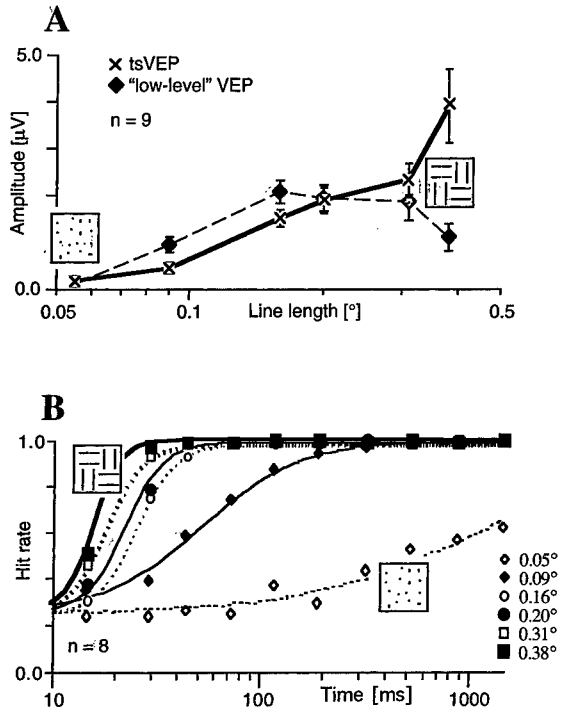

Figure 8. Line-length experiment, electrophysiological (A, top) and psychophysical (B, bottom) results. A. The diamonds represent the 'low-level VEP', peaking at an intermediate line length. The crosses represent the tsVEP, rising monotonically with line length. B. The probability of correctly identifying the location of a test patch in a 4AFC vs. stimulus presentation time. The smooth curves represent a logistic function fit. All psychometric functions represent an acceptable fit and show that saliency increases monotonically with line length.

2 lines vertical). If the 'U's are rotated by 180°, the global checkerboard can hardly be seen (Figure 6 bottom left). In this experiment we measured the tsVEP in a steady-state paradigm [12], and the appropriate Fourier-amplitude was vector-averaged across subjects. The results show a close correlation of saliency with tsVEP amplitude. This finding supports the hypothesis that the tsVEP actually is associated with neuronal processes underlying image segregation.

Line length – Saliency and tsVEP amplitude

To assess more quantitatively the relationship between tsVEP amplitude and psychophysical saliency in one visual dimension, we studied the influence of line length and used a test-mask paradigm for psychophysical measurements.

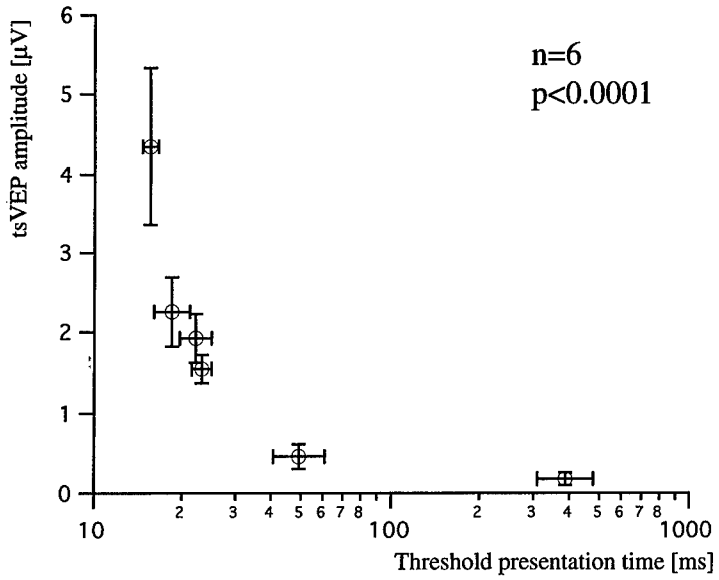

Figure 9. Line-length experiment, comparison of electrophysiological and psychophysical measures from Figure 8. A close correlation between tsVEP amplitude and threshold presentation time obtains across the line lengths tested.

Increasing line length can be thought of as increasing orientation gradient (Figure 7).

The tsVEPs were extracted in the frequency domain as in [12]. Two types of responses as grand mean from 9 subjects are plotted in Figure 8A: The crosses represent the tsVEP amplitudes resulting from a linear combination similar as in Figure 5, the diamonds represent a linear combination that cancels higher order components, leaving the 'low-level VEP' (cf. Figure 11, right). With increasing line length, the low-level VEP displays an intermediate maximum, whereas the tsVEP continues to rise monotonically until the line elements nearly touch each other. This different behavior suggests that two different mechanisms are tapped.

To measure the saliency, we employed a four alternative forced choice task: Instead of a global checkerboard, only a single check was presented. This check was embedded in a background of oriented lines, with a position right, top, left or bottom of the fixation point. The distance between the center of the check and the fixation spot was 2.4°. This test pattern appeared for a certain time and was followed by a mask of alternatingly oriented line elements. In a constant stimulus design the presentation time was varied between 14.6 ms (the frame interval) and 1460 ms in 10 steps. The stimuli were presented in an interleaved block design, each presentation time was

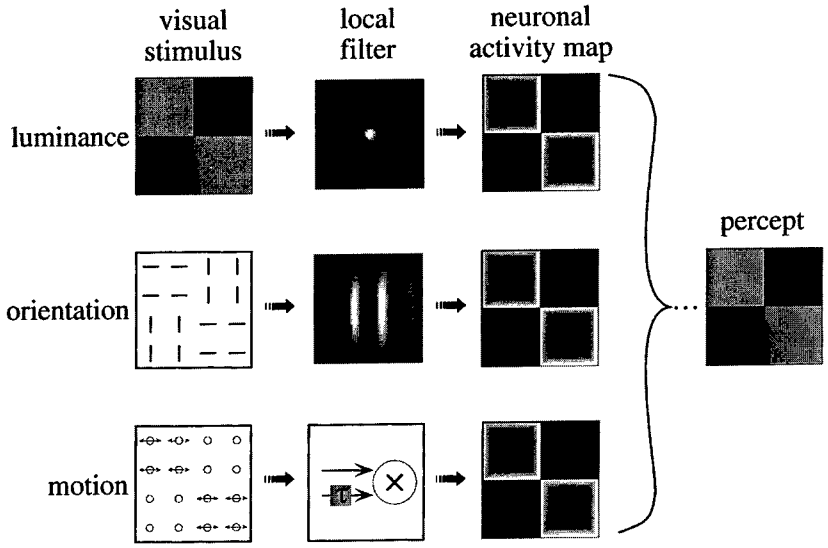

Figure 10. Model scheme of texture segregation. The image (left), which is segregated into four fields by one of three exemplary visual dimensions, is processed by local filters (second column, not to scale, the local filters correspond to known neuron types) into one common 'neuronal activity map' (third column). On this common activity map, which may simply be the sum of the outputs from the filter map in every visual dimensions, the gradient detectors operate. Finally, after more unknown steps, the percept 'checkerboard' arises.

tested 8 times per block, each line length was presented in two blocks. After the experiment, logistic functions were fitted using a maximum-likelihood procedure [13]. Figure 8B demonstrates that all psychometric functions represent an acceptable fit. Both inverse slope and time of steepest slope decrease monotonically with increasing line length.

The electrophysiological and psychophysical measures are compared in Figure 9 for those subjects for whom both measures were available. Obviously, a very close correlation ($P < 0.0001$, Pearson signed rank) between tsVEP amplitude and threshold presentation time obtains across the line lengths tested.

The independence of the texture segregation from the visual dimension

It is known that the texture segregation can appear at different visual dimensions. As it appears inefficient if detectors for gradients and neuronal recognition mechanisms would exist in every visual dimension, we propose the following model to explain the independence of texture segregation from

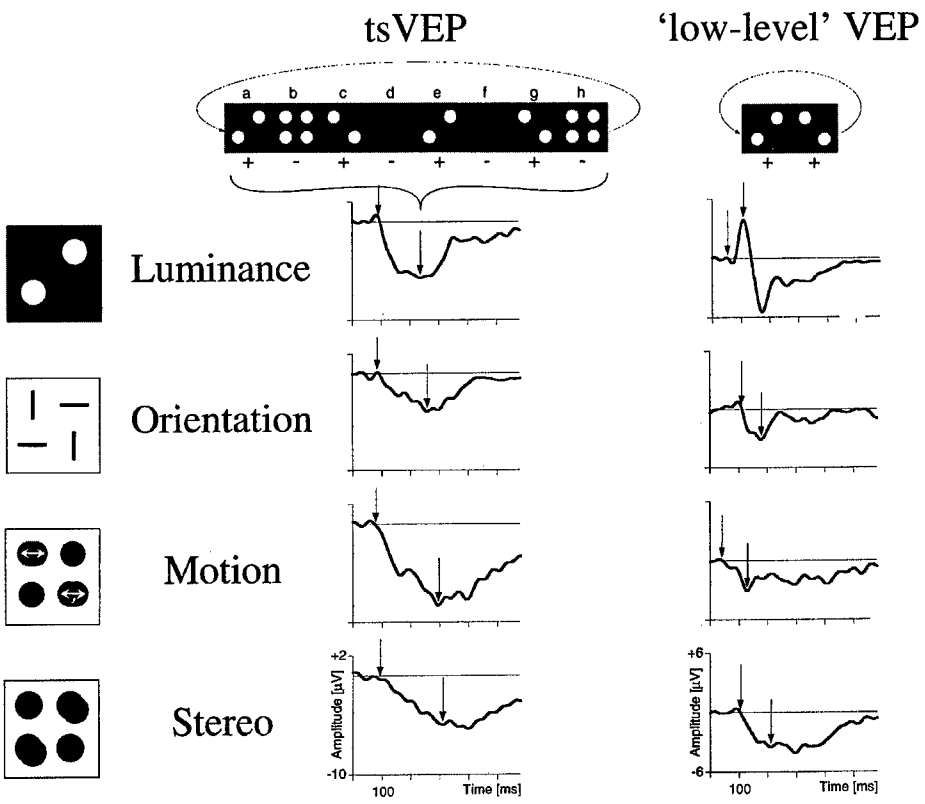

Figure 11. Visual evoked potentials associated with texture segregation (tsVEP, left) contrasted with low-level VEPs (right). On the very left the four visual dimensions are depicted symbolically. The next column depicts the respective tsVEP traces, which were extracted from the raw responses using the linear combination indicated by '+' or '–' in the stimulus pattern sequence at the top. On the right are the 'low-level VEPs' evoked by a 'reversal' of the respective visual dimension. The first arrow in each trace indicates implicit time, the second arrow denotes the major peak. Between the four visual dimensions, the tsVEPs have similarities (each shows a negativity at 230–310 ins) and dissimilarities. The similarities of the tsVEPs are striking when compared to those between the low-level VEPs. This suggests that the tsVEPs reflect a mechanism that has generalized to some degree across visual dimensions. (Modified after [14]).

the visual dimension (Figure 10). This model makes a number of predictions that can be experimentally tested. In the language of the VEPs, the filter outputs relate to the low-level-VEP, and the segregation mechanisms operating within the intensity map would generate the tsVEP.

To test this model, we compared the tsVEP with the low-level-VEP in four visual dimensions (brightness, orientation, movement and stereo). The results can be summarized as follows (Figure 11) [14]: The low-level-VEP

varies very strong among the visual dimensions. Compared to this, the tsVEP appears relatively similar among the visual dimensions (for example it is always negative). This result is consistent with the hypothesis sketched in Figure 10. The details of neuronal function still need to be elucidated. For example it is possible that the steps in Figure 10 are integrated within some neurons' receptive field properties: orientation gradients in monkeys [15, 16] orientation gradients cats [17, 18], motion gradients in monkeys [16, 19], and motion gradients in cats [20].

Conclusion

Texture segregation is an impressive capability of our visual system. Functional correlates of texture segregation in humans provide a link between perception and single cell data in animals. The following aspects of the tsVEP were covered here:

- identification of the tsVEP assumes linearity
- the tsVEP is a negative component around 200 ms
- tsVEPs have been found in all visual dimensions tested: orientation, motion, luminance, and stereo
- psychophysical saliency and tsVEP amplitude are highly correlated
- tsVEPs are similar across dimensions (tested for luminance, orientation, motion and stereo).

Acknowledgment

We gratefully acknowledge support by the Deutsche Forschungsgemeinschaft.

References

1. Treisman A. Preattentive processing in vision. Comput Vis Graph Image Proc 1985; 31: 156–77.
2. Beck J. Similarity grouping and peripheral discriminability under uncertainty. Am J Psychol 1972; 85: 1–19.
3. Julesz B, Bergen JR. Textons, the fundamental elements in preattentive vision and perception of textures. Bell Sys Tech J 1983; 62: 1619–45.
4. Treisman A, Sato S. Conjunction search revisited. J Exp Psychology Human Perception and Performance 1990; 16: 459–78.
5. Nothdurft HC. Texton segregation by associated differences in global and local luminance distribution. Proc Royal Soc London B 1990; 239: 295–320.

6. Bach M, Meigen T. Electrophysiological correlates of texture segregation – Effect of orientation gradient. Invest Ophthalmol Vis Sci (ARVO Suppl.) 1992; 33: #1349.
7. Bach M, Meigen T. Electrophysiological correlates of texture-segmentation in human observers. ARVO Abstracts. Invest Ophthalmol Vis Sci 1990; 31 (suppl): 104.
8. Bach M, Meigen T. Electrophysiological correlates of texture segregation in the human visual evoked potential. Vision Res 1992; 32: 417–24.
9. Lamme VAF, van Dijk BW, Spekreijse H. Texture segregation is processed by primary isual cortex in man and monkey. Evidence from VEP experiments. Vision Res 1992; 32: 797–807.
10. Lamme VA, van Dijk BW, Spekreijse H. Contour from motion processing occurs in primary visual cortex. Nature 1993; 363: 541–3.
11. Lamine VA, van Dijk BW, Spekreijse H. Organization of texture segregation processing in primate visual cortex. Vis Neurosci 1993; 10: 781–90.
12. Meigen T, Bach M. Perceptual ranking vs VEP for different local features in texture segregation. Invest Ophthalmol Vis Sci 1993; 34: 3264–70.
13. Meigen T, Lagrèze W, Bach M. Asymmetries in preattentive line detection. Vision Res 1994; 34: 3103–9.
14. Bach M, Meigen T. Similar electrophysiological correlates of texture segregation induced by luminance, orientation, motion and stereo. Vision Res 1997; 37: 409–14.
15. Knierim JJ, van Essen DC. Neuronal responses to static texture patterns in area V1 of the alert macaque monkey. J Neurophysiol 1992; 67: 961–80.
16. Lamme VA. The neurophysiology of figure-ground segregation in primary visual cortex. J Neurosci 1995; 15: 1605–15.
17. Blakemore C, Tobin BA. Lateral inhibition between orientation detectors in the cat's visual cortex. Exp Brain Res 1972; 15: 439–40.
18. Kastner S, Nothdurft HC, Pigarev I. Neuronal responses to orientation and motion contrast in feline striate cortex. Soc Neurosci Abst 1995.
19. Allinan J, Miezin F, McGuinness EL. Effects of background motion on the response of neurones in the first and second cortical visual areas. In: Edelman GM, Gall WE and Cowan MW, eds. Signal and Sense: Local and Global Order in Perceptual Maps. New York: Wiley-Liss, 1991: 131–41.
20. Kastner S, Nothdurft H-C, Pigarv IN. Neuronal correlates of pop-out in cat striate cortex. Vision Res 1997; 37: 371–6.

Address for correspondence: M. Bach, Univ.-Augenklinik, Killianstr. 5, D-79106 Freiburg, Germany
Phone ++49 (761) 270-4060; Fax: ++49 (761) 270-4052; E-mail:bach@uni-freiburg.de

Documenta Ophthalmologica **95:** 349–358, 1999.

Parallel visual and memory processes

KRISTL CLAEYS[1], LUC CREVITS[1], ELS STUYVEN[2], KOEN VAN DER GOTEN[2], CHRISTOPHE DEPUYDT[3] & ANDRÉ VANDIERENDONCK[2]
[1]*University Hospital Ghent, Department of Neurology, Ghent, Belgium;* [2]*Department of Experimental Psychology, University of Ghent, Belgium and* [3]*University Hospital Ghent, Department of Internal Medicine, Ghent, Belgium*

Abstract. We studied parallel processes: visual processes with the prosaccade, the no-saccade and the antisaccade task on the one hand and memory processes with the random tap task on the other hand. The random tap task is believed to be a pure interference task for the central executive component of working memory. The number of saccadic errors was found not to be influenced by taxing the central executive, while the latency times were significantly increased both in the prosaccade and in the antisaccade task. The effect seen in the antisaccade task was expected since it is a non-automatic activity under central executive control. Because the prosaccade task is an automatic activity, an effect of central executive load was not expected. As an explanation for our findings, we postulate that the prosaccade task is brought under willed control of the central executive.

Key words: antisaccade, central executive, prefrontal, random time interval generation task, saccade, working memory

Abbreviations: AS – antisaccade; CE – central executive; NS – no-saccade; PS – prosaccade; SAS – Supervisory Attentional System; SC – superior colliculus

Introduction

Saccades are fast eye movements which are used to catch rapidly an image of interest on the fovea. *Reflexive saccades* are externally triggered by a target suddenly occurring in the environment: they may be auditively guided or visually guided. Reflexive saccades are triggered by the parietal eye field of the posterior parietal cortex, through its direct projection to the superior colliculus (SC). Prosaccades (PS), made towards a suddenly appearing lateral visual stimulus (Figure 1), are reflexive saccades. Reflexive saccades are inhibited by the dorsolateral prefrontal cortex or area 46 of Brodmann at the level of the SC. *Intentional or voluntary saccades* are internally triggered, with a goal, namely to find and catch a visual target of interest. They are triggered by the frontal eye field, which projects to the SC and also directly to the premotor reticular formation in the brainstem [1, 2]. Antisaccades (AS), made in the direction opposite to a suddenly appearing lateral visual stimulus (Figure 1), are also intentional saccades [3].

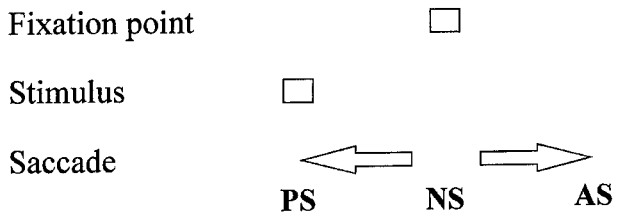

Figure 1. Schematic illustration of the saccadic paradigm: the prosaccade (PS), the no-saccade (NS) and the antisaccade (AS).

In the working memory model, Baddeley and Hitch [4] proposed a division of the short-term memory into three subsystems: the central executive (CE) and two slave systems, a visuospatial sketchpad and a phonological loop. The visuospatial sketchpad is specialized in maintaining visuospatial information for a short period of time, while verbal information is held in the phonological or articulatory loop. The central executive is assumed to supervise and coordinate these slave systems.

Baddeley [5] adopted the concept of the Supervisory Attentional System (SAS) as formulated by Norman and Shallice [6] as the basis for the central executive. The SAS discriminates between two modes of attentional control of cognitive action. At the lower level, routine activities are controlled by existing schemata. At a higher level, the SAS is able to intervene in cases of emergency, novelty, etc., by interrupting and modifying automatic routine activities into non-automatic actions under willed control.

Recent research [7] suggests that the prefrontal cortex has the following important functions: the preservation of transient information across short time intervals for organizing upcoming action, i.e. the working memory function and the inhibition of prepotent but inappropriate responses. These two functions are intimately related and a deficient working memory system can increase the difficulty of resisting prepotent actions. Moreover, a temporarily increase in load on working memory, more specifically on the central executive, results in similar patterns of errors as a permanent dysfunction of working memory, like those observed in prefrontal patients [7].

The purpose of the present study is to test the hypothesis that an increased load of the CE decreases the ability to inhibit prepotent saccades. This would lead to a decreased performance in the antisaccade task, if the antisaccade task would also be under CE control. To load the central executive, the random time interval generation task (random tap task), which is a pure CE task, was used [8].

Subjects and methods

After obtaining informed consent, 30 healthy persons (13 males and 17 females), varying in age from 18 to 83 years, were examined. The mean age was 39 years. Some were students or personnel at the University of Ghent (Belgium), others were relatives and friends of the authors. Subjects were excluded if they had a history of psychiatrial, neurological or ophthalmological disturbances (other than refractive disorder). None of the participants was using drugs other than contraceptives during the week before examination.

All participants were subjected to six tasks: the prosaccade, the no-saccade and the antisaccade task, each in two conditions, i.e. with and without the random tap task [8]. In order to simplify task instructions, the load and no-load conditions pertaining to each saccade task were held together. Order was varied within these blocks. The principle of the Latin square was used to obtain six different sequences, to which each participant was randomly assigned.

Eye movements were registered by means of an Ober2 system, which uses goggles for infrared corneal reflection. Only the movements of the dominant eye were registered. The random tap task was recorded on a second computer connected in parallel with the first computer, to synchronize the registrations of the eye movements and the random tapping. The tasks were done in a dark room relatively free of distractions. The participant was seated on a chair with his goggles at 40 cm distance from the computer monitor. Head position was maintained by asking not to move the head. In the center of the screen a white square (4×4 mm) was used as a fixation point. After 1.5 to 3.0 seconds, this square disappeared. At the same moment, a square appeared at a visual angle of 14° randomly to the left or to the right. After 2.0 to 3.0 seconds, the screen was cleared and the central fixation square reappeared. First, a calibration phase was done in order to adjust a number of parameters (e.g. illuminance) of the eye tracking device of the goggles. Two calibration sessions of eight trials were registered. After calibration, the six conditions were run. Every condition consisted of 30 trials, randomly 15 stimuli to the left and 15 stimuli to the right.

The participants had to make as quickly as possible an eye movement towards the cue in the prosaccade task, and an eye movement in the opposite direction of the stimulus in the antisaccade task. In the no-saccade task, subjects had to fixate the center of the screen in spite of the presence of a lateral stimulus (Figure 1). To perform the tap task, the participants had to tap randomly with their dominant hand, at an unpredictable rhythm on the zero key of the numeric keyboard at a rate of approximately one tap per second.

Table 1. Mean latency time in msec and standard deviation in the prosaccade and the antisaccade task

	Prosaccade		Antisaccade	
	without tapping	with tapping	without tapping	with tapping
Mean latency time (msec)	241.9	282.0[a]	316.6[c]	352.7[b,c]
Standard deviation	41.0	66.9	85.3	87.0

[a] Significantly higher versus prosaccade without tapping, $p<0.0001$.
[b] Significantly higher versus antisaccade without tapping, $p<0.0003$.
[c] Significantly higher versus prosaccade respectively with and without tapping, $p<0.0001$.

Repetition of a pattern and tapping tunes were not allowed. It was stressed that both the saccade task and the random tap task were equally important.

We measured latency time and calculated the percentage of incorrect saccades. Latency time was defined as the time lapse between the beginning of the stimulus and the onset of the saccade. As incorrect saccades we considered: saccades made in the wrong direction (opposite of the cue for prosaccades, towards the cue for antisaccades), when no saccade was made, and in case of the no-saccade task, a saccade when it should have been inhibited. Anticipatory saccades, i.e. saccades performed before the stimulus appeared or saccades with a latency time of less than 100 ms, were not considered as incorrect but were excluded.

The program Evalsac was used to analyze the eye movements [9]. The results of the random tap task were analyzed by a method described by Vandierendonck et al. [8]. Statistical analysis was performed using the MedCalc® computer program (MedCalc Software, Mariakerke, Belgium) [10].

Results

Latency time

Table 1 shows the mean latency time in the prosaccade and in the antisaccade task, without and with tapping. In the no-saccade task, no latency time can be measured, as there is no saccadic eye movement made. Because of the normal distribution of the latency times, the significance of differences was assessed by the Student's *t*-test. The random tapping caused a significant increase of the latency times in the prosaccade task ($p<0.0001$) and in the antisaccade task ($p<0.0003$). The latency times in the antisaccade task both

with and without tapping were significantly longer than the latency times in the prosaccade task with and without tapping respectively ($p<0.0001$).

Number of errors

To get a better idea of the distribution of the number of errors within each task, the number of errors made in the prosaccade, the no-saccade and the antisaccade task both with and without tapping are represented in histograms (Figure 2). As the number of errors were not normally distributed, the significance of differences was assessed by the Wilcoxon test. The number of errors in all of the three saccade tasks were not significantly increased by the random tap task ($p = 0.2$). In the antisaccade task, subjects made significantly more errors compared to the no-saccade and the prosaccade task both with and without tapping ($p<0.0001$).

Latency time and number of errors

The correlation between the difference in latency time with and without tapping on the one hand and the difference in number of errors with and without tapping on the other hand was calculated in the prosaccade and the antisaccade task by the Spearman rank test. In the antisaccade task, there was a significant negative correlation between the difference in latency time with and without tapping versus the difference in number of errors with and without tapping ($r = -0.43$; $n = 30$; 95% confidence interval –0.68 to –0.08; $p = 0.02$; Figure 3). There was no significant correlation found in the prosaccade task.

Discussion

In previous experiments, different tasks have been used to load the central executive component of working memory: e.g. the random number generation task [11], counting backwards [12], the random digit generation task [13], the mental arithmetic task [7]. All these tasks do not only interfere with the central executive but also with either the visuospatial or the phonological slave system, so that clear-cut conclusions can not be obtained. In order to show unequivocally that the CE, rather than the entire working memory system, intervenes in the antisaccade task, the concurrent task should only interfere with the CE without loading on the slave systems. In the random tap task a random rhythm has to be produced. The requirement to be random and to avoid automaticity loads on the central executive, while there is neither empirical nor logical ground to assume that there is interference with the slave systems [8].

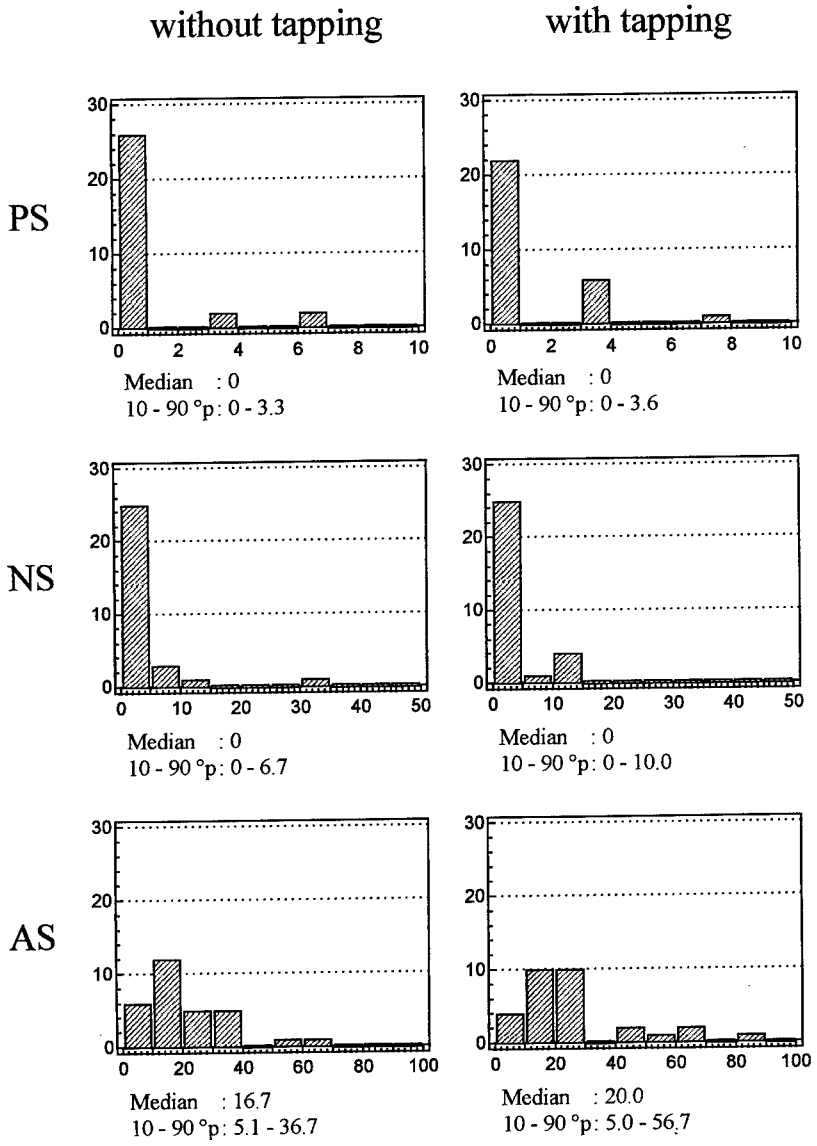

Figure 2. Number of errors made in the prosaccade (PS), the no-saccade (NS) and the antisaccade task (AS) without and with tapping (median, 10-90 th percentiles).

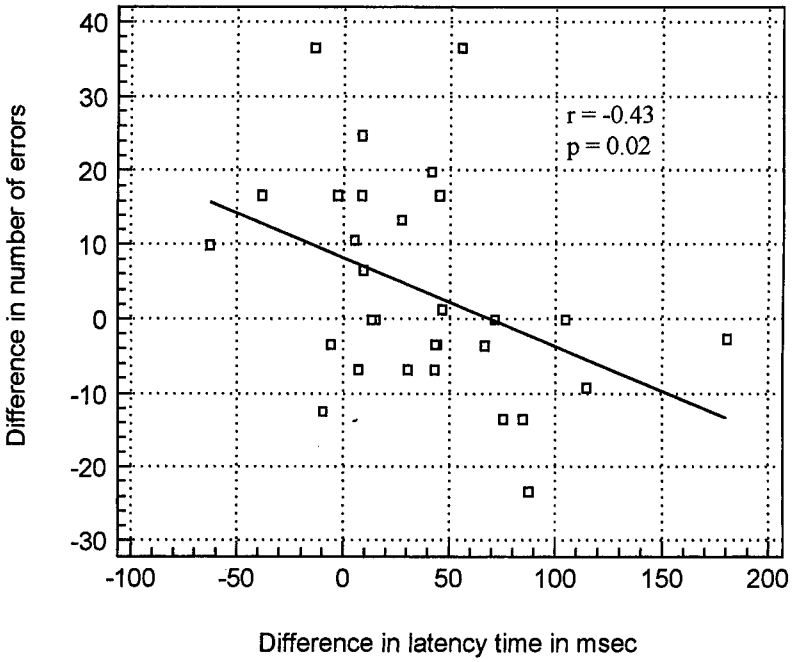

Figure 3. Correlation between the difference in latency time and the difference in number of errors with and without tapping in the antisaccade task (r = –0.43; n = 30; 95% confidence interval -0.68 to –0.08; p =0.02).

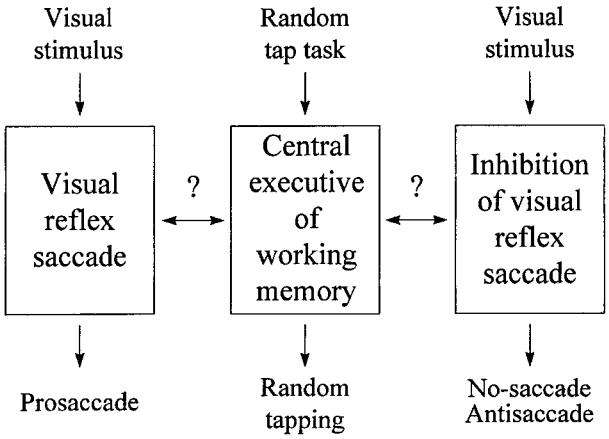

Figure 4. Schematic illustration of parallel visual and memory processes.

Recent evidence [7] shows that eye movements towards a lateral visual target (prosaccades) are performed automatically ,whereas eye movements in a direction opposed to the normal saccadic direction (antisaccades) are performed under attentional control of the central executive (Figure 4).

In accordance with previous findings [7], both the latency times and the number of errors were higher in the antisaccade task compared to the prosaccade task, both with and without taxing the central executive. In the prosaccade task, a significant increase of the latency time was seen under central executive load by random tapping. This is in contrast with the hypothesis that prosaccades would be insensitive to central executive interference [7], as they are believed to be automatic (Figure 4). A possible explanation is that the performance of the prosaccade and the antisaccade task in the same experimental session could bring both tasks under voluntary control. To test this hypothesis, an additional experiment was carried out (K. Van der Goten, in preparation). One group of subjects was asked to perform only the prosaccade task with and without tapping and another group was asked to perform only the antisaccade task with and without tapping. In this experiment, random tapping resulted also in a significant increase of the latency time in both the prosaccade and the antisaccade task. This means that the sequence in which the saccade tasks are performed, is not responsible for the effect of random tapping found in the prosaccade task. Another explanation could be as follows: since the prosaccade is a reflexive automatic action, the SAS (CE) is able to interrupt and modify this automatic routine activity into a non-automatic action under willed control, because subjects were instructed to look as quickly as possible in the direction of the stimulus. Because of the central executive load by the random tap task, a significant increase of latency times in the prosaccade task can then be expected. Antisaccades are the combination of the inhibition of a reflexive saccade towards the stimulus, followed by an intentional saccade in the opposite direction of the stimulus. The no-saccade, where a certain point is fixated in spite of the appearance of a lateral visual target, also requires an inhibition of a reflexive visually guided saccade. The prepotent response to look at the stimulus, in other words the visual reflex saccade has to be inhibited. Therefore, the no-saccade and the antisaccade are non-automatic actions which would be under willed control of the central executive (Figure 4). If the CE is loaded with the random tap task, we can expect higher latency times in the antisaccade task with tapping compared to the antisaccade task without tapping, as demonstrated by our findings.

The number of errors made in all of the three saccade tasks was not influenced by loading the central executive by the random tap task (Figure 2). This means that the latency time is a more sensitive parameter than the number

of errors to investigate the effect of the CE-load. Because of the significant higher number of errors made in the antisaccade task compared to the no-saccade task, with and without tapping, the antisaccade task is considered to be a more difficult task to perform.

In the antisaccade task, a negative correlation was found between the difference in latency time with and without tapping versus the difference in number of errors with and without tapping respectively (Figure 3). In other words, the stronger the effect of the random tapping on the number of errors, the weaker the effect on the latency time in the antisaccade task. This could be explained by one of the following strategies: or the subjects save on the number of errors at the cost of the latency times, or they save on the latency times at the cost of the number of errors.

We can conclude that the ability to inhibit prepotent saccadic responses decreases when the CE is loaded, as is seen in a decreased performance in the antisaccade task. This implies that the antisaccade task would be under CE-control. The effect of CE-load was found on the latency times, not only in the antisaccade task but also in the prosaccade task. As an explanation for this, we postulate that the prosaccade task is brought under willed control of the central executive. The present study also demonstrates that the antisaccade task is a more difficult task to perform than the no-saccade task. To investigate the effect of the CE-load, the latency time seems to be a more sensitive parameter than the number of errors, as no effect of CE-interference is seen in the number of errors, while a significant effect is found on the latency times.

References

1. Stanton GB, Goldberg ME, Bruce CJ. Frontal eye field efferent in the macaque monkey. J Comp Neurol 1988; 271: 473–506.
2. Segraves MA. Activity of monkey frontal eye field neurons projecting to oculomotor regions of the pons. J Neurophysiol 1992; 68: 1967–1985.
3. Pierrot-Deseilligny C, Rivaud S, Gaymard B, Müri R, Vermersch A-I. Cortical control of saccades. Ann Neurol 1995; 37: 557–567.
4. Baddeley AD, Hitch GJ. Working memory. In: Bower GH, ed. The psychology of learning and motivation. New York: New York Academic Press, 1974, vol 8: 47–89.
5. Baddeley AD. Human memory: Theory and practice. London: Lawrence Erlbaum Associates, 1990: 117–141.
6. Norman DA, Shallice T. Attention to action: Willed and automatic control of behaviour. In: Davidson RJ, Schwarts GE, Shapiro D, eds. Consciousness and selfregulation. Advances in research and theory. New York: Plenum Press, 1986, vol 4: 1–18.
7. Roberts RJ, Hager LD, Heron C. Prefrontal cognitive processes: Working memory and inhibition in the antisaccade task. J Exp Psychol 1994; 123: 374–393.
8. Vandierendonck A, De Vooght G, Van der Goten K. Does random time interval generation interfere with working memory executive functions? Eur J of Cognitive Psychol 1998; 10: 413–442.

9. Maes J, De Ridder K. Evalsac program. University of Ghent, Belgium, 1994.
10. Schoonjans F, Zalata A, Depuydt CE, Comhaire FH. MedCalc: A new computer program for medical statistics. Comput Methods Programs Biomed 1995; 48: 257–262.
11. Baddeley AD. The capacity for generating information by randomization. Q J Exp Psychol 1966; 18: 119–129.
12. Glanzer M, Dorfman D, Kaplan B. Short-term storage in the processing of text. Journal of Verbal Learning and Verbal Behavior 1981; 20: 656–670.
13. Gilhooly KJ, Logie RH, Wetherick NE, Wynn V. Working memory and strategies in syllogistic-reasoning tasks. Mem-Cognit 1993; 21: 115–124.

Address for correspondence: L. Crevits, University Hospital Ghent, Department of Neurology, De Pintelaan 185, B-9000 Ghent, Belgium
Phone: 32 9 240 4536; Fax: 32 9 240 4971; E-mail: Luc.crevits@rug.ac.be

Documenta Ophthalmologica **95:** 359–370, 1999.

Parallel visual processes in symmetry perception: Normality and pathology

JOHAN WAGEMANS
University of Leuven, Department of Psychology, Leuven, Belgium

Abstract. Mirror symmetry is one of those regularities for which the visual system seems to have developed a special sensitivity. It is detected robustly and efficiently in a single glance, suggesting that the basic processes do not perform a serial, pointwise comparison of structural elements but rather operate in parallel. Psychophysical evidence relating to the processing mechanisms will be reviewed. Although the focus will be on symmetry perception in normal vision, interesting findings on symmetry perception in observers with deficient vision (e.g., retinitis pigmentosa, visual hemineglect) will also be touched upon briefly.

Key words: attention, corpus callosum, hemineglect, orientation, retinitis pigmentosa (RP), symmetry

Introduction

Mathematically, a symmetric pattern is one which is identical to a transformed copy of it. The type of transformation determines the kind of symmetry one is dealing with. One usually considers four Euclidean transformations or isometries: translation, rotation, reflection, and glide reflection (i.e., a combination of reflection and translation along the axis of reflection, like left and right footsteps in the snow). Three classes of symmetric patterns are distinguished depending on their underlying symmetry group (see Figure 1 for examples). When there are no translations, one has point patterns (Figure 1a); when there are translations in one direction, one has frieze patterns (Figure 1b) and when there are translations in two directions, one has wallpaper patterns or tilings (Figure 1c). Patterns like these are used for decoration everywhere in the world and have been for as long as we know [1]. Their universal appeal is probably based on how well the visual system extracts the underlying regularities. The symmetries are said to be perceived in a single glance [2, 3].

Since the early observations on human symmetry perception by Ernst Mach in the late 19th century and by the Gestalt psychologists early in the 20th century, psychophysical research has attempted to determine the characteristics of how the human visual system extracts regularities such as sym-

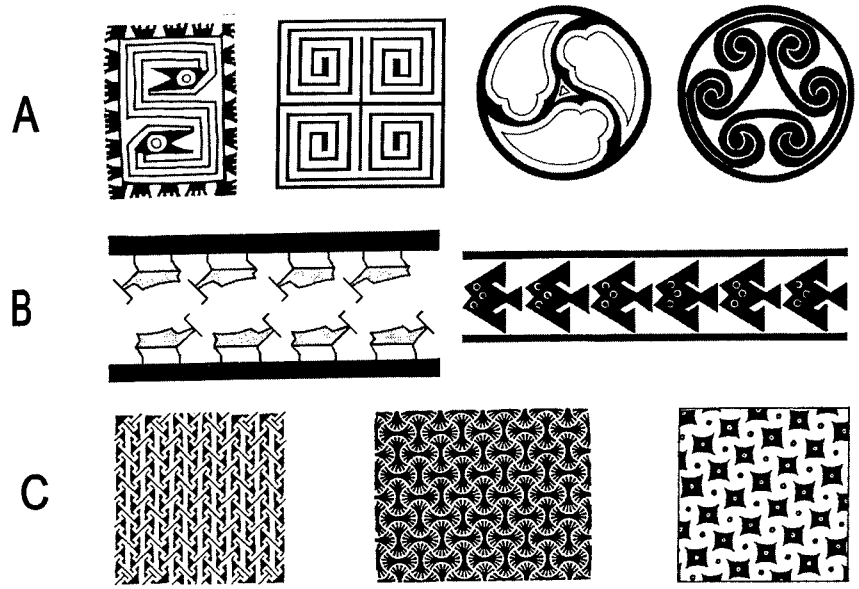

Figure 1. Examples of symmetric patterns used in decorative art taken from diverse cultures. (a) Point patterns with rotation and reflection. (b) Frieze patterns with translation in one direction, rotation, and reflection. (c) Wallpaper patterns with translation in two directions and other isometries.

metries. More recently, computational models of the underlying mechanisms have been proposed and these continue to inspire further theoretical and empirical research. In this paper, I will present a mini-review of this research, with a special focus on the topics which are most relevant to the theme of this special issue, namely, parallel processes and the relevance of both normal and abnormal vision research to unravel the visual system's basic mechanisms. Readers with a more general interest in symmetry detection are referred to two other recent reviews for additional information [4, 5].

Parallel processes

Symmetry is detected efficiently in brief presentations (e.g., 150 ms) suggesting that the underlying mechanisms work preattentively and globally [2, 6, 7]. By this, we mean that they do not require attention and that they work in parallel at different locations of the visual field. They do not seem to require a scrutinous point-by-point comparison to establish all the correspondences needed to verify the mathematical criteria for symmetry. Such a mechanism would necessarily be serial and much slower.

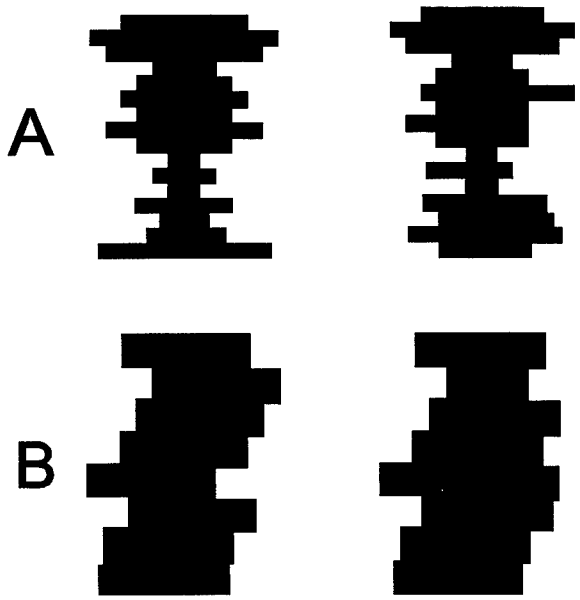

Figure 2. Examples of stimuli used in experiments on parallel versus serial processing of symmetry. (a) At the left is an example of reflection symmetry with 16 steps along the vertical edges; at the right is its asymmetrical counterpart. Number of steps has almost no effect on response times and error rates. (b) At the left is an example of translation symmetry with 8 steps along the vertical edges; at the right is its asymmetrical counterpart. Number of steps has a strong linear effect on response times and error rates. Adapted from [13].

Psychophysically, it is indeed well established that symmetry detection is enormously efficient, versatile and robust [7–11]. More recently, several attempts have been made to confirm the use of parallel, preattentive processes with techniques derived from other areas in cognitive psychology. For example, in visual search tasks it is well known that certain targets are found easily (i.e., preattentively), regardless of the number of distractors, while the search time for others increases almost linearly with the number of items in the display (see [12], for a review). When this occurs, one speaks of parallel and serial search, respectively. In symmetry detection, one can do similar experiments by manipulating the number of corresponding elements and looking at its effect on response time and error rate.

This is what was done in a recent study by Baylis and Driver [13]. They used filled polygons as stimuli and manipulated the number of steps along their jagged edge (4, 8, 16). In Figure 2a is an example of a vertical mirror symmetry with 16 steps, along with an asymmetrical example created by changing 25% of the steps. Although there was a significant linear effect of number of steps on both the response times and the error rates, the slopes

of the functions were very shallow (2–3 ms/step). However, when the symmetry was created by a translation instead of a reflection (see Figure 2b, for examples), the slopes were much steeper (about 40 ms/step). The authors concluded from these results that mirror or reflection symmetry is detected by a parallel process whereas repetition or translation symmetry seems to require a serial process.

Another interesting study with respect to the preattentive nature of symmetry detection has been published by Driver et al. [14]. They tested symmetry detection in a patient with visual hemineglect. This patient, CC, is a 69-year old man with right-hemisphere damage and severe left neglect. He ignores information on the left even though he has no left visual field loss. His hemineglect can thus be characterized as an attentional rather than a sensory deficit. If detection of vertical symmetry depends on the comparison of the left and right halves of a pattern, one would expect such a patient with visual hemineglect to perform at chance level. Indeed, that was what they found when he was tested with shapes similar to those in Figure 2a but with rounded edges. When the shapes were oriented differently, with a horizontal axis of symmetry, he performed almost perfectly, demonstrating that his poor performance with vertical symmetry really resulted from his left neglect and not from failing to understand the task or the notion of symmetry.

Much more interesting is a second experiment performed on CC which looked at the effect of symmetry on figure/ground segregation. When asked how they see the display in Figure 3a, most people would say they see it as white shapes against a black background, whereas the display in Figure 3b is usually seen as black shapes against a white background. That effect is due to symmetry: with ambiguous figure/ground displays, the visual system tends to see figures that are symmetrical [15, 16]. Surprisingly, CC showed the same behavior: he saw the symmetric shapes in 80% of the trials. This result suggests that symmetry is detected preattentively, at a level preceding the involvement of attention. It is only when the patient is explicitly asked to detect symmetry that he probably consciously compares pattern halves, a process which fails with vertical symmetry because of his left visual neglect.

Orientation and location effects

Orientation of the axis of symmetry and location in the visual field have long been known to affect symmetry detection [17, 18]. Mirror symmetry is easier to detect when the axis is oriented vertically, then horizontally, and then obliquely (for reviews of the empirical evidence, see [19, 20]). Moreover, symmetry detection is easy only when the axis of symmetry is centered at the fovea; performance declines rapidly when it is presented eccentrically [21].

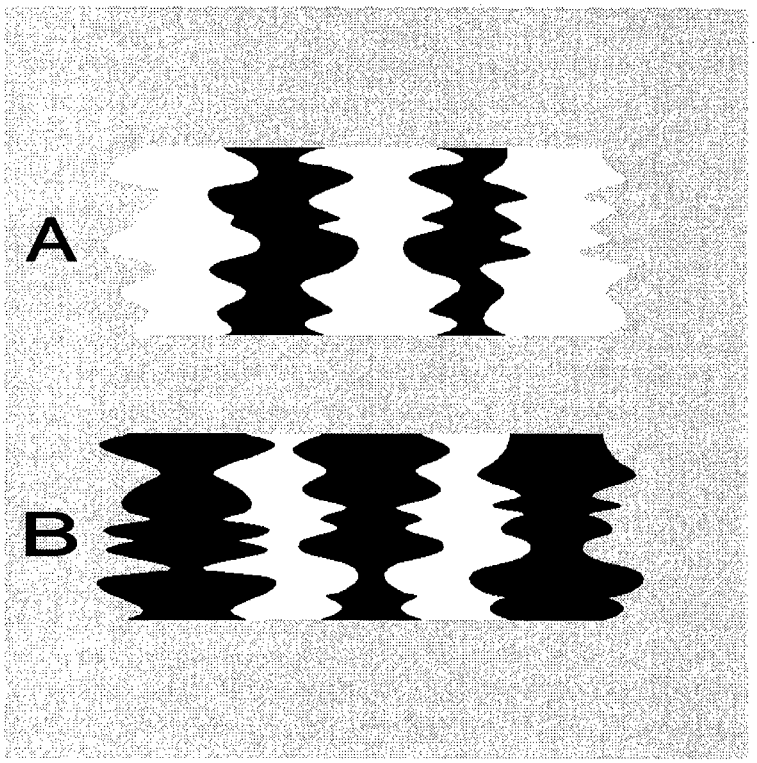

Figure 3. Examples of symmetry effects on figure/ground segregation. In (a) one tends to see white shapes on a black background, while in (b) black shapes on a white background are seen. In both cases there is a preference to see the symmetric shapes as figures. The same is true for a patient with visual hemineglect who fails, however, to report symmetry when asked explicitly. Adapted from [14].

All these results have led several people to suggest that the salience of vertical symmetry in central vision depends on the anatomical and physiological properties of the visual system, such as the bilateral symmetry of the cortex [17, 22] and the abundance of vertically and horizontally tuned orientation-selective cells [23, 24].

In relation to this, it is interesting to see whether the effect of axis orientation on symmetry detection follows the same function as the well-established psychophysical functions for orientation discrimination in gratings and oriented line segments (for reviews, see [25, 26]). Most interesting in this respect are the oblique orientations. If the effect of axis orientation on symmetry detection is based on neural sensitivities, one would expect performance to drop off gradually with increasing deviations away from vertical and horizontal. That is not typically what is found. In one of our own studies we found

performance to be somewhat better at 45° or 135° (i.e., the main diagonals) than at other oblique orientations [19]. This result has been confirmed in more recent work by Wenderoth [20].

He presented dot patterns with the axis of symmetry at a whole range of orientations from 0° to 180° in 10° steps. When number of correct responses was plotted against axis orientation, one could see clearly that there was increased performance near the main diagonals, which goes against what one would expect from orientation-tuned cells [27, 28]. The same result was obtained with response times, although somewhat weaker.

Because the main diagonals, right (45°) and left (135°), were not actually included in the preceding experiment, Wenderoth designed a second experiment to look at these orientations in more detail. This experiment had 16 axis orientations: horizontal (0°), vertical (90°), right-diagonal (45°) plus six oriented slightly away from them (5°, 10°, and 15°, in each direction), and left-diagonal (135°) plus six neighboring axes. Again, he found better performance at the main diagonals, with gradually decreasing performance when the axis of symmetry was turned away from the main diagonals. To his surprise, vertical and horizontal symmetries now produced much lower performance. Because all of the data points represented an equal number of trials, with all trial types mixed randomly, the explanation might be that now attention was directed first towards the most frequent axis orientation, which was oblique in this experiment. For the same reason, the peak of performance may have been at 45° and 135° because they represented the two means of the bimodal distribution of axis orientations.

To verify that explanation, a third experiment was performed with the main diagonals now no longer at the mean of the distribution. This experiment had 16 axis orientations too: horizontal (0°), from 15° to 45° in 5 steps, vertical (90°), and from 135° to 165° in 5° steps. Again, there was a tendency towards better performance at the diagonals than at the other oblique orientations. In other words, the diagonal symmetries are more salient than the other oblique symmetries because of an inherent advantage to the visual system, not because they happened to be the mean orientation of several oblique orientations of the axis of symmetry. In this experiment, horizontal symmetry was also much easier than vertical symmetry, probably because most of the orientations were now near horizontal, not near vertical.

In sum, it is clear that the orientation effects on symmetry detection cannot be based completely on hardwired factors such as better orientation-tuning for vertical and horizontal: The main diagonals seem to be cardinal orientations too and factors such as the frequency of the distribution at least partially determine performance.

Nevertheless, the normal salience of vertical symmetry at fixation and reduced salience with deviating axis orientations and away from fixation, has led some people to suggest an anatomical basis for symmetry detection. They argue for a point-by-point matching process between symmetrically opposite loci in each cortical hemisphere which would be mediated by fibres crossing over through the corpus callosum [29, 30]. Three predictions derived from this so-called 'callosal hypothesis' were tested in a recent paper by Herbert and Humphrey [31].

First, the orientation tuning of symmetry detection at fixation should be quite narrow around the vertical. In an experiment with briefly flashed dot patterns, a sharp drop in performance was indeed obtained, even at only 15° away from the vertical. However, symmetry detection was still possible, and quite good in fact, for other orientations than the vertical. Second, the vertical advantage should decrease abruptly or disappear for brief presentations of patterns away from fixation. In another experiment, the vertical advantage was reduced both with very brief exposures (30–70 ms) and somewhat longer exposures (100–150 ms) but it did not disappear completely. Finally, the corpus callosum must be intact for the vertical advantage to be expressed. Herbert and Humphrey [31] tested two individuals born without a corpus callosum and compared their performance with that of age-matched controls. One subject, SG, appeared to detect horizontal symmetry more reliably than vertical, while the other subject, MG, detected horizontal and vertical symmetry equally well at fixation. However, both could still detect mirror symmetry at all orientations and locations.

In sum, although the authors presented these results as evidence in support of the callosal hypothesis, one could just as well focus on the fact that symmetry could still be detected at nonvertical orientations, at noncentral locations in the visual field and without a corpus callosum.

Mechanisms

In general, symmetry detection is remarkably flexible. Although some results are in line with what we know from the visual system's anatomy and physiology, other results suggest the involvement of psychological factors that are difficult to understand in terms of hardwired neural mechanisms.

This has led many modellers to distinguish between at least two levels of explanation or two stages of processing: low-level versus high-level, preattentive versus attentive, global versus local, etc. [17, 23, 32, 33]. More recently, the role of grouping small-scale items such as dots or oriented line fragments into larger-scale tokens as a more global way of establishing symmetry in multi-element patterns, has been supported psychophysically [6,

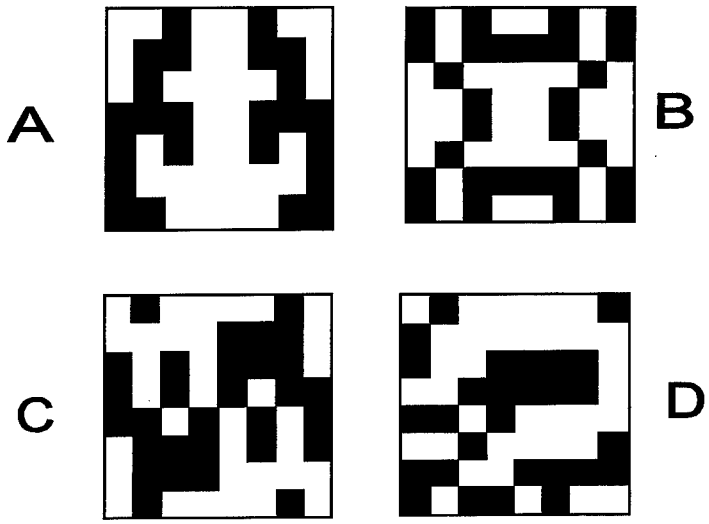

Figure 4. Examples of stimuli used in experiments on symmetry discrimination by patients with retinitis pigmentosa (RP). (a) Reflection symmetry about a vertical axis, (b) two-fold reflection symmetry (vertical-horizontal), (c) rotational symmetry (180°), and (d) asymmetry. Patients with RP make consistently more errors in categorizing such patterns. Adapted from [36].

34, 35] and has been incorporated into computational models [7, 34, 36]. A review of this work would be beyond the present paper's scope (see [5]).

One study which has been presented as relating to the issue of low-level versus high-level factors (i.e., retinal versus cortical, more specifically), may be of particular interest to this special issue. Szlyk et al. [37] looked at symmetry detection in retinitis pigmentosa (RP), a group of hereditary retinal degenerations, characterized by the progressive degeneration of rod photoreceptors resulting in a loss of peripheral visual field and nightblindness [38]. They presented block patterns like those in Figure 4 for 250 ms and observed that RP subjects (with at least 20/30 acuity and a visual field of at least 20° of either side of the fovea) performed significantly lower than control subjects. Further experiments were then aimed at testing different hypotheses to account for this difference, based on the reported anatomical and physiological changes in retinas of patients with RP.

Hypothesis 1 states that the loss in accuracy in symmetry discrimination in patients with RP may be due to a decrease in photopigment optical density, which would reduce the effective luminance of the patterns [39]. However, even a 1.0 log unit reduction in the luminance of the patterns did not significantly alter symmetry discrimination in subjects with normal vision. Hypothesis 2 states that the results may be accounted for by a loss in spatial

contrast sensitivity [40]. However, even with patterns of 5% contrast subjects with normal vision had more accurate symmetry discrimination than did patients with RP when presented with patterns of 93% contrast. Hypothesis 3 states that the loss of symmetry discrimination accuracy in patients with RP may be due to reductions in temporal frequency sensitivity [41]. However, patients with RP did worse at 255, 500, and 1000 ms than the control subjects did at 16 ms. Hypothesis 4 states that these losses in accuracy of symmetry discrimination in the patients with RP may be accounted for by decreased photoreceptor spatial density [42]. In a final experiment, symmetry discrimination was measured by presenting targets at increasing eccentricities in subjects with normal vision. They reached a similar level of performance at a 20° eccentricity as the patients' performance with centrally presented targets but scaling by the cortical magnification factor [43] did not improve performance. Symmetry discrimination was also tested in patterns in which visual information was reduced by randomly blanking individual pixels. With only 25% of the elements remaining, control subjects' performance matched the performance of patients with RP with non-degraded patterns.

In sum, there seems no retinally based explanation which alone can account for the poorer performance of the patients with RP on the symmetry discrimination task. This does not rule out that the deficits in symmetry discrimination may result from a combination of retinally based factors, or from a spatially heterogeneous loss of retinal function, but it seems more likely that the alterations of the sensory input (as a result of the degeneration of rod photoreceptors) may have affected the perceptual encoding of the relationships among pattern elements which are involved in symmetry detection. Further research seems needed to establish the validity of this conclusion.

Conclusions

This mini-review allows several conclusions to be drawn. First, there is solid evidence to show that the human visual system is very good at perceiving mirror symmetry. Especially when it is oriented vertically and centered at the fovea, there is no need to perform a pointwise matching; symmetry is then detected globally and in parallel, even preattentively as clearly demonstrated in a case study with visual hemineglect. Although performance decreases when the axis is turned away from vertical or displaced away from fixation, detection is still too good to be strictly tied to the neuroanatomy and -physiology of the visual system. This is further supported by results of two case studies with patients born without corpus callosum. Finally, patients with RP perform markedly poorer in symmetry discrimination tasks but it is unclear how to explain this effect. Further research on both normal and

abnormal vision seems needed to unravel the underlying mechanisms of the human visual system's remarkably apt detection of mirror symmetry.

Acknowledgements

The author was supported by a grant from the FWO-Vlaanderen (G.0210.97N).

References

1. Washburn DK, Crowe DW. Symmetries of culture. Seattle, WA: University of Washington Press, 1988.
2. Carmody DP, Nodine CF, Locher PJ. Global detection of symmetry. Percept Motor Skills 1977; 45: 1267–1273.
3. Locher PJ, Nodine CF. The perceptual value of symmetry. Computers & Mathematics with Applications 1989; 17: 475–484.
4. Wagemans J. Detection of visual symmetries. Spatial Vision 1995; 9: 9–32.
5. Wagemans J. Characteristics and models of human symmetry detection. Trends in Cognitive Sciences 1997; 1: 346–352.
6. Locher P, Wagemans J. The effects of element type and spatial grouping on symmetry detection. Perception 1993; 22: 565–587.
7. Wagemans J, Van Gool L, Swinnen V, Van Horebeek J. Higher-order structure in regularity detection. Vision Res 1993; 33: 1067–1088.
8. Barlow HB, Reeves BC. The versatility and absolute efficiency of detecting mirror symmetry in random dot displays. Vision Res 1979; 19: 783–793.
9. Tapiovaara M. Ideal observer and absolute efficiency of detecting mirror symmetry in random images. J opt Soc Am A 1990; 7: 2245–2253.
10. Wagemans J, Van Gool L, d'Ydewalle G. Detection of symmetry in tachistoscopically presented dot patterns: Effects of multiple axes and skewing. Percept Psychophys 1991; 50: 413–427.
11. Wenderoth, P. The effects of dot pattern parameters and constraints on the relative salience of vertical bilateral symmetry. Vision Res 1996; 36: 2311–2320.
12. Treisman A. Properties, parts, and objects. In: Boff KR, Kaufman L, Thomas JP (eds) Handbook of perception and human performance (Vol. 1). New York, NY: Wiley, 1986: 35-1–35-70.
13. Baylis GC, Driver J. Parallel computation of symmetry but not repetition within visual shapes. Visual Cognition 1994; 1: 377–400.
14. Driver J, Baylis GC, Rafal RD. Preserved figure-ground segregation and symmetry perception in visual neglect. Nature 1992; 360: 73–75.
15. Bahnsen P. Eine Untersuchung über Symmetrie und Asymmetrie bei visuellen Wahrnehmungen. Z Psychol 1928; 108: 129–154.
16. Kanizsa G, Gerbino, W. Convexity and symmetry in figure-ground organization. In: Henle M (ed) Art and artefacts. New York: Springer, 1976: 23–32.
17. Julesz, B. Foundations of cyclopean perception. Chicago: University of Chicago Press, 1971.
18. Mach E. The analysis of sensations. (Originally published in German, 1886). New York: Dover, 1959.

19. Wagemans J, Van Gool L, d'Ydewalle G. Orientational effects and component processes in symmetry detection. Quart J Exp Psychol 1992; 44A: 475–508.
20. Wenderoth P. The salience of vertical symmetry. Perception 1994; 23: 221–236.
21. Saarinen J. Detection of mirror symmetry in random dot patterns at different eccentricities. Vision Res 1988; 28: 755–759.
22. Corballis MC, Beale IL. The psychology of left and right. Hillsdale, NJ: Erlbaum, 1976.
23. Jenkins B. Component processes in the perception of bilaterally symmetric dot textures. Percept Psychophys 1983; 34: 433–440.
24. Jenkins B. Orientational anisotropy in the human visual system. Percept Psychophys 1985; 37: 125–134.
25. Appelle S. Perception and discrimination as a function of stimulus orientation: The 'oblique effect' in man and animals. Psychol Bull 1972; 78: 266–278.
26. Essock EA. The oblique effect of stimulus identification considered with respect to two classes of oblique effects. Perception 1980; 9: 37–46.
27. Campbell FW, Kulikowski JJ, Levinson J. The effect of orientation on the visual resolution of gratings. J Physiol (Lond) 1966; 187: 427–436.
28. Mitchell DE, Freeman RD, Westheimer G. Effect of orientation on the modulation sensitivity for interference fringes on the retina. J opt Soc Am 1967; 57: 246–249.
29. Braitenberg V. Reading the structure of brains. Network 1990; 1: 1–11.
30. Milner AD, Jeeves MA. A review of behavioral studies of agenesis of the corpus callosum. In: Russell IS, van Hof MW, Berlucchi G (eds) Structure and function of cerebral commisures. College Park, MD: University of Maryland Press, 1979: 428–448.
31. Herbert AM, Humphrey GK. Bilateral symmetry detection: Testing a 'callosal' hypothesis. Perception 1996; 25: 463–480.
32. Bruce V, Morgan MJ. Violations of symmetry and repetition in visual patterns. Perception 1975; 4: 239–249.
33. Palmer SE, Hemenway K. Orientation and symmetry: Effects of multiple, rotational, and near symmetries. J Exp Psychol [Hum Percept Perf] 1978; 4: 691–702.
34. Labonté F, Shapira Y, Cohen P, Faubert J. A model for global symmetry detection in dense images. Spatial Vision 1995; 9: 33–55.
35. Pashler H. Coordinate frame for symmetry detection and object recognition. J Exp Psychol [Hum Percept Perf] 1990; 16: 150–163.
36. Dakin SC, Watt RJ. Detection of bilateral symmetry using spatial filters. Spatial Vision 1994; 8: 393–413.
37. Szlyk JP, Seiple W, Xie W. Symmetry discrimination in patients with retinitis pigmentosa. Vision Res 1995; 35: 1633–1640.
38. Newsome DA. Retinitis pigmentosa, Usher's syndrome, and other pigmentary retinopathies. In: Newsome DA (ed) Retinal dystrophies and degenerations. New York: Raven Press, 1988: 161–194.
39. Kilbride PE, Fishman M, Fishman GA, Hutman LP. Foveal cone pigment density difference and reflectance in retinitis pigmentosa. Arch Ophthal 1986; 104: 220–224.
40. Marmor MF. Contrast sensitivity versus acuity in retinal disease. Br J Ophthal 1986; 70: 553–559.
41. Dagnelie G, Massof RW. Foveal cone involvement in retinitis pigmentosa progression assessed through psychophysical impulse response parameters. Invest Ophthal visual Sci 1993; 34: 243–255.
42. Flannery JG, Farber DB, Bird AC, Bok D. Degenerative changes in a retina affected with autosomal dominant retinitis pigmentosa. Invest Ophthal visual Sci 1989; 30: 191–211.

43. Rovamo J, Virsu V. An estimation and application of the human cortical magnification factor. Exp Brain Res 1979; 37: 495–510.

Address for correspondence: J. Wagemans, University of Leuven, Department of Psychology, Tiensestraat 102, B-3000 Leuven, Belgium
Phone: (+32) 16-32 59 69; Fax: (+32) 16-32 60 99;
E-mail: johan.wagemans@psy.kuleuven.ac.be

Documenta Ophthalmologica **95:** 371–374, 1999.

DOCUMENTA OPHTHALMOLOGICA Contents Volume 95

Volume 95 No. 1 1998 (ISCEV 10.3)

Volume 95 No. 2 1998

Volume 95 No. 3–4 1998/1999 (ISCEV 10.4)

Special issue
Parallel Visual Processes in Health and Disease

Guest editor: Werner Spileers

AUTHOR INDEX Volume 95

Documenta Ophthalmologica **95:** 375–378, 1999.

DOCUMENTA OPHTHALMOLOGICA

Instructions to ISCEV authors – 1999

Presentation of the manuscript

Manuscripts must be written in English; American spellings are preferred. An original and two legible photocopies of the manuscript, with three sets of illustrations, should be mailed to:

Dr. J.V. Odom, Editor
Department of Ophthalmology
RC Byrd Health Sciences Center
P.O. Box 9193
Morgantown, WV 26506, USA

All manuscripts and correspondence should be sent by air mail in durable envelopes. No fax transmittal is permitted except for urgent corrections.

All manuscripts will be reviewed by members of the ISCEV Editorial Board and additional referees. They may be returned to authors for revision as appropriate. The Society encourages both members and non-members of ISCEV to submit articles at any time.

No page charges are levied on authors or their institutions. The length of manuscripts is no longer restricted to six pages for Symposium papers.
Noncompliance with Instructions to Authors as to the proper preparation of manuscripts will result in their unnecessary delay in processing.

Preparation of the Manuscript

General
The entire manuscript (including references and tables) should be typed double-spaced on one side of quality white bond paper 21 x 29 cm or 8.5 x 11 inches. Machine pitch should be set the same as that of the printing element (10 pica or 12 elite). Margins should be at least 3 cm (1.25 inches).

All pages (including the tables, figures, legends, and references) should be numbered consecutively, in the upper right-hand corner preceded by the surname of the first author.

Abbreviations, units, and other
Only SI units and abbreviations should be used although some quantities may be used in common units, e.g. mm Hg. Abbreviations should be explained when they first appear in the text. If a non-standard abbreviation is to be used extensively, it should be defined in full on page 2 as mentioned below. Whenever in doubt use SI (Système International) Units.

Acronyms and initialisms should be used in moderation and only after parenthetical identification following first use of the phrase. If such abbreviations are other than those common to the specialty (ERG, EOG, VECP, PERG, etc.) they should be set out in a glossary on the abstract page. To facilitate electronic search, it is preferable to use the full term in titles, abstracts, and key words.

Patients should be identified by number and not by name or initials. The Editorial Board has adopted the policy that any animal experiments published in the ISCEV Documenta Ophthalmologica must conform to the general recommendations of the Association for Research in Vision and Ophthalmology on the humane and conservative use of animals in research and must conform to the laws of each author's country.

Words should be used for numbers one through nine in the general text and for all numbers beginning a sentence. Numerals should be used for 10 and above, for all numbers with units of measure, and in a series of numbers when the highest number is above nine.

Manuscript Format

The manuscript should be arranged in the following order:

Title Page (page 1)

- Title (the title should be concise and accurate, but should contain adequate information regarding the contents). Capitalize only the first word.
- Subtitle (this may be used to supplement and thereby shorten an excessively long main title).
- Author's full first and last names (if more than one, use "&" before the last name).
- Affiliation(s) should be identified (including the city and country), and footnoted with superscript numerals for the respective authors.

Type a rule across the page and then add:

- The complete mailing address and telephone number of the corresponding author. A fax number, if available, should also be provided.

Key words / Abstract / Abbreviations (page 2)

- Key words (to a maximum of 6, in alphabetical order, suitable for indexing and electronic search).
- Abstract (brief and informative, not to exceed 250 words, and only one paragraph).
- Abbreviations (arranged alphabetically, only those which are not familar and/or commonly used).

Main Text

- The main section usually is arranged as Introduction, Materials (or Subjects) and Methods, Results, and Discussion, without page breaks.
- Headings and subheadings (not numbered) should be made clear by spacing and indentation. Do not use all capital letters.
- The approximate location of figures and tables should be indicated in the margin.
- New paragraphs should be indicated by clear indentation
- Breaking a word at the end of a line should be avoided whenever possible.
- The use of footnotes should be avoided. However, if essential, they should be typed on appropriate pages, but clearly separated from the text with a line above them.
- Mathematical formulas should have a clarification of all symbols and an accompanying "translation" of the meaning, e.g., "this formula shows that when the highly variable factor λ is found to exceed unity, the viscosity of the medium δ is no longer significant".
- Acknowledgements (including grant support etc. if any): should follow the text and precede the references.

References

- References are cited in *numerical order*, the numbers being placed in square brackets. Citations of personal communications and unpublished data should be avoided unless

absolutely necessary. When used, such citations should appear in the text only, e.g., "(E.D. Smith, personal communication)", and not in the reference list.
- Abbreviate titles of periodicals according to style of the Index Medicus (USA).
- Follow the format (arrangement, punctuation) shown below (Vancouver Style):

Article in periodical

1. Günther E, Zrenner E. Rod and cone contribution to adaptation processes in cat retinal ganglion cells. Doc Ophthalmol 1990; 75: 83–95.

Book

2. Cohen I. Statistical power analysis for the behavioural sciences. Revised ed. New York: Academic Press, 1977: 217–48.

Chapter in book

3. Brown SA, Fox TT. Focal electroretinograms in systemic diseases. In: Tinsley SW, Smith IA, eds. Pediatric ophthalmology. Philadelphia: JR Lippincott, 1985: 345–55.

- Never use underlining or italics of articles or books.

Tables
- Each table should be mentioned in the text. Careful thought should be given to the orientation of each table when it is constructed. Tables which can be arranged so that they can be read without rotating the page are preferred.
- Tables may be edited by the publisher to permit more compact typesetting.
- Tables should be numbered consecutively with arabic numerals, followed by the title. Horizontal rules should be indicated; vertical rules are not used.
- Definitions and explanations should appear as table-footnotes, marked with superscript letters.
- Each table should be typed on a separate page.

Figures
- Each figure should be mentioned in the text.
- Line drawings should be in a form suitable for reproduction without modification. Extremely small type should be avoided as figures are often reduced in size.
- Photographs should be supplied as black-and-white, high contrast glossy prints. Colour prints may be inserted at the author's own expense.
- Figures as well as Legends should be identified by arabic numbers. Where multipart figures are used, each part should be clearly identified in the legend, preferably with (lower case) letters.
- The top of the figure should be indicated on the back. Figures which need to be placed landscape should be avoided if possible.
- Identify each illustration, on the back, by lightly writing the first author's name and figure number.

General Information

Style Manuals
The following three books are recommended as guides in writing scientific papers:
- Council of biology editors style manual. A guide for authors, editors and publishers in the biological sciences, 5th ed., Bethesda, Md: Council of Biology Editors, 1983. 796
- O'Connor M, Woodford FP (eds.): Writing scientific papers in English. Amsterdam: Elsevier, 1976.
- Reynolds L, Simmonds D: Presentation of data in science. Publications, slides, posters, overhead projections, tape-slides, television. Dordrecht: Kluwer, 1984.

Proofs

- When proofs are submitted to the corresponding authors, ***it is imperative*** **that they be checked and returned by airmail only to the ISCEV Editor**, Dr. J.V. Odom, Department of Ophthalmology, RC Byrd Health Sciences Center, P.O. Box 9193, Morgantown, WV 26506, USA, within 48 hours of their receipt.
- The ISCEV Editor will check all proofs, but it is the author's responsibility to guarantee that there are no technical errors.
- Alterations other than typographical errors must be held to a minimum; the author will be charged for the labor required to make extensive changes.

Offprints

- The authors will receive 50 offprints free of charge.
- Ordering information for additional offprints will be sent with the proofs to the corresponding author.

Copyright Transmittal

- Copyright for all published ISCEV material is held by Kluwer Academic Publishers. Submission of a paper for publication implies that copyright reverts to the publisher from the author and also that the article has not been published and is not being considered for publication elsewhere.
- Permission to reproduce, in whole or in part, any material published in the Documenta Ophthalmologica must be obtained from the publisher.

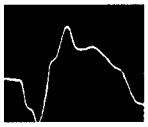

ISCEV

YOU COULD HAVE HAD THIS ISSUE FOR FREE
if you had registered as an ISCEV MEMBER!

The International Society for Clinical Electrophysiology of Vision (ISCEV) has the goals

- To promote and extend the knowledge of clinical electrophysiology of vision
- To promote cooperation and communication between workers in the field of clinical and basic electrophysiology of vision

The annual membership fee includes the five ISCEV issues of Documenta Ophthalmologica for free (a regular subscription is necessary if all 12 issues are wanted). Moreover, members have a considerably reduced registration fee at the Society's symposia.

You are invited to join the ISCEV and share your experiences with other members of the society. Just submit the application form below.

- -

Application form

I wish to become a member of the International Society for Clinical Electrophysiology of Vision (ISCEV).

Name .....Academic Degree .....

Position .....

Address .....

.....

.....

Tel: ..... Fax: .....E-mail: .....

Mail the form to: Signed .....

Professor Colin Barber
Secretary-General of ISCEV
Medical Physics Department
University Hospital
Nottingham NG7 2UH
Tel +44 115 970 9131; Fax +44 115 942 2745;
E-mail: Colin.Barber@nottingham.ac.uk.

You will be invoiced for the annual subscription (approximately $110, payable by credit card). If you think you justify for student rate (half price) please supply documentary evidence of status.

Manuscripts intended for publication in *Documenta Ophthalmologica* should be written in English and should be submitted in triplicate to the following address: The Editorial Office, Kluwer Academic Publishers, P.O. Box 17, 3300 AA Dordrecht, The Netherlands, Telephone: (31) 78 6392236 Fax: (31) 78 6392555.

Editorial statement. *Documenta Ophthalmologica* publishes articles in the field of ophthalmology. Apart from regular journal articles longer manuscripts will also be considered for publication, for example monographs, theses or reviews.

ISCEV. *Documenta Ophthalmologica* is also the official journal for the International Society for Clinical Electrophysiology of Vision (ISCEV). Manuscripts related to electrophysiology and its application to various retinal, optic nerve, or visual pathway disorders can be submitted to Dr. J.V. Odom, Department of Ophthalmology, RC Byrd Health Sciences Center, P.O. Box 9193, Morgantown, WV 26506, USA.

The year program of *Documenta Ophthalmologica* includes 1 issue on the History of Ophthalmology under the auspices of the Cogan Ophthalmic History Society.

Detailed *Instructions to authors* are available from the Editorial Office of the publisher. *Instructions to ISCEV authors* appear in every ISCEV issue.

Offprints. 50 offprints of each article will be provided free of charge. Additional offprints can be ordered when proofs are returned to the publisher.

Consent to publish in this journal entails the author's irrevocable and exclusive authorization of the publisher to collect any sums or considerations for copying or reproduction payable by third parties (as mentioned in Article 17, Paragraph 2, of the Dutch Copyright Act of 1912 and in the Royal Decree of June 20, 1974 (S.351) pursuant to Article 16b of the Dutch Copyright Act of 1912) and/or to act in or out of court in connection herewith.

This journal is indexed/abstracted in *Biological Abstracts, CAB Abstracts, Current Contents, Current Contents/Clinical Medicine, EMBASE/Excerpta Medica, Index Medicus, The ISI Alerting Services, Medical Documentation Service, Ocular Resources Review, Reference Update, Science Citation Index and Science Citation Index Expanded.*

The Kluwer Academic Publishers Information Online.
Visit our Website at http://www.wkap.nl